CONTRACTOR REPORT

SAND84—7011
Unlimited Release
UC—62

Innovative Solar Thermal Dish Technology Development

W. E. Schwinkendorf
The BDM Corporation
1801 Randolph Rd., SE
Albuquerque, NM 87106

Prepared by Sandia National Laboratories Albuquerque, New Mexico 87185 and Livermore, California 94550 for the United States Department of Energy under Contract DE-AC04-76DP00789

Printed September 1984

Issued by Sandia National Laboratories, operated for the United States Department of Energy by Sandia Corporation.

Printed in the United States of America
Available from
National Technical Information Service
U.S. Department of Commerce
5285 Port Royal Road
Springfield, VA 22161

NTIS price codes
Printed copy: A06
Microfiche copy: A01

SAND84–7011
Unlimited Release
Printed September 1984

Distribution
Category UC–62

Innovative Solar Thermal Dish Technology Development

W. E. Schwinkendorf
The BDM Corporation
1801 Randolph Rd., SE
Albuquerque, NM 87106

Under Sandia Contract No. 52-3671

Abstract

A Cassegrainian point focus solar concentrator system has been analyzed and a conceptual design developed. In this system, the receiver is located at the vertex of the primary mirror eliminating limitations of receiver size and weight associated with standard parabolic dish collectors. Disadvantages include increased reflection loss at the secondary mirror and increased beam spread associated with the longer focal length. A non-imaging, trumpet shaped tertiary reflector located at the receiver aperture increases the system efficiency by 15 to 20 percent. Because the secondary mirror may reach very high temperatures, a reflective film cannot be used as a mirror surface. Recommended instead is thin polished stainless steel stamped into shape and used as the mirror substrate with vacuum deposited silver used for the reflecting surface. A transparent coating is then required to protect the silver. Both the secondary and primary mirrors require radial supports on the back surface to minimize deflection under wind loading. The Cassegrainian system is more efficient than the standard dish only at high operation temperatures and for large receivers. However, the cost per kilowatt into the receiver aperture is less for the Cassegrainian, due primarily to the high cost of piping and insulation running to the receiver of the standard dish. Further efforts in the analysis and design of the Cassegrainian concept appear warranted.

FOREWORD

This report documents the work accomplished during the Innovative Solar Termal Dish Technology Development program, contract 52-3671, administered by Sandia National Laboratories, Albuquerque, New Mexico. This program was divided into four tasks:

Task I Optical System Design and Analysis
Task II Conceptual Structural Design
Task III System Comparison
Task IV Reporting

In Task I a Cassegrainian collector system was analyzed and optimized in terms of performance. A conceptual structural design and investigation of mirror materials and fabrication techniques was performed in Task II. The Cassegrainian system was compared to standard parabolic dish collectors and linear parabolic trough collectors in Task III.

I would like to acknowledge the assistance provided to this program by the following Sandia personnel:

R. W. Hunke
G. S. Kinoshita
R. L. Alvis
R. L. Champion

The following BDM Corporation personnel contributed to this effort:

W. E. Schwinkendorf, Program Manager
S. S. Waterbury
R. S. Leonard
R. W. Herman

TABLE OF CONTENTS

TABLE OF CONTENTS (Concluded)

LIST OF FIGURES

LIST OF FIGURES (Continued)

LIST OF FIGURES (Concluded)

LIST OF TABLES

LIST OF TABLES (Concluded)

CHAPTER I
INTRODUCTION

The purpose of this program was to investigate the feasibility of a Cassegrainian point focus solar concentrator and compare its performance and cost to standard parabolic dish collectors (PDC). A Cassegrainian concentrator consists of a paraboloidal primary and a hyperboloidal secondary mirror arranged so that the focal point of the system is at the vertex of the primary mirror. In a standard PDC the receiver is cantilevered from the primary mirror and located at the focal point of the primary. This places a limit on the size and weight of the receiver since larger receivers will block more insolation and will require more costly structural supports. The piping to the receiver is an additional cost and a source of heat loss. The advantage of the Cassegrainian is that there is no limitation regarding size or weight of the receiver, or regarding the amount of insulation applied to the receiver. In addition, piping costs and heat losses are reduced.

Optically, there are some disadvantages with a Cassegrainian solar concentrator. The first is the additional reflection off the secondary mirror, reducing the power in the reflected beam. The second is blocking of insolation caused by the secondary mirror, and the third is the effect of beam spread due to the increased system focal length. The first disadvantage is inherent in the design and cannot be eliminated. However, the second and third disadvantages affect the system performance inversely, i.e., when the blocking is increased by moving the secondary mirror closer to the primary, the beam spread decreases since the system focal length is decreased, and vice versa. These counteracting effects suggest an optimum position of the secondary reflector for maximum efficiency.

Results of the analyses of the Cassegrainian system indicate three main findings. They are as follows:

(1) As the system focal length decreases by increasing the primary rim angle or decreasing Z/F_p, the intercept factor increases as

a result of decreased beam spread. Here Z is the distance between the vertices of the secondary and primary, and F_p is the focal length of the primary.

(2) There is an optimum Z/F_p for each rim angle, or more generally, for a given amount of beam spread. This more general description of optimum Z/F_p is necessary, since the beam spread varies with the amount of slope error present so that the optimum Z/F_p is a function of rim angle and slope error.

(3) Slope errors on the primary have much more effect than those on the secondary. Secondary slope errors were varied from 1 to 8 milliradians with only about 1.0 percent decrease in optical efficiency when a tertiary reflector was used. Primary surface errors greater than 4 milliradians produced a significant, and unacceptable, decrease in efficiency.

Analyses were performed to compare the optical performance of a Cassegrainian system and a Ritchey-Chretien configuration in which the shapes of the hyperboloidal secondary and paraboloidal primary of the Cassegrainian have been modified to correct for spherical aberration and coma. It was found that, although the Ritchey-Chretien configuration has a higher peak radiation intensity at the center of the receiver, its total optical efficiency is no greater than the optical efficiency of the Cassegrainian. This occurs because the blocking factor of the secondary mirror of the Ritchey-Chretien system is increased above that of the Cassegrainian when the hyperboloidal secondary is modified to eliminate coma.

To correct for the effects of beam spread on the performance of the standard Cassegrainian concentrating system, a non-imaging terminal concentrator, or tertiary reflector, in the shape of a hyperbolic trumpet was integrated into the concentrator system. It has the advantage of affecting only the edges of the beam, reducing total reflecton losses. Analyses indicated an improvement in optical efficiency of 15 to 20 percent when the tertiary is used with the Cassegrainian system.

The optimization study considered a standard Cassegrainian with a tertiary reflector and a concentration ratio of 1200. The results of these studies are as follows:

(1) As the primary mirror rim angle increases, the optical efficiency increases.

(2) The optical efficiency can be optimized as a function of the distance between the primary and secondary.

These performance results indicate that the best performance occurs at large rim angles. However, as the rim angle increases, the surface area of the reflectors increase reducing the effectiveness of the reflector area and increasing cost. At a 60 degree rim angle the power into the receiver per unit of total concentrator area is optimized at 0.694 kW/m^2. The characteristics of the optimized Cassegrainian are summarized in figure I-1, where all surface reflectivities are assumed to be 0.95.

Performance comparisons were made with a parabolic dish concentrator (PDC) with a receiver located at the focal point of the primary mirror. Since the design and analysis of a receiver was not within the scope of this program, only conductive losses from the receiver and piping were considered. As insulation is applied to the receiver and piping, the blocking factor increases while the heat loss decreases. The optimum amount on insulation is that which minimizes total power loss due to heat loss and blocking. This optimum amount of insulation, and a rim angle of 60 degrees which maximizes the optical efficiency, was used in comparing the PDC with the Cassegrainian. Since the insulation on the Cassegrainian receiver does not block any insolation, the insulation thickness is unrestricted.

Comparisons were made at receiver operating temperatures of 370° C and 815° C, and receiver diameters of 0.609 and 1.22 meters. Steady state operating efficiencies were calculated, as well as a daily efficiency based on capacitance losses from heating the pipes running to the receiver during startup. Steady state and daily efficiencies for the PDC and Cassegrainian system are shown in table I-1.

CR:	1200	BLOCKING FACTOR:	.058
θ_R:	60 DEGREES	INTERCEPT FACTOR:	.973
Z/F_p:	.79	OPTICAL EFFICIENCY:	.827
VERTEX TO VERTEX SPACING:		2.39 m	
POWER PER UNIT SURFACE AREA:		0.694 kW/m^2	

PRIMARY

RADIUS:	3.5 m
FOCAL LENGTH:	3.0311 m
SURFACE AREA:	41.53 m^2
REFLECTOR AREA:	39.31 m^2

SECONDARY

RADIUS:	.84 m
ECCENTRICITY:	1.7241
DEPTH OF REFLECTOR:	.184 m
SURFACE AREA:	2.31 m^2
REFLECTOR AREA:	2.22 m^2

TERTIARY

HEIGHT:	1.11 m
ANGLE OF ASYMPTOTES:	23.9 DEGREES
RADIUS OF UPPER RIM:	0.504 m
SURFACE AREA:	2.08 m^2

Figure I-1. Characteristics of Optimized Cassegrainian Concentrator

TABLE I-1. DAILY EFFICIENCY COMPARISON BETWEEN THE PDC AND CASSEGRAINIAN CONCENTRATORS

Receiver Dia (meters)	T_{oper} (°C)	PDC Steady	PDC Daily	Cassegrainian Steady	Cassegrainian Daily	Difference Between PDC and Cassegrainian
0.609	370	.867	.854	.815	.815	-4.6%
1.22	370	.833	.820	.811	.811	-1.1%
0.609	815	.815	.832	.803	.813	+1.2%
1.22	815	.791	.762	.809	.809	+6.2

A thermal analysis of the secondary mirror indicates that it can reach a temperature of 230°F. This prevents the use of any of the available reflective films. An investigation of materials which could be used for the secondary mirror was performed. Based on this investigation and a preliminary structural analysis, a conceptual design was developed which consists of a thin (0.0762 cm thick) polished stainless steel mirror supported on the back surface with steel hat-shaped radial supports attached to the steel mirror with structural acrylic adhesive. Vacuum deposited silver would be applied to the polished surface of the steel mirror to enhance its reflectivity to 0.95 or greater. A coating of SOL-GEL or Dow Corning's 1-2577 silicone would be applied for environmental protection.

Analysis of the tertiary and the intensity distribution across the receiver aperture indicates that the tertiary mirror would become too hot if the tracking error was excessive. Thus, the mirrors must be actively cooled using cooling channels brazed to the outer surface. The mirror itself would be fabricated from bright rolled aluminum using a spinning process. Silver would be vacuum deposited on the inner surface and a protective coating applied.

A cost and performance analysis was performed for the Cassegrainian collector, a standard PDC and a linear parabolic trough collector (LPT).

The results are summarized in table I-2. For large, high temperature receivers, the Cassegrainian efficiency is greater than that of the PDC. However, for all situations the Cassegrainian system is lower in cost per kilowatt of power entering the receiver. This is due to the high cost of piping and insulation associated with the PDC, and the low efficiency of the LPT.

TABLE I-2. COST AND PERFORMANCE COMPARISON SUMMARY

Cost Item	Cassegrainian	PDC	LPT
Primary Mirror	2847.00	2847.00	
Secondary Mirror	362.60		
Secondary Support	11.00		
Testiary Mirror	217.50		
Receiver Support (126kg)		17.34	
Piping and Insulation		1794.00	
Total Cost per m^2 of Aperture	$89.33	$121.00	$110.80

STEADY STATE PERFORMANCE AND COST

		Cassegrainian		PDC		LPT	
RECEIVER TEMP ^oC	RECEIVER Dia.(m)	PERFORMANCE (kW/m^2)	COST ($/kW)	PERFORMANCE (kW/m^2)	COST ($/kW)	PERFORMANCE (kW/m^2)	COST ($/kW)
370	0.609	0.815	109.60	0.867	139.60		
370	1.22	0.811	110.15	0.833	145.25		
815	0.609	0.813	109.90	0.832	145.40		
815	1.22	0.809	110.40	0.791	153.00		
350	0.0318					0.63	$175.90

CHAPTER II
OPTICAL SYSTEM DESIGN AND ANALYSIS

A. INTRODUCTION

1. Cassegrainian Configuration

The Cassegrainian optical configuration consists in general form of a concave primary mirror and a convex secondary mirror. This secondary mirror folds the optical path in order to locate the system focal point at a more convenient location as illustrated in figure II-1. The system was originally proposed in 1672 for astronomical telescopes, because it would have several practical and optical advantages over the Newtonian design. The main advantage is a long focal length system which can be designed into a relatively compact package, reducing bulk and weight. The focal point for the system can also be located in a more convenient position, increasing the flexibility of the design. Also, since another reflector surface has been added to the system, several optical aberrations can be reduced or eliminated. The two aberrations most easily eliminated are spherical aberration and coma. The Cassegrainian system, corrected for spherical aberration and coma is commonly called the Ritchey-Chretien, named for the astronomers who collaborated on its design, or it is called by its generic name, the aplanatic Cassegrainian. The true Cassegrainian, consisting of a paraboloidal primary and confocal hyperboloidal secondary, is optically similar to an equivalent paraboloid having a primary focal length equal to the Cassegrainian system focal length.

A solar concentrator using the Cassegrainian configuration takes advantage of the compact system size and convenient focal point position. Additionally, there are practical advantages regarding the mechanics of the system and thermal transport. Since the receiver is located at the primary vertex rather than at the primary focal point, there are no limitations regarding the size, weight, or insulation of the receiver or the piping leading to the receiver, since they are behind the primary mirror, and will not block incoming insolation.

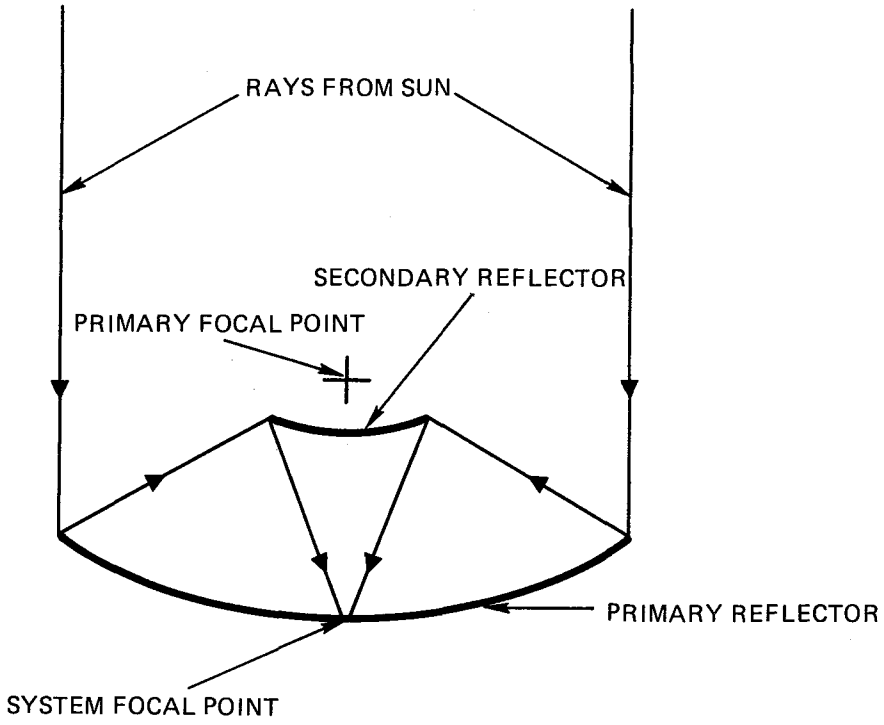

Figure II-1. Illustration of Cassegrainian Optical Configuration

Optically, there are some disadvantages with a Cassegrainian solar concentrator. The first is the additional reflection off of the secondary mirror, reducing the power in the reflected beam. The second is blocking of insolation caused by the secondary mirror, and the third is the effect of beam spread due to the increased system focal length. The first disadvantage is inherent in the design and cannot be eliminated. However, the second and third disadvantages affect the system performance inversely, i.e., when the blocking is increased by moving the secondary mirror closer to the primary, the beam spread decreases since the system focal length is decreased, and vice versa. These counteracting effects suggest an optimum position of the secondary reflector for maximum efficiency.

2. Previous Work on Cassesgrainian Solar Concentrators

There have been several papers published on Cassegrainian concentrators, however, much of this work has been limited to perfect

optics, or specific designs. No analysis of aplanatic Cassegrainian concentrators has been published, except for general statements regarding their possible improvement in system performance.

The Soviet journal Geliotekhnika has published several papers on analysis of Cassegrainian solar concentrators (1-6) and experimental results of actual concentrators (7-9). They have also published a paper describing a small Cassegrainian using an inflatable film secondary (10).

The published U.S. work has been limited to perfect optics and simple treatment of errors (11-15). Neither Soviet or U.S. authors have considered the effects of misalignment or thermal effects on the secondary mirror.

3. Analytical Methods

There are two general methods of analysis used for predicting the performance of Cassegrainian concentrators. The first method is purely analytical, using generally closed form solutions. Unfortunately, to reduce the complexity of the solutions, simplifications are usually made, which reduce the completeness of the solution.

The second method of analysis uses ray-tracing computer codes. This method has the advantage of being able to analyze arbitrary mirror shapes without requiring any simplification. The main disadvantage is the increased computer time required to analyze a concentrator, although with modern high speed computers this disadvantage has become less important. It was determined that a ray trace analysis would be the most useful for this study.

Several codes were reviewed for their utility in this application. The first was HELIOS (16) a "cone optics" code originally designed for heliostat/power tower applications. This code has been used in the past for analyzing parabolic dish concentrators (PDC), but was somewhat inflexible when used in this manner. This program, in its present form, was incapable of analyzing secondary reflectors and since it would require significant modification to be useful, it was eliminated as a candidate for this project. The optical design code, CODE V (17), was considered but rejected as too expensive and sophisticated for the level

of analysis required in this study. Although CODE V would be very useful for final optimization of a Cassegrainian concentrator, it was considered too expensive for a general parametric study.

Several other codes were considered such as the cone optics code developed by Schrenk (18). This code had been modified to study Cassegrainian concentrators (14), but apparently was not sufficiently documented or flexible enough for general use. Another code, actually an illumination code available at LANL (19), looked very promising but was not sufficiently documented for general use.

The code chosen to do the analysis was a Monte-Carlo ray trace code, the Concentrator Optical Performance Simulation (COPS), developed by Honeywell (20). This code traces rays through the concentrator, reflecting off of each surface assuming a first surface reflection. Additionally, RMS slope errors are modeled by perturbing the surface normal at the intersection of the ray and the reflector surface based on a user-selected standard deviation of error. The sun is modeled with a nonuniform flux distribution. Using this method, a large number of rays, typically 20000, are traced through the system, and the number of hits on the focal plane are stored in a "bullseye" array to show the intensity distribution at the receiver. From the intensity distribution plot, it is possible to calculate the intercept factor for various geometric concentration ratios.

COPS, being a Monte-Carlo method, relies on a random number generator supplying random numbers uniformly distributed between 0 and 1. Since the random number generator will not distribute between 0 and 1 with exact uniformity, there is a small amount of error with this method. However, the lack of uniformity is small and is not considered to be a significant problem.

COPS was originally developed to analyze concentrator types other than the Cassegrainian, and so a subroutine describing the Cassegrainian geometry was written in order to use the COPS driver program and auxiliary subroutines. The flowchart describing the algorithm used for the Cassegrainian geometry is shown in figure II-2.

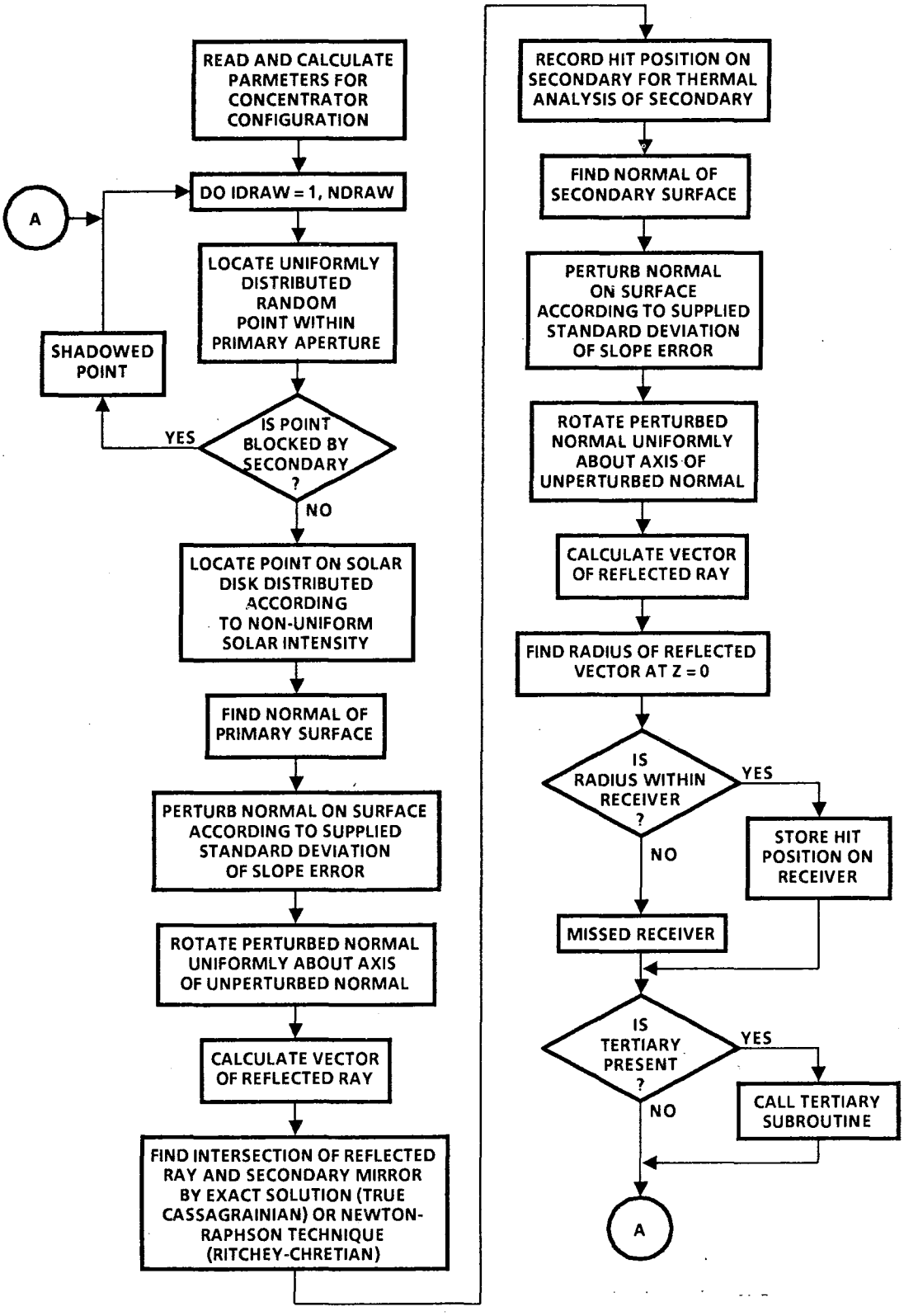

Figure II-2. COPS Flowchart

The listing for the program and flowcharts for the auxiliary subroutines, along with some of their development can be found in reference 20 and appendix B of this report.

B. OPTICS OF CASSEGRAINIAN SOLAR CONCENTRATORS

1. Definitions

The standard Cassegrainian concentrator consists of a paraboloidal primary and a hyperboloidal secondary--both conic sections. Their shapes can be described by basic conic section formulas. The following is a collection of the various terms used in this study to describe the standard Cassegrainian geometry and its performance. The geometric parameters are shown in figure II-3.

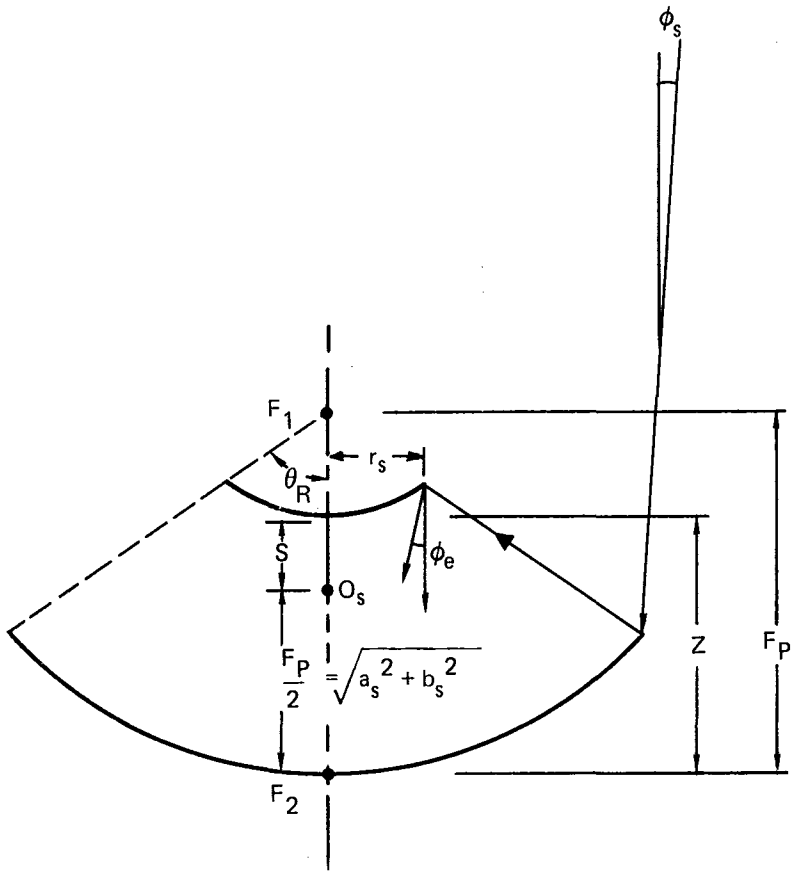

Figure II-3. Geometric Parameters of Cassegrainian Concentrator

a. Primary Focal Length (Fp)

The distance between the vertex of the paraboloid and the primary focal point.

b. Magnification (M)

A function of the eccentricity (ε_s) of the secondary reflector (defined in the next section) relating the focal length of the primary to the system focal length such that

$$M = \frac{\varepsilon_s + 1}{\varepsilon_s - 1} \qquad \text{(Eq. II-1)}$$

c. Optical Extent

A constant for a fixed aperture radius defined as:

$$\sin^2\phi_s \; r_p^2 = \text{constant} \qquad \text{(Eq. II-2)}$$

where ϕ_s is the sun half angle, and r_p is the radius of the aperture, in this case the primary mirror radius.

This constant defines the maximum concentration ratio that can be obtained for a given entrance angle to the focal point (F_2). In figure II-3, the entrance angle is ϕ_e, so

$$\sin^2\phi_s \; r_p^2 = \sin^2\phi_e \; r_{spot}^2 = \text{constant} \qquad \text{(Eq. II-3)}$$

where r_{spot} is the radius of the beam on the focal plane. The theoretical concentration ratio is defined as

$$CR_{THEO} = \frac{r_p^2}{r_{spot}^2} = \frac{\sin^2\phi_e}{\sin^2\phi_s} \qquad \text{(Eq. II-4)}$$

This definition of concentration ratio has neglected the effects of slope errors and optical aberrations, but does give some insight into the rela-

tionship between the size of the spot at the focal plane, and the entrance angle.

d. Slope Error (σ)

The macroscopic RMS deviation of the reflector surface from the geometrically defined surface. In this study, this deviation is normally distributed about the surface normal vector and uniformly distributed, i.e. not limited to radial errors only.

e. Geometric Concentration Ratio (CR)

The ratio of the aperture area to the receiver area, or

$$CR = \frac{r_p^2}{r_r^2} \qquad \text{(Eq. II-5)}$$

The geometric concentration ratio is not restricted to correspond to CR_{THEO}, as CR_{THEO} assumes that 100 percent of the beam is within the radius r_{spot}. CR is merely a ratio of areas, and does not assume anything about the amount of the beam that is within r_r.

f. Intercept Factor at Receiver (IF_R)

The ratio of the insolation within r_r to the total insolation reflected from the secondary.

g. Blocking Factor (BF)

The ratio of the secondary mirror area projected onto the aperture plane to the total aperture area, or

$$BF = \frac{r_s^2}{r_p^2} \qquad \text{(Eq. II-6)}$$

h. Intercept Factor at Secondary (IF_s)

The ratio of the insolation intercepted by the secondary mirror to the total insolation reflected off of the primary.

i. Optical Efficiency (η_o)

The ratio of the total insolation intercepted by the aperture area to the amount within r_p, or

$$\eta_o = (1\text{-}BF)(IF_s)(IF_R)\rho_p\rho_s \qquad \text{(Eq. II-7)}$$

where ρ_p and ρ_s are the reflectivities of the primary and secondary mirrors.

2. Optical Configuration of Cassegrainian Solar Concentrators

In this study, the variable geometric parameters are the primary rim angle (θ_R) and the spacing (Z) between the primary and secondary vertex. The constant parameters are the radius of the primary (r_p) which is held at 3.5 meters, and the position of the system focal plane, which is located at the vertex of the primary. In most cases the radius of the secondary (r_s) has been sized to intercept 100 percent of the insolation reflected by the primary, so

$$r_s = f(\theta_R, Z, \sigma_p) \qquad \text{(Eq. II-8)}$$

also,

$$F_p = f(\theta_R, r_p) \qquad \text{(Eq. II-9)}$$

The spacing Z between the primary and secondary has been normalized to F_p and will generally be referred to as the fraction Z/F_p.

Figure II-3 shows the relationships between the hyperbolic secondary and the parabolic primary. F_1 is the shared focal point of the parabola and one of the hyperbolic focal points. The focal point of the system is at the second hyperbolic focal point, which in this case is located at the vertex of the parabola, F_2. Locating the system focal point at F_2 simplifies the relationships between the primary and secondary, and was appropriate for this study, although the system focal point could be located anywhere along the system axis.

For this study, the center for the hyperboloid is located halfway between the primary focal point and the primary vertex, so the distance from O_s to either focal point is $F_p/2$, defined as F_s. Also,

$$F_p/2 = F_s = \sqrt{a_s^2 + b_s^2} \qquad \text{(Eq. II-10)}$$

The eccentricity of a hyperbola is defined as

$$\varepsilon_s = \frac{\sqrt{a_s^2 + b_s^2}}{a_s} = \frac{F_p/2}{a_s} \qquad \text{(Eq. II-11)}$$

where a_s is the distance from O_s to the vertex of the hyperbola defined by

$$a_s = Z - F_p/2 \qquad \text{(Eq. II-12)}$$

The values of a_s and b_s define the surface geometry of the hyperboloid surface through the relation

$$\frac{z^2}{a_s^2} - \frac{r_s^2}{b_s^2} = 1 \qquad \text{(Eq. II-13)}$$

where in this relation z is measured from O_s to the hyperboloid surface. If Z is normalized to Z/F_p, then

$$a_s = F_p\,(Z/F_p - 1/2) \qquad \text{(Eq. II-14)}$$

and

$$\varepsilon_s = \frac{F_p/2}{F_p(Z/F_p - 1/2)} = \frac{1}{2(Z/F_p) - 1} \qquad \text{(Eq. II-15)}$$

so that ϵ_s is dependent only on the normalized spacing Z/F_p. This result also carries into the magnification M such that

$$M = \frac{Z/F_p}{1-Z/F_p} \qquad \text{(Eq. II-16)}$$

Jones (21) has presented the concept of an equivalent parabola, i.e. the Cassegrainian configuration can be mathematically replaced by a parabola with the same aperture radius and system focal length, such that

$$F_{sys} = F_p M \qquad \text{(Eq. II-17)}$$

This is useful for visualizing the effects of M on the system performance.

The entrance angle, ϕ_e, for an equivalent parabola is

$$\phi_e = \theta_{R_e} + \phi_s \qquad \text{(Eq. II-18)}$$

where θ_{Re} is the rim angle of an equivalent parabola. This definition of ϕ_e neglects the effect of slope errors.
Also,

$$\theta_{Re} = \tan^{-1} \frac{r_p}{F_{sys} - \frac{r_p^2}{4 F_{sys}}} \qquad \text{(Eq. II-19)}$$

Substituting into the relationship for CR_{THEO},

$$CR_{THEO} = \frac{\sin^2 (\theta_{Re} + \phi_s)}{\sin^2 \phi_s} \qquad \text{(Eq. II-20)}$$

Clearly, when θ_{Re} increases, CR_{THEO} increases. However, when F_{SYS} increases by increasing Z/F_p, θ_{Re} decreases, reducing CR_{THEO}. However, increasing Z/F_p decreases the blocking factor. This indicates that there will be an optimum Z/F_p for a given rim angle. Figure II-4 shows a plot of the blocking factor and ideal beam radius at the focal plane for θ_R = 60 degrees. It must be stressed that the beam radius shown is the theoretical minimum for 100 percent intercept and is not physically attainable because of various optical aberrations and deviations on the reflector surfaces (slope errors). As can be seen, beam spread rapidly increases when Z/F_p reaches about .85, and so there is little need to examine configurations of Z/F_p greater than .85, since the ideal concentration ratio drops to ~1950.

For an ideal concentrating system, a short focal length is most desirable. However, a Cassegrainian concentrator actually increases the focal length, thus reducing CR_{THEO}, making the Cassegrainian look less desirable from a purely optical viewpoint. There are other factors to consider, however. The first factor is the effect of optical aberrations on the image or spread of the beam. Up to now only ideal optics were considered. It is beyond the scope of this study to cover all the effects of optical aberrations on concentrator systems, except in very general terms.

The most important aberration in concentrating systems is coma. This is an off axis aberration which causes the beam to be larger at the focal plane than predicted by ideal optics. Coma is inherent in parabolic systems and cannot be corrected for with a single mirror. However, a Cassegrainian has two reflectors, allowing more degrees of freedom in reflector geometry, and therefore the capability of correcting coma and other aberrations. The reflector surfaces are no longer conic but of general aspheric shape. The most common name for the corrected Cassegrainian is the Ritchey-Chretien. There have been several derivations of the required reflector curvatures published in the telescope literature. The one that was used in this study is by Wetherell and Rimmer (22). The required reflector relationships will be presented in the next section.

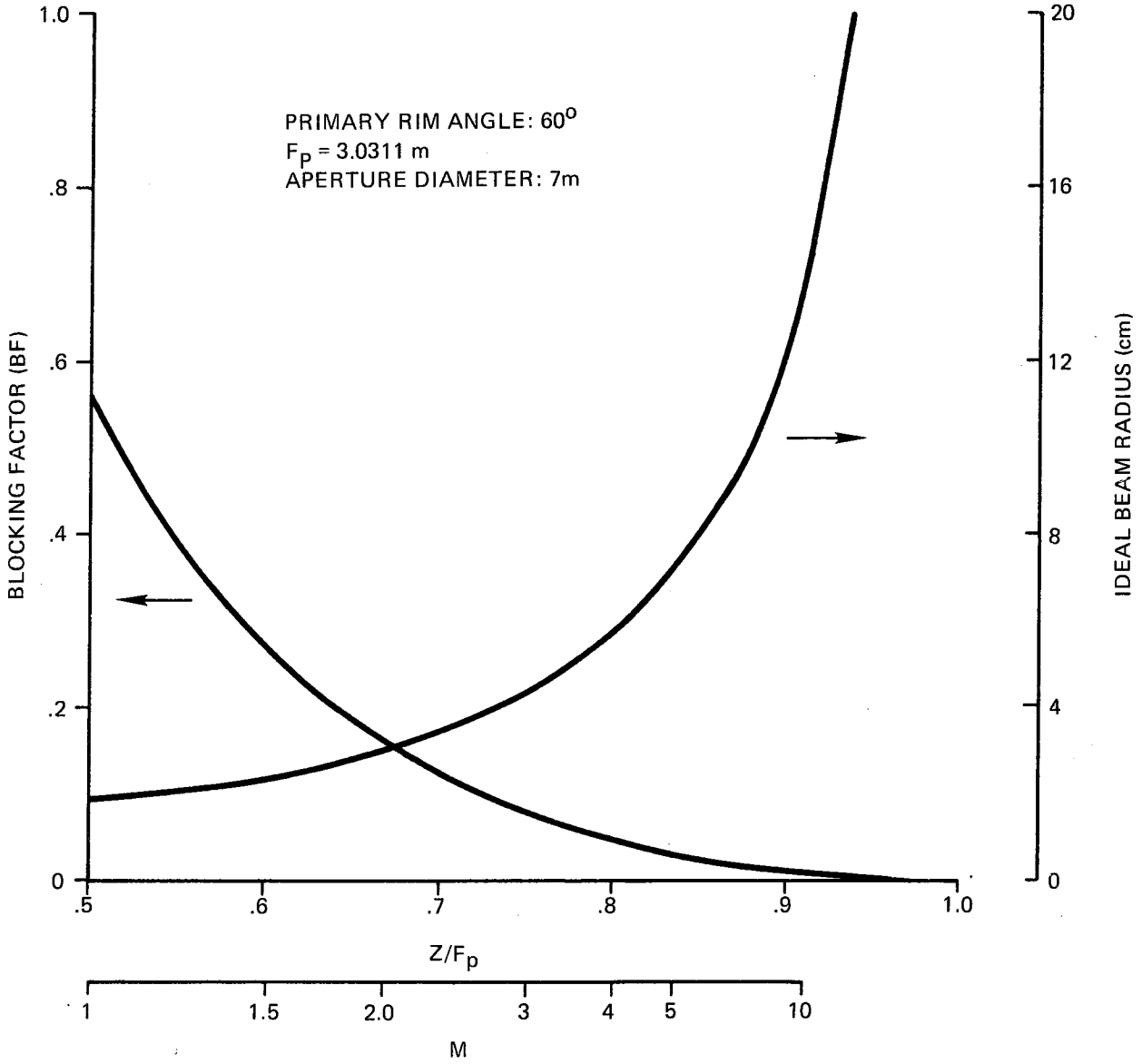

Figure II-4. Ideal Blocking Factor and Beam Radius Versus Z/F_p

Other factors which make the Cassegrainian more attractive involve structural, thermal, and practical considerations. These considerations will be discussed in detail in later sections.

3. Definitions and Relationships for Ritchey-Chretien Concentrators

The general form of the reflector surface equation is a sag equation of the form

$$Z(r) = \frac{C_p r^2}{1+(1-\kappa_p C_p^2 r^2)^{1/2}} \qquad \text{(Eq. II-21)}$$

for the primary.

Terms and definitions used in the above equation are

$$C_p = \frac{-1}{2\ F_p} \qquad \text{(Eq. II-22)}$$

$$\kappa_p = \frac{-2}{m^3} \qquad \text{(Eq. II-23)}$$

$$m = \frac{Z/F_p}{1-Z/F_p} \qquad \text{(Eq. II-24)}$$

for the primary, and

$$C_s = \frac{1-m^2}{2\ m\ F_p} \qquad \text{(Eq. II-25)}$$

$$\kappa_s = -2\left[\frac{m+1}{(m-1)^3} + \frac{2m}{(m-1)^2}\right] \qquad \text{(Eq. II-26)}$$

for the secondary, where C_s and κ_s are substituted for C_p and κ_p in equation II-21. As before, the spacing between the primary and secondary vertex is referred to the primary focal length, and the system focal plane is located at the vertex of the primary. In this form, the system will be corrected for coma and spherical aberration.

4. Application of a Tertiary Reflector

To correct for the effects of beam spread on the performance of the concentrating system, a tertiary reflector, or more generally, a nonimaging terminal concentrator was integrated into the Cassegrainian system in the third phase of the optical study. There has been considerable work regarding nonimaging concentrators by Winston, et. al. (23, 24, 25), and their conclusion is that for a terminal concentrator for high power systems such as this one, a hyperbolic trumpet concentrator is the most desirable. It has the advantage of affecting only the edges of the beam, reducing the total reflection losses. Figure II-5 shows the geometry of the tertiary reflector as it has been integrated into the Cassegrainian. A minimum of three parameters are required to describe the shape and size of the tertiary; they are the virtual spot diameter $2 F_H$, the exit aperture diameter 2a, and the tertiary truncation height Z_T. The virtual spot diameter is what the concentrator "sees" as a target, and any part of the beam that is outside 2a, but inside $2 F_H$ will be redirected into 2a. The part of the beam that is outside $2 F_H$ will be rejected, or reflected out the top of the tertiary.

Z_T is subject to two restrictions which set a minimum and maximum for its value. The first restriction is that the upper rim of the tertiary must not block any rays that are reflected from the primary towards the secondary. The second restriction is that the rim of the tertiary must intersect the entire beam that is reflected from the secondary towards the virtual spot. This relationship is shown in figure II-6 for the case when the maximum and minimum are equal.

The shape of the tertiary is a hyperbola, and is described by

$$\frac{r^2}{a^2} - \frac{z^2}{b^2} = 1 \qquad \text{(Eq. II-27)}$$

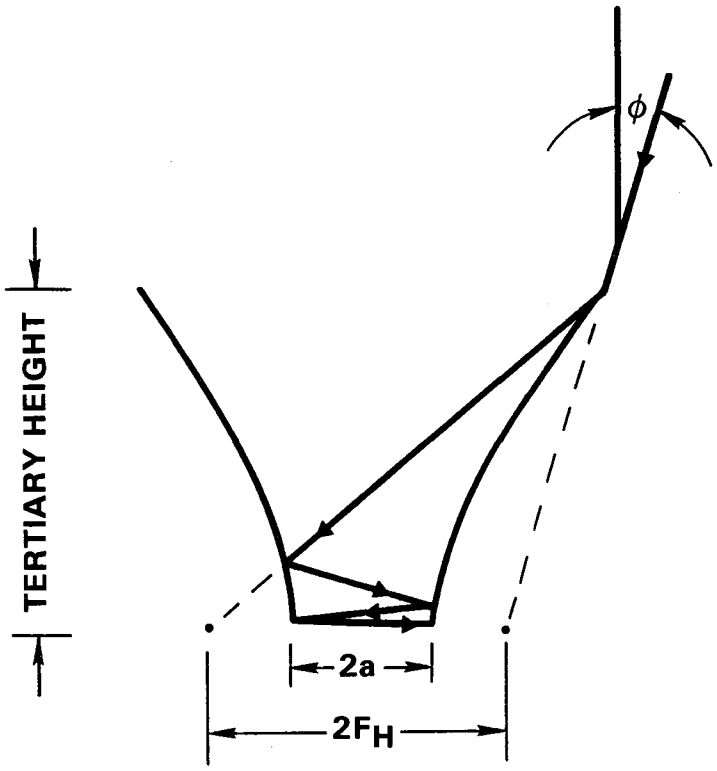

Figure II-5. Tertiary Reflector Geometry

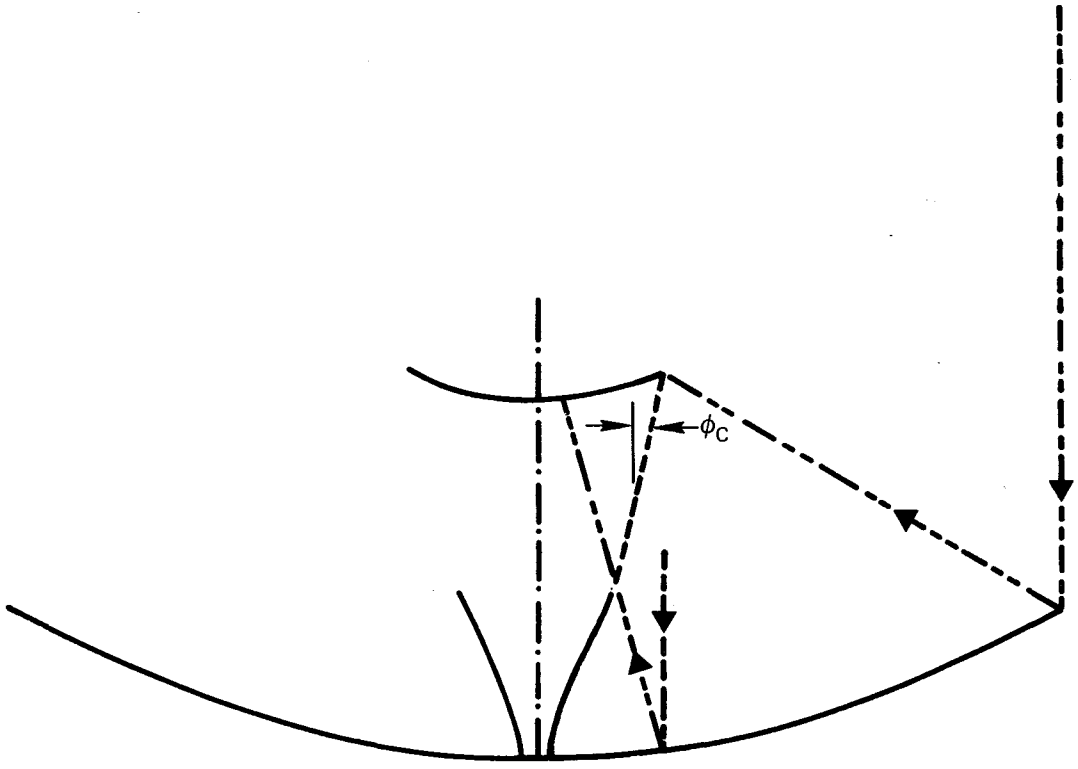

Figure II-6. Optimal Z

where

$$b = \sqrt{F_H^2 - a^2} \qquad \text{(Eq. II-28)}$$

The asymptotic angle for the hyperbola is

$$\theta_a = \sin^{-1} \frac{a}{F_H} \qquad \text{(Eq. II-29)}$$

If "a" is constant and F_H increases, θ_a decreases causing the hyperbola to have more vertical asymptotes. This results in a taller tertiary if the entire beam is to be intercepted. To reduce the size of the tertiary, it is necessary to reduce F_H so that it is smaller than the actual beam. This results in a percentage of the beam being rejected by the tertiary. This percentage can be estimated by approximating the intensity of the beam at the focal plane with a normal distribution. The standard deviation of the beam intensity is determined by examining the IF_R from previous computer runs for the Cassegrainian system without the tertiary. With this information, F_H can be set to intercept any desired percentage of the total beam, subject to the restrictions on Z_T.

5. Scope of Analysis

This optical analysis consists of three phases. The first phase is a parametric analysis of the standard Cassegrainian concentrator, examining the effects of varying the primary rim angle, the spacing Z/F_p, and varying the RMS slope errors on the primary and secondary mirrors using the COPS simulation program. The second phase examines the performance of the Ritchey-Chretien for selected parameters to assess the relative change in performance due to the Ritchey-Chretien geometry. The third phase integrates a nonimaging tertiary reflector into the standard Cassegrainian design. This configuration is also analyzed with the COPS code for selected parameters. Table II-1 lists the range of the parameters used for phase one.

TABLE II-1. PARAMETERS USED FOR CASSEGRAINIAN OPTICAL STUDY

Rim Angle (θ_R) 45, 60, 75 degrees
Vertex Spacing (Z/F_p) .55, .65, .70, .75, .80, .85
Primary Slope Error (σ_p) 2, 4, 8 mrad
Secondary Slope Error (σ_s) 1, 2, 3 mrad

C. RESULTS OF OPTICAL ANALYSIS

1. Standard Cassegrainian

The results for the Cassegrainian study are in the form of four plots. They are as follows:

(1) Integrated power into receiver versus receiver radius
(2) Intensity at the receiver versus receiver radius
(3) Intercept factor versus concentration ratio
(4) Optical Efficiency versus Z/F_p.

The reflectivity of the primary and secondary mirrors has been set to 100 percent in these plots. To compare these results with those of other concentrators, it will be necessary to multiply the appropriate values by ρ_p and ρ_s. The bulk of these plots are located in the appendix.

Generally, the results indicate three main findings. They are as follows:

(1) As the system focal length decreases by increasing the primary rim angle or decreasing Z/F_p, the intercept factor increases as a result of decreased beam spread, as was indicated by theory. This effect is shown in figure II-7.
(2) There is an optimum Z/F_p for each rim angle, or more generally, for a given amount of beam spread. This more general description of optimum Z/F_p is necessary, since the beam spread varies with the amount of slope error present so that the optimum Z/F_p is a function of rim angle and slope error. A plot of optical efficiency versus Z/F_p is shown in figure II-8.
(3) Slope errors on the primary have much more effect than those on the secondary.

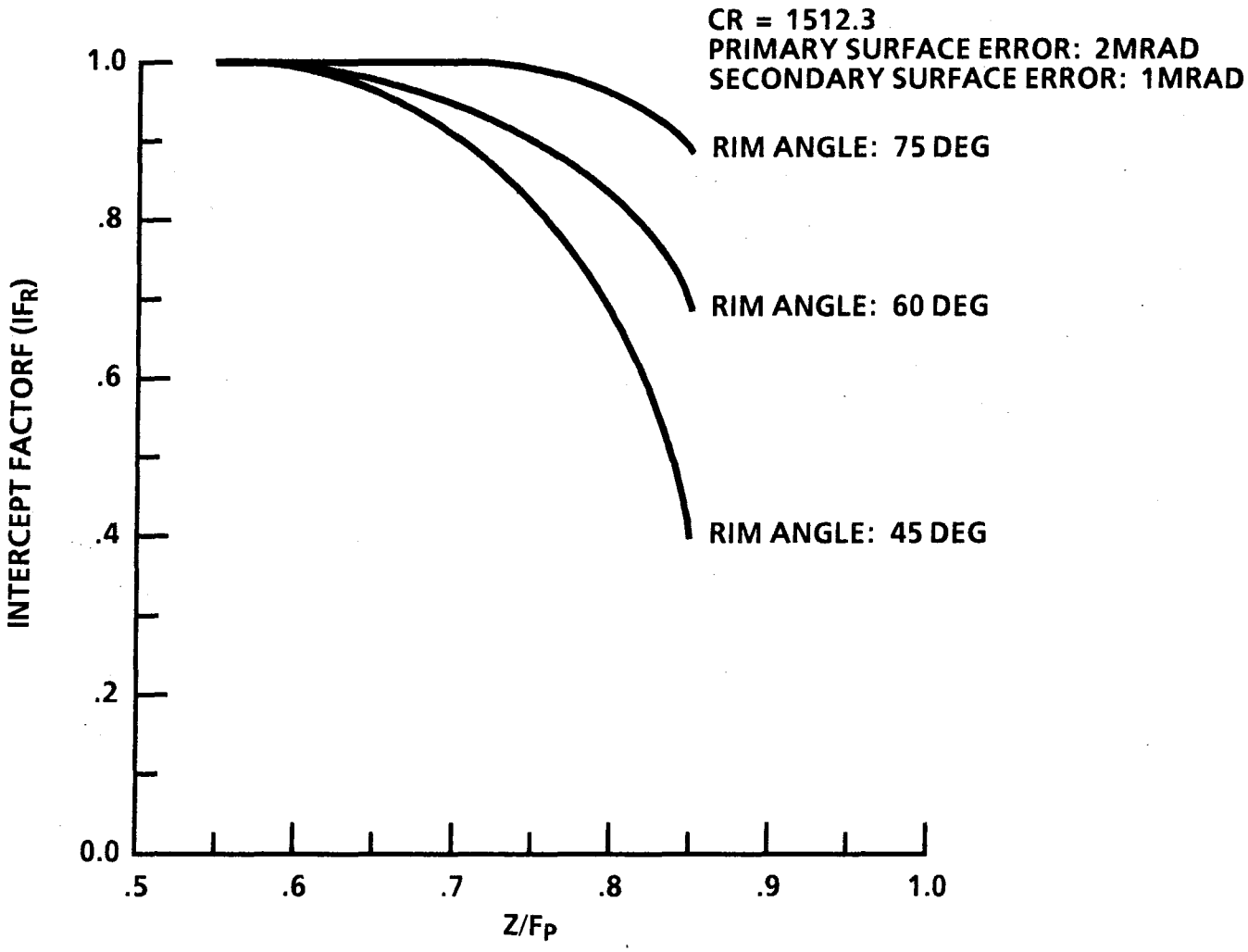

Figure II-7. Intercept Factor Versus Z/F_P

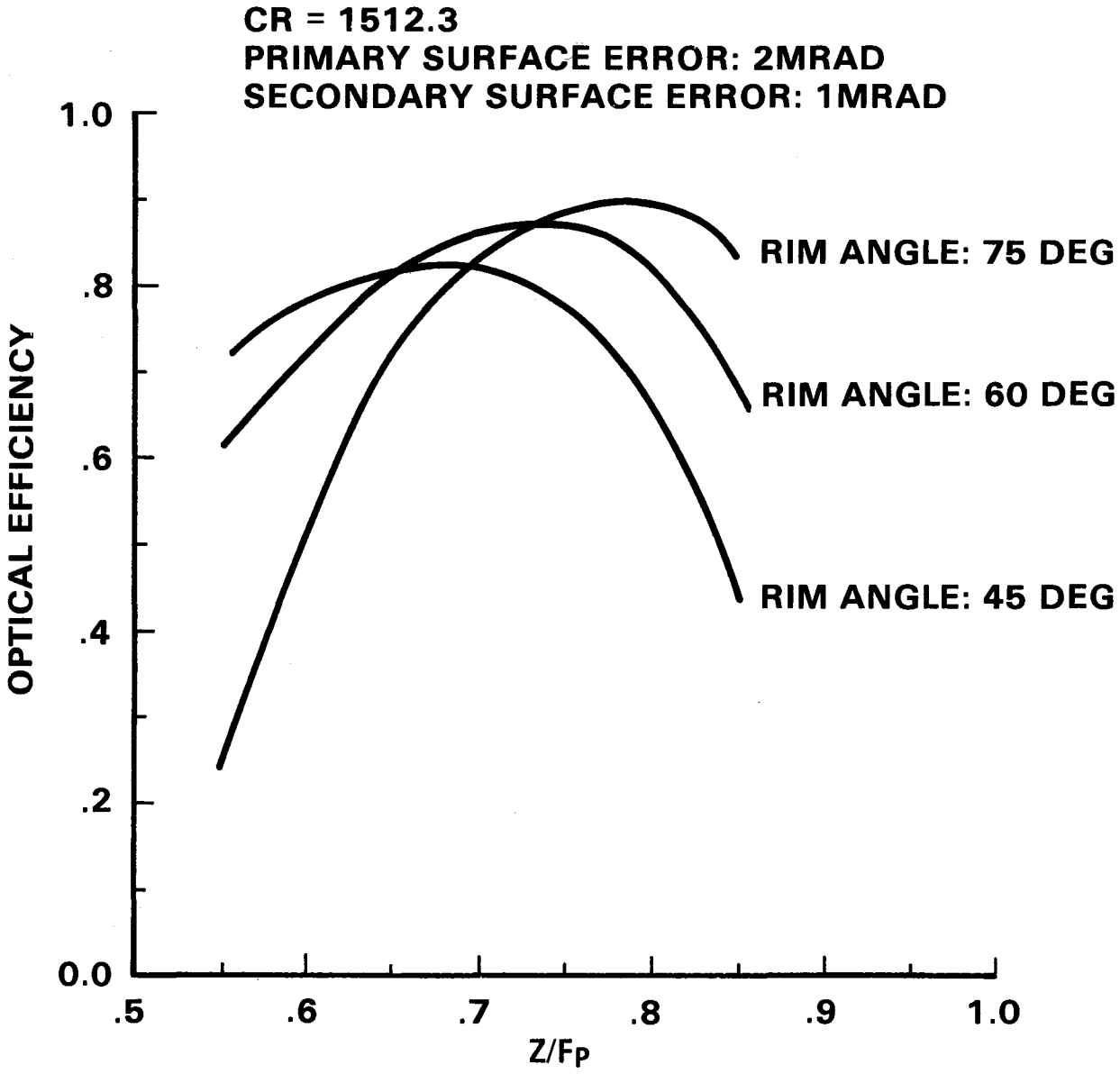

Figure II-8. Optical Efficiency Versus Z/F_P

Table II-2 lists the maximum efficiency point for various conditions of rim angle and slope error at concentration ratios of 1200 and 1500. Figures II-9 and II-10 show the maximum optical efficiency and corresponding intercept factor versus primary rim angle for σ_p = 2, 4, and 8 milliradians. As θ_R increases, reducing the primary focal length, it is possible to increase Z/F_p, and thus the magnification, keeping the system focal length relatively constant. However, as Z/F_p increases, r_s decreases, reducing the blocking factor which in turn increases the optical efficiency of the concentrator. Figure II-11 shows the blocking factor versus rim angle for the maximum efficiency points.

Slope errors on the secondary mirror do not significantly affect the performance of the system. This was analytically determined by Kirgizbaev (4), and has been verified here. Increasing σ_s from 1 to 8 mr decreased the efficiency by only 9 percent. Some anomalies in the data appear in the case of θ_R = 75, σ_p = 8 mrad. In this case, it appears that the system with σ_s = 2 has a higher efficiency than the system with σ_s = 1. This contradiction is due only to roundoff and the effect of a not quite uniform distribution generated by the random number generator. The values for the intercept factor at CR = 1200 to four decimal places are .5747 for σ_s = 1 and .5766 for σ_s = 2, within .002 of each other. The third decimal place is considered to be subject to variations caused by the random number generator, and so the accuracy of the results is considered to be about $\pm$.005. Using this accuracy criteria, the anomalous values discussed above are essentially equal.

2. Ritchey-Chretien

As with the standard Cassegrainian, the results from the COPS runs are in the form of four plots which are located in the appendix. The results are summarized in table II-3. Figures II-12 and II-13 show the optical efficiency and intercept factor as functions of the rim angle.

Comparing optical efficiency first, there is little difference between the Ritchey-Chretien and the standard Cassegrainian. At CR = 1200, the standard appears better by about 1 percent, but at CR = 1500, the Ritchey-Chretien regains that loss, so that η_{max} is the

TABLE II-2. MAXIMUM EFFICIENCY RESULTS FOR STANDARD CASSEGRAINIAN

Primary Rim Angle (θ_r)		45		60					75				
Primary Slope Error (σ_p)		2	4	2	4			8	2	4		8	
Secondary Slope Error (σ_s)		1	1	1	1	2	8	2	1	1	2	1	2
Z/F_p for Max Efficiency	CR = 1200	.70	.65	.75	.70	.7	.70	.65	.80	.75	.75	.70	.70
	CR = 1500	.70	.65	.75	.70	.70	.65	.65	.80	.75	.75	.70	.70
Max Efficiency (η_{max})	CR = 1200	.85	.71	.90	.77	.77	.72	.54	.92	.81	.81	.57	.58
	CR = 1500	.83	.66	.87	.73	.73	.68	.49	.90	.77	.77	.53	.53
IF_R at η_{max}	CR = 1200	.97	.86	.98	.72	.90	.85	.68	.96	.91	.91	.72	.73
	CR = 1500	.94	.80	.96	.86	.85	.85	.63	.98	.87	.87	.67	.67
Blocking Factor at η_{max}		.117	.172	.089	.143	.143	.143	.224	.063	.116	.116	.204	.20

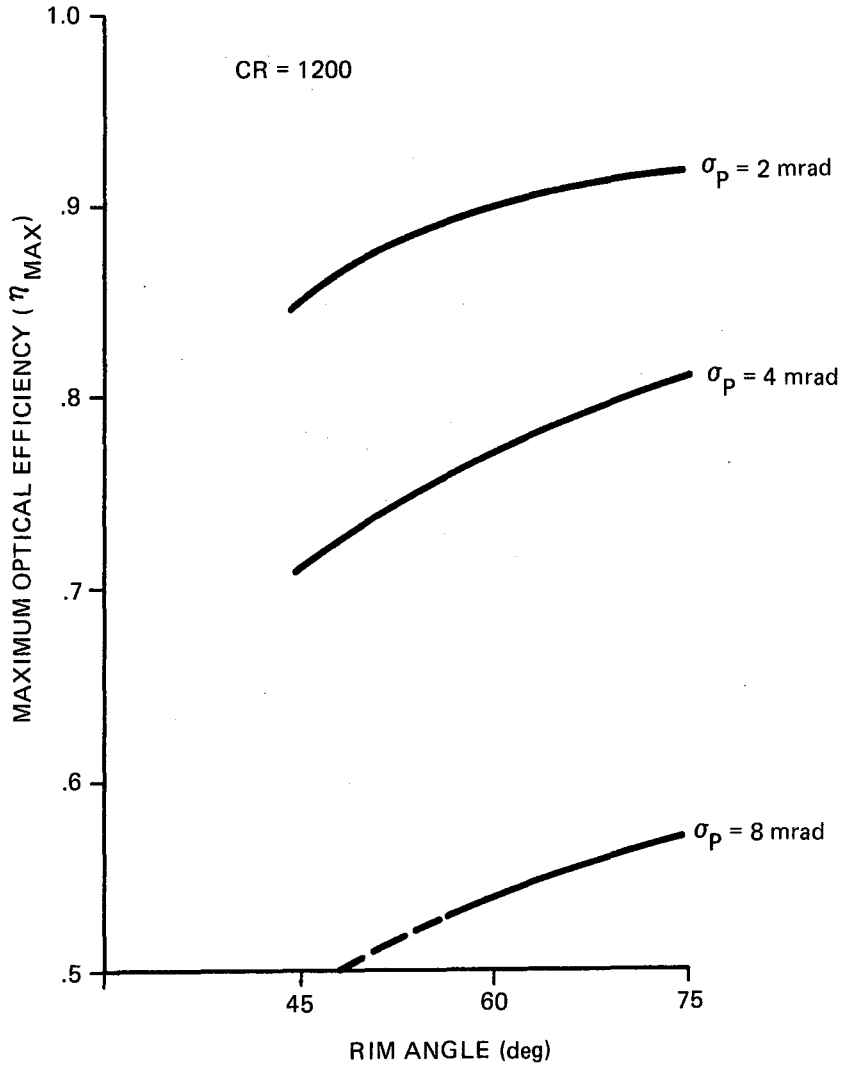

Figure II-9. Maximum Optical Efficiency Versus Rim Angle for the Standard Cassegrainian where σ_s = 2 mr

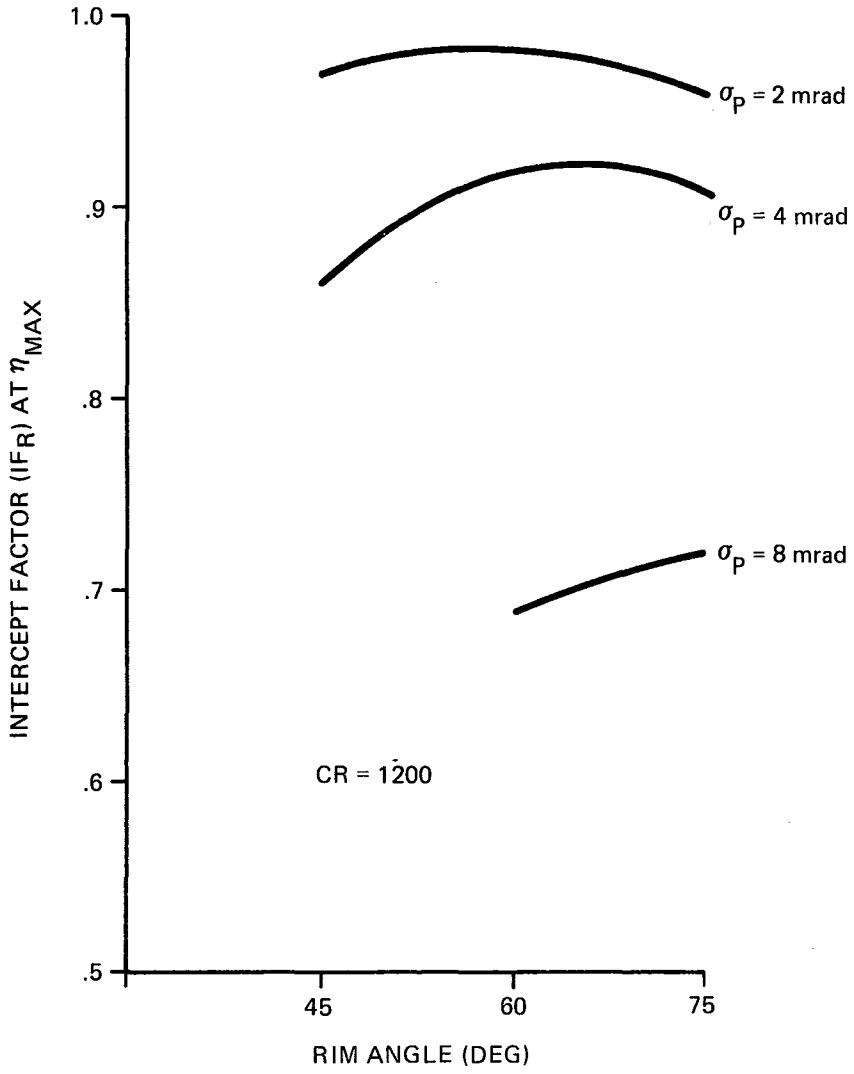

Figure II-10. Intercept Factor at Maximum Optical Efficiency for the Standard Cassegrainian where σ_s = 2 mr

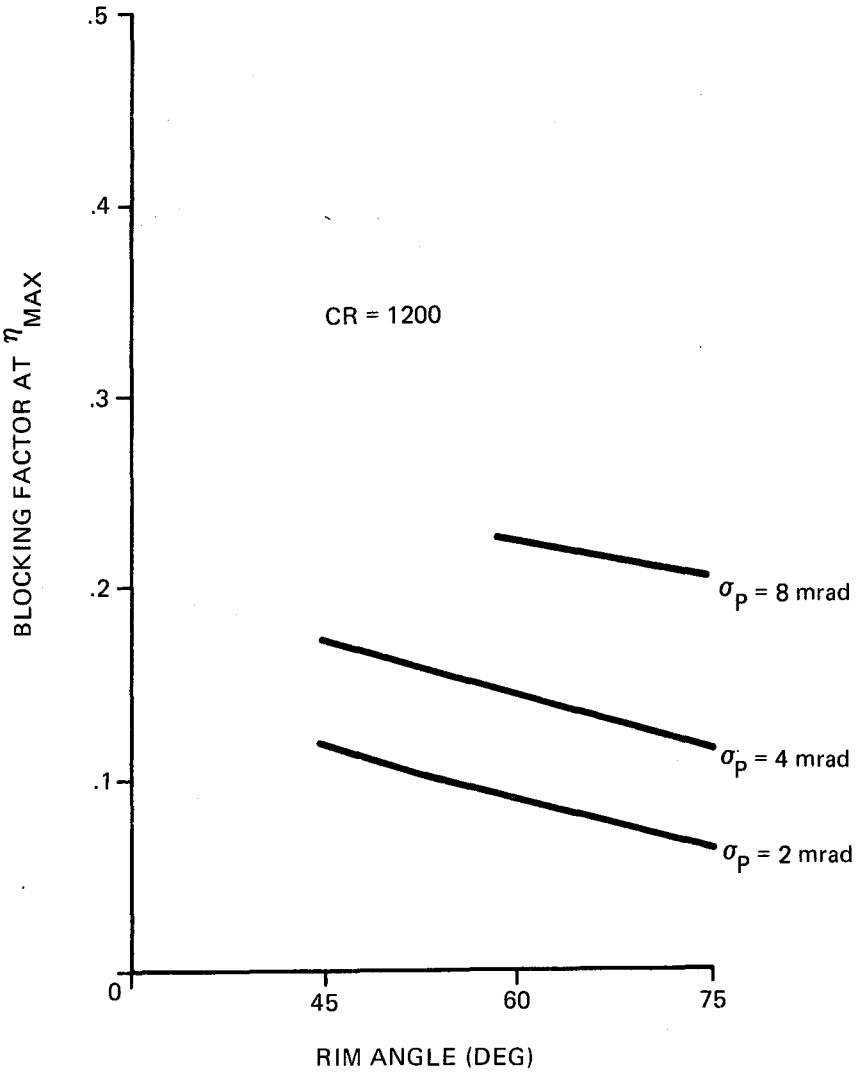

Figure II-11. Blocking Factor at Maximum Optical Efficiency for the Standard Cassegrainian where σ_s = 2 mr

TABLE II-3. MAXIMUM EFFICIENCY RESULTS FOR RITCHEY-CHRETIEN

Primary Rim Angle (θ_r)		60		75		
Primary Slope Error (σ_p)		2	4	4		8
Secondary Slope Error (σ_s)		1	2	1	2	1
Z/F_p for Max Efficiency	CR = 1200	.75	.70	.75	.75	.70
	CR = 1500	.75	.70	.75	.75	.70
Max Efficiency (η_{max})	CR = 1200	.89	.76	.81	.81	.56
	CR = 1500	.88	.73	.78	.77	.52
IF_R at η_{max}	CR = 1200	.98	.91	.93	.93	.74
	CR = 1500	.97	.87	.89	.89	.69
Blocking Factor at η_{max}		.098	.160	.131	.131	.246

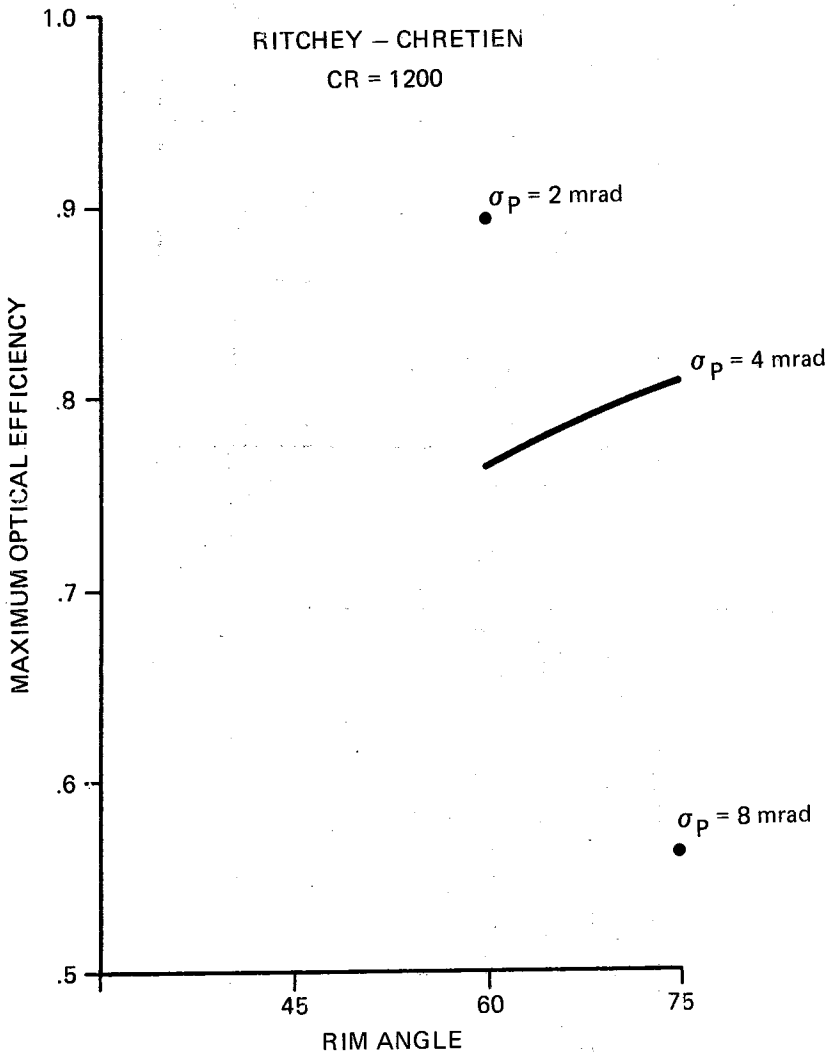

Figure II-12. Maximum Optical Efficiency for Ritchey-Chretien Versus Rim Angle where σ_S = 2 mr

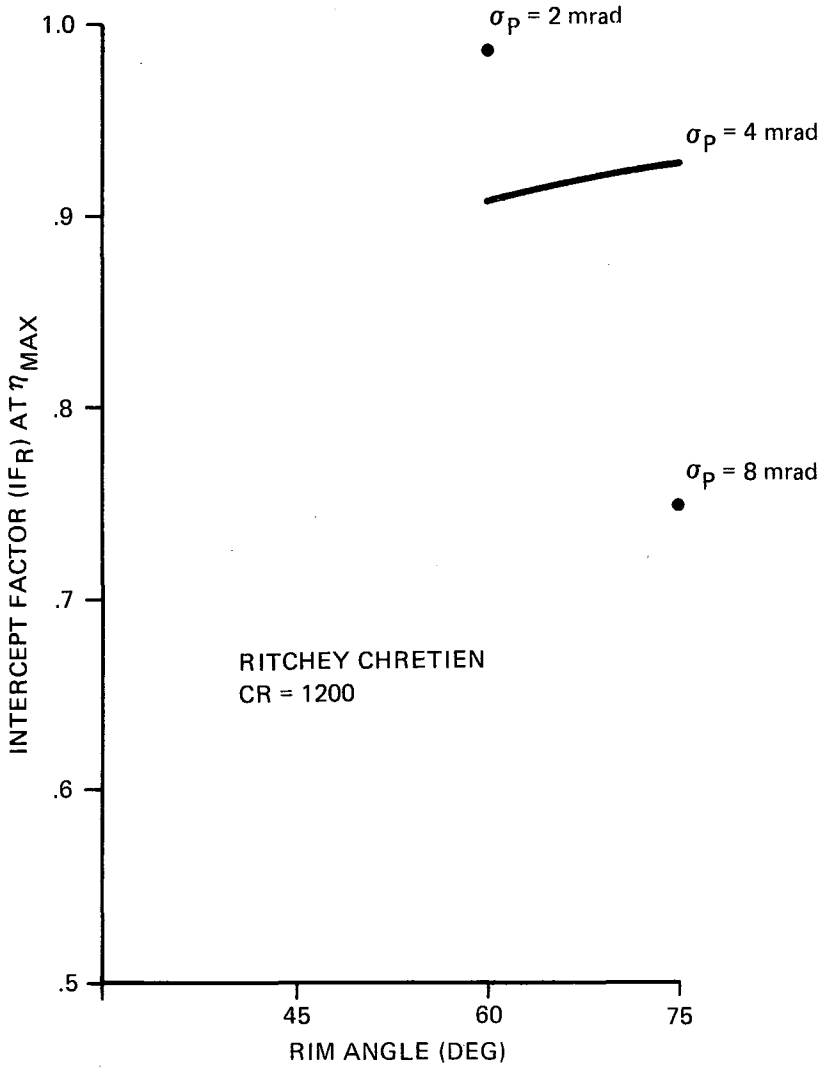

Figure II-13. Intercept Factor at Maximum Optical Efficiency for Ritchey-Chretien Versus Rim Angle where σ_S = 2 mr

same or slightly better. The intercept factor for the Ritchey-Chretien, however, is always higher than that for the standard Cassegrainian. This would be expected, since the Ritchey-Chretien has been corrected for optical aberrations which spread the beam. Since beam spread is less with the Ritchey-Chretien, the IF_R will be higher for a given CR.

The blocking factor, the final term used to calculate optical efficiency, is higher for the Ritchey-Chretien, since the primary focal length for it is slightly smaller than for the standard Cassegrainian, which results in a slightly larger secondary reflector for a given spacing Z/F_p. As before, the slope errors on the primary affect the concentrator performance much more than those on the secondary.

The general result of this comparison between the standard Cassegrainian and the Ritchey-Chretien is that IF_R increases when the Ritchey-Chretien is implemented, but the blocking also increases, resulting in little, if any improvement in optical efficiency. Figure II-14 shows a comparison of the intensity distribution at the receiver plane for the standard Cassegrainian and the Ritchey-Chretien. The profile for the Ritchey-Chretien is slightly more peaked than that for the standard Cassegrainian, due to the reduction in optical aberrations. However, the profile is still affected by optical aberrations and slope errors on the reflector surfaces. Much of the beam spread is caused by slope errors.

3. Cassegrainian with Tertiary Reflector

The third phase of the optical analysis integrated a tertiary reflector into the standard Cassegrainian. This configuration showed the greatest promise, and therefore a greater attempt at optimizing this design was made. There were several stages of this analysis. The first stage used the standard Cassegrainian as was used for the Cassegrainian only analysis. The virtual spot radius, F_H, was sized so that the tertiary would capture 97.5 percent and 99.5 percent of the total insolation reflected off of the secondary. The value of 97.5 percent was chosen since approximately 1.5 percent of the energy was absorbed by the tertiary itself, leaving 96 percent available for the receiver, which yielded the minimum required IF_R of .96. The value of 99.5 percent was

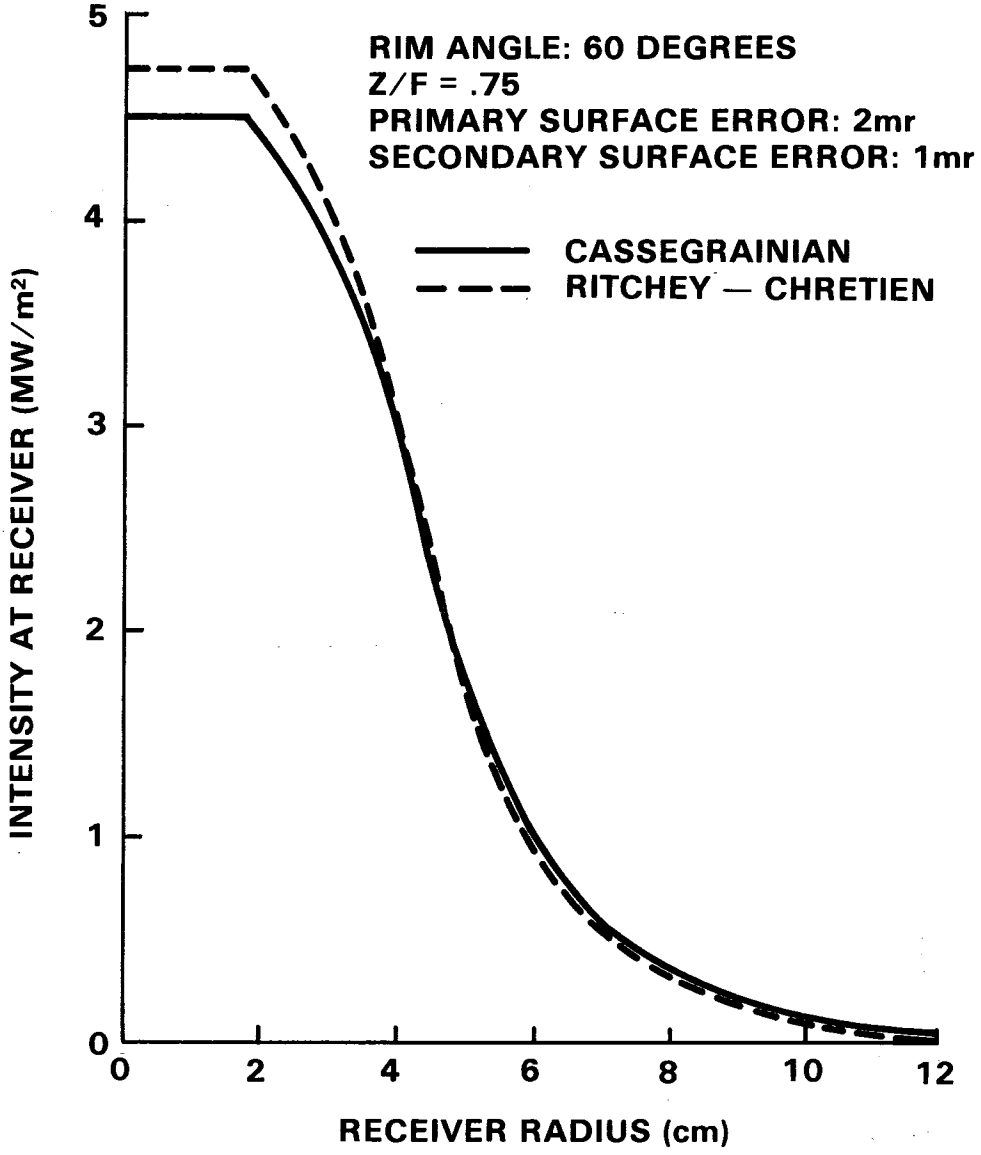

Figure II-14. Comparison of Intensity Distributions

chosen as being essentially equal to 100 percent. Since F_H was determined by assuming that the receiver plane energy distribution could be approximated by a normal distribution, 99.5 percent was chosen since it corresponds to $F_H = 2.81\sigma$, where σ is the standard deviation of the energy distribution at the focal plane. Above .995, the additional amount of energy capture requires an excessively large F_H.

The second stage of this analysis was similar to the first except that the radius of the secondary was reduced. It was observed that the outer rings of the secondary were intercepting very little insolation reflected from the primary, so that r_s could be reduced without sacrificing performance. A small amount of insolation would not be intercepted by the secondary, but this loss would be compensated for by the decreased blocking factor. Additionally, the "source" for the tertiary would be smaller, allowing steeper hyperbolic asymptotes which result from a higher CR or larger F_H.

The third stage of the tertiary analysis built on the second stage. The reduced secondary radius was used, and to further decrease the blocking factor, Z/F_D was increased. This final stage was where the tertiary was most useful, since as Z/F_D was increased, the beam spread became larger. The other difference between stages two and three was that the capture ratio was no longer set at .975 or .995. Instead, the desired CR was set to 1200 and F_H was made as large as possible without allowing the tertiary to block rays reflected from the primary. As was stated earlier, there is a maximum and minimum boundary for the height of the tertiary, Z_T, which is a function of F_H and the exit aperture. Since the exit aperture was set by CR=1200, Z_T is a function of F_H, and so the maximum F_H is limited by the Z_T which begins to block rays reflected from the primary mirror. Figure II-6 illustrates this relationship.

Stages one and two were performed with a primary rim angle of 60 degrees, since it was determined to be a good compromise between performance and primary reflector surface area. Later, it will be shown that this resulted in an optimum reflector effectiveness. Also, σ_p was set at 4 mrad. Stage 3 allowed variations of θ_R up to 90 degrees, to assess the relative changes in performance.

Table II-4 lists the results for stage one of the tertiary study. Optical efficiency and intercept factor are shown graphically in figures II-15 and II-16, respectively. As seen in figure II-15, the optical efficiency does not peak at a given Z/F_p for the range of Z/F_p considered. Rather, η_{max} increases with increasing Z/F_p up to 0.8. This is due to the beam spread having less effect on IF_R, since the beam is redirected to the desired receiver size. For example, when the capture ratio is set at .975, the intercept factor ranges from .97 to .95, while Z/F_p ranges from .65 to .80, and CR ranges from 1200 to 2200. Since IF_R and BF are the only terms used to define optical efficiency in this case, it is apparent that BF has the most effect on η.

It is important to recognize the difference between the capture ratio and intercept factor. The capture ratio is the ratio between the total energy reflected from the secondary towards the receiver compared to the energy that is not rejected from the tertiary. The intercept factor is the ratio of the total energy reflected from the secondary towards the receiver compared to the energy that is incident on the receiver. The capture ratio and intercept factor differ by the amount of energy that is absorbed by the tertiary. If the reflectivity of the tertiary was 100 percent, the capture ratio and intercept factor would be equal.

This effect of absorbtion by the tertiary can be seen in the plot of IF_R versus CR, figure II-16. As Z/F_p increases, the beam spread increases, and the tertiary acts on a larger percentage of the beam for a constant CR, increasing the amount of absorbtion and thereby reducing IF_R. Similarly, for a constant Z/F_p and increasing CR, the receiver aperture decreases so that the tertiary acts on more of the beam. This absorbed power is shown in table II-4 for a tertiary reflectivity of 0.95.

Figures II-17 and II-18 show the required tertiary height for a given CR and Z/F_p for capture ratios of .995 and .975. The dashed segments of the curves represent conditions where the tertiary would block some of the insolation reflected from the primary towards the secondary. This condition is not acceptable and was not analyzed beyond what is shown in the figures.

TABLE II-4. CASSEGRAINIAN WITH TERTIARY RESULTS

Cassegrainian Plus Tertiary
(Full Size Secondary)

CR	Z/F_p	r_s (m)	Rim Angle: 60° σ_p = 4 mr σ_s = 3 mr $\rho_p = \rho_s$ = 1.0 Capture Ratio: .995 Z_T (m)	IF_R --	η -	Q_{abs}* (kW)	Q_r** (kW)	Capture Ratio: .975 Z_T (m)	IF_R --	η -	Q_{abs} (kW)	Q_r (kW)
1200	.65	1.585	.45	.99	.79	.11	30.4	.08	.97	.77	.10	29.8
1500	.65	1.585	1.09	.99	.79	.18	30.4	.18	.97	.77	.18	29.7
2200	.65	1.585	--	--	--	--	--	.68	.96	.77	.37	29.6
1200	.70	1.322	.72	.99	.84	.23	32.4	.20	.97	.82	.25	31.7
1450	.70	1.322	1.23	.99	.84	.32	32.4	---------- not analyzed ----------				
1500	.70	1.322	--	--	--	--	--	.36	.96	.82	.37	31.6
2200	.70	1.322	--	--	--	--	--	.97	.96	.82	.63	31.4
1200	.75	1.085	1.20	.98	.89	.44	34.2	.47	.97	.87	.50	33.6
1500	.75	1.085	--	--	--	--	--	.70	.96	.87	.64	33.5
1990	.75	1.085	--	--	--	--	--	1.24	.96	.86	.89	33.2
1200	.80	0.866	--	--	--	--	--	.88	.96	.90	.89	34.6
1475	.80	0.866	--	--	--	--	--	1.16	.95	.89	1.09	34.4

* Power absorbed by the tertiary with ρ_T = 0.95

** Power incident on the receiver aperture

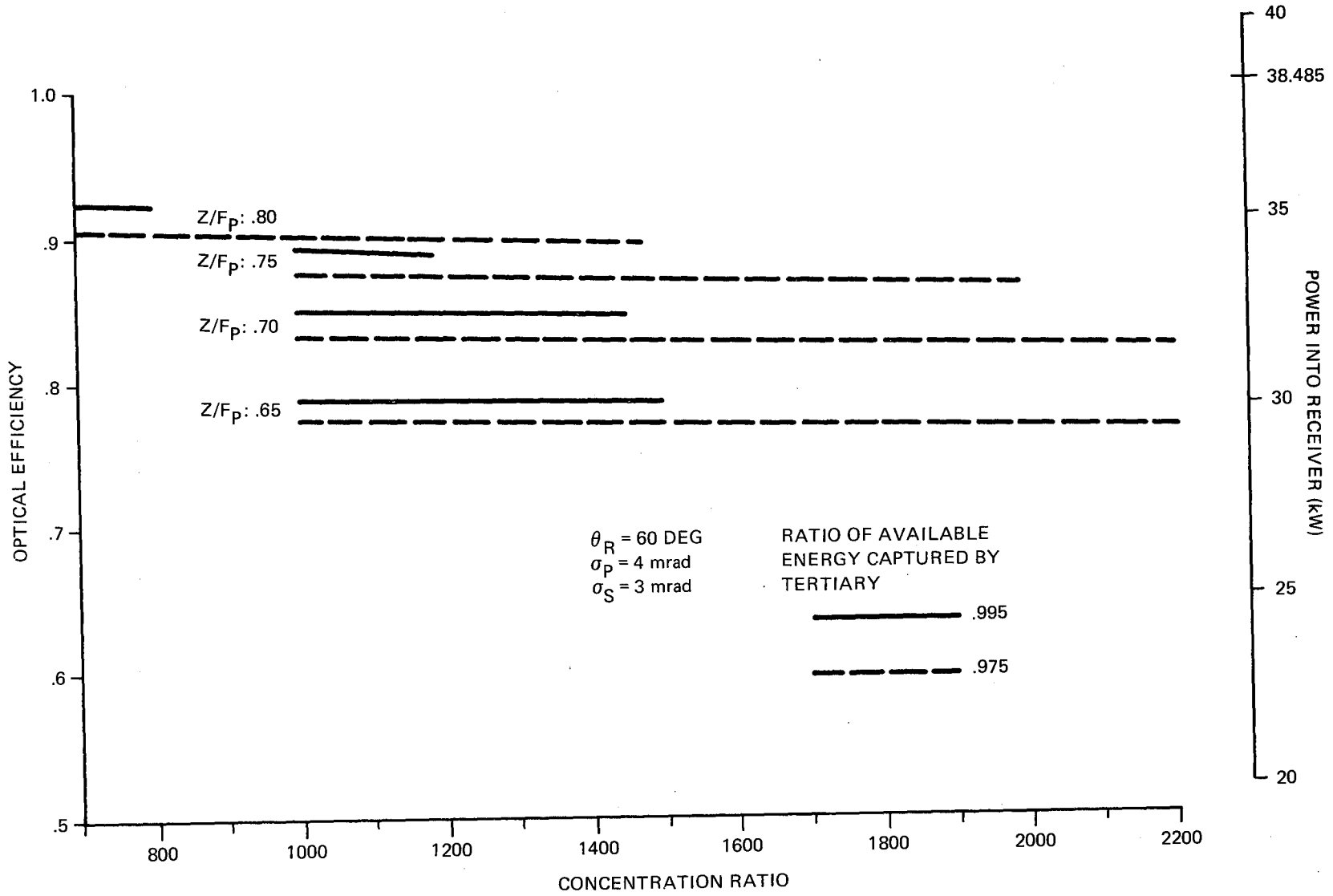

Figure II-15. Optical Efficiency and Power Delivered to the Receiver Versus Concentration Ratio for Cassegrainian System with Tertiary Reflection

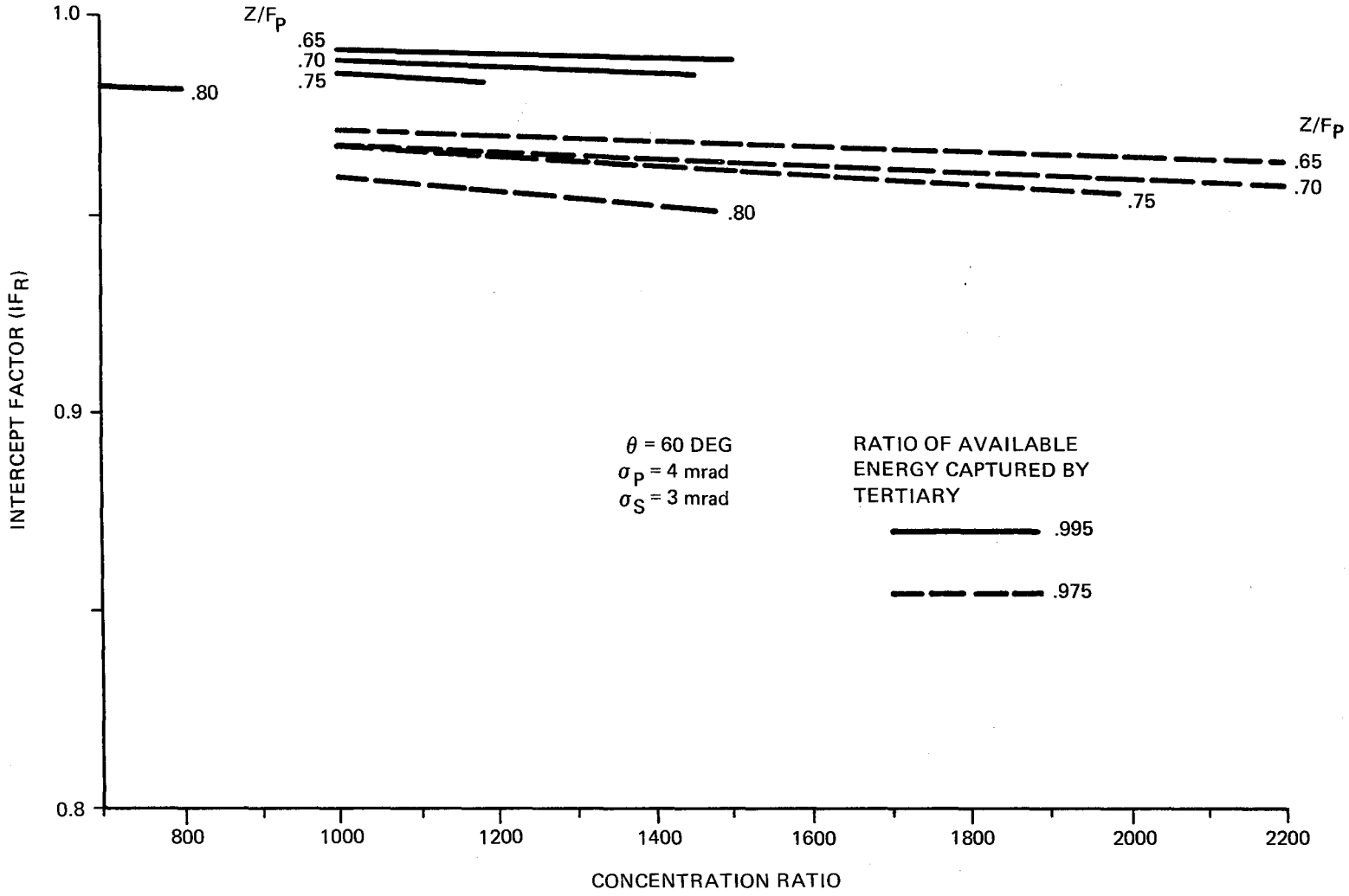

Figure II-16. Intercept Factor Versus Concentration Ratio for Cassegrainian System with Tertiary Reflector

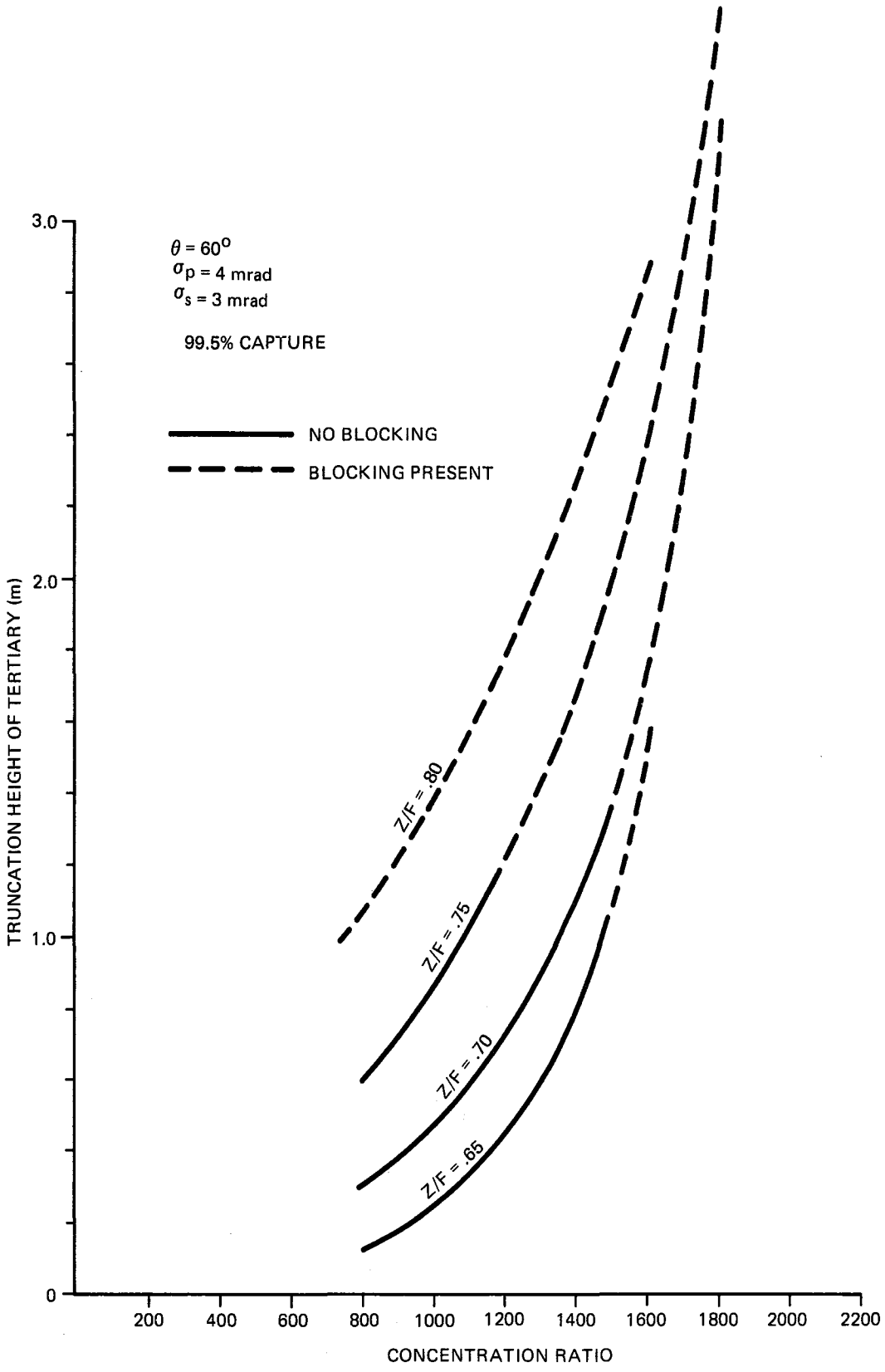

Figure II-17. Tertiary Height Versus CR for Capture = .995

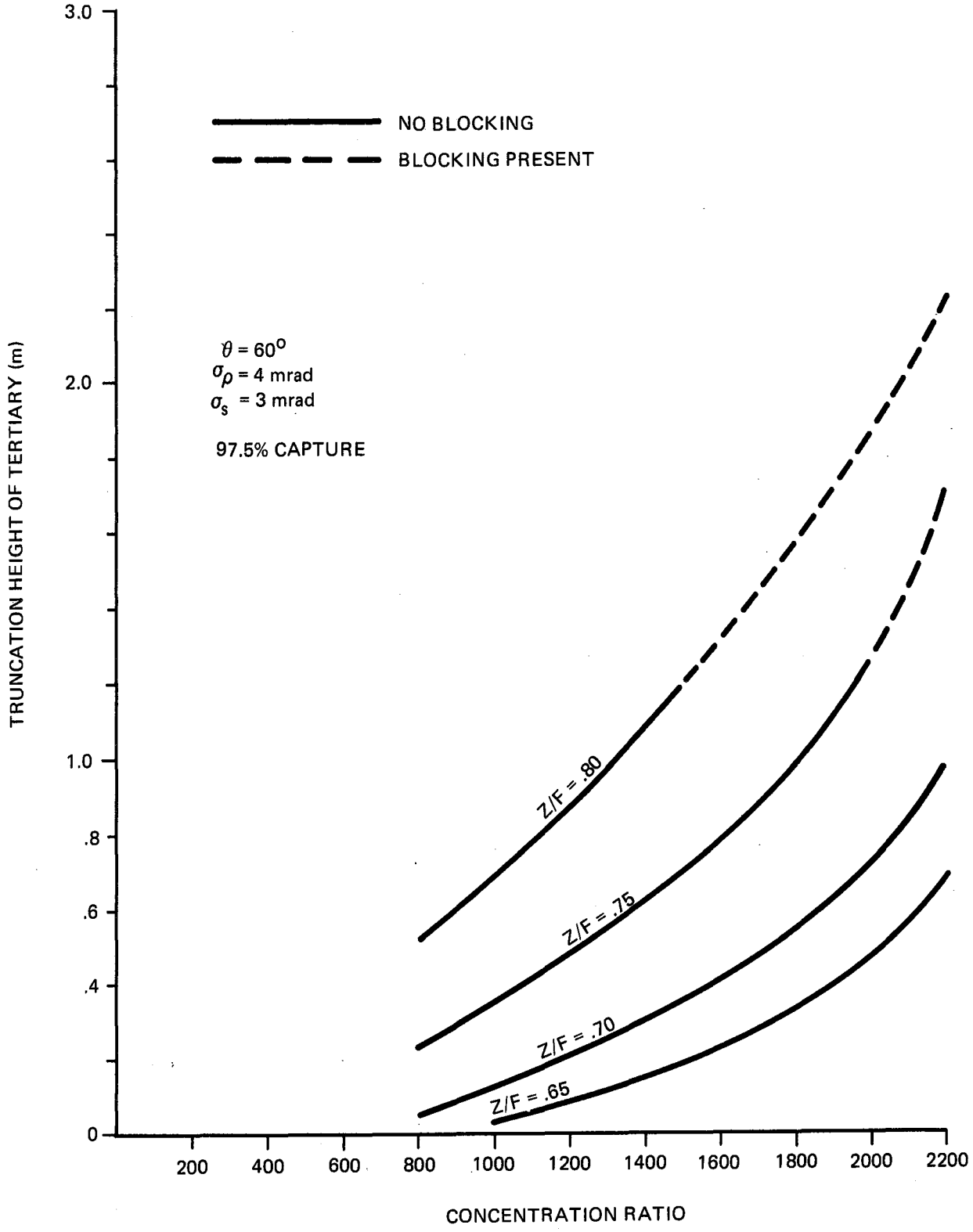

Figure II-18. Tertiary Height Versus CR for Capture = .975

As the capture ratio decreases, and therefore F_H, the required tertiary height decreases. This fact illustrates one trade-off present in the implementation of the tertiary: as the capture ratio and/or CR increases, the size of the teriary also increases. Depending on fabrication requirements, it might be more advantageous to decrease the capture ratio to reduce the cost of the tertiary.

Comparing the optical performance of the standard Cassegrainian with the Cassegrainian plus tertiary, a significant improvement is apparent. The maximum efficiency for the standard Cassegrainian is .77 at $\theta_R = 60^o$, σ_p = 4 mrad at CR = 1200. For the tertiary, η_{max} = .90 at σ_p = 4 mrad, a 17 percent improvement. At CR = 1500, η_{max} = .73 at $\theta_R = 60^o$ for the standard Cassegrainian, and .87 for the tertiary, a 19 percent improvement.

Stage two of the tertiary analysis involved reducing the radius of the secondary reflector. Table II-5 lists the results of this exercise. Reducing r_s reduces the required tertiary height for a given CR and capture ratio, or allows a higher CR. A general reduction in required material was achieved in this stage with a small increase in performance.

TABLE II-5. CASSEGRAINIAN WITH TERTIARY RESULTS - REDUCED SECONDARY

RIM ANGLE: 60° σ_p= 4 mr σ_S= 3 mr $\rho_p = \rho_S$ = 1.0

CR	Z/F$_P$	r$_S$ (m)	CAPTURE RATIO: .995					CAPTURE RATIO: .975				
			Z$_T$ (m)	IF$_R$	η	Q$_{ABS}$ (kW)	Q$_r$ (kW)	Z$_T$ (m)	IF$_R$	η	Q$_{ABS}$* (kw)	Q$_r$** (kw)
1200	.75	.98	.99	.98	.89	.41	34.4	.42	.97	.88	.66	33.7
1300	.75	.98	1.14	.98	.89	.46	34.4	NOT ANALYZED				
1500	.75	.98	-	-	-	-	-	.60	.96	.87	.61	33.6
2200	.75	.98	-	-	-	-	-	1.18	.96	.87	.96	33.3
1500	.80	.82	-	-	-	-	-	1.09	.95	.90	1.07	34.7

* POWER ABSORBED BY THE TERTIARY WITH ρ_τ = 0.95
** POWER INCIDENT ON THE RECEIVER APERTURE

4. Misalignment Effects

During stage two, questions were raised about the effects of misalignment of the reflectors; consequently, a study was done to determine the magnitude of these effects. The three modes of reflector misalignment studied were axial, radial, and rotational. The secondary reflector is the most sensitive to misalignment, and most likely to be misaligned; consequently, most of the misalignment study focused on the secondary. Due to placement of the tertiary directly above the focal plane, radial and axial misalignment were considered unlikely. Rotational misalignment was considered a possibility but was not critical for the following reasons. Since the "target" for the beam is the circle defined by F_H, the area of the target will only be reduced by the cosine of the misalignment angle of the tertiary thus producing a negligible increase in the amount of the beam that is outside of the target circle. However, as the tertiary is rotated, one side of its rim will be less likely to intercept the edge of the beam, but since the beam intensity is of approximately normal distribution, the power at the edge of the beam is low, and the fraction of the total power that is not intercepted is relatively small. Analyses were made at misalignments of 1, 2, and 4 degrees, and in all cases the percentage of lost power was less than .2 percent.

The entire secondary misalignment study was performed for a rim angle of 60 degrees $Z/F_p = .75$, $\sigma_p = 4$ mrad, and CR = 1600, but the results are generally applicable for other configurations. Figure II-19 shows the misalignment geometry.

There are four loss mechanisms present in the Cassegrainian plus tertiary configuration which are affected by misalignment of the secondary. These are as follows:

(1) Insolation not intercepted by the secondary,
(2) Insolation not intercepted by the tertiary,
(3) Insolation rejected by the tertiary,
(4) Insolation absorbed by the tertiary.

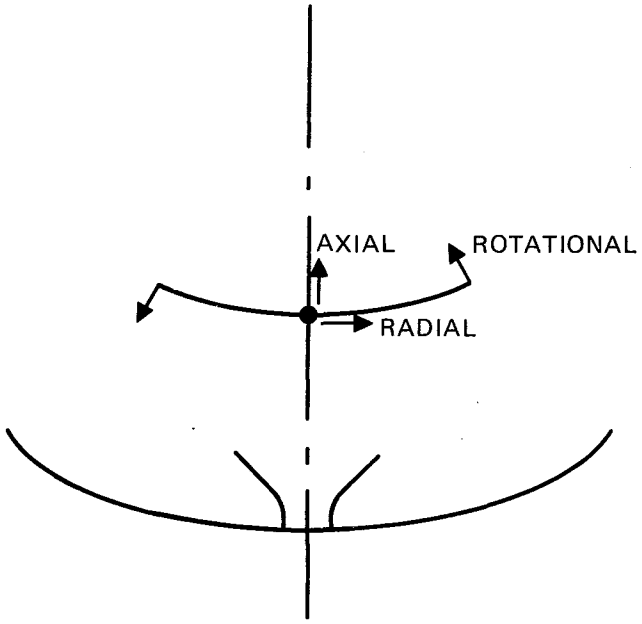

Figure II-19. Modes of Misalignment

These loss mechanisms have been plotted as a fraction of the total insolation intercepted by the primary aperture as a function of each of the misalignment modes in figures II-20 through II-22. Consider axial alignment first. As the secondary reflector is moved in the positive direction, i.e., up, the percentage of the beam that is not intercepted by the secondary decreases, since the radius of the beam impinging on the secondary is decreasing. Also, the focal point, i.e. "waist" of the beam is moving up, causing the focal plane of the system to "see" a larger diameter portion of the beam. This effect is shown in figure II-23, with the tertiary deleted for clarity. Since the tertiary will capture only that portion of the beam within the radius F_H, more of the beam will be rejected than when the waist of the beam is at Z=0, the system focal plane. Also, more absorption will occur, since the tertiary is acting on a larger portion of the beam. As the secondary is moved down, i.e. negative misalignment occurs, the effects are similar, except that a larger portion of the beam is not intercepted by the secondary.

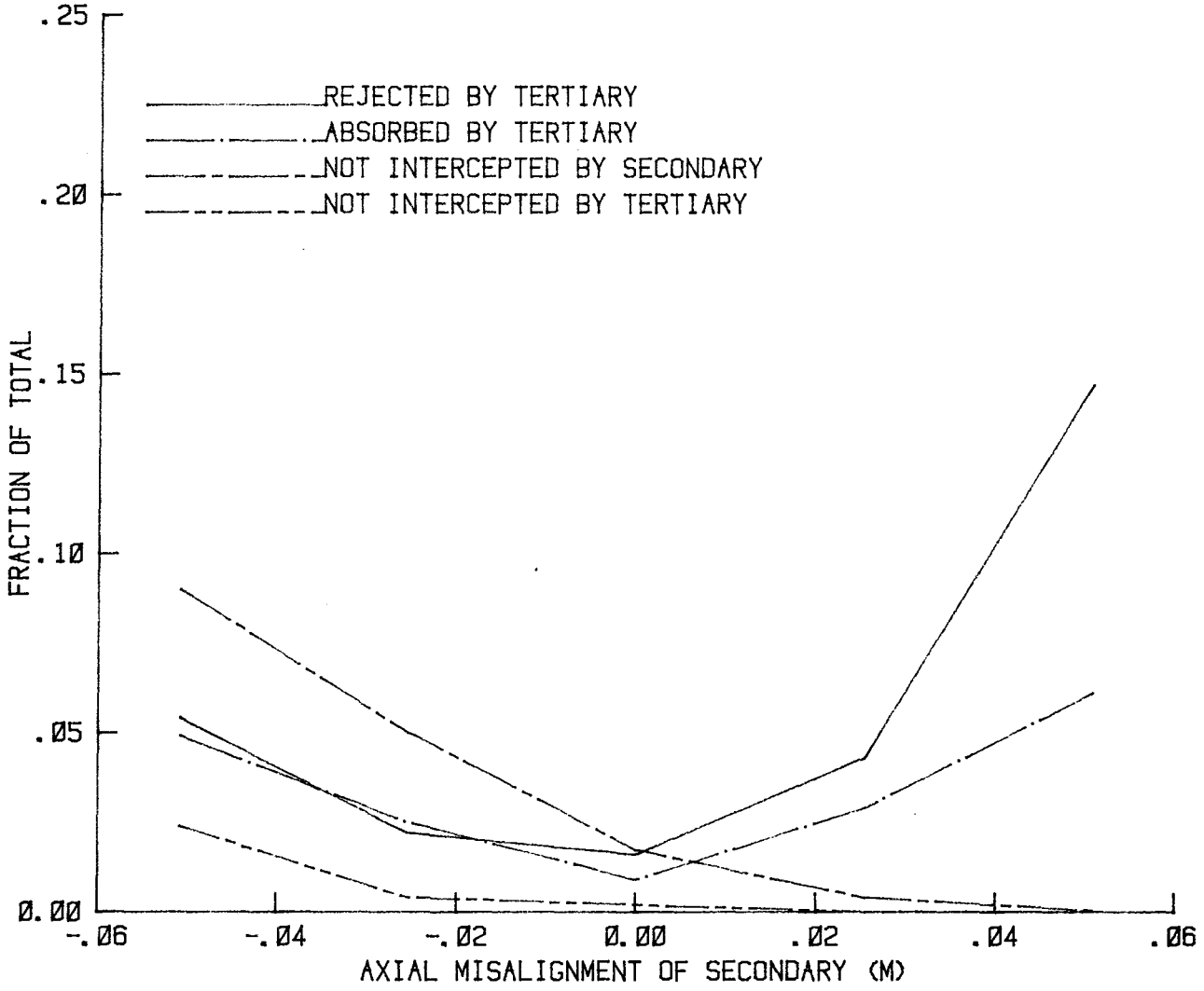

Figure II-20. Effects of Axial Misalignment

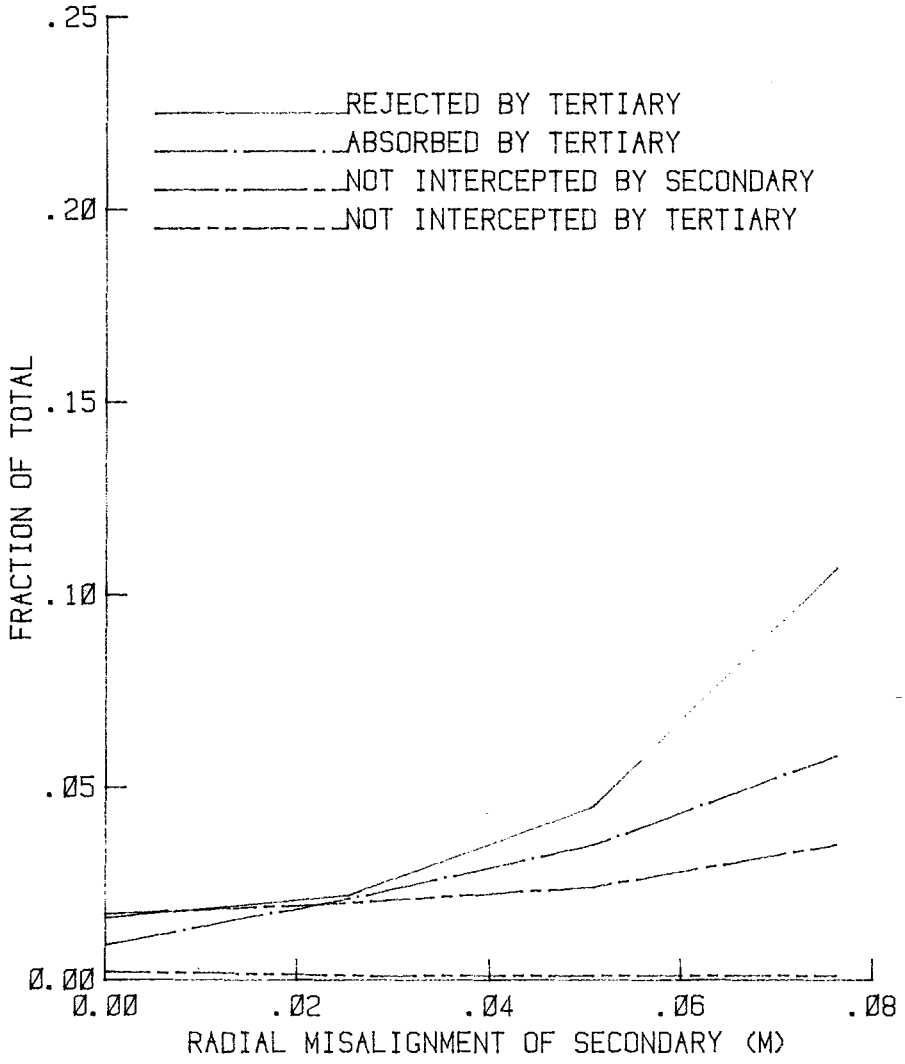

Figure II-21. Effects of Radial Misalignment

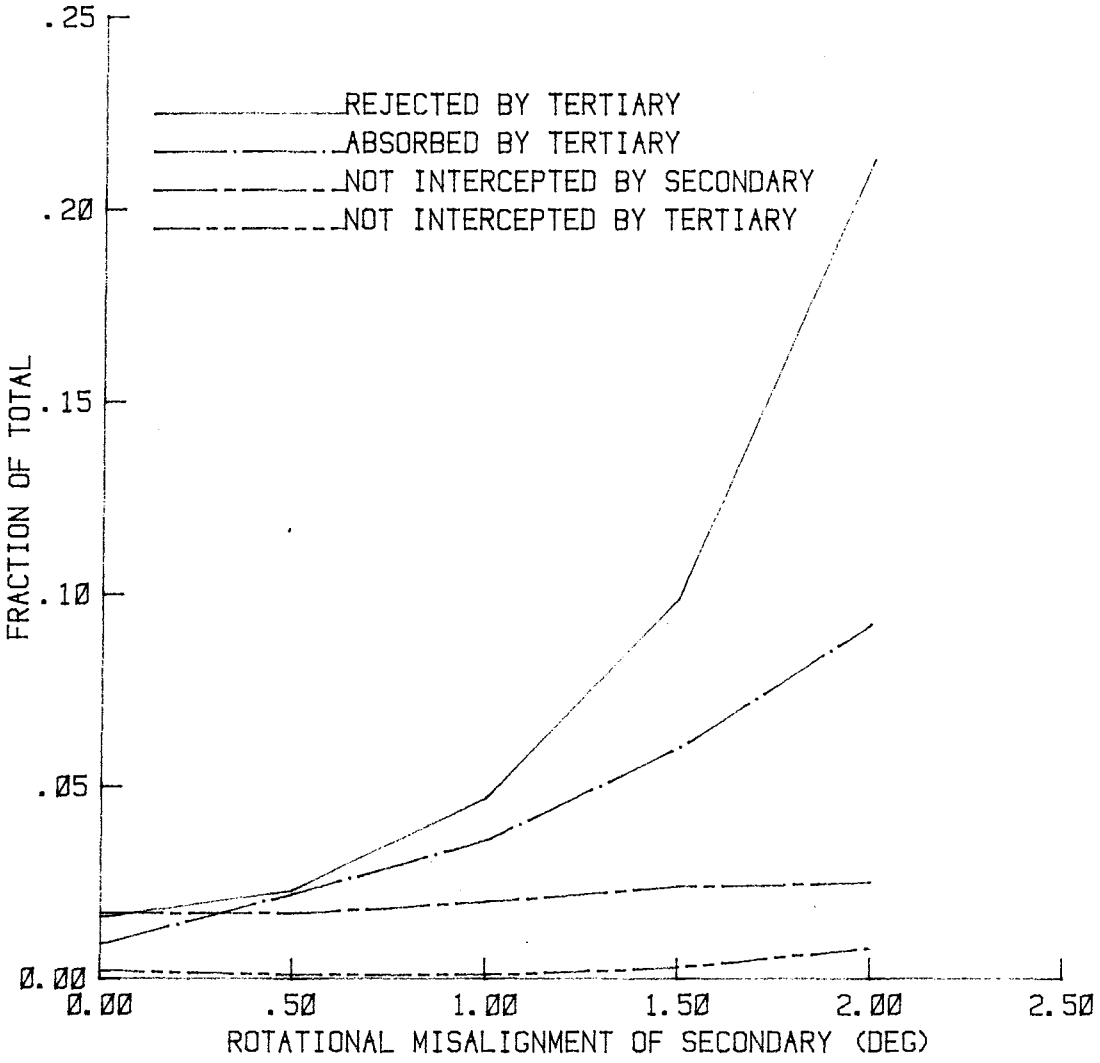

Figure II-22. Effects of Rotational Misalignment

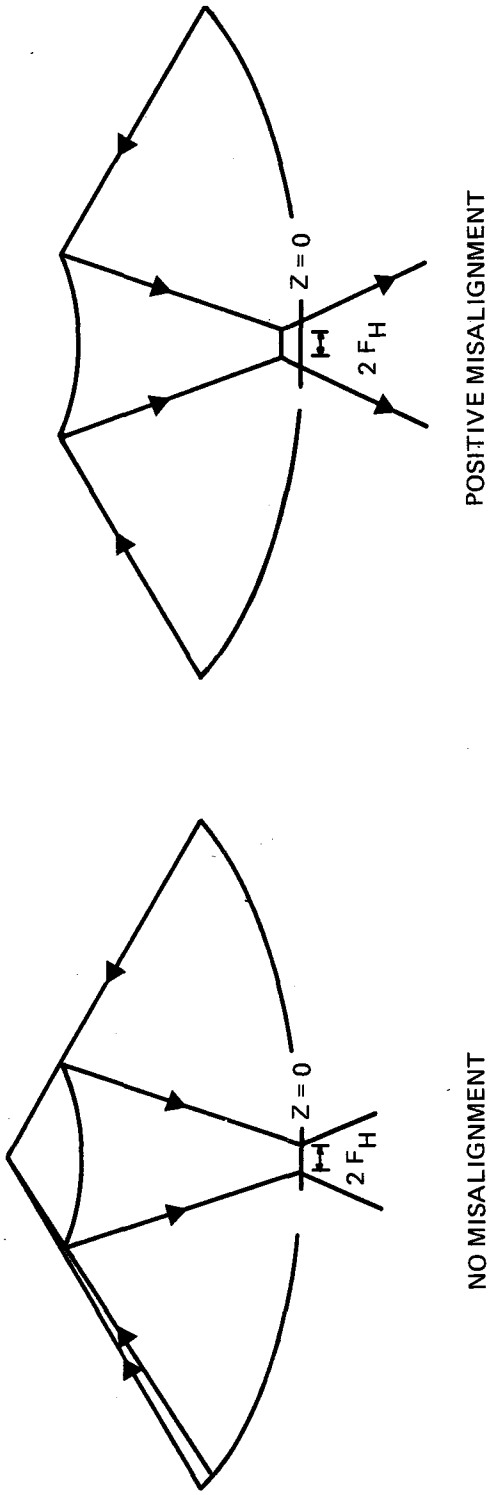

Figure II-23. Schematic of Positive Axial Misalignment Effects

Radial and rotational misalignment are similar to each other. The beam tends to be deflected from the optical axis, moving the waist of the beam radially. The effect of this is that more of the beam is outside the radius F_H, and is therefore rejected or absorbed by the tertiary. Of the three misalignment modes, the system is most sensitive to rotational misalignment, as expected.

Figures II-24 through II-29 have combined the three misalignment modes to display their effects on intercept factor and optical efficiency. The combination of different misalignments has a synergistic effect so that some tolerance on all three must be set. There are many variables that need to be known before a true tolerance may be set, but a rough tolerance could be set by allowing the performance of the Cassegrainian with tertiary in misalignment to be no worse than the standard Cassegrainian. This sets the minimum optical efficiency at 0.77. With this criterion, the maximum combined misalignment of the secondary is:

Radial:	.0254 m
Axial:	$\pm$.0254 m
Rotational:	.5 deg.

This criterion is somewhat arbitrary and would need to be reexamined in a final design, however, it does give a general idea of the magnitude of the tolerance required.

5. Final Variation of Parameters for Cassegrainian with Tertiary

Stage three of the tertiary analysis returned to a perfectly aligned system. This stage had as its goal to maximize the optical efficiency of the system at CR = 1200. The primary rim angle was allowed to vary up to 90 degrees, and the secondary radius was varied to optimize between the blocking factor and interception of insolation reflected from the primary. F_H was increased to maximize IF_R. In all cases the tertiary was sized to avoid any blocking of rays reflected from the primary. Tables II-6 and II-7 list the results from the configurations analyzed.

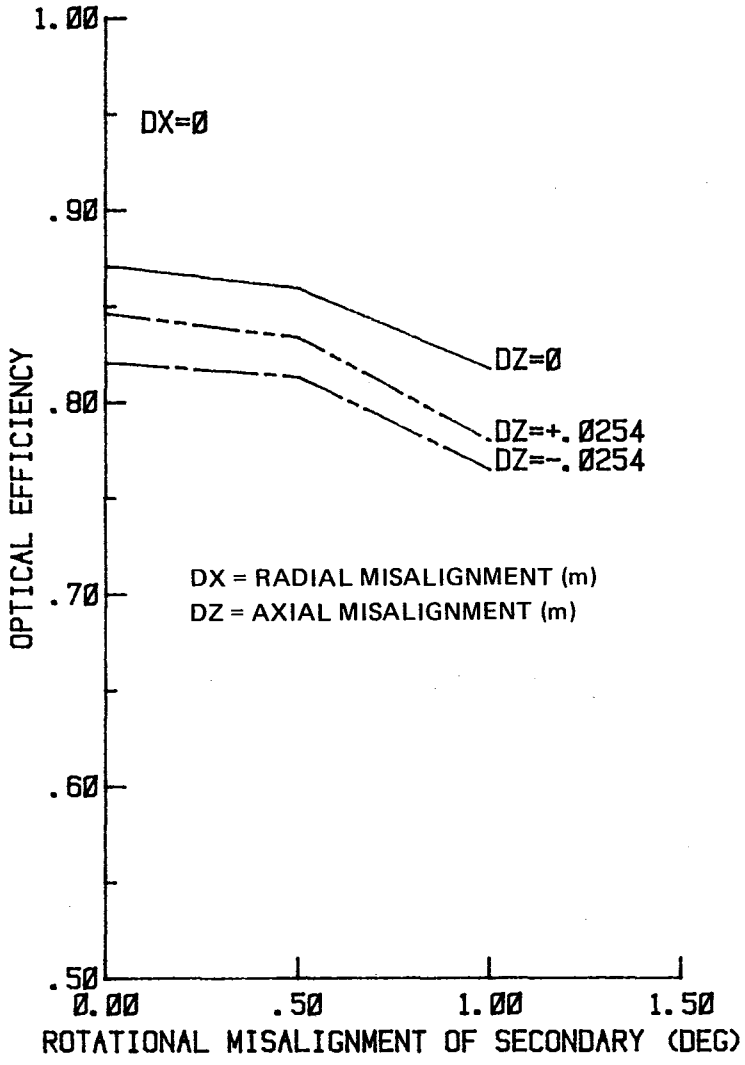

Figure II-24. Optical Efficiency Versus Combined Misalignment

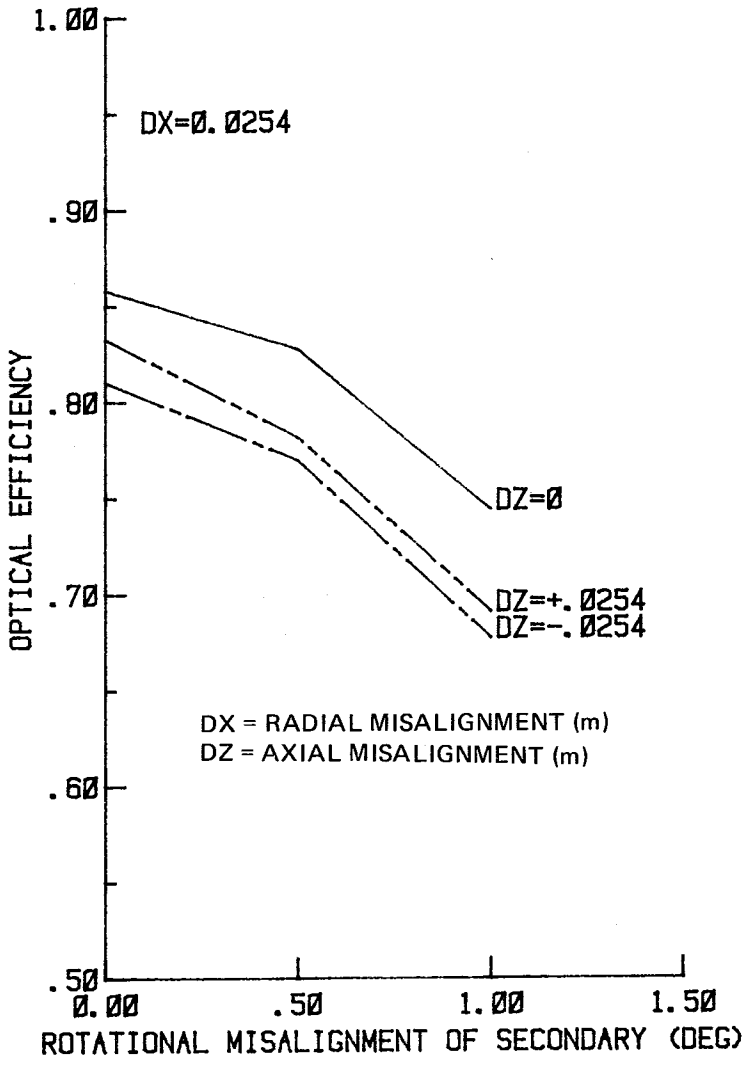

Figure II-25. Optical Efficiency Versus Combined Misalignment

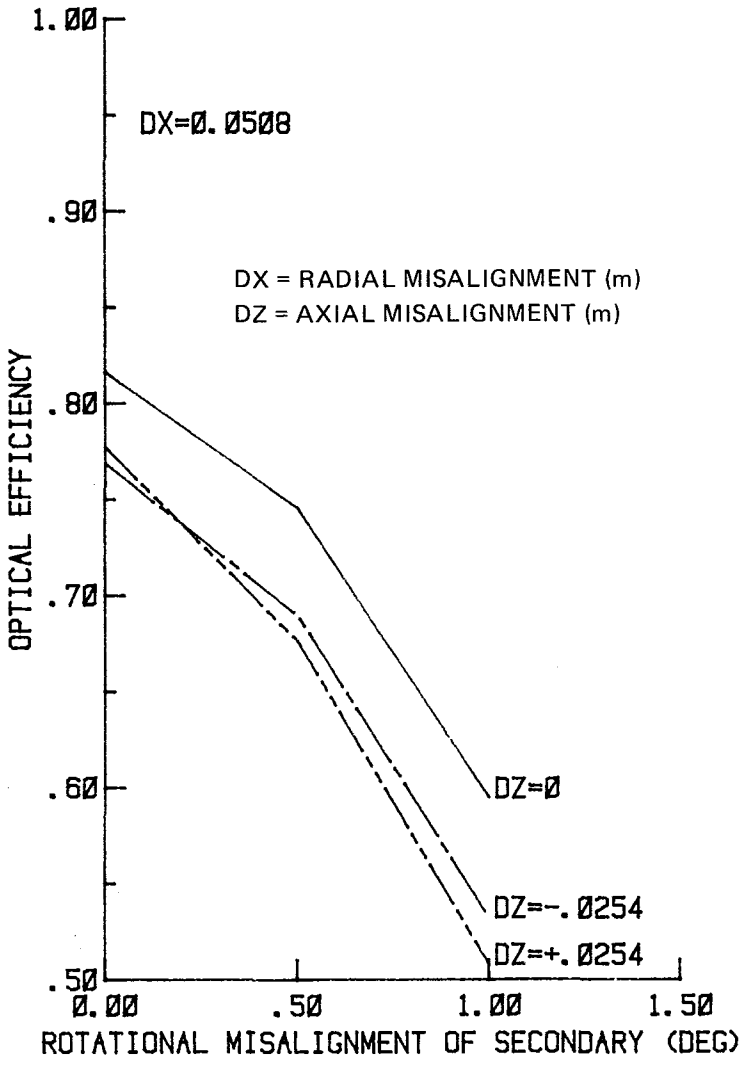

Figure II-26. Optical Efficiency Versus Combined Misalignment

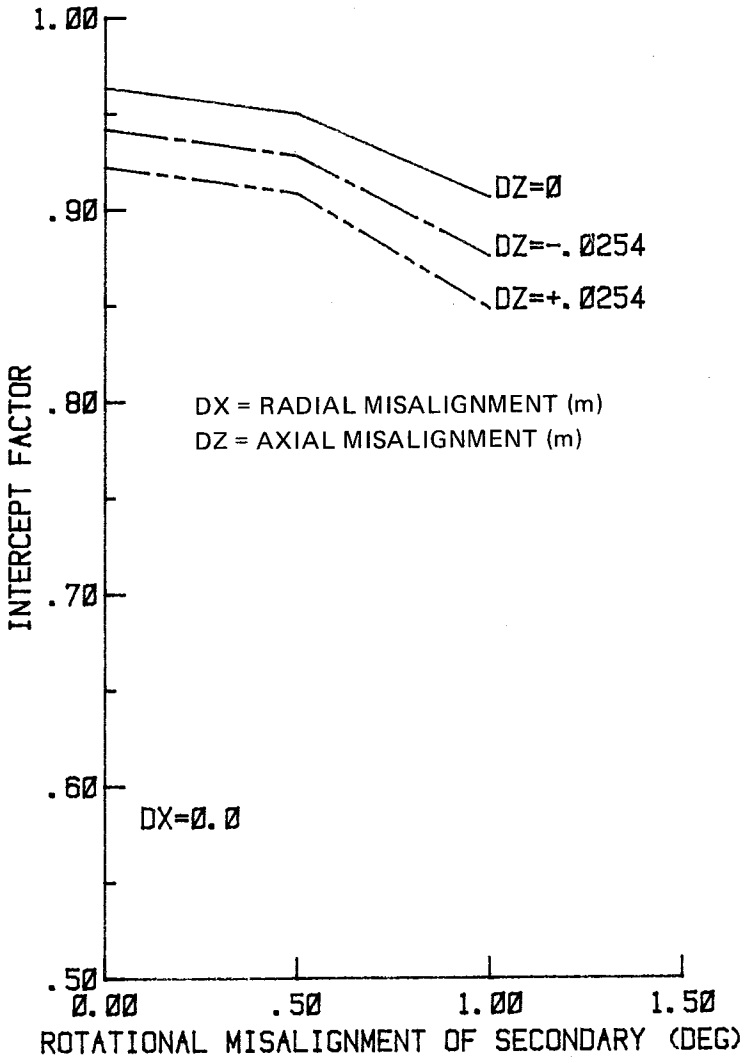

Figure II-27. Intercept Factor Versus Combined Misalignment

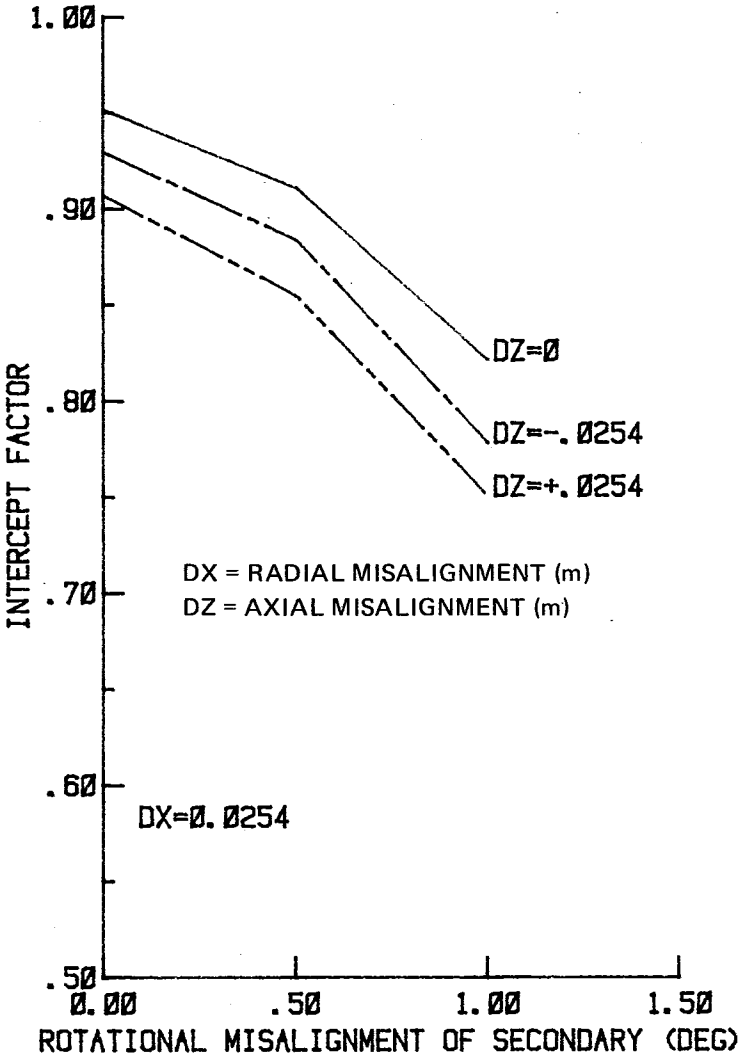

Figure II-28. Intercept Factor Versus Combined Misalignment

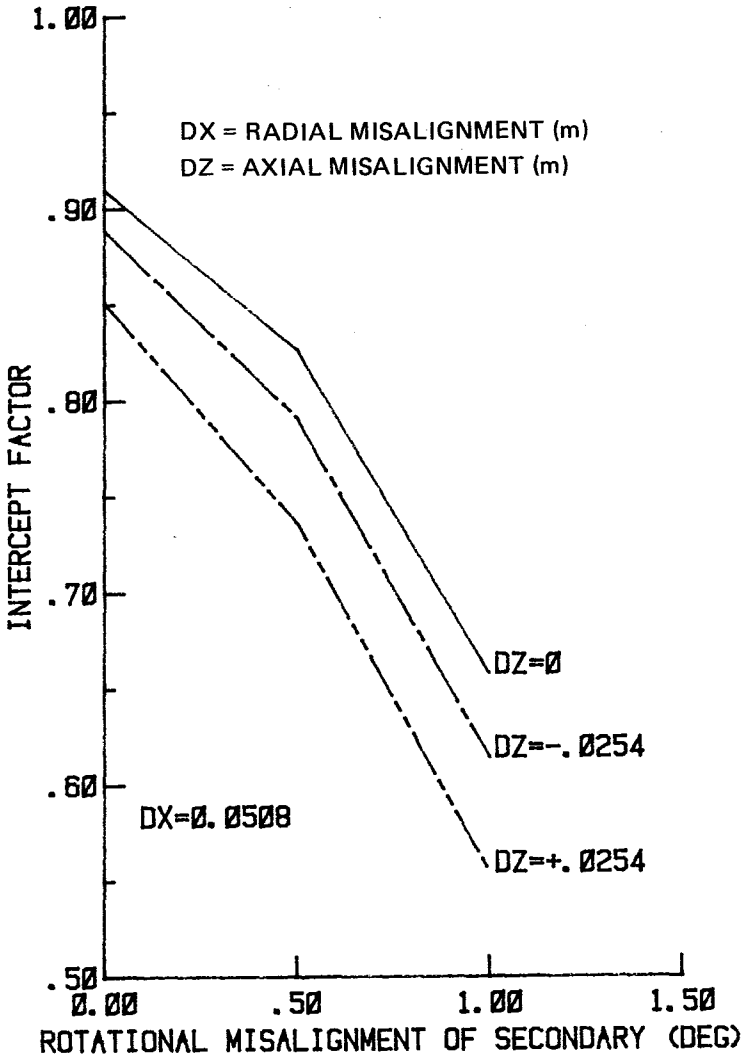

Figure II-29. Intercept Factor Versus Combined Misalignment

TABLE II-6. RESULTS OF OPTIMIZED RIM ANGLE AND Z/F_p, $\theta_R = 60^o$

Cassegrainian Plus Tertiary $\theta_R = 60^o$ CR = 1200

Z/F_p	σ_p (mrad)	σ_s (mrad)	r_s (m)	BF	IF_s	Z_T (m)	θ_a*	F_H (m)	η_o	IF_R
.75	4	4	1.00	.082	.995	1.167	26.55	.226	.903	.984
.79	4	4	0.84	.058	.998	1.112	23.94	.249	.917	.973
.80	4	2	0.82	.055	.9995	1.058	23.93	.249	.916	.967
.81	4	3	0.80	.052	1.000	0.793	26.06	.230	.897	.945
.81	4	4	0.80	.052	1.000	0.902	24.90	.240	.902	.951
.81	4	4	0.77	.048	0.9995	1.079	22.96	.259	.913	.960
.82	4	3	0.74	.045	0.9998	1.028	22.87	.260	.908	.952
.82	4	8	0.74	.045	0.9997	1.028	22.87	.260	.905	.945
.82	4	8	0.74	.045	0.9997	1.061	22.59	.263	.906	.946
.85	4	4	0.60	.029	0.9986	0.948	21.56	.275	.886	.914

* Asymptotic angle of the tertiary

TABLE II-7. RESULTS OF OPTIMIZED RIM ANGLE AND Z/F_p, $\theta_R = 75^o, 90^o$

Z/F_p	σ_p (mrad)	σ_s (mrad)	r_s (m)	BF	IF_s	Z_T (m)	θ_a*	F_H (m)	η_o	IF_R
				Cassegrainian Plus Tertiary			$\theta_R = 75^o$, CR = 1200			
.83	4	3	.73	.044	.9996	0.688	28.10	.2145	.922	.965
.83	4	4	.73	.044	.9996	0.869	23.94	.231	.930	.973
.84	4	3	.68	.038	.9997	0.778	26.06	.230	.925	.962
.84	4	4	.68	.038	.9997	0.839	25.35	.236	.928	.965
.85	4	4	.55	.025	.9996	0.744	24.04	.248	.902	.925
				Cassegrainian Plus Tertiary			$\theta_R = 90^o$, CR = 1200			
.85	4	2	.656	.035	.993	0.396	34.15	.180	.927	.965
.85	4	2	.656	.035	.993	0.566	30.34	.200	.936	.975
.85	4	8	.656	.035	.993	0.663	28.76	.210	.936	.975
.87	4	4	.560	.026	.996	0.619	27.34	.220	.934	.962
.87	4	4	.550	.025	.991	0.633	27.07	.222	.930	.963
.90	4	4	.404	.013	.985	0.509	26.70	.225	.877	.904

* Asymptotic angle of the tertiary

Several observations can be made from these results. First, as the rim angle increases, optical efficiency increases. This is mainly due to the reduction in system focal length with increasing rim angle, which results in less beam spread. Since there is less beam spread at higher rim angles, a higher intercept factor is possible for a given F_H. Second, the optical efficiency optimizes as a function of Z/F_p. This observation is not consistent with the results from the first two stages of the tertiary study, but only because the first two stages used relatively low values of Z/F_p. In this stage, the beam spread can be excessive at high values of Z/F_p, much more than the tertiary can redirect, resulting in low intercept factors at very high values of Z/F_p.

To assess the effects of increased secondary slope error several cases were checked at two different values. The effects are relatively slight, as would have been predicted from the Cassegrainian only analysis. At θ_R = 60 degrees and Z/F_p = .82, increasing σ_s from 3 mrad to 8 mrad decreased IF_R less than 1 percent.

These performance results indicate that the best performance occurs at large rim angles. However, there are other considerations. As the rim angle increases, the surface area of the reflectors increases. This reduces the effectiveness of the reflector area and increases cost. Table II-8 lists the surface area for each rim angle at the optimum Z/F_p for maximum efficiency. This table is also shown graphically in figure II-30. As expected, the primary reflector dominates the surface area requirements. As the primary rim angle increases, the surface area requirements of the secondary and particularly the tertiary decrease, but do not affect the additional requirements of the primary.

The last column in table II-8 lists the power-per-unit surface area of the three reflectors. This ratio shows that if the desired result is to maximize the effectiveness of the surface area of the reflectors, or maximize the power-per-unit surface area, the desired rim angle would be 60 degrees. Above 60 degrees, the surface area increases faster than does the power delivered to the receiver, below 60 degrees the ratio also drops, but not as fast.

TABLE II-8. SURFACE AREA FOR MAXIMUM POWER CONFIGURATION

Reflector Surface Area for Maximum Power Configuration
CR = 1200 σ_p = 4 mrad σ_s = 3-4 mrad

Rim Angle (deg)	Z/F_p	Primary Area		Secondary			Tertiary		Concentrator Area		Power/Area*
		Total (m^2)	Reflective (m^2)	Z (m)	Total Area (m^2)	r_s (m)	Height (m)	Total Area (m^2)	Total (m^2)	Reflective (m^2)	(ρ_p=ρ_s=.95) (kW/m^2)
45	.79	40.09	38.08	3.34	2.06	0.8	1.38	2.50	44.65	42.64	.692
60	.79	41.53	39.31	2.39	2.31	0.84	1.11	2.08	45.92	43.70	.694
75	.83	43.69	42.00	1.89	1.83	0.73	0.87	1.45	46.97	45.28	.687
90	.85	46.91	45.55	1.49	1.55	0.655	0.66	1.00	49.46	48.10	.657

*Power per unit of total area

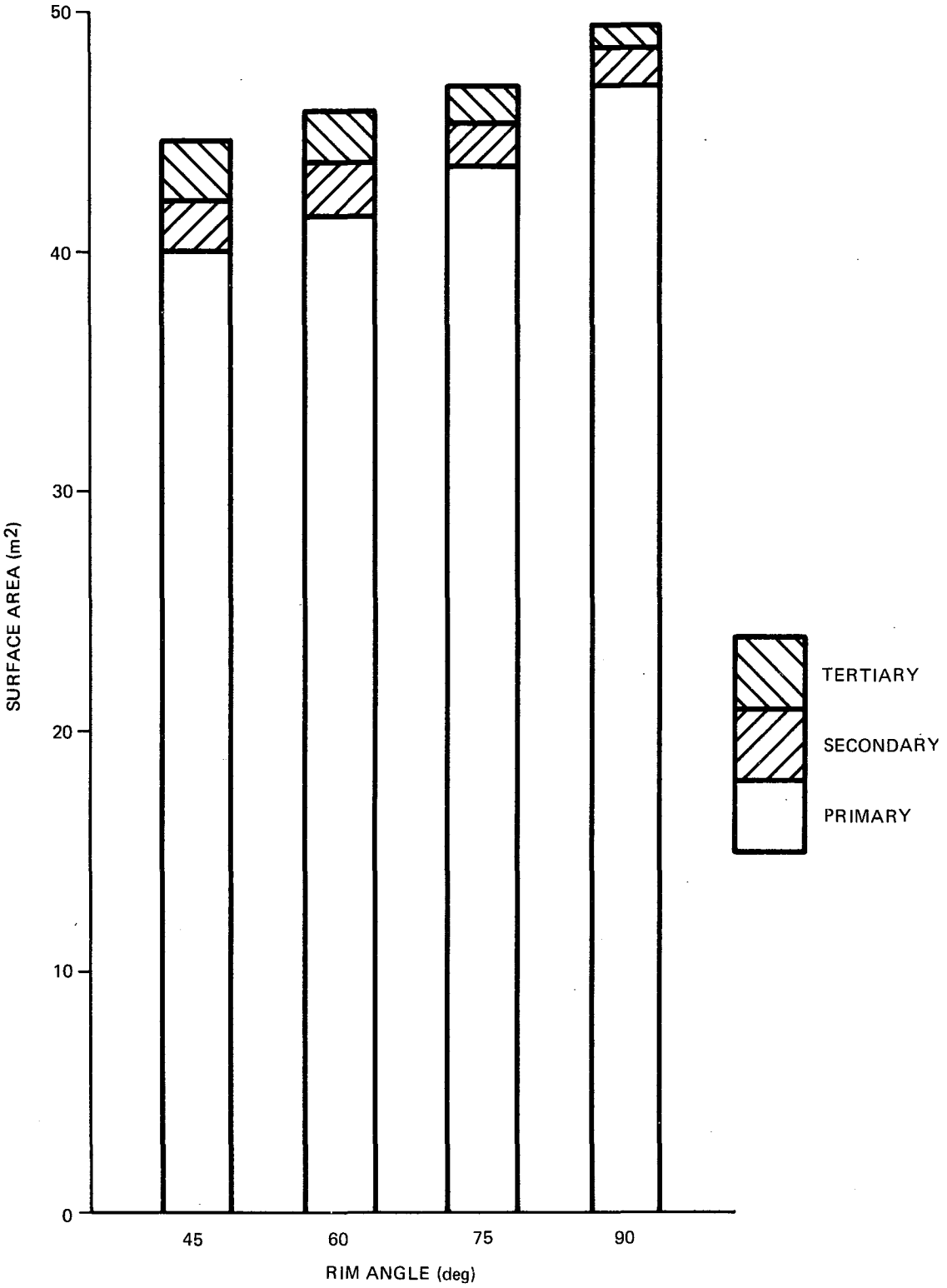

Figure II-30. Required Surface Area for Maximum Power Configuration

Figure II-31 illustrates the trade-off between blocking factor and intercept factor for maximizing optical efficiency with a tertiary reflector. For a 60 degree angle, the optimum Z/F_p is 0.79. In the range of Z/F_p shown, the curves are very similar to those produced for the Cassegrainian only study. The characteristics of this optimum configuration are defined in table II-9.

6. Summary and Conclusions

In this chapter we have presented the results of a study of the optical performance of a Cassegrainian concentrator system. We have determined that the Ritchey-Chretien configuration has little or no advantage over the standard Cassegrainian. Although the Ritchey-Chretien decreases the effect of coma, thereby increasing the intercept factor, the blocking factor of the secondary reflector increases so that the total efficiency remains about the same as for the Cassegrainian.

The efficiency of the standard Cassegrainian can be increased significantly (15 to 20 percent) through the use of a nonimaging trumpet tertiary located at the vertex of the primary reflector. Also, the optical performance of the system is highly dependent on the slope errors and specularity of the primary mirror, but is almost independent of the errors (at least up to 8 mr) associated with the secondary reflector surface.

The overall optical performance of the Cassegrainian with the tertiary is a function of geometrical factors including the position of the secondary relative to the primary, misalignment of the secondary, the size of the secondary and tertiary, and the primary rim angle. A rim angle of 60 degrees maximizes the power-per-unit area of the collector surface, and a Z/F_p of 0.79 maximizes the optical efficiency at 83 percent, assuming that the reflectivities of all surfaces are 0.95 and that the concentration ratio is 1200.

If the rim angle of the Cassegrainian was increased beyond the 60-degree angle which was chosen based on optimum power-per-unit collector area, the performance of the Cassegrainian would be improved further, but at the expense of a lower effectiveness of the reflector surfaces.

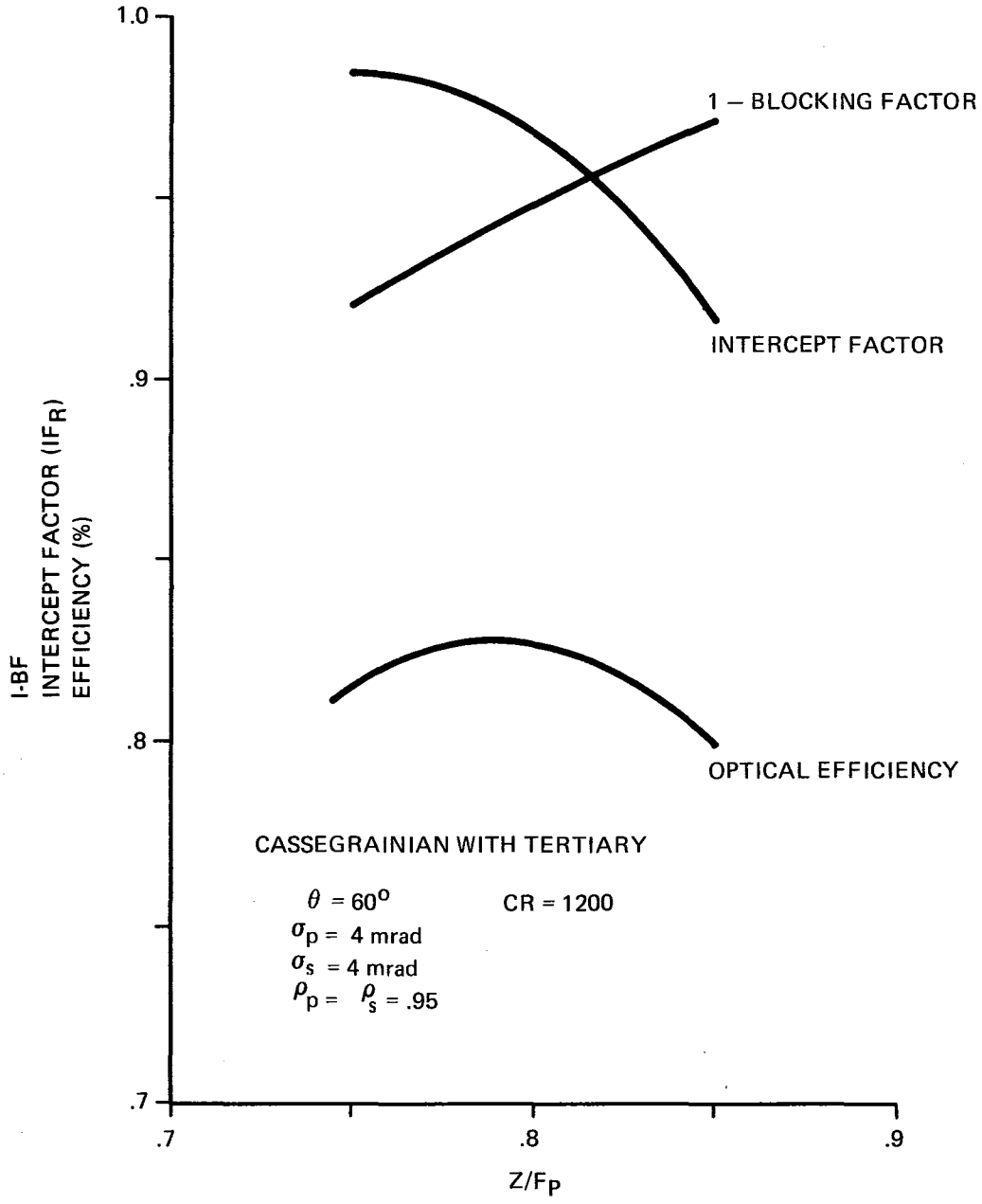

Figure II-31. Optimum Z/F_p for Cassegrainian with Tertiary

TABLE II-9. CHARACTERISTICS OF OPTIMIZED CASSEGRAINIAN COLLECTOR

Primary Mirror	
Rim angle	60^{o}
Focal length	3.0311 m
σ_p	$\leq$ 4 mr
Diameter	7 m
Secondary Mirror	
Distance from primary/vertex	2.395 m
Diameter	1.68 m
Depth	0.184 m
Area	2.31 m^2
σ_p	$\leq$ 8 mr
a_s	0.879 m
b_s	1.2346 m
Tertiary	
Height	1.11 m
Radius at the top	0.503 m
Radius at receiver	0.101 m
Virtual radius	0.249 m
a_t	0.101 m
b_t	0.2246 m
System Performance	
Mirror Reflectivities	0.95
Concentration Ratio	1200
Intercept Factor (IF_R)	0.973
Optical Efficiency	0.83
Power/Total Area	0.694 kW/m^2

The Ritchey-Chretien configuration could potentially improve the performance of the Cassegrainian. Higher orders of correction could reduce the abberation still present in the system. This approach has been followed by ASPCO (26), although their design uses a rim angle over 90 degrees and a blocking factor over 0.10. If a high order Ritchey-Chretien with smaller rim angles and blocking could be formulated, and if this design were coupled to a tertiary reflector, perhaps the surface slope error tolerances could be relaxed.

CHAPTER III

COMPARISON OF CASSEGRAINIAN CONCENTRATORS WITH OTHER CONCENTRATOR GEOMETRIES

A. INTRODUCTION

Since the Cassegrainian concentrator is being proposed as a replacement for the other concentrator types, a comparison is necessary to allow for rational decisions concerning their application. The obvious comparison is between the Cassegrainian and the parabolic dish concentrator (PDC). The other concentrator in wide use is the linear parabolic trough (LPT) which will also be compared to the Cassegrainian, although to a lesser extent because of the very different concentration ratios between point focus and line focus concentrators.

Since receiver design is not a part of this study, this comparison will not consider losses from radiation and convection by way of the receiver cavity or window. The losses that will be compared are radial conduction and convection losses from piping and the receiver, and losses due to blocked insolation due to insulation and structural supports. These losses are evaluated at receiver operating temperatures of 370°C and 815°C. Additionally, two receiver diameters are considered: a 0.609-meter and a 1.22-meter diameter receiver. Heat losses are evaluated for calm and 15-mph wind conditions.

B. COMPARISON WITH A PARABOLIC DISH COLLECTOR

Figures III-1 through III-4 show the power loss due to blockage and radial heat loss from receivers located at the focal point at a PDC. The values for blocking assume a 1 kW/m^2 insolation value, which will be assumed throughout this study, and the conductivity of the insulation is assumed to be 0.061 W/m^oC. As expected, there is an optimum insulation thickness for each operating temperature and receiver diameter. Figures III-5 and III-6 show the power loss due to blockage and radial heat loss

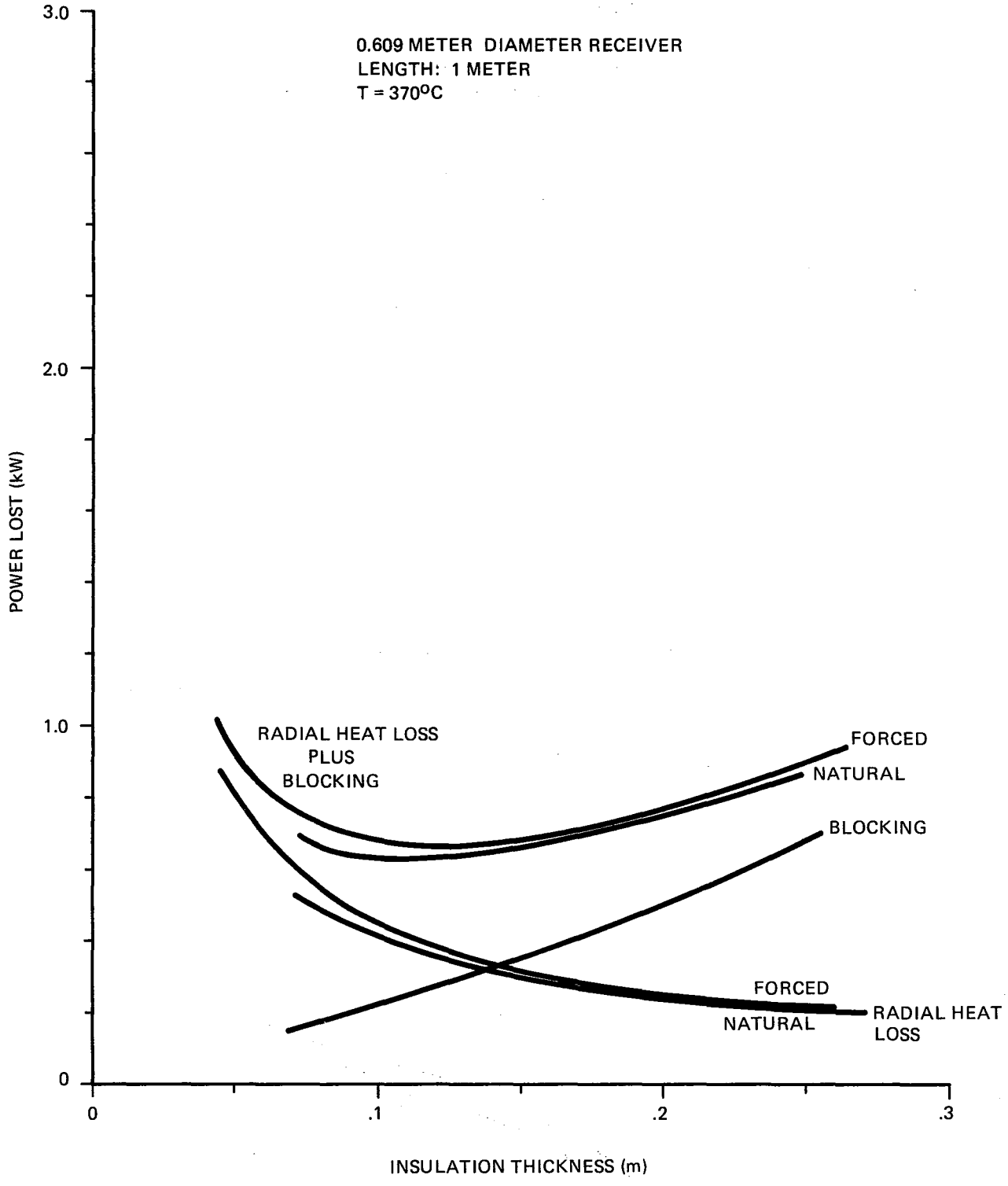

Figure III-1. Power Loss at 370°C from a 0.609 Meter Diameter Receiver

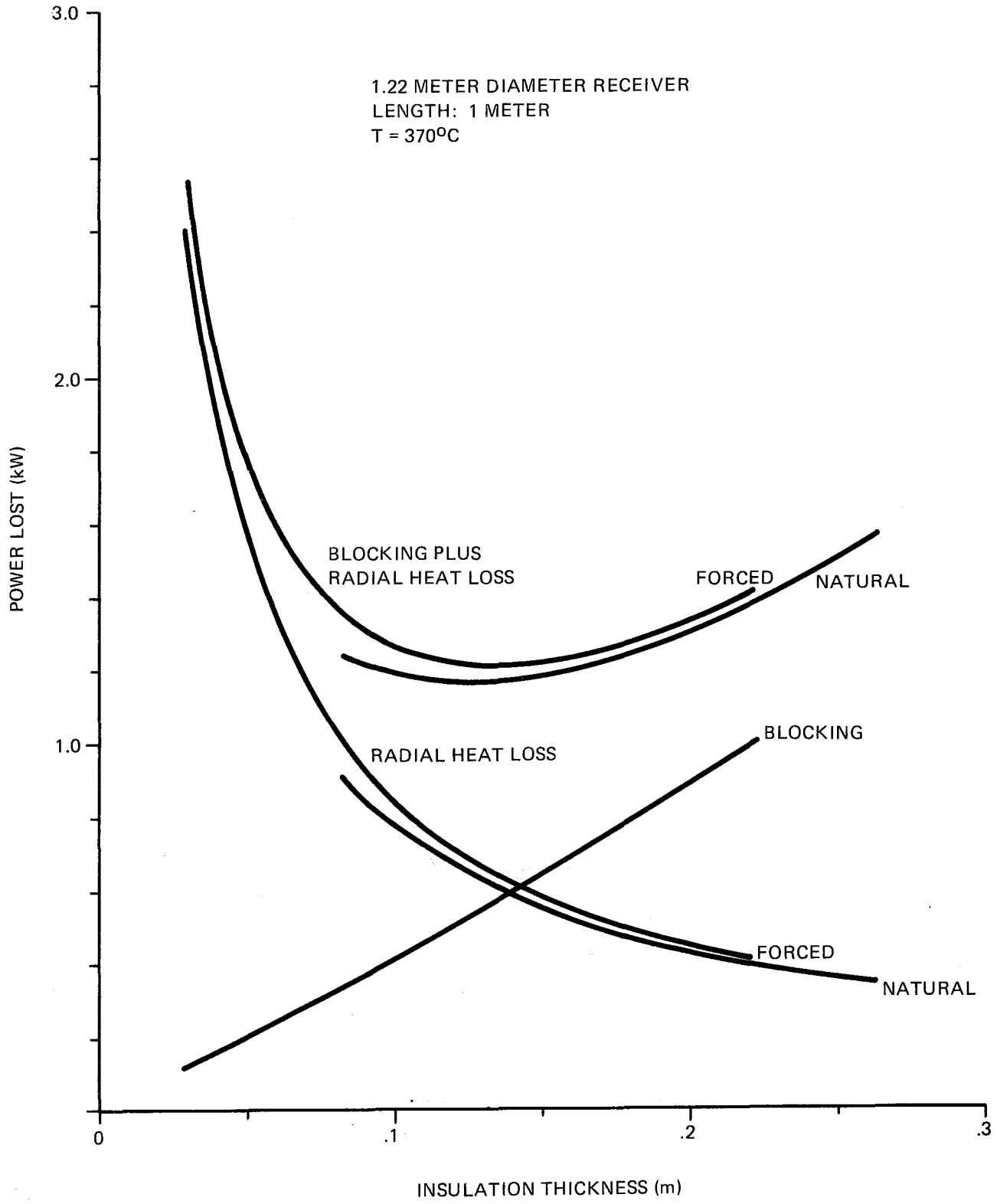

Figure III-2. Power Loss at 370°C from a 1.22 Meter Diameter Receiver

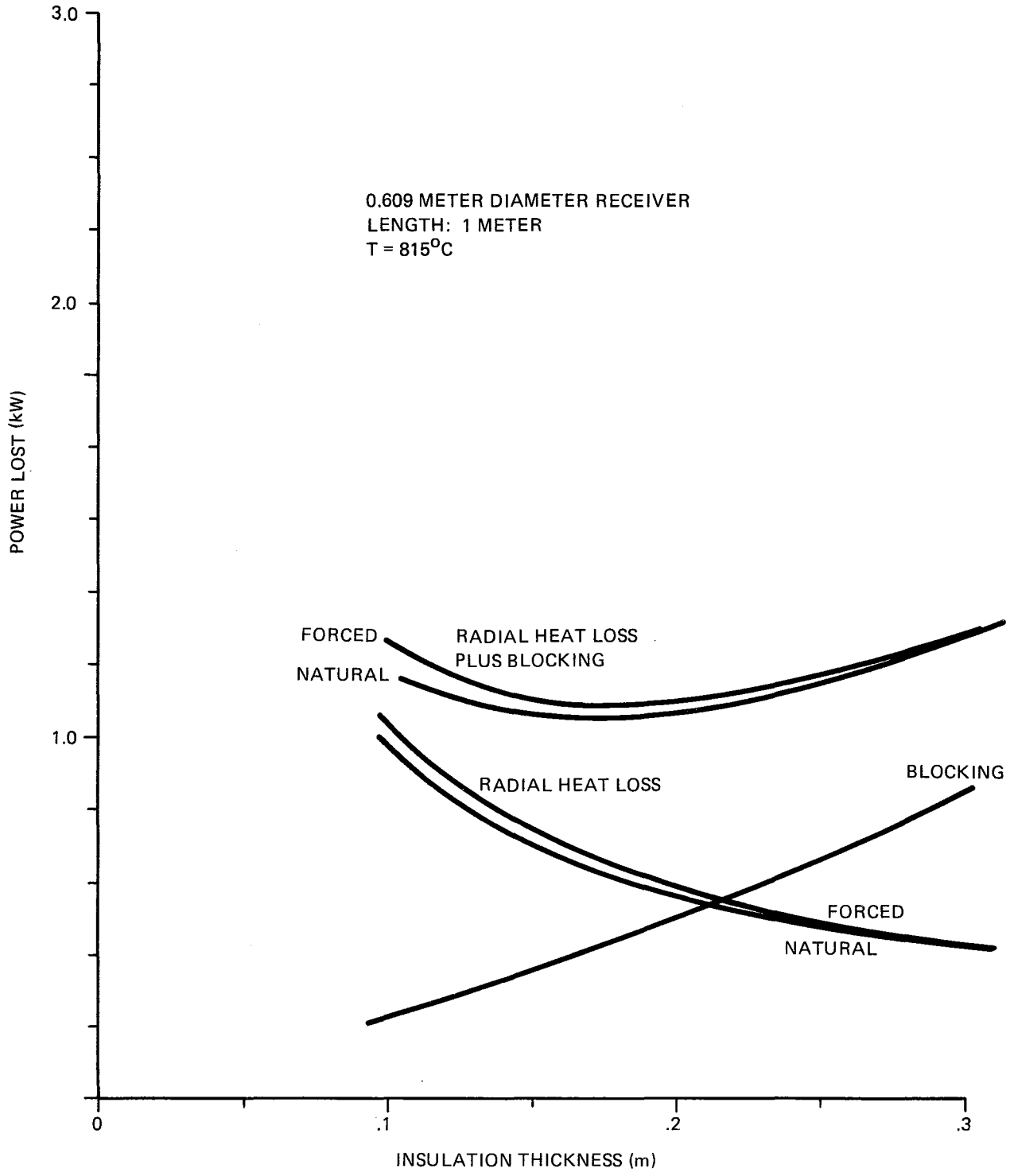

Figure III-3. Power Loss at 815°C from a 0.609 Meter Diameter Receiver

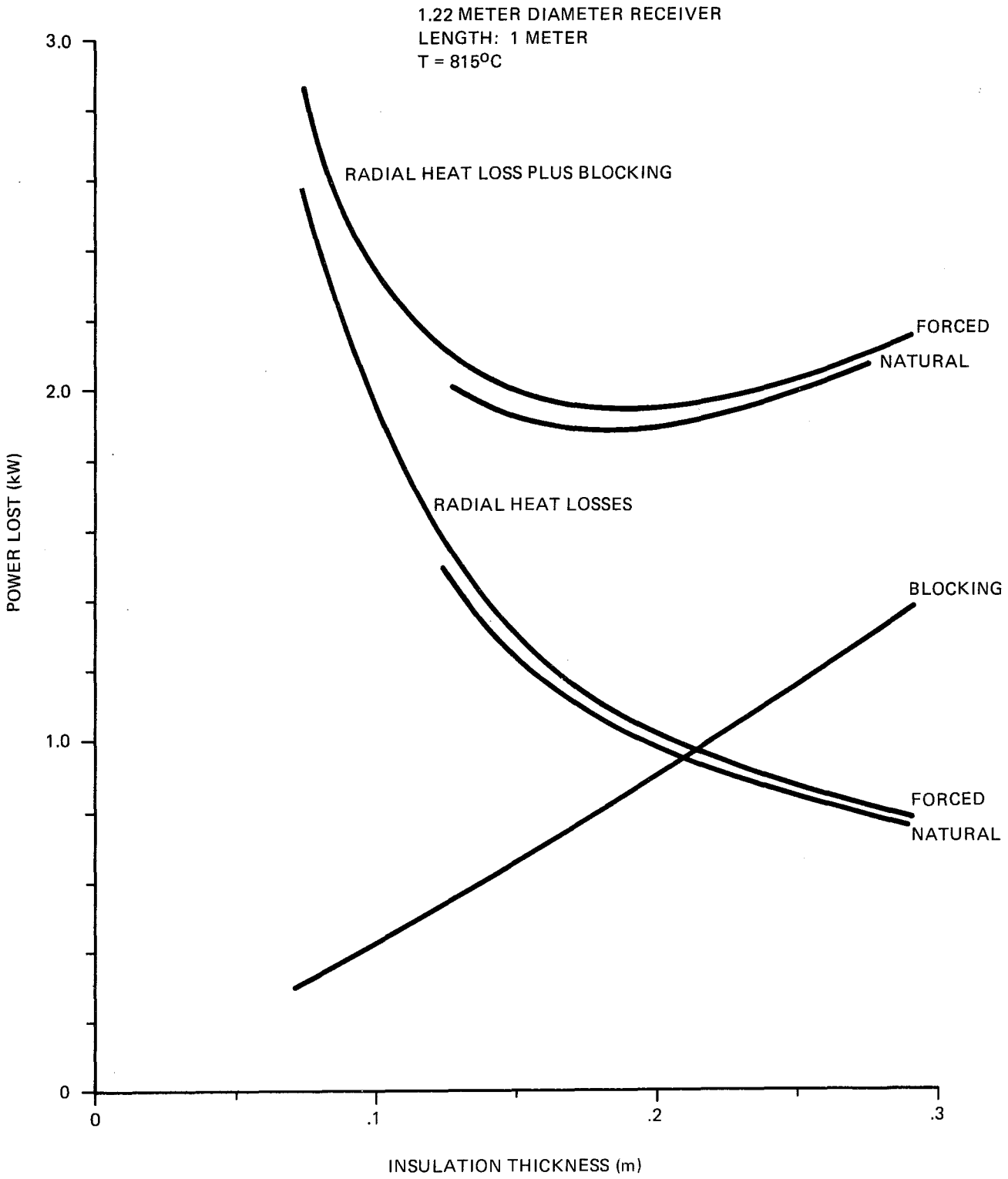

Figure III-4. Power Loss at 815°C from a 1.22 Meter Diameter Receiver

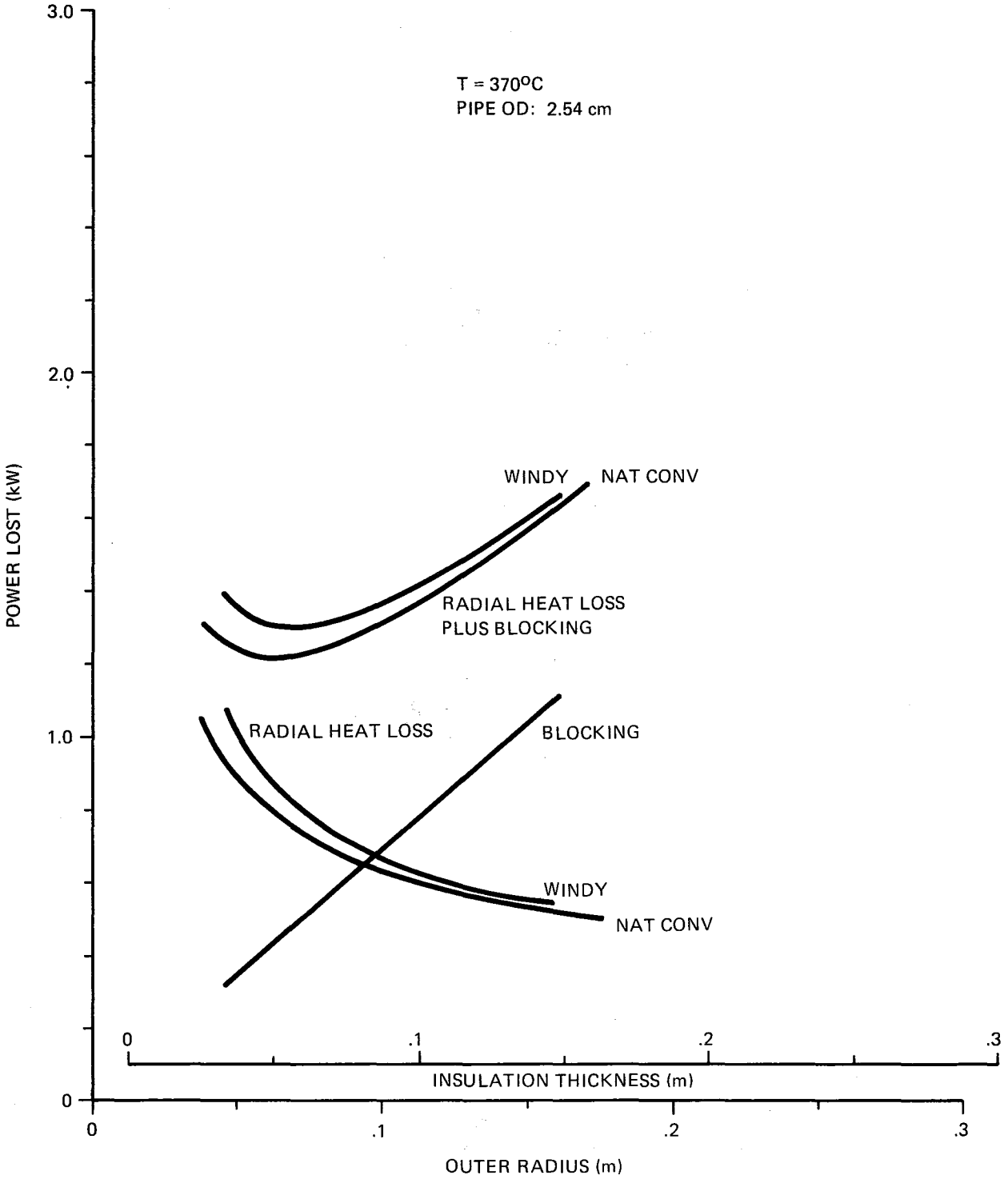

Figure III-5. Piping Loss at 370°C

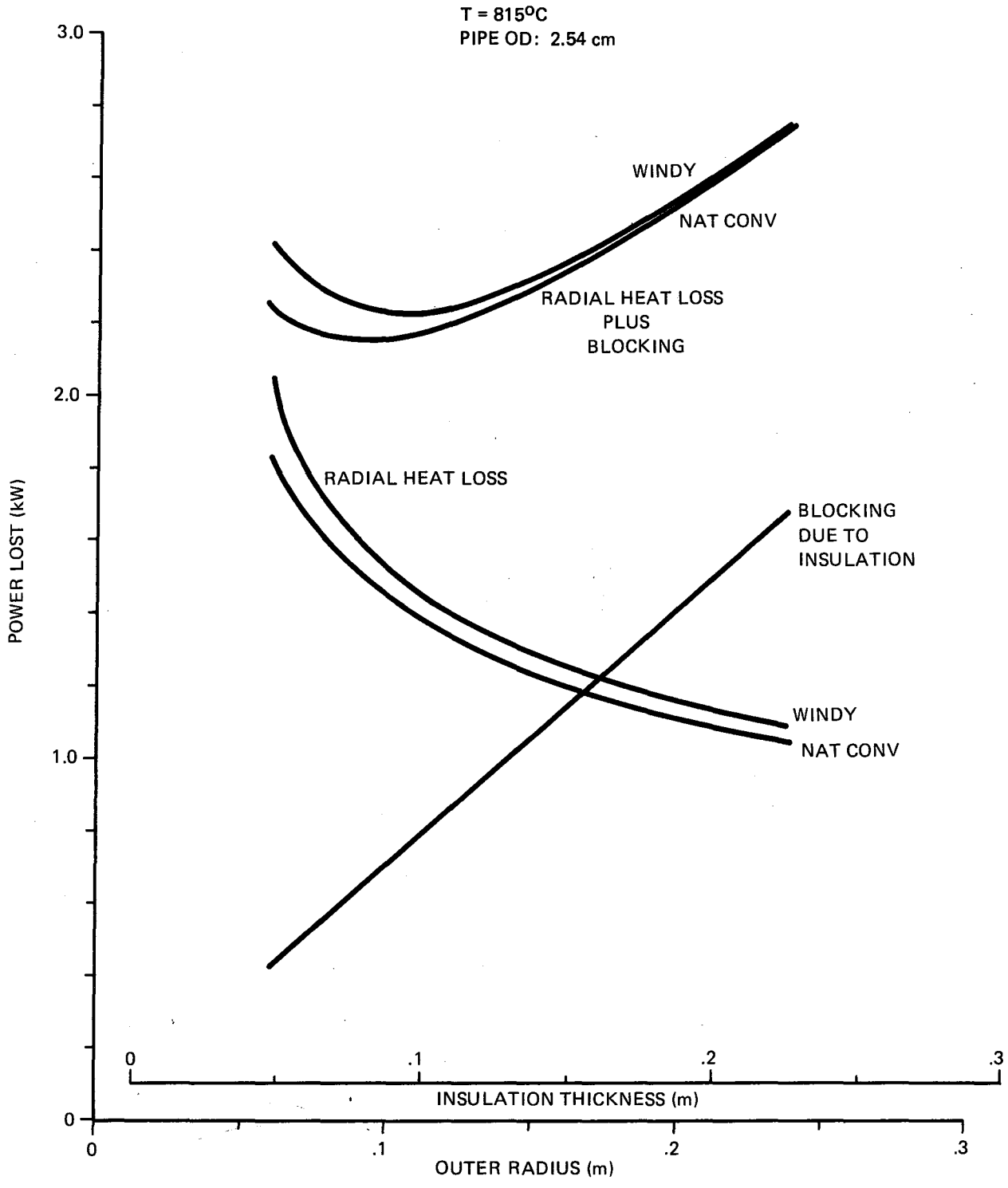

Figure III-6. Piping Loss at 815°C

from 2.54-cm diameter pipe running from the pedestal to the receiver and back.

A PDC was analyzed using COPS for primary rim angles of 45, 60, and 75 degrees, with a slope error of 4 mrad. The results of these analyses are listed in table III-1. The optical efficiency peaks at 60 degrees, consequently the results for 60 degrees will be used for comparison with the Cassegrainian. Notice that no blocking has been applied. To compare the PDC to the Cassegrainian, the various radial heat losses and blocking losses will be subtracted from the values for power into the receiver without blocking or heat loss. Table III-2 lists the blocking and heat losses that are present for the PDC at both operating temperatures and receiver diameters. Table III-3 lists the blocking due to the secondary reflector support and the receiver radial heat loss for the Cassegrainian. Since the insulation on the Cassegrainian receiver does not block incoming insolation, the insulation thickness is unrestricted. To calculate radial heat losses from the Cassegrainian receiver, the insulation thickness was set at .25 m for operation at 370°C, and at .30 m for operation at 815°C, although the thickness could be increased, thus further reducing heat losses. The comparison of steady state heat loss and efficiency between the PDC and Cassegrainian is shown in table III-4. This comparison has not considered any losses from the aperture of the receiver, because these can be affected greatly by the design of the receiver, and receiver design was not a part of this study.

TABLE III-1. PARABOLIC DISH CONCENTRATOR PERFORMANCE RESULTS

Parabolic Dish Concentrator Performance

CR = 1200
σ_p = 4 mrad
ρ_p = .95
No blocking applied

Rim Angle	IF	η_o	Power (kW)	Surface Area (m^2)
45	.98	.931	35.83	40.09
60	.9852	.936	36.02	41.53
75	.957	.909	34.99	43.69

TABLE III-2. PDC LOSSES DUE TO BLOCKING AND RADIAL HEAT LOSSES

Rim Angle: 60 degrees

Receiver supports three 7.62cm x 7.62cm O.D. square tubing

(Only two supports considered for blocking; third is shadowed by piping)

0.609 meter OD Receiver, 370°C Operating Temperature

Unit	O. Dia (m)	Blocking (kW)	Heat Loss (kW)	Total (kW)
Receiver supports	.076	.469	--	.469
Receiver	.848	.565	0.38	.945
Piping	.138	.423	0.82	1.243
Total	--	1.457	1.20	2.657

0.609 meter OD Receiver, 815°C Operating Temperature

Unit	O. Dia (m)	Blocking (kW)	Heat Loss (kW)	Total (kW)
Receiver supports	.076	.460	--	.460
Receiver	.960	.724	0.65	1.374
Piping	.212	.641	1.49	2.131
Total	--	1.825	2.14	3.965

1.22 meter OD Receiver, 370°C Operating Temperature

Unit	O. Dia (m)	Blocking (kW)	Heat Loss (kW)	Total (kW)
Receiver supports	.076	.421	--	.421
Receiver	1.482	1.725	0.65	2.375
Piping	.138	.379	0.82	1.199
Total	--	2.525	1.47	3.995

1.22 meter OD Receiver, 815°C Operating Temperature

Unit	O. Dia (m)	Blocking (kW)	Heat Loss (kW)	Total (kW)
Receiver supports	.076	.412	--	.412
Receiver	1.607	2.028	1.06	3.088
Piping	.212	.572	1.49	2.062
Total	--	3.012	2.55	5.562

TABLE III-3. CASSEGRAINIAN LOSSES DUE TO BLOCKING AND RADIAL HEAT LOSSES

Rim angle: 60 degrees

Z/F_p: 0.79

Secondary dia: 1.68m

Secondary Mirror Supports: three 3.81cm x 3.81cm

Op. Temp. (°C)	Unit	O.D. (m)	Blocking (kW)	Heat Loss (kW)	Total (kW)
	Support	0.38	.304	--	.304
370	0.609m receiver	1.12	0.0	.2	.2
370	Total (0.609m Rcvr)				.504
370	1.22m receiver	1.72	0.0	.35	.35
370	Total (1.22m Rcvr)		0.0	.35	.654
815	0.609m receiver	1.22	0.0	.3	.30
815	Total (0.609m Rcvr)		0.0	.3	.604
815	1.22m Receiver	1.82	0.0	.45	.45
815	Total (1.22m Rcvr)		0.0	.45	.754

NOTE: Blocking due to the secondary reflector is already considered in the optical efficiency, and so is deleted here.

TABLE III-4. COMPARISON BETWEEN CASSEGRAINIAN AND PDC

PDC: Rim Angle: 60 degrees

ρ_p: .95

σ_p: 4mrad CR = 1200

η_o: .936 P = 36.02 kW (no losses)

Cassegrainian: Rim Angle: 60 degrees

Z/F: .79

$\rho_p = \rho_s$: .95

σ_p: 4mrad

σ_s: 4mrad

η_o: .828 CR = 1200

P: 31.87 kW (no losses)

Op. Temp (°C)	Rcvr. Dia (m)	PDC P (kW)	PDC Losses (kW)	PDC Actual (kW)	PDC ηSteady	Cassegrainian P (kW)	Cassegrainian Losses (kW)	Cassegrainian Actual (kW)	Cassegrainian ηSteady	Difference Between PDC and Cassegrainian
370	0.609	36.02	2.657	33.36	.867	31.87	.504	31.37	.815	-4.5%
370	1.22	36.02	3.965	32.05	.833	31.87	.654	31.22	.811	-0.6%
815	0.609	36.02	3.995	33.02	.832	31.87	.604	31.27	.813	-0.5%
815	1.22	36.02	5.562	30.46	.791	31.87	.754	31.12	.809	+4.6%

Another loss inherent in the PDC and not in the Cassegrainian is a daily capacitance loss from heating the pipes running to the receiver. An estimate of these losses and a list of the properties of materials used for the capacitance heat loss estimation are as follows:

Syltherm HTF

$\rho \simeq 800.9$ kg/m^3

$C_p \simeq 1.84$ kJ/kg^{o}C

Pipe (steel sch. 40)

ID = .02665m

OD = .0334m

$\rho = 7800$ kg/m^3

$C_p = .475$ kJ/kg^{o}C

Insulation (Calcium Silicate)

OD = .138m for T = 370^{o}C

OD = .212m for T = 815^{o}C

$\rho = 208.2$ kg/m^3

$C_p = .837$ kJ/kg^{o}C

Length of piping run: 7.7m from concentrator pedestal to receiver.

Using these material properties and pipe/insulation measurements, the capacitance losses can be calculated based on the following formula:

$$Q_{cap} = \rho C_p A_{cs} L \Delta T$$

where

Q_{cap} = the capacitance loss due to heating the material from ambient temperature to the operation temperature (kJ)

A_{cs} = cross-sectional area of material (m^2)

L = length of pipe (m)

ΔT = temperature change of material (^{o}C)

The values for Q_{cap} for each material are listed below for both operating temperatures.

T_{oper} = (370°C)	T_{oper} = (815°C)
T_{inlet} = (343.3°C)	T_{inlet} = (788°C)
T_{amb} = (32.2°C)	T_{amb} = (32.2°C)
$Q_{cap.\ fluid}$ = 4114 kJ	$Q_{cap.\ fluid}$ = 8868 kJ
$Q_{cap.\ pipe}$ = 5910 kJ	$Q_{cap.\ pipe}$ = 13,983 kJ
$Q_{cap.\ insul.}$ = 3160 kJ	$Q_{cap.\ insul.}$ = 6183 kJ
Q_{total} = 13184 kJ	Q_{total} = 29034 kJ

Next, a daily efficiency can be calculated according to:

$$\eta_{Daily} = \frac{\eta_{Steady\ State} * A_{AP} * I_{DN} - Q_{Total}}{I_{DN} * A_{AP}}$$

where

$\eta_{Steady\ State}$ = Previously calculated efficiency (from table III-4)

A_{ap} = aperture area of concentrator (m^2)

I_{DN} = average daily direct normal insolation (25.6 MJ/day - m^2 for Albuquerque)

Q_{Total} = total capacitance loss calculated above (kJ)

A comparison of the daily efficiencies for the Cassegrainian and the PDC is shown in table III-5. Capacitance effects due to receiver warmup and field piping have been deleted since they are common to both systems. At T = 815°C, the Cassegrainian has a higher efficiency than the PDC.

These estimates assume that operation is not possible below the operating temperature of 370°C or 815°C. This analysis demonstrates that capacitance losses are a significant portion of the daily operating efficiency.

TABLE III-5. DAILY EFFICIENCY COMPARISON BETWEEN THE PDC AND CASSEGRAINIAN CONCENTRATORS

Receiver Dia (meters)	T_{oper} (°C)	PDC Steady	PDC Daily	Cassegrainian Steady	Cassegrainian Daily	Difference Between PDC and Cassegrainian
0.609	370	.867	.854	.815	.815	-4.6%
1.22	370	.833	.820	.811	.811	-1.1%
0.609	815	.832	.803	.813	.813	+1.2%
1.22	815	.791	.762	.809	.809	+6.2%

In addition to the performance comparison, the cost of piping and insulation associated with a PDC and which is not required for a Cassegrainian system was determined. These costs are based on the Richardson Cost Estimating Guide, 1983-1984 edition, and includes labor costs. The thickness of insulation is based on the optimum performance at 815°C shown in figure III-6. The components of this cost analysis are shown in figure III-7 which indicates that the added cost to the PDC for piping and insulation to the receiver is $738 for material and $1056 for field labor.

C. COMPARISON WITH A LINEAR PARABOLIC TROUGH (LPT).

The LPT used to compare with the Cassegrainian is the Solar Kinetics Inc. (SKI) T700 concentrator. The performance of this unit has been tested by Sandia National Laboratories (SNLA) (27). Table III-6 lists the physical characteristics of the T700, along with the equations describing its overall efficiency. There were three receivers used when testing the T700, resulting in three efficiency equations. In the comparison between the Cassegrainian, PDC, and LPT, all three will be shown. SNLA tested the T700 at high insolation levels (greater than 900 W/m^2), and at outlet temperatures up to 350°C (662°F). This temperature is the maximum recommended operating temperature, and so performance cannot be

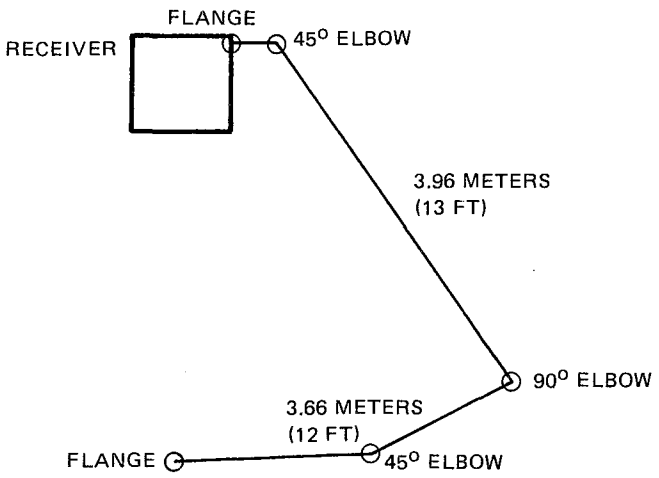

PIPING: 1-INCH A106 CARBON STEEL SCHEDULE 40
INSULATION: 3-INCH DOUBLE THICK CALCIUM SILICATE WITH ALUMINUM JACKET

ITEM	QUANTITY	UNIT PRICE		TOTAL		
		MAT'LS	LABOR	MAT'LS	LABOR*	TOTAL
PIPE	15.2m (50 ft)	6.81/m	8.10/m	103.84	123.48	227.32
PIPE SUPPORTS	8	10.00 ea	6.10 ea	80.00	48.80	128.80
ELBOWS — 90°	2	4.96 ea	21.56 ea	9.92	43.12	53.04
ELBOWS — 45°	4	6.33 ea	21.56 ea	25.32	86.24	111.56
FLANGES	4	12.76 ea	17.64 ea	51.04	70.56	121.60
BOLTS, GASKETS, ETC.	4	4.33 ea	13.13 ea	17.32	52.52	69.84
PIPE INSULATION	15.2m (50 ft)	21.12 ea	29.58 ea	322.00	451.00	773.00
FLANGE INSULATION	4	12.88 ea	18.04 ea	51.52	72.16	123.68
ELBOW INSULATION	6	12.88 ea	18.04 ea	77.28	108.24	185.52
				738.24	1056.12	1794.36

*FIELD LABOR

Figure III-7. Piping and Insulation Costs for a PDC

TABLE III-6. T700 PHYSICAL CHARACTERISTICS

Manufacturer		Solar Kinetics, Inc. 3300 Centry Circle Irving, TX 75060 (214) 721-1070
Operating Temperature:		20^{o} - 350^{o}C (68^{o} - 662^{o}F)
Module Size:		6.1m x 2.13m (240 x 84 in.)
Aperture:		12.80m^2 (137.76 ft^2)
Rim Angle:		90 degrees
Reflector:		3M FEK-244 Acrylic-Film Mirrors Second-Surface Aluminized Measured Reflectance: 0.84 @ 660 nm
Focal Length:		55.9cm (22 in.)
Concentration Ratio:		Aperture Width/Receiver Diameter 51:1 (4.13-cm-OD absorber) 67:1 (3.18-cm-OD absorber)
Receiver:	Type:	Absorber Diameter: 4.13cm (1.625 in.) Black-Chrome-Plated Steel Tubing Measured Emittance: 0.20 (300^{o}C)
	1	6.35-cm-dia Pyrex-Glass Envelope
		Absorber Diameter: 3.18cm (1.257 in.) Black-Chrome-Plated Steel Tubing Measured Emittance: 0.20 (300^{o}C)
	2	5.21-cm-dia Quartz-Glass Envelope
	3	5.21-cm-dia Pyrex-Glass Envelope

Efficiency Equations (I greater than 900 W/m^2)

1. $73.3 - .0444\ DT - .00012\ DT^2$
2. $66.7 - .01699\ DT - .0000862\ DT^2$
3. $66.2 - .00293\ DT - .0000966\ DT^2$

$DT = T_{amb} - T_{ave}$ (^{o}C)

determined at 370°C, unless performance equations are extrapolated upward. Therefore, the efficiency of the T700 will be evaluated at 350°C.

Since all the heat losses from an LPT are directly from the absorber tube, an estimate of the losses that occur from the absorber cavity for a point focus concentrator was needed. Since receiver design was not part of this study, receiver heat loss data were obtained from reports on the Shenandoah STEP concentrator (references 28 and 29). These data are reproduced below.

Shenandoah Concentrator Data

$\eta_{overall} = .716$

$\eta_{optical} = .820$

Shenandoah Receiver Thermal Performance at T = 370°C

$Q_{radiation} = 1.76$ Watts

$Q_{convection} = 1.05$ Watts

$Q_{conduction} = 0.25$ Watts

The receiver efficiency, η_{rcvr}, can be calculated by

$$\eta_{rcvr} = \frac{\eta_{overall}}{\eta_{optical}} = \frac{.716}{.820} = .873$$

This includes all the losses associated with the receiver. Since the optimum insulation thickness, and therefore the conduction heat losses have been determined previously in this study, it is necessary to delete Q_{cond} from the receiver efficiency. This can be done by

$$\eta_{cav} = 1 - (1 - \eta_{rcvr}) \frac{Q_{conv} + Q_{rad}}{Q_{rad} + Q_{conv} + Q_{cond}}$$

or $\eta_{cav} = .883$

Applying this cavity efficiency to the efficiencies presented in table III-4, the estimated thermal efficiencies are shown in table III-7.

TABLE III-7. SYSTEM THERMAL EFFICIENCY AT 370°C

Rcvr. Diam. (m)	PDC w/o cavity losses	PDC w/cavity losses	Cassegrainian w/o cavity losses	Cassegrainian w/cavity losses
0.609	.867	.766	.815	.720
1.22	.833	.736	.811	.716

Relative overall efficiencies for the Cassegrainian, PDC, and LPT are shown in figure III-8. The efficiencies for the T700 collector have been upgraded by assuming a reflectivity of .95 instead of .87. This was done because the results for the Cassegrainian and the PDC used .95 as the reflectivity. As can be seen, the efficiency for the LPT is significantly lower than that for the point focus concentrators. At this temperature, the LPT is hampered by its low concentration ratio and inability to insulate the receiver. At lower temperatures, however, this disadvantage would become less serious.

Using MISR cost data, the quoted cost of mirror modules and receiver assemblies is $491,000 for one MISR module which consists of 180 T-700 collectors. An analysis of component costs indicate that the mirror and receiver stands comprise 80 percent of this cost, or $2182.00 per mirror ($167.70/m^2). In quantities of 20 MISR modules, or 3600 T-700 collectors, the quoted cost was $392,800 for the mirror modules and receiver assemblies. This translates into $1745.80 per mirror ($134.00/m^2).

The unit cost of an LPT mirror in production quantities can be obtained using equation III-1.

$$C_T = C_0 R^K \qquad \text{(Eq. III-1)}$$

$$K = \frac{\ln (P_T/P_0)}{\ln 2}$$

Where:

C_T = Unit cost of mirror at time T
C_0 = Unit cost of mirror at time 0
R = Experience factor
P_T = Cumulative production at time T
P_0 = Cumulative production at time 0

Current cumulative production of T-700 collectors is approximately 37,200m^2, with a current mirror cost of \$167.70/m^2. If 20 MISR modules were to be fabricated, production would jump to 84,040m^2 and cost would drop to \$134.00/m^2. Using equation 1, the experience factor can be found to be 0.826. Again using equation 1 with a production level of 10,000 collectors (130,100m^2), the calculated mirror cost is \$110.80/m^2.

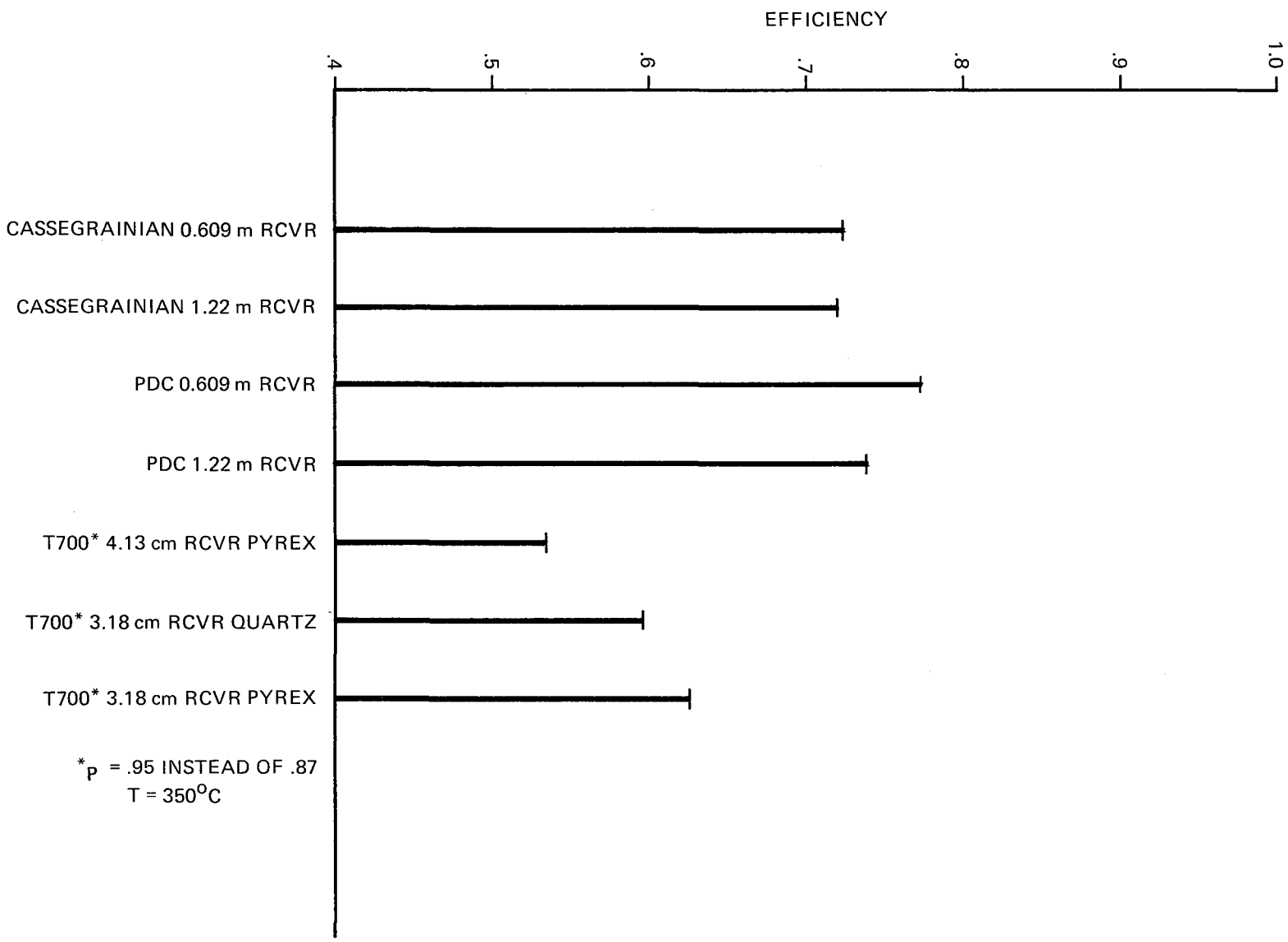

Figure III-8. Comparison of Thermal Efficiency at T = 370°C

CHAPTER IV
MIRROR MATERIALS

In this chapter, the results of an investigation of materials requirements and costs as well as fabrication techniques are presented. The materials must be low cost, amenable to low cost fabrication processes, provide adequate optical and/or structural surfaces, and withstand the temperatures associated with the various mirror surfaces. Each major component (primary, secondary, and tertiary mirrors) have different material requirements as discussed below.

A. PRIMARY MIRROR

1. Conceptual Design

The primary mirror is the largest component of the Cassegrainian collector. This mirror is the major structural element supporting the secondary and tertiary mirrors. In addition to the structural requirements, discussed in more detail in chapter V, the primary must have low surface slope errors and high speculatory. Based on the calculations in chapter II, the combined standard deviation of slope error and specular reflection error should be less than 4 milliradians.

The conceptual design of the primary mirror consists of using thin metal gores stamped into the shape of a paraboloid. Current state-of-the-art tooling can provide a stamped surface with less than 4 milliradian slope error. The mirror surface will consist of a reflective film applied to the metal gores, or petals.

The two types of film considered are manufactured by 3-M, located in St. Paul, Minn. ECP-94 is a front surface silvered polyester film with an acrylic overcoat to protect the silver metallization. This material is 0.00635 cm (0.0025 inch) thick and has a total solar reflectivity of 95 percent. Its cost is about $\$16.14/m^2$. ECP-300X is an experimental front surface silvered acrylic film. This film is about 0.01 cm (0.004 inches) thick and has a reported reflectivity of

97.5 percent. The cost is expected to be about $16.14 to $21.52 per square meter.

Studies have been performed in which various types of gore construction have been investigated. Reference 30 documents one such study by the Boeing Solar Systems Group. This study considered steel and aluminum sheet, glass reinforced plastic, composite laminates and sandwiches, and stiffened monocoque metal skins. This study concluded that a stiffened steel skin, although weighing the most (9.66 kg/m^2), had the lowest manufacturing complexity and technical risk, and the lowest cost ($11.73/$m^2$).

The conceptual design consisted of 22-gage steel gores supported by radial hat section stiffeners as shown in figure IV-1. The steel substrate is primed with epoxy prior to bonding the aluminized polyester film to the surface. Each gore is 3 meters long with an 11 degree spread, shown in figure IV-2. Boeing performed a finite element structural analysis for radial and circumferential stiffeners. Their results indicated that the RMS slope error was 1.067 milliradians with circumferential stiffeners on 0.3 meter (12 inch) centers, whereas the slope error was 0.63 milliradians with radial stiffeners, shown in figure IV-2. These calculations and slope errors were for a wind speed of 50 km/hr.

Recommended manufacturing techniques involve stretch forming the steel sheet substrate. The steel hat section stiffeners and spreaders would be fabricated by first contour roll forming low carbon coil stock into the desired hat section shape. These hat sections would then be parabolically contoured by stretch forming. The stiffeners and spreaders would then be positioned on a stiffener subassembly die and fastened together by spot welding the flanges of the spreaders to the hat section stiffeners.

The formed steel substrate would be vacuum chucked down on an accurately contoured master tool to smooth out any long period surface deformations. The stiffener subassembly would be bonded to the chucked substrate using a rapid cure structural acrylic adhesive. Finally, the stiffener side of the steel panel assembly would be finish coated with a white two-part polyurethane paint.

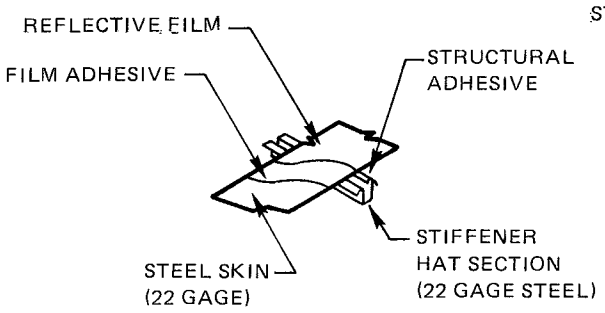

• PANEL COMPONENTS

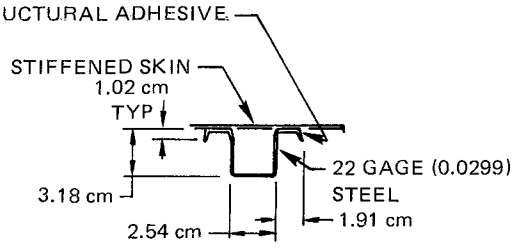

• DETAIL HAT SECTION STIFFENER CROSS-SECTIONAL AREA = 0.871 cm^2

• MATERIAL/USAGE

COMPONENT	MATERIAL
REFLECTIVE FILM	ALUMINIZED 4 MIL POLYESTER FILM WITH ACRYLIC OVERCOAT
STEEL SKIN	STEEL SHEET, LOW CARBON 22 GAGE, COLD ROLLED
STIFFENER HAT SECTION	FORMED STEEL SHEET, LOW CARBON 22 GAGE, COLD ROLLED
STRUCTURAL ADHESIVE	REACTIVE ACRYLIC
FILM ADHESIVE	T.B.D.

Figure IV-1. Details of the Boeing Gore Structure Concept

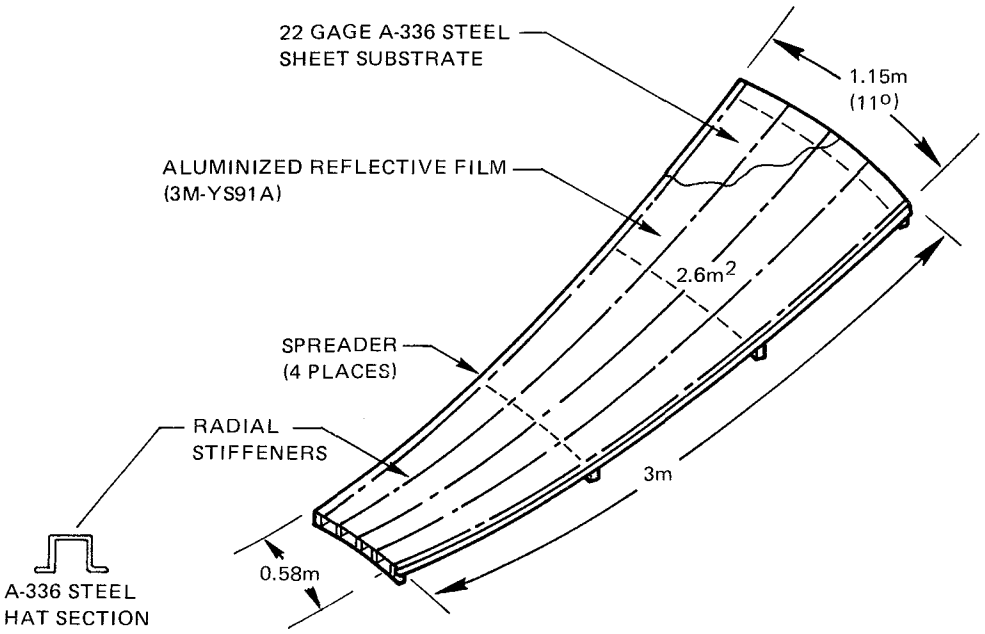

Figure IV-2. Reflector Panel Components for the Boeing Concept

Unfortunately, Boeing did not estimate the manufacturing costs. It would appear that as the substrate thickness decreases, manufacturing and stiffener material costs would increase since a larger number of stiffeners are required. Alternatively, as the substrate thickness increases, fewer stiffeners are required and fabrication costs decrease; however, the cost of the substrate now increases. This implies that there is some optimum substrate thickness, whether the substrate be steel or aluminum, which would minimize total cost while still having less than a 2 milliradian RMS slope error under operating wind loads.

To determine the differences in cost between a thin and thick substrate, BDM performed a simplified flat plate analysis using relations from reference 31. A gore with a spread angle of 20 degrees was assumed. Since the center of the primary is shadowed by the secondary, the arc length of the gore is approximately 2.84 meters (112 inches), and the outer rim length is 1.2 meters (48 inches). Calculations were then performed to determine the support spacing required to limit the slope error to less than 2 milliradians in a design wind speed of 64.4 km/hr (40 mph). The calculations were for a rectangular plate 2.84 meters long with fixed supports on four sides. Results of these calculations are shown in table IV-1.

TABLE IV-1. SUPPORT REQUIREMENTS AND MIRROR COSTS FOR STEEL SUBSTRATES

GORE THICKNESS (cm)	GORE THICKNESS (in)	MAXIMUM SUPPORT SPACING (m)	NUMBER OF SUPPORTS PER GORE	TOTAL PRIMARY WEIGHT (kg)	TOTAL PRIMARY WEIGHT (lb)	TOTAL RAW MATERIAL COST* ($)
0.0777	0.0306	0.40	4	380	837	218
0.203	0.080	0.83	3	731	1612	419
0.351	0.138	1.2	2	1150	2535	659

*Based on a cost of $0.57/kg for cold rolled low carbon steel sheet

The total weight and material cost of the substrate plus stiffeners are shown in table IV-1. Although increasing the substrate thickness decreases the number of stiffeners required, the mirror weight and cost increases dramatically. Although these costs do not include manufacturing costs, the fabrication costs of the primary using the 0.0777-cm-thick steel substrate would need to be an additional $441 to bring its cost up to the cost of a mirror using 0.35-cm-thick steel. This translates into $12 for each additional support used with the thin substrate material.

Based on the preliminary analysis, it appears that the use of thin (0.0777 cm) sheet steel and four radial supports per gore is the most cost-effective approach. However, a detailed optimization study would be required to determine minimum material and fabrication cost. This would require a detailed finite element structural analysis and manufacturing cost estimating. This study would consider the question of welding versus adhesives, and stiffeners versus thicker gores.

Drawing on the Boeing work and the preliminary calculations, a preliminary design for the primary mirror is proposed which consists of 18 20-degree gores or petals. Each gore would be stamped from 22-gage (0.0777 cm or 30.6 mil thick) cold rolled low carbon steel and supported by four hat section radial supports. This configuration would allow less than 1 milliradian slope error in a 64.4 km/hr design wind. The reflector panels, consisting of the steel substrate, radial supports, and circumferential spreaders, would be bolted to the circumferential structural rings shown in figure IV-3. Alignment of the individual panels may be accomplished using this bolted connection. Radial trusses support the circumferential rings.

BDM's design goal is to develop a framework that is easy to fabricate from flat stock, and to which the gores would be fastened using a low cost process while maintaining required optical quality. However, a detailed structural analysis using finite element techniques, and a detailed analysis of manufacturing alternatives and costs would be required to determine the least expensive design.

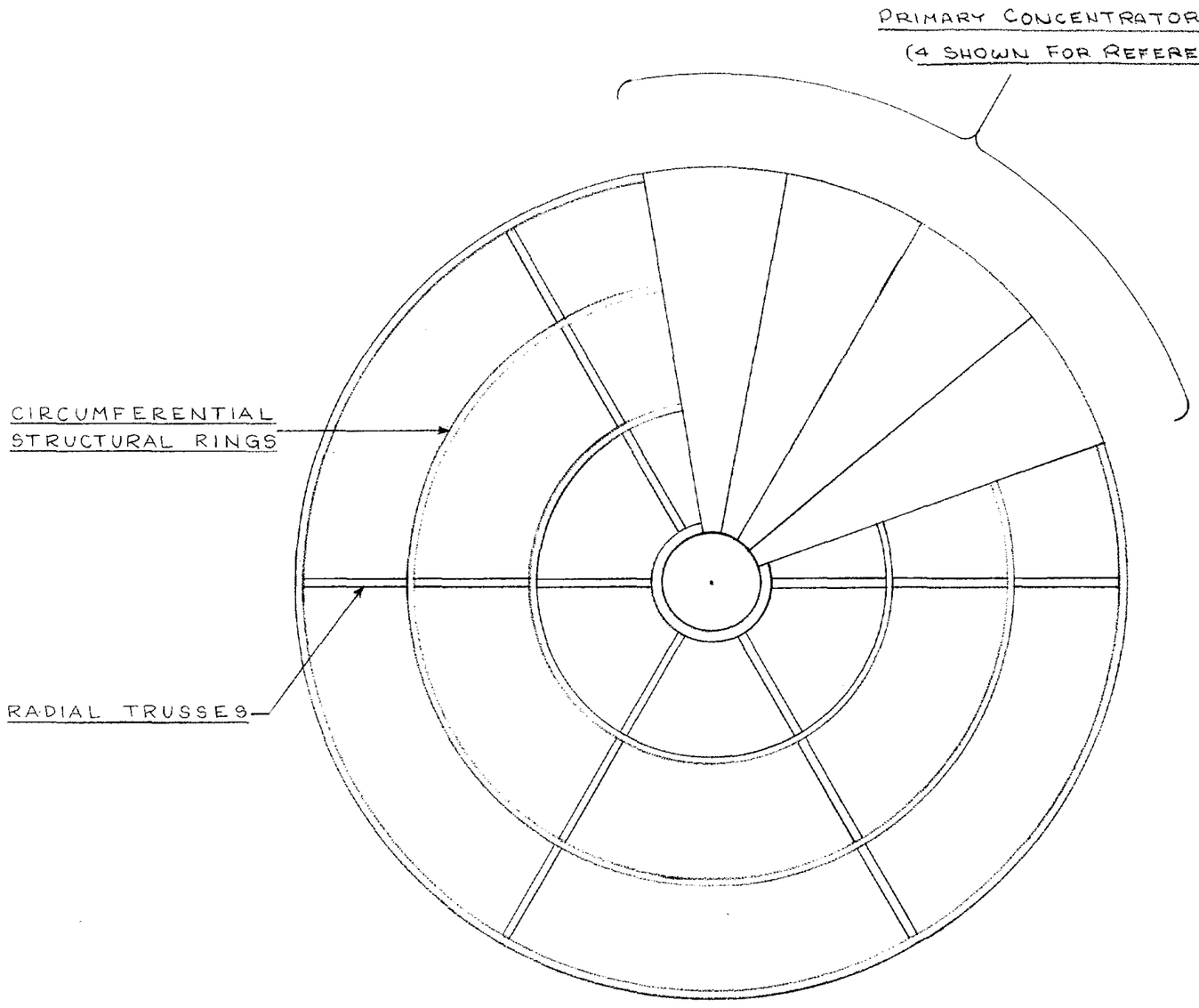

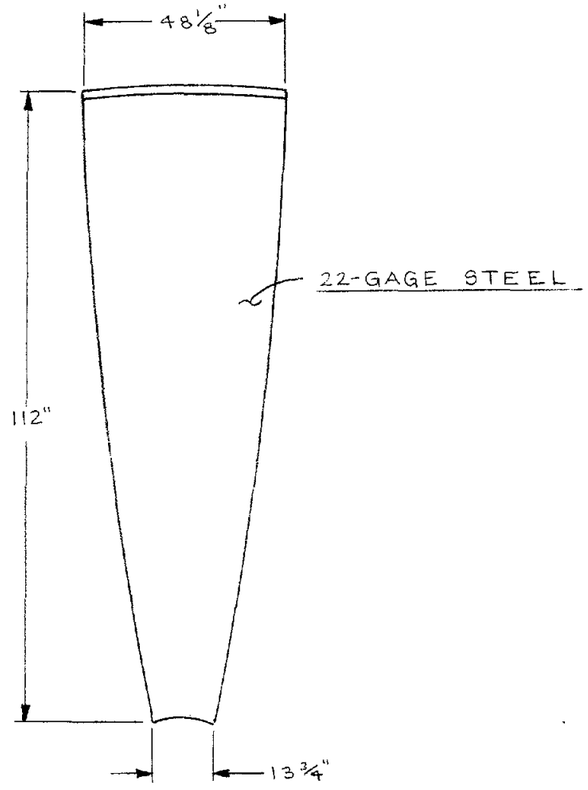

PETAL DETAIL
(FLAT PATTERN REFERENCE LAYOUT)

Figure IV-3. Primary Reflector Support Framework

Total primary costs are shown in the following section for a primary mirror with 39.31 m^2 of reflective area and 41.53 m^2 total area.

2. Cost Estimate

A summary of the cost for a single petal is shown in table IV-2. The assumptions used in developing this cost estimate are as follows:

(1) All costs are in FY 84 dollars.

(2) All work is performed in a single facility. Thus, there is no charge for shipping components, such as stiffeners, from a stamping plant to a final assembly plant.

(3) Large production runs so setup costs are small per unit of production.

(4) Mirror petals are formed by stamping.

(5) A small non-aerospace firm located in Chicago performs the work.

(6) Costs are f.o.b. the fabricator--no transportation to the construction site.

(7) Field erection is not included.

(8) A production level of 10,000 mirrors per year.

(9) No resale value of scrap.

The following sections provide the estimating rationale for each cost component in table IV-2. The various factors and standard hour data used in the following equations have been developed and documented at several aerospace and other manufacturing firms.

a. Petal

Material cost was estimated using equation IV-1.

$$\begin{aligned}\text{Material Cost} &= \$0.57/\text{kg} \times 1.2 \text{ scrap/waste} \\ &\quad \times 1.2 \text{ inventory holding} \times 1.05 \text{ transportation} \\ &\quad \times 1.2 \text{ G\&A and fee} \times 13.3 \text{ kg/petal} \\ &= \$14.00 \end{aligned} \qquad \text{(Eq. IV-1)}$$

The \$0.57/kg is an f.o.b. price obtained from reference 32 and inflated to 1984 dollars assuming a 6 percent inflation rate. The 1.2 scrap/waste factor accounts for workmanship errors and the changes in shape from raw

TABLE IV-2. COST ESTIMATE SUMMARY FOR A SINGLE PETAL OF THE PRIMARY MIRROR

COMPONENT	LABOR COST	MATERIAL COST
Petal	3.85	14.00
Stiffeners (4)	10.40	10.40
Spreaders (4)	10.40	1.90
Spot Welding	2.50	-
Reflective Film	20.20	51.80
Adhesive Bonding	16.00	1.70
Subtotal	63.35	79.80
Contingency (10%)	6.34	7.98
Total	69.69	87.78

Recurring Cost: $0.70
Total Petal Cost: $158.17
Total Mirror Cost: $2847.00
Non-Recurring Die Cost: $350,000

sheet to final product. The 1.2 inventory holding factor accounts for insurance, receiving inspection, and similar costs for holding the raw materials and work in process inventory. This factor is based on BDM experience in the manufacturing operation of several clients. The 1.05 transportation factor allows for the cost to transport raw material from the founding source to the fabricator, and the 1.2 G&A and fee factor is a typical value for manufacturing firms.

The labor for stamping the petals was estimated using equation IV-2.

$$\text{Labor Cost} = \$35/\text{manhour} \times 5 \text{ men} \times 1.1 \text{ supervision} \times 1.2 \text{ support} \div 60 \text{ pieces/hour} = \$3.85 \qquad \text{(Eq. IV-2)}$$

The $35/manhour is the burdened labor rate including salary, direct fringe benefits (FICA, unemployment insurance, vacation, etc.) and plant overhead (utilities, property insurance and taxes, equipment maintenance, allocated materials, and general and administrative expenses). The total of five men includes material handling, machine operator, and packaging personnel. The 1.1 supervision factor is typical, and the 1.2 support labor factor accounts for quality control, test, manufacturing engineering, engineering liaison, and rework labor. A sustained rate of 60 petals per hour was estimated based on industrial experience assuming two dies are required to produce the final parabolic shape. This cost of $3.85 per petal is within the range of $3 to $4 quoted by Deerfield Manufacturing Co., Mason, Ohio for stamping the primary mirror petals.

b. Stiffener

The raw material cost was estimated using equation IV-1 with approximately 2.5 kg of final material per stiffener. The labor was estimated assuming that the hat shape would be obtained by die stamping and the parabolic contour by a subsequent stretch forming operation. The stamping cost was estimated as $1.00 per stiffener using equation IV-2 and assuming a production rate of 250 pieces per hour on a sustained basis.

The cost for stretch forming was estimated using equation IV-3.

Labor Cost = 1.9 manhours/unit x $35/hour
x 1.1 supervision x 1.2 support labor
x 0.0187 learning = $1.60 (Eq. IV-3)

The 1.9 manhours per unit was developed from labor data for over 200 parts from the F-111 program (reference 33). The labor rate, supervision, and support labor factors are the same as in equation IV-2. The 0.0187 factor is the cumulative average factor for 700,000 units on an 80 percent learning curve obtained from F-111 program experience for stretch forming (reference 33).

c. Spreaders

Material cost was estimated using equation IV-1 with an approximate weight of 0.454 kg per spreader. The labor for die stamping and stretch forming the spreaders was assumed to be the same as for the stiffeners.

d. Spot Welding

Welding material costs were assumed to be included in the labor overhead costs estimated using equation IV-4.

Labor Cost = 0.42 manhours/unit x $35/manhours
x 1.2 support labor x 0.14 learning
= $2.50 (Eq. IV-4)

The 0.42 manhours assumes 0.0085 manhours per spot weld and 16 welds per petal, plus 0.27 manhours for handling. The 0.0085 manhours per spot were based on BDM standard hour data and an 85 percent learning curve using equation IV-5.

Manhours = 0.05 standard minutes/spot
x 2 variance x 5.1 learning ÷ 60 min/hr
= 0.0085 (Eq. IV-5)

The 5.1 learning curve factor converts from the standard 1000 units to one unit, whereas the 0.14 learning curve factor in equation IV-4 converts back from one unit to a large quantity. The 2 variance factor accounts for personnel fatigue and delay, supervision, and rework. The handling labor was estimated based on 8 pieces and 0.2 standard minutes per part.

e. Reflective Film

The labor cost of applying the ECP-300x film to the primary mirror was estimated at $\$9.25/m^2$ based on Shenandoah experience. The cost assumed for the ECP-300x is $\$21.52/m^2$ and is the high end of the range quoted by 3-M Corporation. The cost of primer for the petal surface is about $\$2.20/m^2$. For a petal area of $2.19m^2$ the labor cost is $20.20 and material cost is $51.80.

f. Bonding

Labor involved in bonding the petal to the stiffeners includes cleaning, handling, and adhesive application. The area requiring cleaning and adhesive for one stiffener is approximately $0.107m^2$. Using standard data for cleaning of 0.016 hours/m^2 (0.0015 hours/ft^2), cleaning time was estimated to be 0.0017 standard hours. Standard data for painting is 0.355 hours/m^2 (0.033 hours/ft^2) so the time required to apply the adhesive is approximately 0.038 standard hours. The handling time is approximately 0.01 hours. Labor cost for bonding a single stiffener to a petal is found from equation IV-6.

$$\begin{aligned}\text{Labor Cost} &= 0.05 \text{ standard hours} \times 2 \text{ variance} \\ &\times 1.2 \text{ support labor} \times \$35/\text{manhours} \\ &= \$4.00 \text{ per stiffener}\end{aligned} \qquad \text{(Eq. IV-6)}$$

The factors used in equation IV-6 have been defined previously. Since four stiffeners are required per petal, the total labor cost is $16.00.

Assuming an adhesive bond thickness of 0.0254 cm (0.01 inches), the volume of adhesive required per petal is $1.09 \times 10^{-4} m^3$

($6.66\ in^3$). The density of Versilok 201 acrylic is $1031\ kg/m^3$ (8.6 lb/gal) and the cost is $8.40/kg ($3.80/lb). Thus, the cost per petal of raw material is $0.94 per petal. Using equation IV-1, the total material cost per petal is $1.70.

g. Contingency

A factor of 10 percent is added to material and labor estimates to account for omissions in the descriptive data and estimating methods.

h. Recurring Tooling Cost

A charge of $0.70 per petal is added to cover tool maintenance and is calculated using equation IV-7.

Recurring Cost = $350,000 non-recurring tooling
x 0.36 maintenance/year
÷ 180,000 petals/year = 0.70 (Eq. IV-7)

The non-recurring cost of $350,000 is an estimate for tool and die manufacturing and design based on manufacturer estimates. The 0.36 maintenance factor assumes 3 percent per month of non-recurring cost for maintenance.

B. SECONDARY MIRROR

The secondary mirror does not have as stringent optical requirements as the primary; however, it must be capable of withstanding the temperature associated with the incident-concentrated insolation. As shown in chapter II, the combined surface errors may be 8 mr or more without seriously affecting the optical performance of the concentrator. The secondary must be structurally rigid to prevent sagging or vibration. Finally, it must withstand maximum temperatures of about 110°C (230°F).

1. Thermal Analysis

For this analysis, it was assumed that the Cassegrainian concentrator has the characteristics of the optimized system described in

chapter II. This system was optimized in terms of power per unit of collector area and consists of a primary mirror with a 60-degree rim angle, and a 1.68-meter diameter secondary, positioned 2.395 meters from the vertex of the primary. Assuming a primary reflectivity of 0.95, the insolation incident on the secondary is shown in figure IV-4. The radial temperature distribution for various candidate materials is shown in figure IV-5.

This temperature distribution gives the temperature rise above ambient as a function of radius for a solid mirror having a reflectivity of 0.95. The temperature was calculated assuming natural convection and radiation heat loss, a uniform heat flux of 19 kW/m^2 between $r/r_o = 0.25$ ($r = 0.21$ m) and the edge of the mirror on the front surface, and 1000 W/m^2 on the back surface. It was assumed that the back surface is painted with a white paint having a short wavelength absorptance of 0.2 and a long wavelength emittance of 0.91. Fiberglass and stainless steel have low thermal conductivities (0.05 W/m^oC and 16.4 W/m^oC, respectively), and exhibit a high radial temperature gradient in the region of the mirror where the incident insolation drops to zero. The addition of fins to the aluminum mirror decreases the mirror temperature by only 6^oC to 7^oC.

Based on this analysis, the secondary mirror may reach maximum temperatures of 110^oC (230^oF) on a hot 40^oC summer day. This indicates that silvered films, such as 3-M's ECP-94 or ECP-300X cannot be used. The ECP-94 is a front surface silvered polyester with an acrylic flow coat and can operate at maximum temperatures of 104^oC to 116^oC (220^oF to 240^oF). ECP-300X is a second surface silvered acrylic which can withstand a maximum temperature of only 77^oC (170^oF).

The high temperature gradients for steel and fiberglass could cause excessive warping of a solid mirror thereby decreasing the intercept factor at the receiver and lowering the overall efficiency of the concentrator. However, since there is no insolation incident upon the center of the mirror, this section can be removed leaving an annulus region of nearly constant temperature. Removal of the center section of

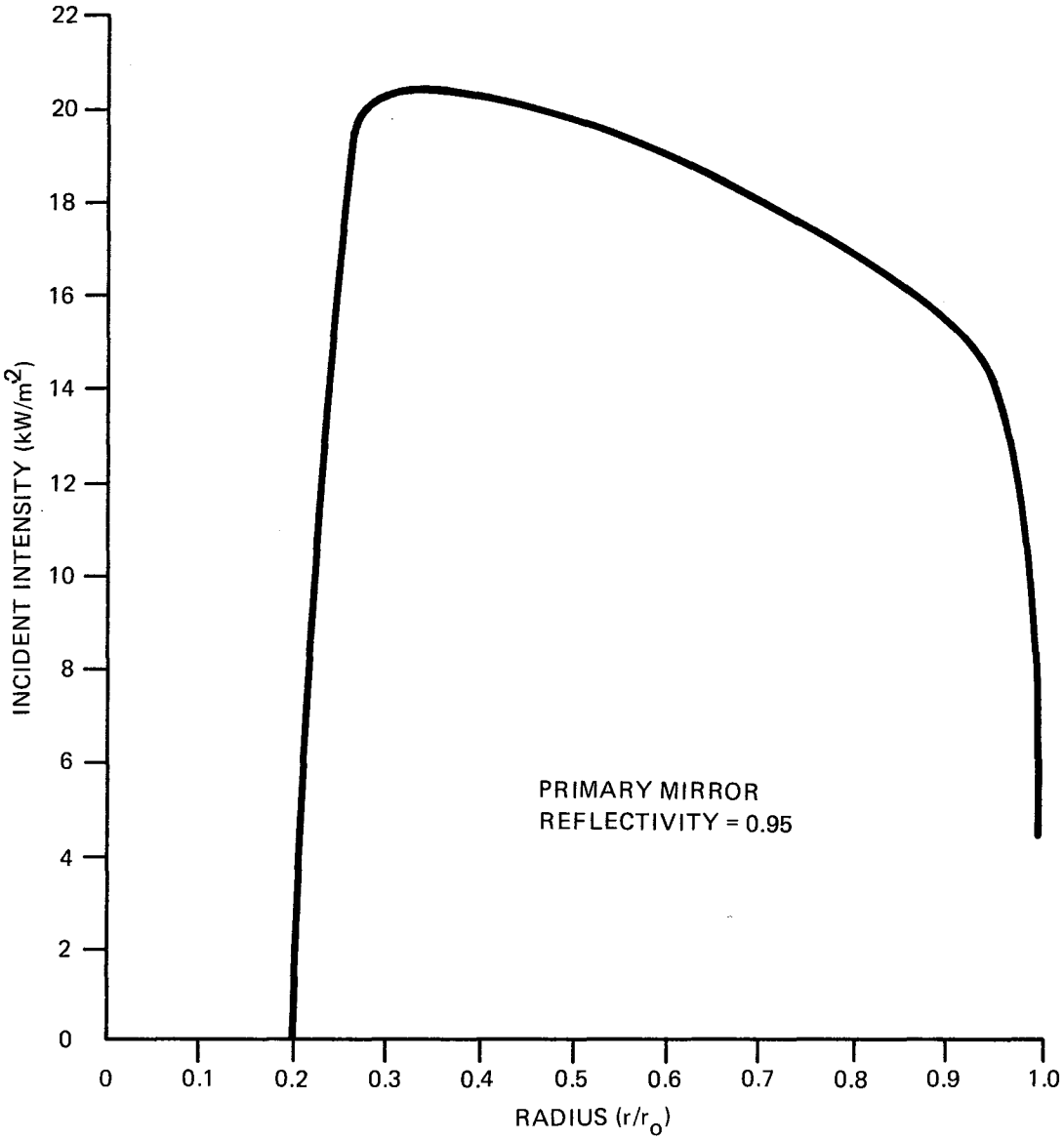

Figure IV-4. Intensity Distribution on the Secondary Mirror

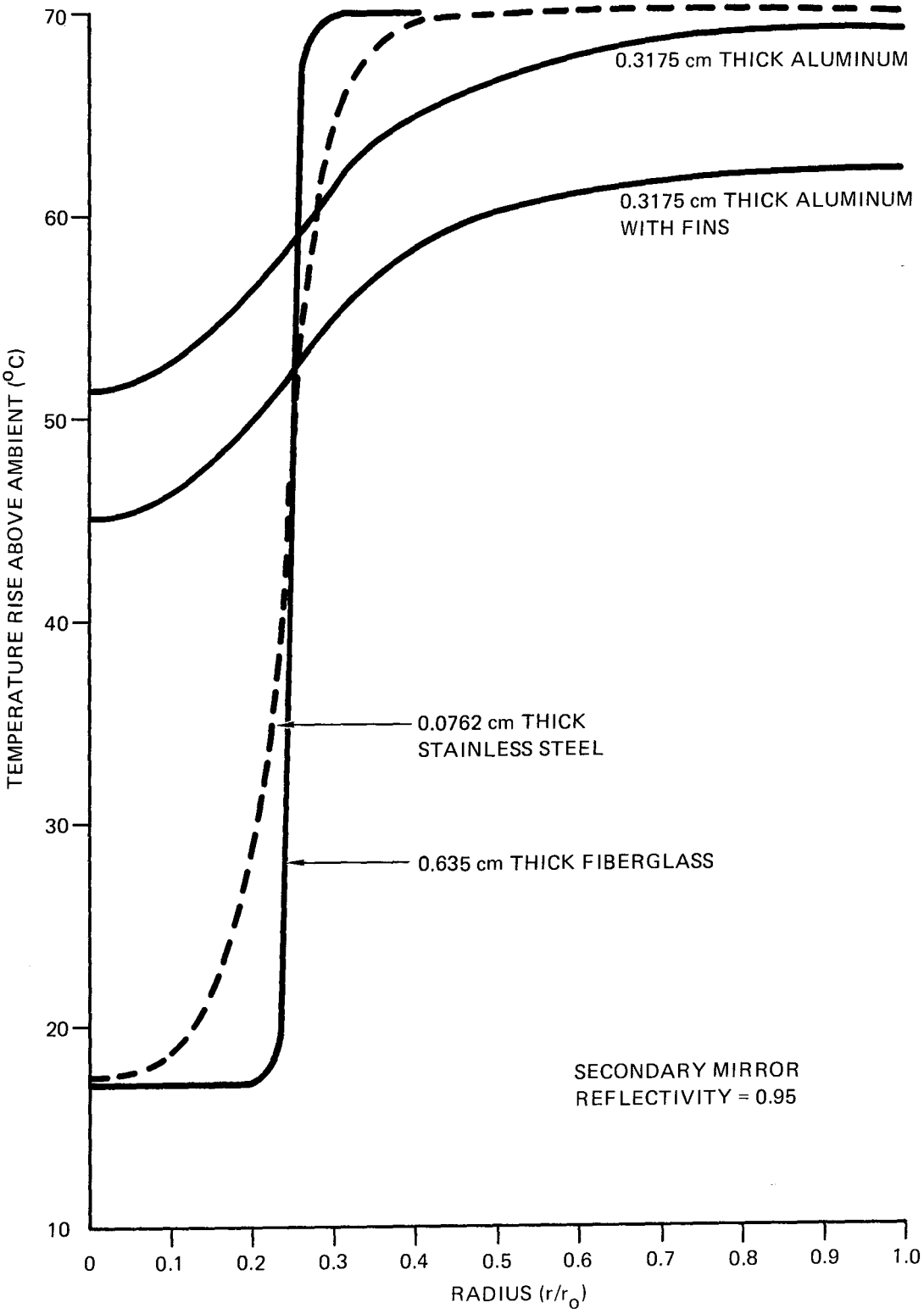

Figure IV-5. Temperature Distribution in the Secondary Mirror

the secondary will also improve its support and allow the mirror to be fabricated in two pieces. This will be discussed in subsection 3.

2. Materials and Fabrication

Several materials were investigated for fabrication of the secondary mirror. These materials may be divided into three categories: structure, reflecting surface, and protective coating. The structural materials investigated included glass, steel, aluminum, and fiberglass. Reflective surfaces included vacuum-deposited and electro-plated silver, and silvered film. The protective coatings include SOL-GEL and Dow Cornings 1-2577 conformal silicone coating. The results of these investigations are discussed in the following paragraphs.

a. Structural Materials

1) Steel

Two concepts were considered using steel as the structural element. These included a low carbon steel with an electrostatic paint coating, and polished stainless steel.

The electrostatic painting of low carbon steel is a standard process used by automobile manufacturers. This process produces a high gloss surface with a 0.102- to 0.127-micron (4 to 5 micro-inch) finish and which will accept a vacuum-deposited silver film. Discussions with Mr. Joseph Smartch of Ford Motor Companies process development group, Detroit, Michigan, indicated that although the paint is baked on for 10 minutes at 123°C (245°F), with a maximum temperature of 140°C (285°F), he thought the paint would delaminate from the steel at the peak operating temperature of the secondary mirror consequently, this concept was abandoned. However, this concept may merit further investigation into higher temperature steel coatings.

Polished stainless steel shows promise as a structural material for the secondary mirror. Discussions with Mr. Paul Tamuzza of Polished Metals Limited, Inc., Bloomfield, New Jersey, indicate that steel is available in rolls 0.915 meters (36 inches), 1.22 meters (48 inches), 1.52 meters (60 inches), and 1.83 meters (72 inches) wide. As the sheet width increases, the quality of finish decreases

significantly. Also, there is only one domestic mill which produces 1.83-meter (72-inch) wide steel rolls, and the thickness of these steel sheets is 0.198 cm (78 mils). Therefore, we have decided to design the secondary in two pieces, each 0.86 meters (33.85 inches) wide before stamping, to achieve the hyperoboloidal shape. By cutting out the center section of the mirror (the region which receives no reflected insolation from the primary), the two sections can be supported around the outer rim and at the center. Such a mirror fabricated from 0.0762-cm (30 mil) steel would weigh 14.1 kg (31 lbs).

A quote was obtained from Polished Metals Limited on a 0.889-meter wide, 0.0762-cm-thick polished 304 stainless steel sheet, 1.78 meters long. In quantities of 20,000 (10,000 mirrors) per year the cost would be $\$33.68/m^2$ or about $80 per mirror polished and coated with PVC for protection, and delivered to Albuquerque, N.M. Polished Metals Ltd. is sending samples of their polished steel to Sandia National Laboratories for optical testing which includes specularity and reflectivity. Samples indicative of production quality of 1.83-meter-wide rolls were measured by SNLA and 95 percent of the hemispherically reflected radiation was retained within a 6-milliradian slit. Since the total solar reflectivity of stainless steel is only about 61 percent, polished steel will require a silver coating to improve the reflectivity of the mirror. Based on GE's investigation of mirror materials for the Shenandoah project, enhancement of a polished steel surface with vapor-deposited silver could produce a highly reflective and specular surface with 96 percent total and 95.9 percent specular solar reflectance. However, GE abandoned this concept, because they felt the high cost of a mirror using vapor-deposited silver on polished stainless steel was prohibitive for the primary mirror.

Estimates for stamping the required shape of the secondary mirror were obtained from the Shenandoah experience. The cost of stamping the secondary mirror into the shape shown in figure IV-6 is approximately $21.80 per square meter of surface area, or $48.40 per mirror. The cost of the stamping die would be about $300,000.

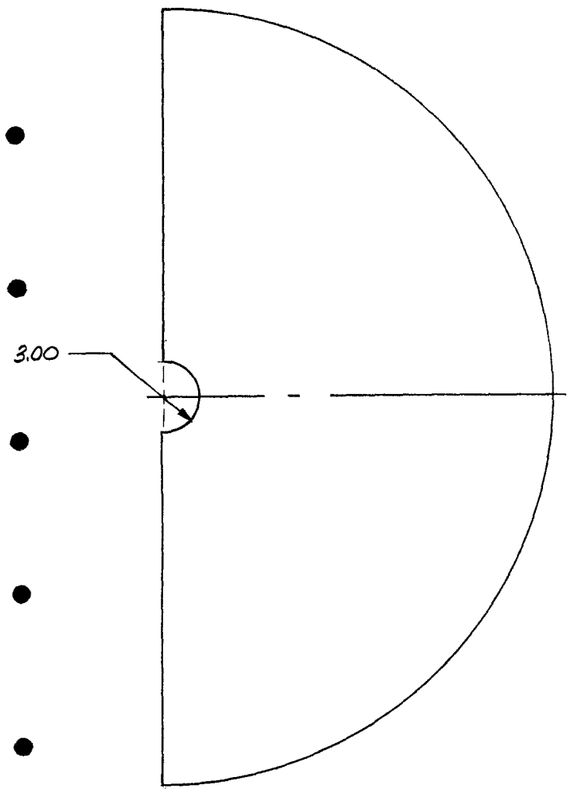

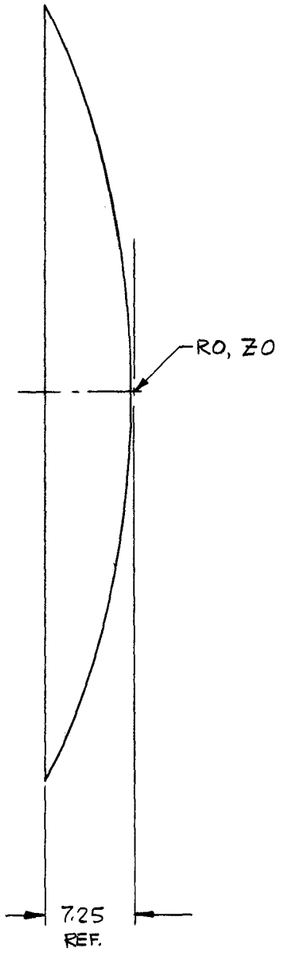

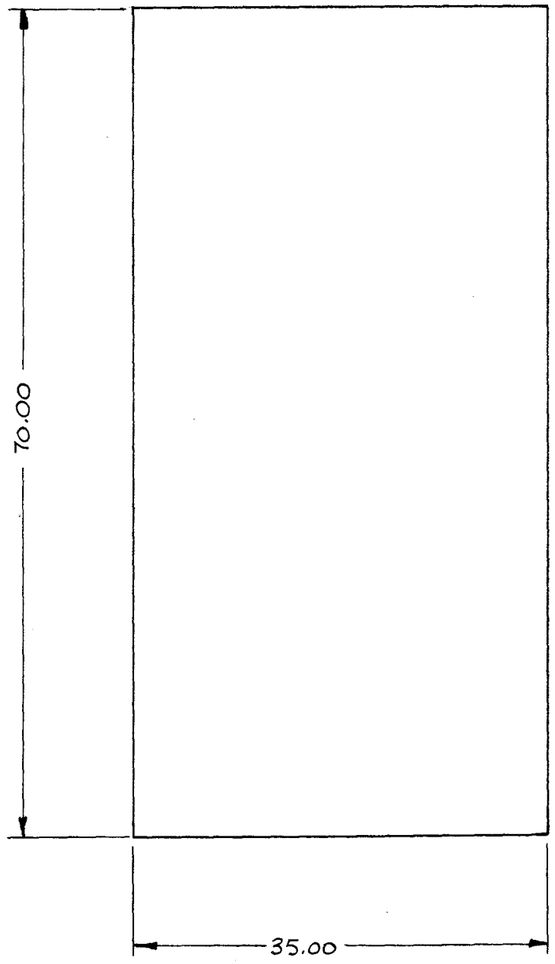

BLANK BEFORE STAMPING

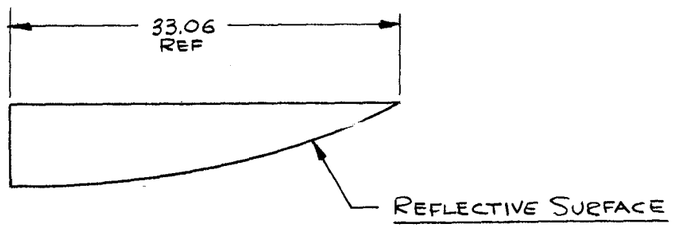

COORDINATES OF FORMED MIRROR (IN.)	
R	Z
0.00	0.00
4.80	0.17
9.60	0.67
14.40	1.49
19.20	2.60
24.00	4.00
28.80	5.62
33.06	7.25

Figure IV-6. Formed Secondary Mirror

2) Fiberglass

This concept involves a high temperature polyester resin with chopped glass fibers for reinforcement and stability. For production quantities these ingredients are combined, mixed, and sheeted out using sheet molding compound (SMC). The SMC is cut to fit the cavity of a steel mold in which it is cured under heat and pressure. Due to the size of the part and the molding pressure, the die or tool cost is the most significant cost for this approach. Reinhold Engineering and Plastics Company of Santa Fe Springs, CA., estimated the cost for this mold at about $250K. The mold would not have any section discontinuities, i.e., ribs, bosses, or flanges that would telegraph through to the reflective surface. A polished surface finish of 0.102 microns (4 microinches) is attainable from the tool bidder, and a part price of $200 was estimated by the molder. This uniform thickness dish would be bonded to a wide flanged peripheral ring with a very thick elastomeric adhesive as the differential stress-forgiving interface with the metalic support structure.

Silver ($\approx$1000Å) would be applied by the vacuum process to the convex side. A thin primary protective film of several hundred angstroms of silicon monoxide would be deposited on the silver before breaking the vacuum.

3) Glass

There are two techniques for obtaining a curved glass mirror, bending and sagging. Donnelly Mirror of Holland, Michigan, routinely bends 0.51-meter (20-inch) diameter spherical mirrors and has the ability to bend 1.09-meter (43-inch) spherical mirrors, but cannot bend a mirror as large as that required for the Cassegrainian secondary (1.72 meters or 67.7 inches).

Glass Mountain Optics in Austin, Texas, is one of two companies in the United States capable of sagging a 1.78-meter-square sheet of glass. For structural integrity, the required thickness is 1.27 to 1.9 cm (1/2 to 3/4 inch). Pyrex or Schott Glass is not available in sheets large enough for the secondary, so that front surface silvered

reflectance requirements of the secondary. Chemical brightnening of commercially available aluminum produced total solar reflectivities of about 88 percent. An 800Å layer of silver deposited on polished aluminum produced a total solar reflectivity of 95 percent.

Discussions with ALCOA indicate that Al 5657 is dipped, anodized, and sold only in coils to protect the finish. It is currently sold only to automobile manufacturers who use the material as trim, and who have the equipment required to de-coil the aluminum and cut it to size. ALCOA produces a highly reflective aluminum sheet with the trade name of COILZAK. This material has a bright rolled surface which is anodized. The anodized surface has a total reflectivity of 80 percent and costs $4.96 per kilogram ($2.25 per pound). The bare sheet without anodize is $3.86 per kilogram ($1.75 per pound). ALZAK is essentially COILZAK which has been chemically brightened before anodizing. The reflectivity of ALZAK has been measured by SNLA (reference 34). The total solar hemispherical reflectance was 85 percent, the specular reflectance at 500 nm into a 6 milliradian slit was 72 percent, and the total hemispherical reflectance at 500 nm was 89 percent. Thus, at 500 nm, only 81 percent of the total reflected radiation was with 6 milliradians as compared to 95 percent for polished steel. The cost of nonanodized ALZAK is about $6.33 per kilogram ($2.87 per pound).

The concept would be to obtain sheets of 0.159-cm (0.0625-inch) thick CC50, an internal ALCOA designation, with one surface bright rolled (nonanodized COILZAK) and stamp the sheet into the required shape for the secondary mirror. Silver would then be vacuum deposited onto the bright surface and a protective coating applied. The cost of the bright rolled aluminum would be about $40 per mirror ($17.22/m^2). If chemical brightening is required, the cost would be $64 per mirror.

Discussions with Mr. John Powers at the ALCOA Research Laboratory indicated that vacuum-deposited silver may adhere better to an anodized surface than to a bare aluminum surface. If this is the case, forming would be required first since forming would cause the anodize to craze. Anodizing would increase the cost by about $11 per mirror.

Two materials appear to have the required properties, Dow Corning (DC) 1-2577 conformal silicone coating, and a coating of inorganic oxides applied by the SOL-GEL process being developed and tested by SNLA.

The DC1-2577 is a transparent silicone resin which is flexible over a temperature range of -65°C to 200°C, has high resistance to moisture, and a light transmissivity of 92 percent. This material has two methods of cure, a room temperature cure and accelerated heat cure from 75°C to 100°C after addition of DC176 catalyst. The Shore D Durometer hardness with the heat cure is 39 points. According to the manufacturer this material weathers well (20 year life) and resists ultraviolet light and dirt accummulation.

Following the application of the silver reflective surface, the surface would be primed with Dow Corning's 1200 or 1204 primer. After evaporation of the solvent vehicle from the primer, Dow Corning's 1-2577 would be applied by a flow coating procedure resulting in a thickness of 1 to 2 mils. This results in a hard protective silicone surface. Although silicone coatings have a high moisture permeability coefficient, the silicon monoxide will protect the silver. The heat cured DC1-2577 has a water vapor transmission of 0.00345 gms/cm^2/cm. The 1-2577 will protect the reflective surface from abrasion by impinging dust as well as cleaning and handling operations. The application of the Dow Corning primer and coating is estimated at $2.50 per mirror for material and $28 for processing, for a total cost of $30.50 for a secondary mirror.

The SOL-GEL process is a coating technique which allows various inorganic oxides to be deposited on large surfaces at relatively low costs. In this process, glasslike macromolecules are formed in an alcohol solution at room temperature by chemical polymerization. Before the solution transforms to a stiff, amorphous gel, it can be diluted and applied to a surface by dipping, spraying, or other thin film coating technique. After drying, the porous gel coating is heated to convert it to a dense, transparent glass layer. Sandia is investigating the use of this process to protect the silver layer deposited on steel. Several parameters affect the properties and applicability of the coating including composition, thickness, firing temperature, firing time, and

soda lime glass must be used. Annealed glass 1.83 m x 1.83 m (72 x 72 inches) is available from Pittsburg Plate Glass (PPG) for $171 per sheet.

When sagging a piece of glass this large, a 30 percent failure rate is expected. In addition, a mold this large will warp producing a nonuniform piece of glass which will require polishing to obtain the desired surface configuration. The high thermal expansion of metal molds cause this deformation, and graphite molds sublimate at sag temperatures and damage the glass surface. The major cost in providing a sagged glass mirror is in the polishing, which costs $0.3885/cm^2 ($2.50/in^2). The area of the secondary mirror is 2.31 m^2 and with a 50 percent price break for production quantities, the mirror would cost about $4700. A 1.27-cm-thick glass mirror will weigh 62.3 kg (137 lbs).

Due to the cost, weight, and fragility, glass was eliminated as a possible structural mirror material.

4) Aluminum

During the early phases of the Shenandoah project, General Electric (GE) investigated several mirror concepts including polished or chemically brightened aluminum panels. Two concepts considered are shown in figure IV-7, where the 5657 is a high magnesium aluminum alloy which has a H-25 temper and is amenable to polishing.

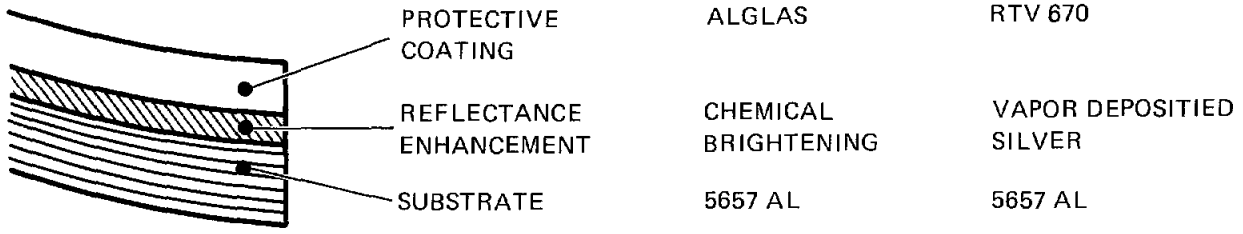

Figure IV-7. Reflector Surface Candidates Investigated in the Shenandoah Project

Tests indicated that polishing aluminum improved the diffuse reflectance but had no great effect on the total solar reflectance. Thus, reflectance enhancement is necessary to meet the

reflectance requirements of the secondary. Chemical brightnening of commercially available aluminum produced total solar reflectivities of about 88 percent. An 800Å layer of silver deposited on polished aluminum produced a total solar reflectivity of 95 percent.

Discussions with ALCOA indicate that Al 5657 is dipped, anodized, and sold only in coils to protect the finish. It is currently sold only to automobile manufacturers who use the material as trim, and who have the equipment required to de-coil the aluminum and cut it to size. ALCOA produces a highly reflective aluminum sheet with the trade name of COILZAK. This material has a bright rolled surface which is anodized. The anodized surface has a total reflectivity of 80 percent and costs $4.96 per kilogram ($2.25 per pound). The bare sheet without anodize is $3.86 per kilogram ($1.75 per pound). ALZAK is essentially COILZAK which has been chemically brightened before anodizing. The reflectivity of ALZAK has been measured by SNLA (reference 34). The total solar hemispherical reflectance was 85 percent, the specular reflectance at 500 nm into a 6 milliradian slit was 72 percent, and the total hemispherical reflectance at 500 nm was 89 percent. Thus, at 500 nm, only 81 percent of the total reflected radiation was with 6 milliradians as compared to 95 percent for polished steel. The cost of nonanodized ALZAK is about $6.33 per kilogram ($2.87 per pound).

The concept would be to obtain sheets of 0.159-cm (0.0625-inch) thick CC50, an internal ALCOA designation, with one surface bright rolled (nonanodized COILZAK) and stamp the sheet into the required shape for the secondary mirror. Silver would then be vacuum deposited onto the bright surface and a protective coating applied. The cost of the bright rolled aluminum would be about $40 per mirror ($17.22/m^2). If chemical brightening is required, the cost would be $64 per mirror.

Discussions with Mr. John Powers at the ALCOA Research Laboratory indicated that vacuum-deposited silver may adhere better to an anodized surface than to a bare aluminum surface. If this is the case, forming would be required first since forming would cause the anodize to craze. Anodizing would increase the cost by about $11 per mirror.

b. Reflective Surfaces

As discussed in the previous section, the reflectivity of polished metals (60 percent for steel and 78 percent for aluminum) is inadequate for the Cassegrainian secondary mirror. A reflectivity of at least 95 percent is desired so that even chemically brightened aluminum is inadequate. Thus, some form of reflectivity enhancement is required for the polished metals. Two types of reflective surfaces have been considered, deposited silver and silvered film.

There are several methods of depositing a silver coating, the two considered here include electroplating and vacuum deposition. Electroplating produces a heavy silver coating with a nonuniform thickness. This method does not produce as good an optical surface as a thin coating, and is much more expensive. Robert Siegel Plating Co., St. Louis, MO., has tanks large enough to plate one half of a secondary mirror. They estimated that 0.005 cm (0.002 inches) of silver would be required for the plating process. At $352/kg ($10/oz) the silver would cost $437 for a single mirror, and the cost of plating, rinse, cleaning and polishing would add another $200 per mirror. Thus, the cost of silver plating the secondary would be $637 or $266/$m^2$.

Vacuum depositing silver appears to be less expensive. Temiscal Corp., Concord, CA., estimated that depositing 1000Å of silver onto a fiberglass or metal substrate would cost ($21.50/$m^2$ or $2.00/$ft^2$). This cost includes cleaning, packaging and deposition of a silicon monoxide coating which would protect the silver surface from corrosion. Total cost for a mirror would be $50.00.

The two types of film considered, ECP-94 and ECP-300X were discussed in the section on the primary mirror. These films cannot withstand the maximum temperature that the secondary mirror is expected to reach.

c. Protective Coatings

To protect the deposited silver coating, a thin, transparent coating is required which will withstand weathering without discoloration or delamination, and which exhibits low dirt retention.

Two materials appear to have the required properties, Dow Corning (DC) 1-2577 conformal silicone coating, and a coating of inorganic oxides applied by the SOL-GEL process being developed and tested by SNLA.

The DC1-2577 is a transparent silicone resin which is flexible over a temperature range of -65°C to 200°C, has high resistance to moisture, and a light transmissivity of 92 percent. This material has two methods of cure, a room temperature cure and accelerated heat cure from 75°C to 100°C after addition of DC176 catalyst. The Shore D Durometer hardness with the heat cure is 39 points. According to the manufacturer this material weathers well (20 year life) and resists ultraviolet light and dirt accummulation.

Following the application of the silver reflective surface, the surface would be primed with Dow Corning's 1200 or 1204 primer. After evaporation of the solvent vehicle from the primer, Dow Corning's 1-2577 would be applied by a flow coating procedure resulting in a thickness of 1 to 2 mils. This results in a hard protective silicone surface. Although silicone coatings have a high moisture permeability coefficient, the silicon monoxide will protect the silver. The heat cured DC1-2577 has a water vapor transmission of 0.00345 gms/cm^2/cm. The 1-2577 will protect the reflective surface from abrasion by impinging dust as well as cleaning and handling operations. The application of the Dow Corning primer and coating is estimated at $2.50 per mirror for material and $28 for processing, for a total cost of $30.50 for a secondary mirror.

The SOL-GEL process is a coating technique which allows various inorganic oxides to be deposited on large surfaces at relatively low costs. In this process, glasslike macromolecules are formed in an alcohol solution at room temperature by chemical polymerization. Before the solution transforms to a stiff, amorphous gel, it can be diluted and applied to a surface by dipping, spraying, or other thin film coating technique. After drying, the porous gel coating is heated to convert it to a dense, transparent glass layer. Sandia is investigating the use of this process to protect the silver layer deposited on steel. Several parameters affect the properties and applicability of the coating including composition, thickness, firing temperature, firing time, and

firing atmosphere. Typical densification temperatures are 500°C to 600°C; however, some compositions densify at 400°C to 450°C. Processing at the higher temperatures will cause problems with aluminum mirrors due to softening and excessive deformation. Because this coating material is still in the development stage, material and processing costs are not available.

3. Structural Considerations

Approximate methods based on relations in reference 31 were used to determine deflections of the secondary reflector. The initial analysis assumed the secondary was formed from a single sheet of steel. Assuming the mirror is clamped around its outer periphery by a support ring which in turn is supported at three points, preliminary analysis indicates that based on stress, deflection, and vibration criteria, a steel shell 0.476 cm (3/16 in) thick is required. The thickness of the secondary could be reduced by adding stiffeners. However, this approach would increase manufacturing costs, and depending on the method of attaching the stiffeners to the mirror, may affect the optical quality of the mirror due to differential thermal expansion between the stiffeners and mirror.

Since no radiation is incident on the central region of the secondary mirror, an alternative design is to remove the central portion and fabricate the mirror in two sections. This allows fabrication of a higher quality mirror surface from narrower sheet stock, and minimizes thermal gradients and associated warping. The mirror can now be supported at the outer edge and around the center as shown in figure IV-8. The center support is hung from the apex of the main tripod support structure.

Deflection analyses were performed assuming fixed supports around the outer and inner edges of the mirror. Under operational wind loadings, the deflection was excessive for 0.0762 cm (30 mil) stainless steel. In order to achieve a slope error less than 4 milliradians due to wind loading, 16 radial hat section supports are required. However, 12-gage (0.266 cm or 0.1046 in thick) steel will have a slope error less than 4 milliradians with no additional supports.

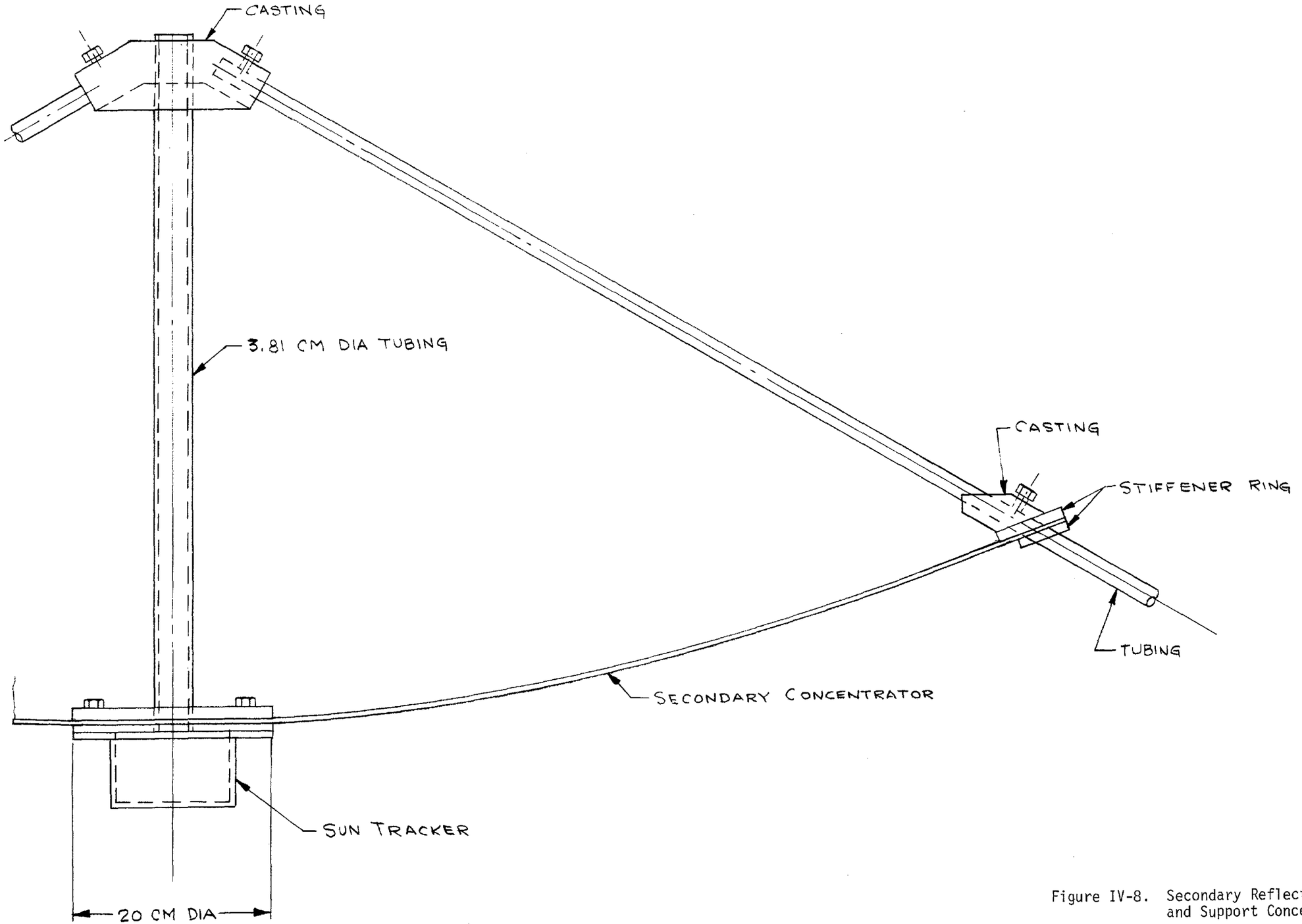

Figure IV-8. Secondary Reflector Stiffening and Support Concept

Using the material costs in table IV-3, 22-gage stainless steel costs $\$17.65/m^2$, so the cost of polishing is about $\$16.03/m^2$. Therefore, 12-gage polished steel would cost $\$83.47/m^2$ and weigh 48.7 kg (107 lbs). The 22-gage mirror would cost $\$33.68/m^2$ plus the cost of the supports, which is about $4.60 per mirror for material, and would weigh 22.3 kg (49 lbs). The cost difference between using thick and thin steel is $195 per mirror so that $7 per support can be allocated for fabrication of the supports and assembly of the supports to the mirror. Thus, it appears that using hat section supports, shaped in the manner described in the section on the primary mirror, and bonded to 22-gage polished steel is the least expensive alternative.

If aluminum were used as the mirror substrate, a sheet 0.381 cm (0.15 in) thick is required to limit the deflected to less than 4 milliradians without supports. This would increase the cost to $\$65.23/m^2$ for non-anodized ALZAX. If a 0.159 cm (0.0625 in) thick aluminum sheet were used, then twelve supports would be required.

Although it appears that thin sheet metal bonded to hat section supports is the least expensive, lowest weight, alternative, the question arises as to how to attach the supports to the sheet metal mirror without degrading the optical quality of the mirror. Boeing suggested using an acrylic structural adhesive (reference 30) and this appears to be an excellent solution. When using acrylic adhesives, great care need not be taken in cleaning the surfaces to be bonded (reference 35). At 94°C (200°F) the shear strength of Versilok 201 acrylic adhesive is still 2.5×10^6 kg/m^2 (3600 psi) when bonding unprepared steel surfaces (reference 36). General purpose acrylics can be cycled between -40 to 120°C (-40°F to 250°F) and posses sufficient flexibility to withstand different coefficients of thermal expansion. Acrylics can be formulated to withstand temperatures up to 205°C (400°F) and to have characteristics ranging from flexible to rigid (reference 33). Thus, it appears acrylic adhesive can be used to bond the supports to the secondary mirror to provide adequate strength under operational wind loadings, and without degrading the optical quality of the mirror due to differential thermal expansion between the mirror and supports.

TABLE IV-3. MATERIAL PRICES FOR PLATE AND SHEET

Material	Weight (kg/m^2)	Cost* ($/m^2$)	Cost* ($/kg)
Stainless Steel			
28 gage (0.389 mm/0.0153")	3.05	9.90	3.25
22 gage (0.777 mm/0.0306")	6.09	17.65	2.90
20 gage (0.935 mm/0.0368")	7.32	20.34	2.78
12 gage (2.66 mm/0.1046")	20.81	67.44	3.24
Plate (6.35 mm/0.25")	48.82	178.00	3.65
Carbon Steel Plate			0.57
Carbon Steel Sheet			
22 gage (0.777 mm/0.0306")	6.09	3.50	0.57
16 gage (1.56 mm/0.0613")	12.20	7.01	0.57
10 gage (3.50 mm/0.1379")	27.43	15.76	0.57
Aluminum			
20 gage (0.813 mm/0.032")	2.20	8.43	3.83
14 gage (1.63 mm/0.0641")	4.41	10.87	2.46
8 gage (3.26 mm/0.1285")	8.83	20.64	2.34

*Costs based on data from Engineering News Record

4. Summary and Recommendations

A summary of the various mirror concepts is provided in table IV-4. Further testing is required on these concepts to determine weathering and optical performance. However, the total solar reflectance of 1000Å silver deposited on aluminum, steel, or fiberglass should be about the same. GE reports 96.5 percent for silver on polished steel. The spectral reflectance is currently unknown; however, the spectral reflectance of polished steel is 95 percent of the total into 6 mr versus 81 percent for polished aluminum. Therefore, it appears that polished steel will provide improved performance, but at a slightly higher cost. In addition, the SOL-GEL process can be used with steel but is questionable for application to aluminum.

Based on these considerations, we recommend that polished steel be used as the secondary mirror structure with vacuum-deposited silver as the reflecting surface. Further testing is required to determine which protective coating would perform the best at lowest cost.

5. Cost Estimate of Selected Conceptual Design

In this section a detailed cost estimate and rationale is provided for the secondary mirror using a polished steel structure. A summary of the costs is shown in table IV-5, and the cost analysis is provided in the following sections.

a. Reflector

The cost of polished stainless steel was defined previously as $\$33.68/m^2$ for a total mirror cost of $77.80. Labor costs were estimated to be $3.85 per half of the secondary mirror using equation IV-2.

b. Stiffener

The raw material cost was estimated using equation IV-1 and assuming 0.68 kg per stiffener and low carbon steel. The labor costs were obtained using equation IV-2 for the stamping operation and assuming 250 units per hour production rate, and equation IV-3 for the stretch forming operation.

TABLE IV-4. PRELIMINARY COSTS OF SECONDARY MIRROR CONCEPTS

Mirror Construction	Cost ($/m^2)	Total Mirror Cost ($)	Tooling Cost
Polished steel (22 gage)	33.68		
Supports	2.00		
Stamping	21.80	204.60	
Vacuum-deposited silver	21.50		$300K
DC1-2577 coating	13.20		
Molded Fiberglass	86.10		
Vacuum deposited silver	21.50	289.40	$250K
DC1-2577 coating	13.50		
Soda lime glass	51.10		
Sagging and polishing	1,937.00	4,753.00	$300K
Silver deposition	0.54		
ALZAK	27.60		
Support	2.00		
Stamping	21.80	191.10	
Vacuum deposited silver	21.50		$300K
DC1-2577 coating	13.20		

TABLE IV-5. COST ESTIMATE SUMMARY FOR ONE-HALF OF THE SECONDARY MIRROR

COMPONENT	LABOR COST	MATERIAL COST
Reflector	3.85	38.90
Stiffener (9)	23.40	6.40
Spreader (8)	20.80	10.80
Spot Welding	5.20	-
Silver Deposition	23.90	-
Protective Coating	14.70	-
Adhesive Bonding	15.40	0.85
Subtotal	107.25	56.95
Contingency (10%)	10.70	5.70
Total	117.95	62.65

Recurring Cost: $0.70
Total Half Mirror Cost: $181.30
Total Mirror Cost: $362.60
Non-Recurring Die Cost: $300,000

c. Spreaders

Material cost was estimated using equation IV-1 assuming 1.3 kg per spreader and 8 spreaders per secondary mirror half. The labor costs were obtained using equations IV-2 and IV-3.

d. Spot Welding

Labor costs were estimated using equation IV-4 and assuming 36 spots per half mirror and 17 parts for handling.

e. Silver Deposition

Manufacturers estimates for vacuum deposition of silver was $\$21.50/m^2$ or \$23.90 for $1.11m^2$. This cost quote includes labor and materials.

f. Protective Coating

Manufacturer cost estimates for coating the silvered mirror with Dow Corning 1-2577 silicone were $\$13.20/m^2$ including labor and material.

g. Bonding

Labor cost estimates for bonding the secondary mirror to the stiffeners using acrylic adhesive were developed using equation IV-6. For an area of $0.028m^2$ per stiffener, the cleaning time is 4.5×10^{-4} hours and the adhesive application time is 9.9×10^{-3} standard hours per stiffener. Handling time is approximately 0.01 hours. Thus, labor cost for bonding is \$1.71 per stiffener or \$15.40 per half mirror. The volume of adhesive required per half mirror is $6.4 \times 10^{-5} m^3$ so the cost of adhesive is \$0.55 per half mirror. Using equation IV-1, the total material cost is \$0.85.

C. TERTIARY MIRROR

1. Thermal Analysis

The temperature distribution of the tertiary mirror was determined for the absorbed insolation shown in figure IV-9. This absorbed radiation distribution was determined with the COPS computer code assuming a 95 percent reflectivity on all the mirrors. As shown in

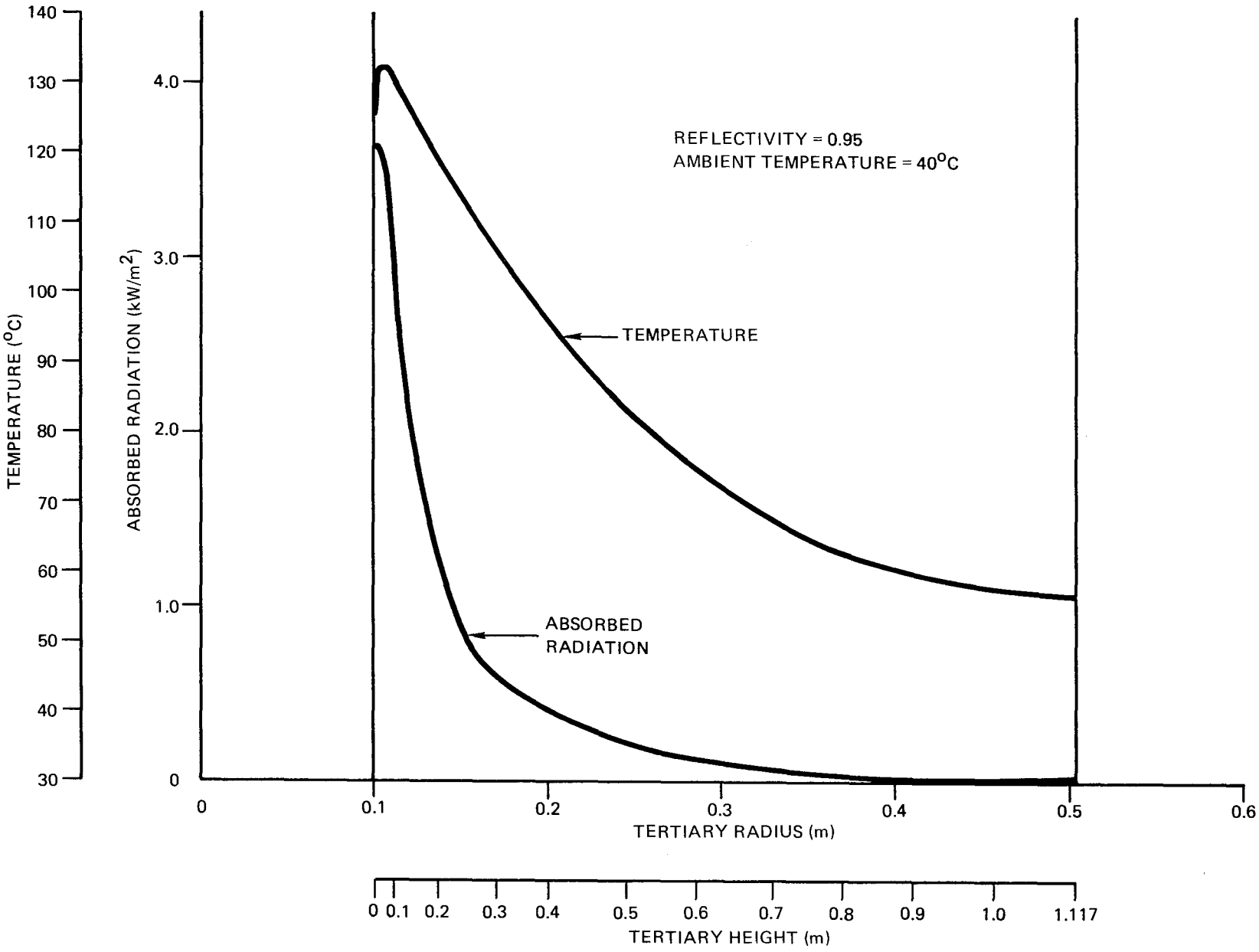

Figure IV-9. Absorbed Insolation and Temperature Distribution of the Tertiary Mirror

figure IV-9 the peak temperature searches about 132°C for an ambient temperature of 40°C. This temperature and distribution of insolation assumes perfect tracking, so that only the fringes of the beam reflected from the secondary are picked up and reflected into the receiver. Even small tracking errors can increase the intensity of radiation on the tertiary by 2 orders of magnitude. Just inside the outer radius of the receiver, the intensity rises rapidly to 500 kW/m^2 as shown in figure IV-10. Thus, to protect the tertiary it should be actively cooled through the use of tubes brazed onto the outer surface.

2. Material and Fabrication

Because the tertiary can reach excessive temperatures without adequate cooling, it must have a high reflectivity and high thermal conductivity. Since high optical performance, in terms of slope errors and specularity, does not seem to be required, the tertiary may be fabricated from ALZAK coated with 800-1000Å of vacuum-deposited silver. Because of the trumpet shape, the tertiary would be fabricated by a spinning process.

The cost of spinning 0.159-cm (1/16-inch) thick aluminum into the shape shown in figure IV-11 was estimated to be $88.00 per reflector by Metal Spinners, Inc., of Angola, Ind. One time tooling cost for a polished steel casting was quoted at $2800. A summary of the costs involved in fabricating the tertiary is provided in table IV-6.

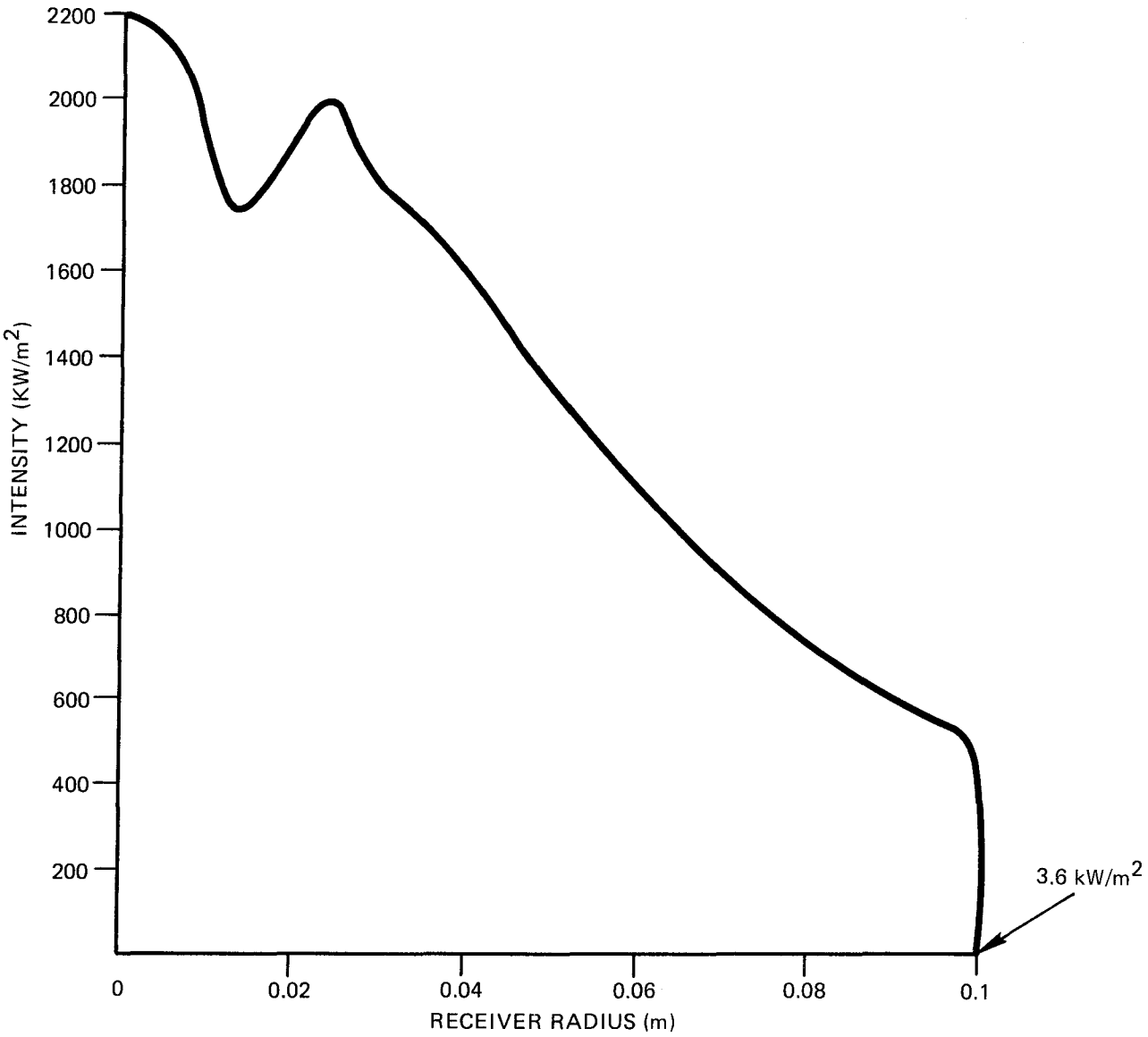

Figure IV-10. Intensity Distribution Across the Receiver Aperture

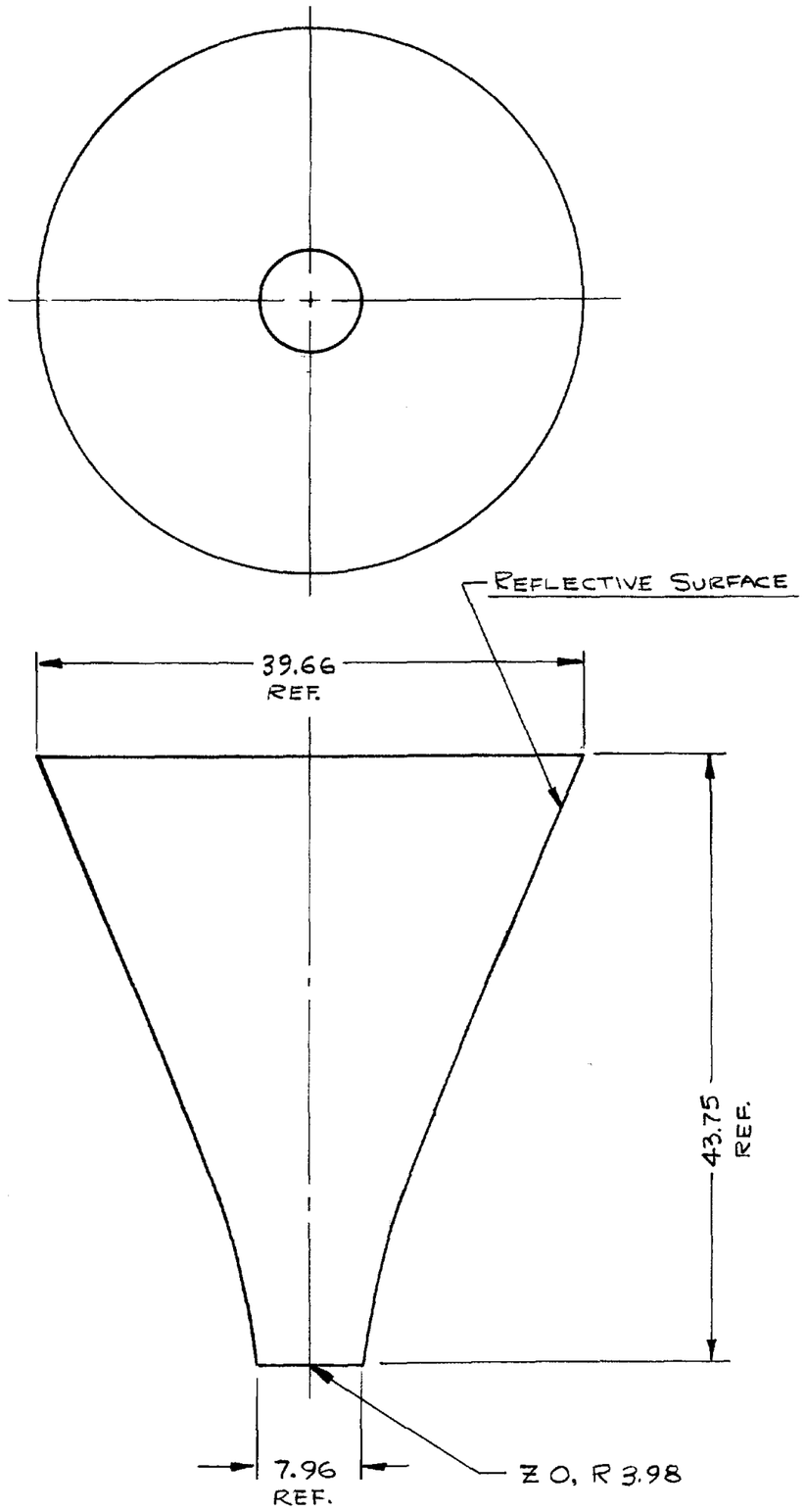

COORDINATES OF FORMED MIRROR (IN.)	
R	Z
3.98	0.00
4.12	2.40
4.51	4.80
5.10	7.20
5.83	9.60
6.65	12.00
8.93	18.00
11.37	24.00
13.90	30.00
16.47	36.00
19.07	42.00
19.83	43.75

Figure IV-11. Tertiary Configuration

TABLE IV-6. TERTIARY COSTS

Material	Unit Cost ($/m^2)	Total Mirror Cost
Unanodized ALZAK	27.55	57.30
Spinning	42.32	88.00
Vacuum-Deposited Silver	21.50	44.70
DC1-2577 Coating	13.20	27.50
TOTAL MIRROR COST		$217.50

CHAPTER V
STRUCTURAL ANALYSIS AND DESIGN

In this chapter, the structural requirements based on dead weight and wind loadings are determined for the Cassegrainian concentrator. These requirements are compared to the structural requirements for a receiver located at the focal point of the primary mirror. In addition, conceptual designs for attaching the receiver to the primary mirror and attaching the collector to the Shenandoah tracker are developed.

A. DESIGN CONSIDERATIONS

1. Codes and Standards

Building codes establish a minimum design for structures with the main concern being prevention of injury and loss of life. Design standards, such as AISC Steel Specification and ACI 318-77 Building Code Requirements for Reinforced Concrete, are structured so that designs will have a very low probability of failure when compared to the probability distribution of strength for the particular material. For new structural systems, especially those in the alternative energy field which do not involve human safety, the codes are not directly applicable and often impose unnecessary economic penalties; however, the codes can provide design guidance. For example, the ANSI code was used for determining wind loads, and the other two codes were used as design guides. However, most of the design was based on first principles.

2. Design Criteria

The main design criterion was to limit the angular deflection of the secondary reflector to $\pm$ 0.5 degrees under operating conditions. The operating condition was assumed to be a wind speed one half of the design wind speed for structures located in the Albuquerque area.

3. Wind Speeds and Forces

The ANSI code (reference 37) specifies a design wind speed of approximately 112.7 km/hr (70 mph) for Albuquerque. Table A-7 of the

same reference lists the extreme fastest mile wind speeds for Albuquerque along with the probability of their being exceeded in a given year. These speeds and occurrence probabilities are given in table V-1.

TABLE V-1. ANNUAL PROBABILITIES OF EXCEEDING A SPECIFIED WIND SPEED

Annual Probability of exceeding a wind speed of km/hr (mph)	0.04	0.02	0.01
	119.1 (74)	125.5 (78)	133.6 (83)

Based on 45 years of data, one standard deviation for the above probabilities is 4.8, 6.4, and 8 km/hr respectively. The fastest mile wind speed recorded was 136.8 km/hr (85 mph). An operating wind speed of 64.4 km/hr (40 mph), and a survival wind speed of 125.5 km/hr (78 mph) plus one standard deviation or 132 km/hr (82 mph) were chosen as baseline figures.

The basic wind force was calculated using ANSI A58.1 equation 3 which is:

$$q_z = 0.00482\ K_z\ (IV)^2 \qquad \text{(eq. V-1)}$$

where

q_z = wind pressure (kg/m^2) at height z
k_z = velocity pressure exposure coefficient
= 0.98 for exposure C at 9.15 meters (30 ft)
I = importance factor = 1.0
V = wind speed in km/hr

This equation was derived from the fundamental equation $p = \frac{1}{2}\rho V^2$ where

ρ = density of air.

Figure V-1 provides plots of basic wind pressure as a function of wind speed and height. The pressure loads are 21.5 kg/m^2 (4.4 psf) for V = 64.4 km/hr (40 mph) and 84.9 kg/m^2 (17.4 psf) for V = 128.7 km/hr (80 mph) at 7.62 meters (25 feet) above the ground.

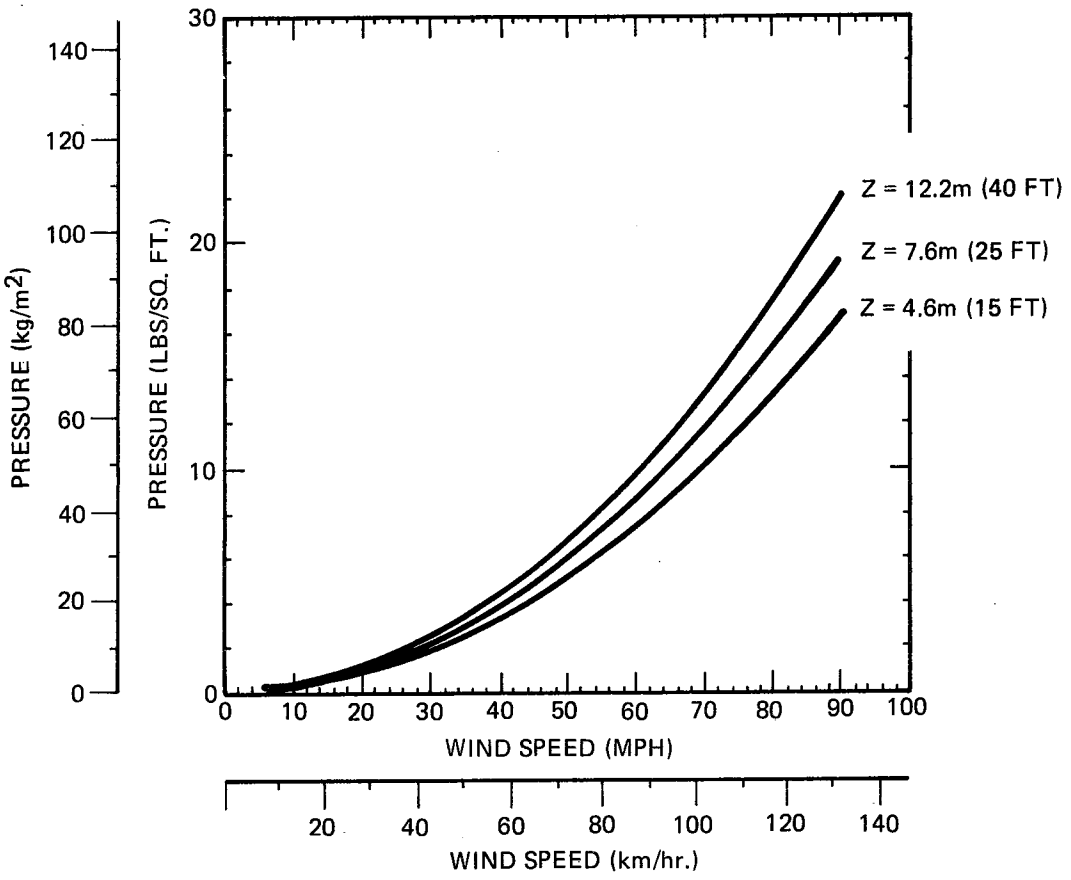

Figure V-1. Pressure Versus Wind Speed

4. Gust Factors

Basic wind pressure is modified by gust factors which take into account the type of structure as well as dynamic amplification factors for flexible structures. The equation used to determine the gust factor was taken from the ANSI A58.1 code. The gust factor for open framework structures is given by equation V-2.

$$\overline{G} = 0.65 + \frac{P}{\beta} + \frac{(3.32T_1)^2_S}{1 + 0.002\ C}^{1/2} \qquad \text{(eq. V-2)}$$

where

$\overline{G}$ = gust response factor for main force resisting system of a flexible structure

P = $1-(1-P_a)^n$ where P_a = annual probability of exceeding a given wind speed. This is the probability of exceeding design wind speed during n years

β = structural damping in percent (2%)

C = average horizontal dimension of the structure normal to the wind in feet

T_1 = exposure factor

$$T_1 = \frac{2.35\ (D_o)}{(7/30)^{1/\alpha}} \qquad \text{(eq. V-3)}$$

where

D_o = is the surface drag coefficient from ANSI A58.1 (table A-6)

α = power law coefficient from the same table

Plots of gust factors for different lifetimes versus the probability of the design wind speed being exceeded in a given year are shown in figure V-2. Figure V-3 shows plots of gust factors for different annual probabilities of occurrence versus the design lifetime. Table V-2 tabulates the plotted data. For this study, a design life of 50 years was assumed, with an annual probability of occurrence of 0.02 for a maximum wind speed of 125.5 km/hr (78 mph).

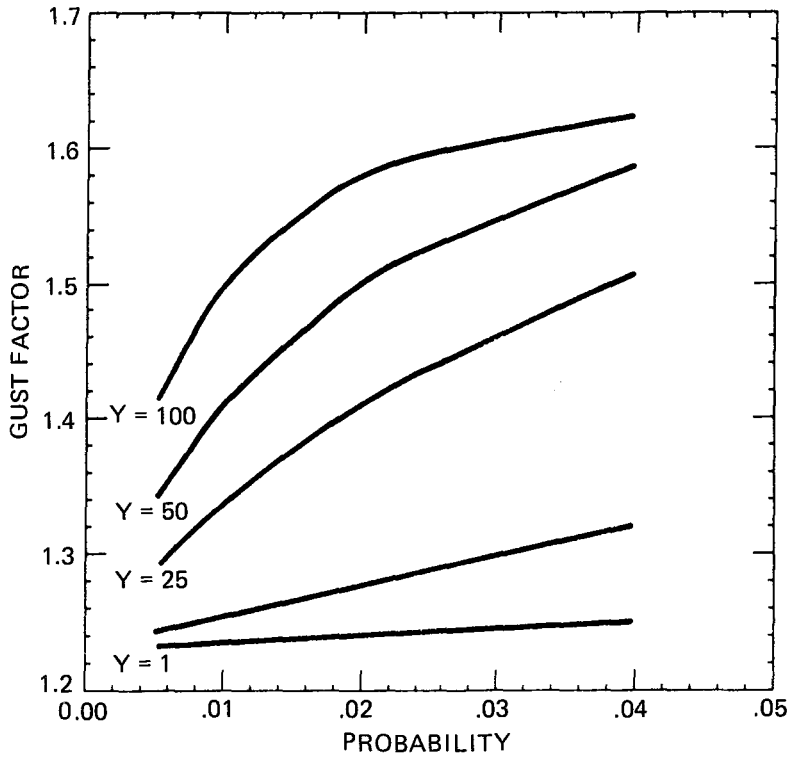

Figure V-2. Gust Factors as a Function of Design Period

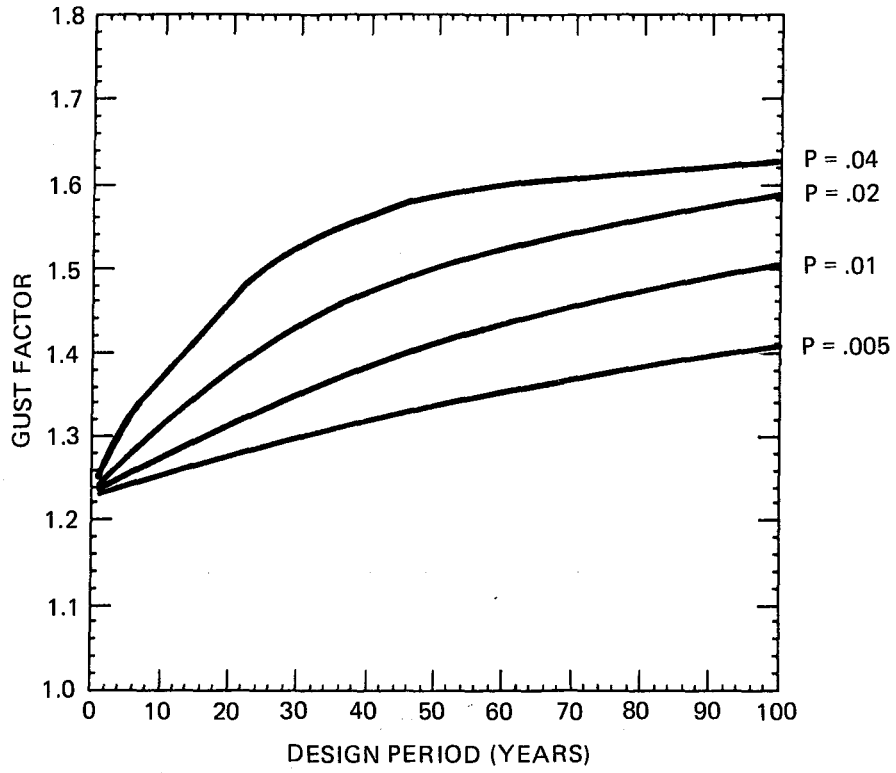

Figure V-3. Gust Factors as a Function of the Probability of Exceeding the Design Wind Speed

TABLE V-2. GUST FACTORS LISTED BY DESIGN PERIOD AND PROBABILITY OF OCCURRENCE

DESIGN PERIOD = 1 YEAR(S)

ANNUAL PROB.	PROBABILITY	GUST FACTOR
.04	.04	1.25
.02	.02	1.24
.01	.01	1.23
.005	.005	1.23

DESIGN PERIOD = 5 YEAR(S)

ANNUAL PROB.	PROBABILITY	GUST FACTOR
.04	.185	1.32
.02	.096	1.28
.01	.049	1.25
.005	.025	1.24

DESIGN PERIOD = 25 YEAR(S)

ANNUAL PROB.	PROBABILITY	GUST FACTOR
.04	.64	1.51
.02	.397	1.41
.01	.222	1.34
.005	.118	1.29

DESIGN PERIOD = 50 YEAR(S)

ANNUAL PROB.	PROBABILITY	GUST FACTOR
.04	.87	1.59
.02	.636	1.51
.01	.395	1.41
.005	.222	1.34

DESIGN PERIOD = 100 YEAR(S)

ANNUAL PROB.	PROBABILITY	GUST FACTOR
.04	.983	1.62
.02	.867	1.59
.01	.634	1.5
.005	.394	1.41

TABLE V-2. GUST FACTORS LISTED BY DESIGN PERIOD AND PROBABILITY OF OCCURRENCE (Concluded)

PROBABILITY OF ANNUAL OCCURRENCE = .04

NUM OF YEARS	GUST FACTOR	PROBABILITY
1	1.25	.04
5	1.32	.185
25	1.51	.64
50	1.59	.87
100	1.62	.983

PROBABILITY OF ANNUAL OCCURRENCE = .02

NUM OF YEARS	GUST FACTOR	PROBABILITY
1	1.24	.02
5	1.28	.096
25	1.41	.397
50	1.51	.636
100	1.59	.867

PROBABILITY OF ANNUAL OCCURRENCE = .01

NUM OF YEARS	GUST FACTOR	PROBABILITY
1	1.23	.01
5	1.25	.049
25	1.34	.222
50	1.41	.395
100	1.5	.634

PROBABILITY OF ANNUAL OCCURRENCE = .005

NUM OF YEARS	GUST FACTOR	PROBABILITY
1	1.23	.005
5	1.24	.025
25	1.29	.118
50	1.34	.222
100	1.41	.394

Therefore, based on these data, the design wind pressures are as follows:

$q_o = 1.51\ (21.5) = 32.4\ Kg/m^2$ (6.64 psf) operating

$q_s = 1.51\ (84.9) = 128.2\ Kg/m^2$ (26.3 psf) survival

The probability is 0.636 that these loads will be exceeded at least once in 50 years. The probability is less than 0.4 that the above design forces would be exceeded at least once in 25 years.

These pressures were translated into forces for two cases. Case 1 is for the plane of the secondary reflector parallel to the wind flow. Case 2 is for the plane of the secondary reflector perpendicular to the wind flow. The area against which the wind is acting for each case is shown in table V-3.

5. Drag Effects

The drag coefficient for case 1 is approximately 1.15 which is much less than the gust factor of 1.51. Therefore, the gust factored load will govern the design for this case. For case 2, the drag coefficient for a flat circular plate is between 1.96 and 2, (reference 38), using the drag factor results in a higher operating load (136 Kg or 300 pounds) and survival load (533 Kg or 1175 pounds). These two forces were used in sizing the structural supports for the secondary reflector.

TABLE V-3. WIND FORCES ON SECONDARY REFLECTOR

Case	Area	Operating Force Kg (pounds)	Survival Force Kg (pounds)
1	0.4 m^2(4.31 ft^2)	12.9 (28.4)	51.4 (113.4)
2	3.142 m^2(33.8 ft^2)	101.8 (224.4)	403.7 (890)

B. DESIGN CONSTRAINTS

A structure needs both adequate strength and stiffness to be functional. Strength is a function of the geometry (moment of interia), the cross-sectional area, and the yield or ultimate strengths of the material. Stiffness is a function of the modulus of elasticity, cross-sectional area and, geometry (moment of inertia).

The major design concern was elastic stability or buckling. The stability equation used to verify the adequacy of support diameter and wall thickness also considered the effects of a uniform lateral load on the strut, due to wind. This equation, taken from reference 39, is reproduced below:

$$S = \frac{5}{384}\frac{\omega \ell^4}{EI}\left[12\,\frac{(2\sec(u)-2-u^2)}{5u^4}\right] \qquad \text{(eq. V-4)}$$

where

ω = 2 qr

r = radius of support

q = wind pressure (lateral load on column)

ℓ = length

E = modulus of elasticity

I = moment of inertia

$$u = \frac{\ell}{2}\quad\frac{P}{EI} \qquad \text{(eq. V-5)}$$

where

P = axial load

Equation V-4 demonstrates that the material, through the modulus of elasticity, has a significant influence on the size of the structural members.

Table V-4 lists the properties for the six materials considered. PVC was considered because of its low cost and ready availability; however, its low modulus of elasticity made it unsuitable for this application.

Fiberglass and kevlar have approximately the same modulus of elasticity as the PVC. The fact that their modulus of elasticity is at least a factor of 3 lower than the remaining 3 materials: aluminum, graphite and steel, means that supports made from these materials will be thicker. This results in more shadowing and therefore less energy. Since the optimizing function is cost per unit of energy, lighter weight materials are not as important as low cost and minimum cross section. Consequently, steel and aluminum are the most likely candidates.

C. CONCEPTUAL DESIGN

A number of support concepts ranging from a single to a quadpod support were studied. These concepts, along with different support strut orientations are shown in figure V-4.

These arrangements were developed to emphasize specific structural behavior. Concept A has one strut (14) in tension with the bottom two struts, carrying both a compressive load from the weight of the secondary reflector and lateral wind loads. Concept B is the mirror image of A except for strut 24 which is in compression. The difference between concepts C and D is that in C struts 15 and 35 carry most of the secondary mirror weight while struts 25 and 45 support the lateral loads. The unistrut concept F was developed to minimize shadowing, however, the deflection requirements impose the need for guy wires.

After these preliminary concepts were developed, the effects of gravity loads due to the changing orientation of the receiver as it tracked the sun were studied. The effect of tracking and the changing direction of the load vector prevented designing the members for a single load condition.

TABLE V-4. PROPERTIES OF STRUCTURAL MATERIALS

Property	Units	MATERIAL					
		PVC	Kevlar Aramid/Epoxy Woven	Glass Fabric Epoxy	Aluminum 6061-T6	Graphite Epoxy int. Modulus	Steel A36
Tensile Modulus	Ksi GPa	1,100. 7.6	$(3.1\text{-}4.5)\times10^3$ 31	3,600 24	10,000	25,000 173	29,000
Tensile Strength	Ksi MPa	14 96	75 517	65 448	40	235 1620	50
Compressive Strength	Ksi MPa	12 83	12 83	55 379	--- ---	222 1515	--- ---
Flexural Strength	Ksi Mpa	21 145	50 345	85 585	--- ---	255 1755	--- ---
Density	Kg/m^3 lbs/cu.in	1,578 0.057	1,356 0.049	1,799 0.065	2,657 0.096	1,551 0.056	7,861 0.284
Thermal Conductivity	W/m^oK		0.21	0.24		1.15	16.7
Thermal Expansion	$x10^{-6}$ in/in/F $x10^{-6}$ cm/cm/^oC		0 0	5.9 10.6	12.6 2.31	---	6.5 1.17
Approximate Cost	$/$cm^3$	0.0027	0.054	0.016	0.0064	0.075	0.0045
	$/$in^3$	.0445	0.882	0.26	0.105	1.232	0.0737
	$/lb	0.78	18.00[1]	4.00[1]	1.12[3]	22.00[1]	0.26

Average for Mean Values

[1]Material cost only. Data obtained from phone quotes.

[2]Material cost only. Data from Engineering News-Record.

[3]Material cost only. Engineering News-Record Jan. 26, 1984, p. 36.

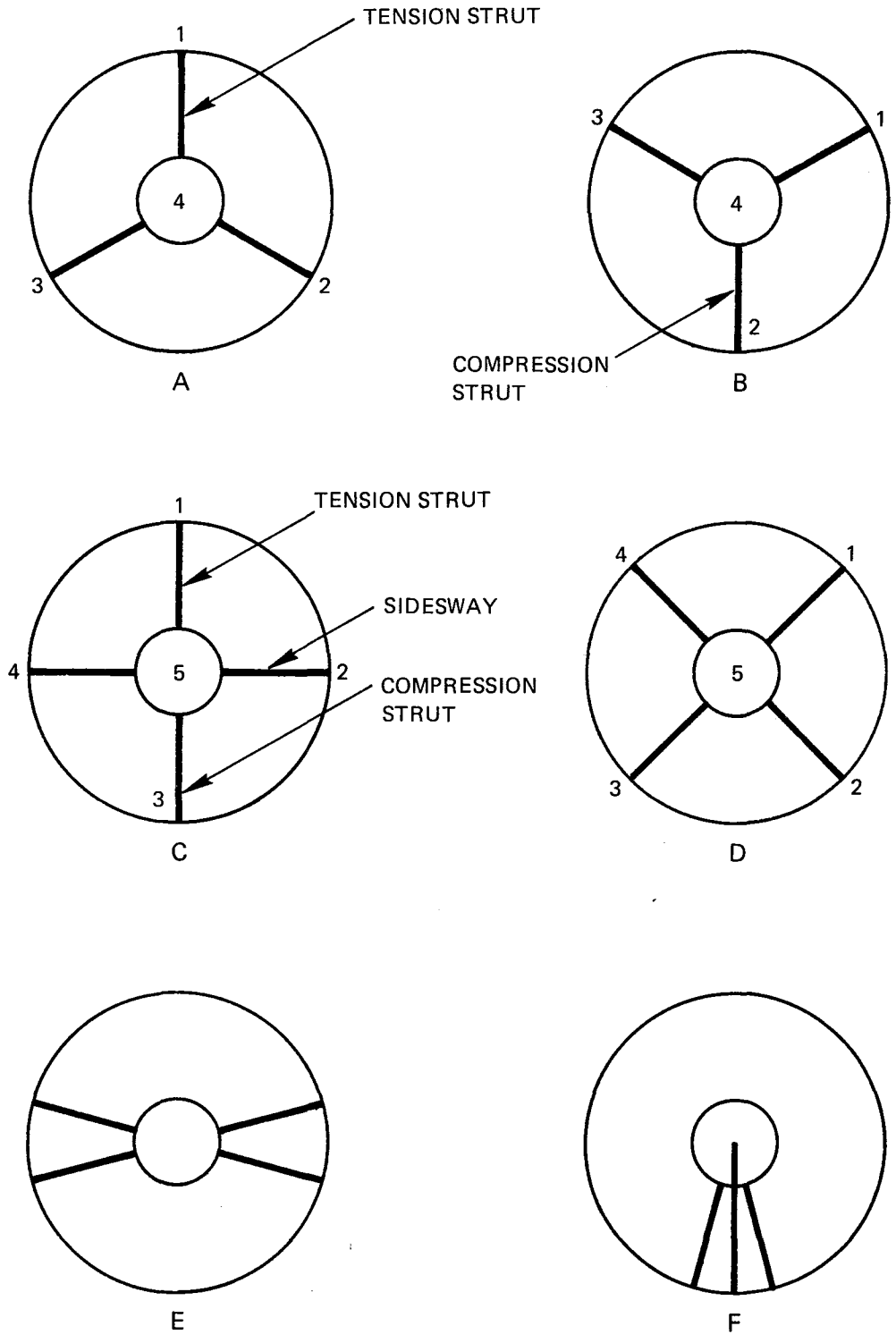

Figure V-4. Secondary Reflector Support Concepts

Some results of the preliminary analysis are presented in Tables V-5, V-6, and V-7. Table V-5 is a comparison of member sizes as a function of joint fixety for a tripod support configuration. The data indicate that a fixed joint allows a material weight savings of at least a factor of 2 or 3 over that of a simple support. The drawback is that true fixity is hard to achieve, and results in a more complex hence costlier design.

Table V-6 compares circular and rectangular shapes for a single support using deflection limits of $\delta \leq 0.635$ cm as the sizing criterion. While there is not much difference in weight, the rectangular cross section has a smaller blockage factor, i.e., a narrower section facing the sun.

Due to variations in the position and orientation of the collector caused by tracking, there is some question as to whether a single support is stiff enough. In addition, comparisons of the weight of the struts in tables V-5 and V-6 indicate that a single support weighs more than three struts in the tripod configuration. Thus, a tripod support was chosen for this phase of development.

The critical loading condition was taken to be a survival wind perpendicular to the secondary reflector. This induced an axial load in each support. In addition, the survival wind loading was applied laterally over the length of the supports. Elastic stability (buckling) governed the member selection. Table V-7 lists member sizes for the materials being considered. A fixed joint condition was assumed, justified in part by the fact that it would be possible to prevent first mode buckling by stiffening the struts in the middle, by producing tapered struts, or bracing the struts against one another. The latter would create a structural system stiffer than a single member. The first two columns contain support dimensions based on simple stability criteria for an axially loaded column. The third column gives member sizes for an axially loaded column with a lateral load. The sizing criterion was to limit deflection to less than 0.635 cm (1/4 inch).

TABLE V-5. TRIPOD SUPPORT DIMENSIONS AS A FUNCTION OF MATERIAL AND JOINT FIXITY

MATERIAL	ELASTIC MODULUS (GPa)	PINNED JOINTS SIZE (cm)	PINNED JOINTS WEIGHT (Kg/m)	FIXED JOINTS SIZE (cm)	FIXED JOINTS WEIGHT (Kg/m)
PVC	7.58	8.89 x 0.476	1.98	5.4 x 0.3175	0.95
KEVLAR	21.4	6.35 x 0.476	1.19	5.08 x 0.3175	0.64
FIBERGLASS	24.8	6.35 x 0.476	1.58	3.81 x 0.635	1.15
ALUMINUM	69	5.08 x 0.3175	1.29	3.81 x 0.159	0.49
GRAPHITE	172.4	3.81 x 0.3175	0.54	2.54 x 0.3175	0.34
STEEL	200	3.81 x 0.3175	2.74	2.54 x 0.3175	1.74

TABLE V-6. SINGLE SUPPORT DIMENSIONS AS A FUNCTION OF MATERIAL AND SHAPE BASED ON DEFLECTION CRITERIA AT $\delta \leq 0.635$ cm

MATERIAL	MINIMUM I DEFLECTION CRITERIA*	CIRCULAR CROSS SECTION (DIA x t cm) (cm^4)	WEIGHT (Kg/m)	RECTANGULAR CROSS SECTION	
				SIZE (cm)	Kg/m
PVC	1022.7	16.8 x 0.714	5.68	15.2 x 10.2 x 0.744	5.71
KEVLAR	363.0	12.1 x 0.635	2.92	12.7 x 7.62 x 0.476	2.43
FIBERGLASS	312.2	11.4 x 0.635	3.68	12.7 x 7.62 x 0.476	3.21
ALUMINUM	112.4	8.89 x 0.476	3.90	10.2 x 5.08 x 0.476	3.54
GRAPHITE	45.0	6.35 x 0.635	1.96	6.35 x 6.35 x 0.476	1.64
STEEL	38.7	6.35 x 0.476	8.62	6.35 x 6.35 x 0.476	8.32

*Minimum moment of inertia which allows the deflection criteria to be met.

TABLE V-7. SUPPORT DIMENSIONS TRIPOD CONCEPT

MATERIAL	STABILITY CRITERION SIMPLE SUPPORT SIZE (cm)	STABILITY CRITERION FIXED SUPPORT SIZE (cm)	DEFLECTION CRITERION $\delta \leq 0.635$ cm SIZE (cm)
PVC	0.635 x 6.35	1.27 x 3.81	0.794 x 11.43
KEVLAR	0.476 x 5.08	0.318 x 3.81	0.635 x 7.62
FIBERGLASS	0.318 x 5.08	0.318 x 3.81	1.11 x 6.35
ALUMINUM	0.318 x 2.54	0.318 x 2.54	0.635 x 5.08
GRAPHITE	0.635 x 2.54	0.159 x 2.54	0.476 x 3.81
STEEL	0.476 x 2.54	---	0.318 x 3.81

After examining the data in table V-7 and considering the fact that steel is the cheapest material, a steel tube 3.81 cm (1.5 inches) in diameter, with a wall thickness of 0.3175 cm (0.125 inches) is recommended as the best secondary mirror support. The weight of this support per meter is 1.74 Kg and costs approximately $0.57 per kilogram, therefore, the cost per support is $3.67 for a support 3.7 meters long.

Table V-8 compares the weight of the 3.7-meter-long tripod struts for the Cassegrainian system with the struts required to support a receiver at the focal point of the primary. As expected, heavy receivers would required much thicker supports; however, the supports for a 91 kg (200 lb) receiver would be about the same as those required to support the secondary mirror.

TABLE V-8. CONCEPT COMPARISON FOR TRIPOD SUPPORT CONFIGURATION

Secondary Tripod Fixed Support		Receiver Mounted at Primary Focal Point 126 kg Receiver		363 kg Receiver	
Weight (kg/m)	Cost ($/collector)	Weight (kg/m)	Cost ($/collector)	Weight (kg/m)	Cost ($/collector)
1.74	11.00	2.74	17.34	3.91	24.74

Conceptual details for attaching the tripod supports to the primary and secondary mirrors are shown in figure V-5.

D. RECEIVER MOUNT CONCEPTS

A concept of mounting the receiver to the primary mirror and to a tracker are shown in figure V-6. In this concept two main structual members provide attachment between the primary mirror and a torque tube. The distance between these members will depend on the size of the receiver. The receiver is located above the torque tube and between the structural members supporting the concentrator on the torque tube. This concept makes use of a single pylon, shown in figure V-7 and is adapted

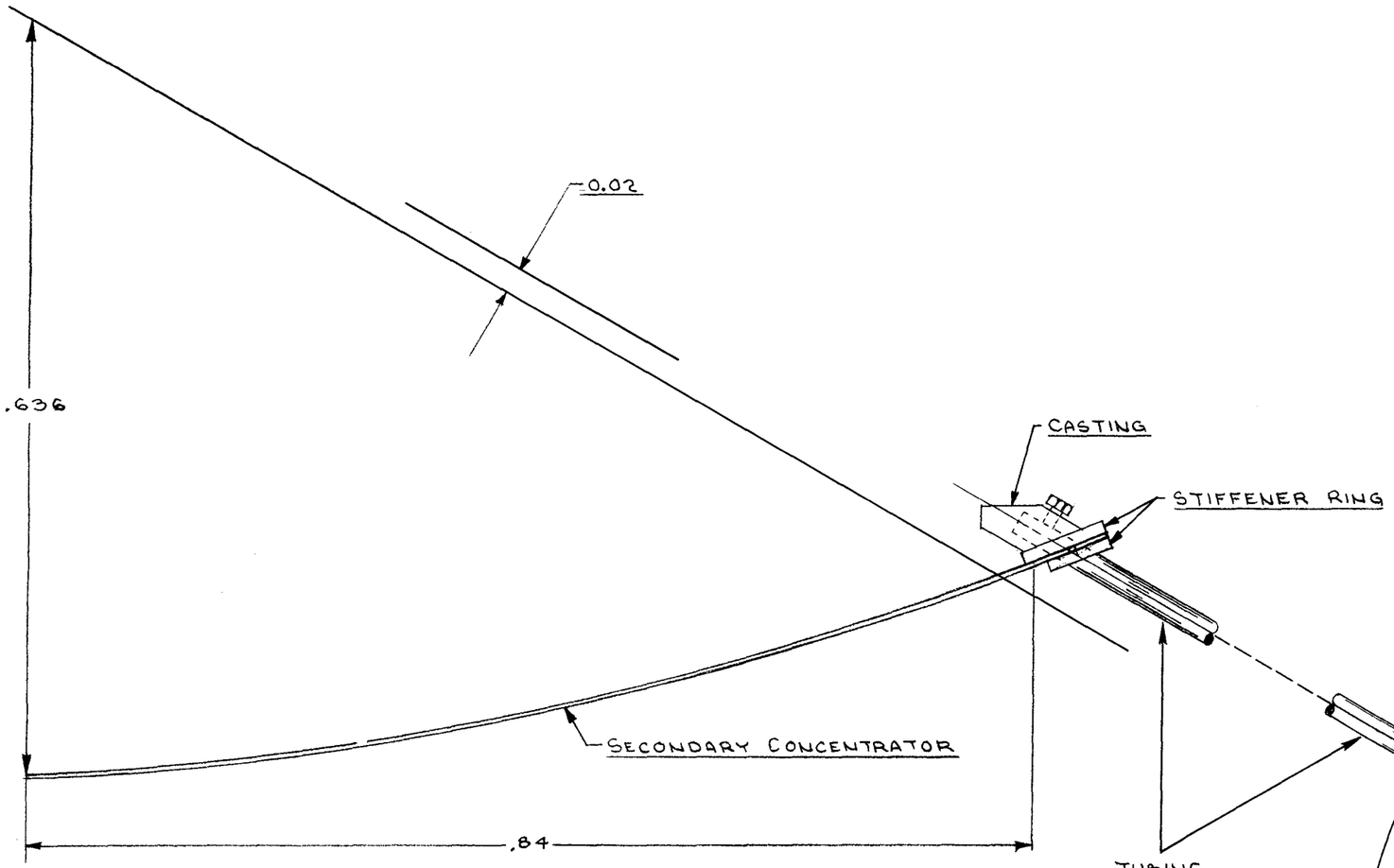

(NOTE: ALL DIMENSIONS ARE IN METERS)

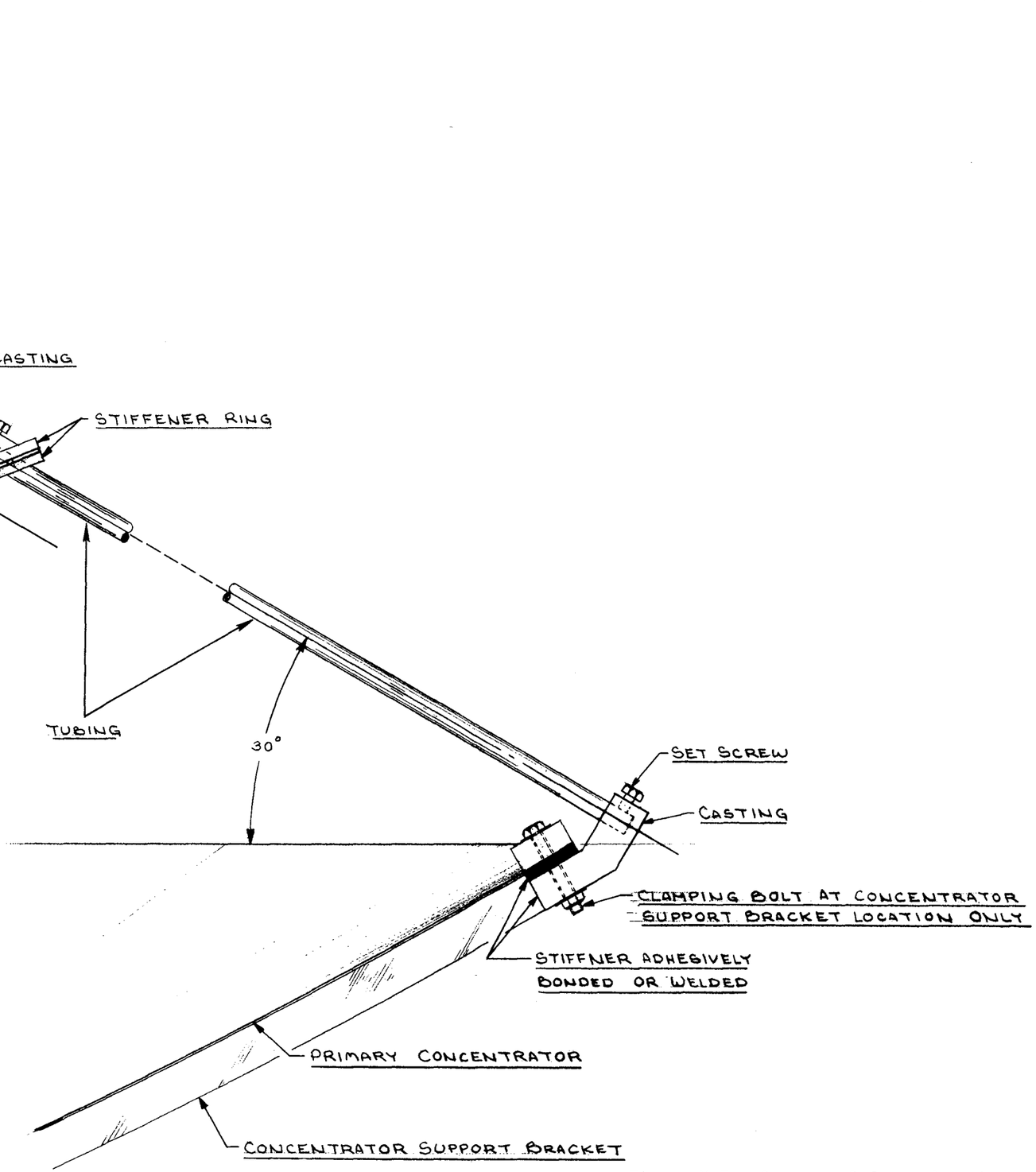

Figure V-5. Conceptual Strut Attachments

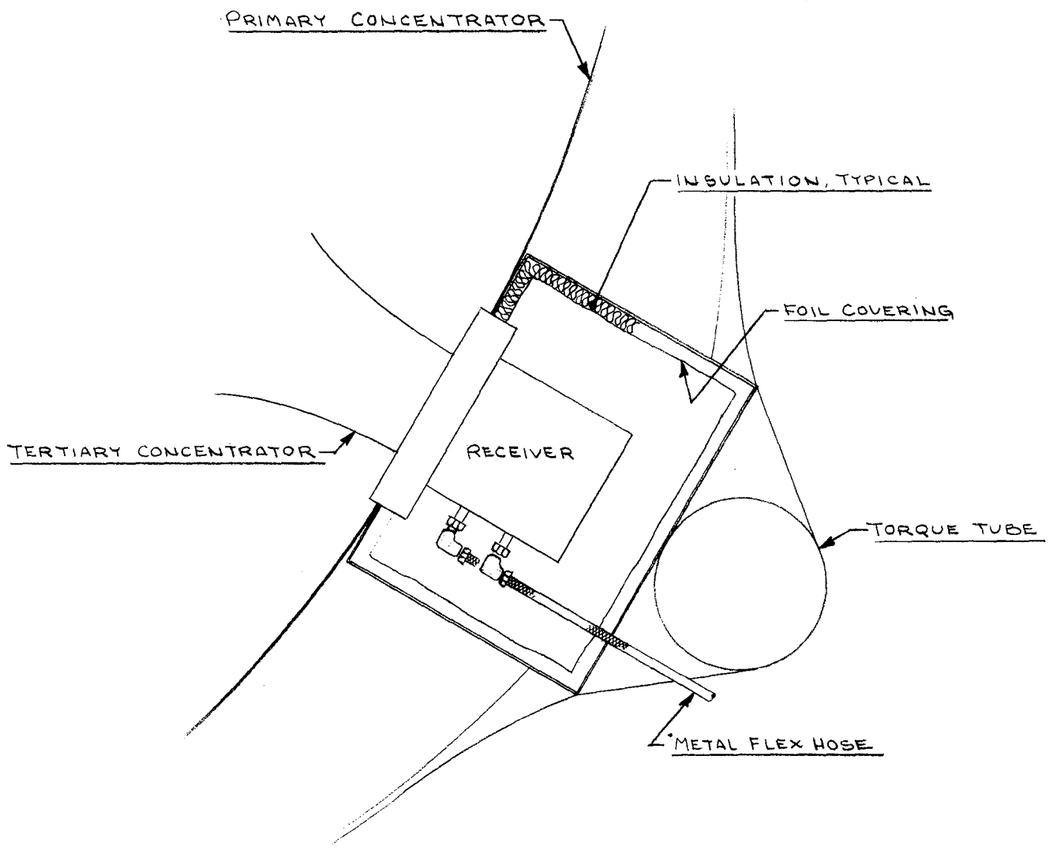

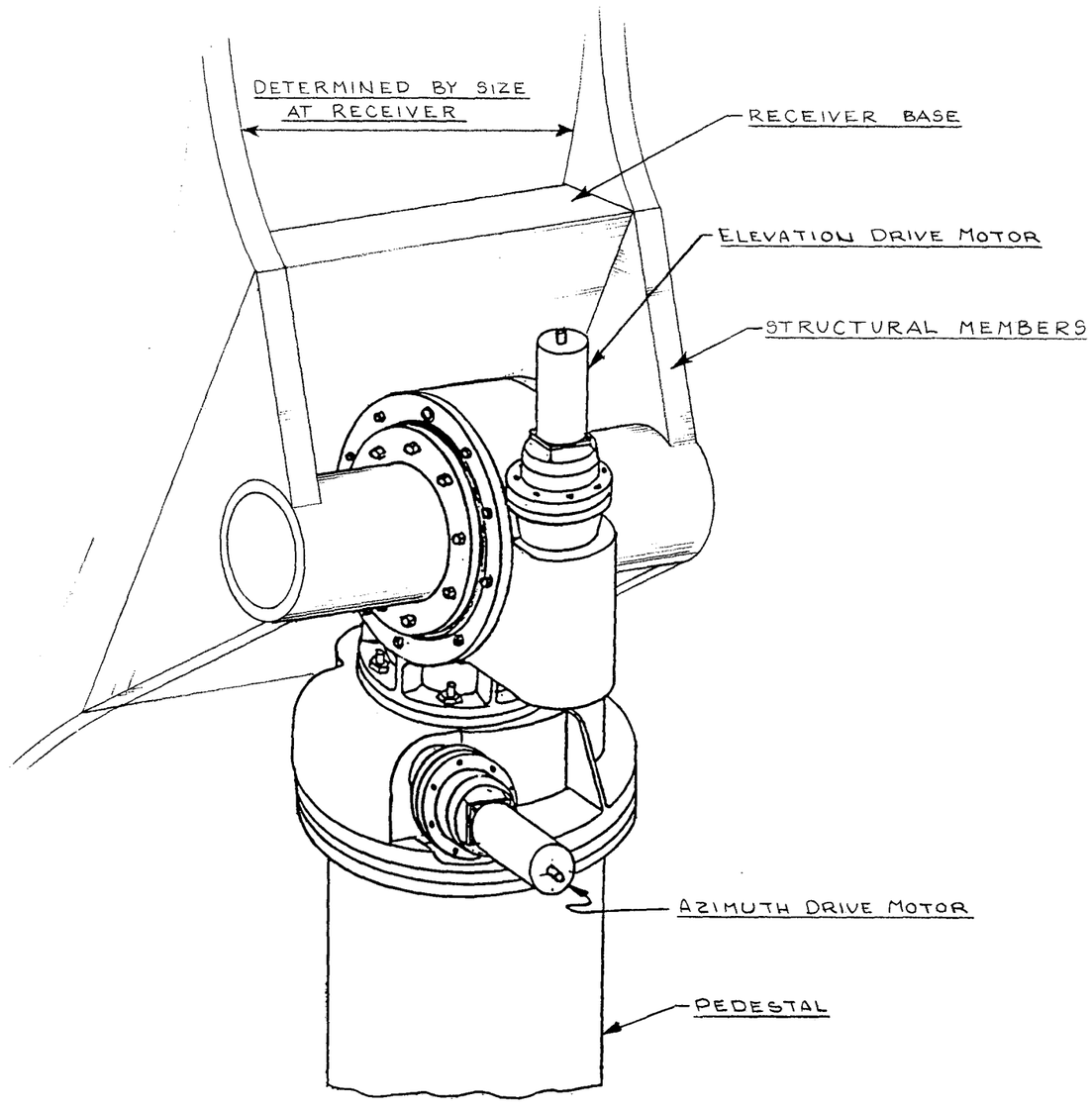

Figure V-6. Receiver to Tracking Mechanism Mounting Detail

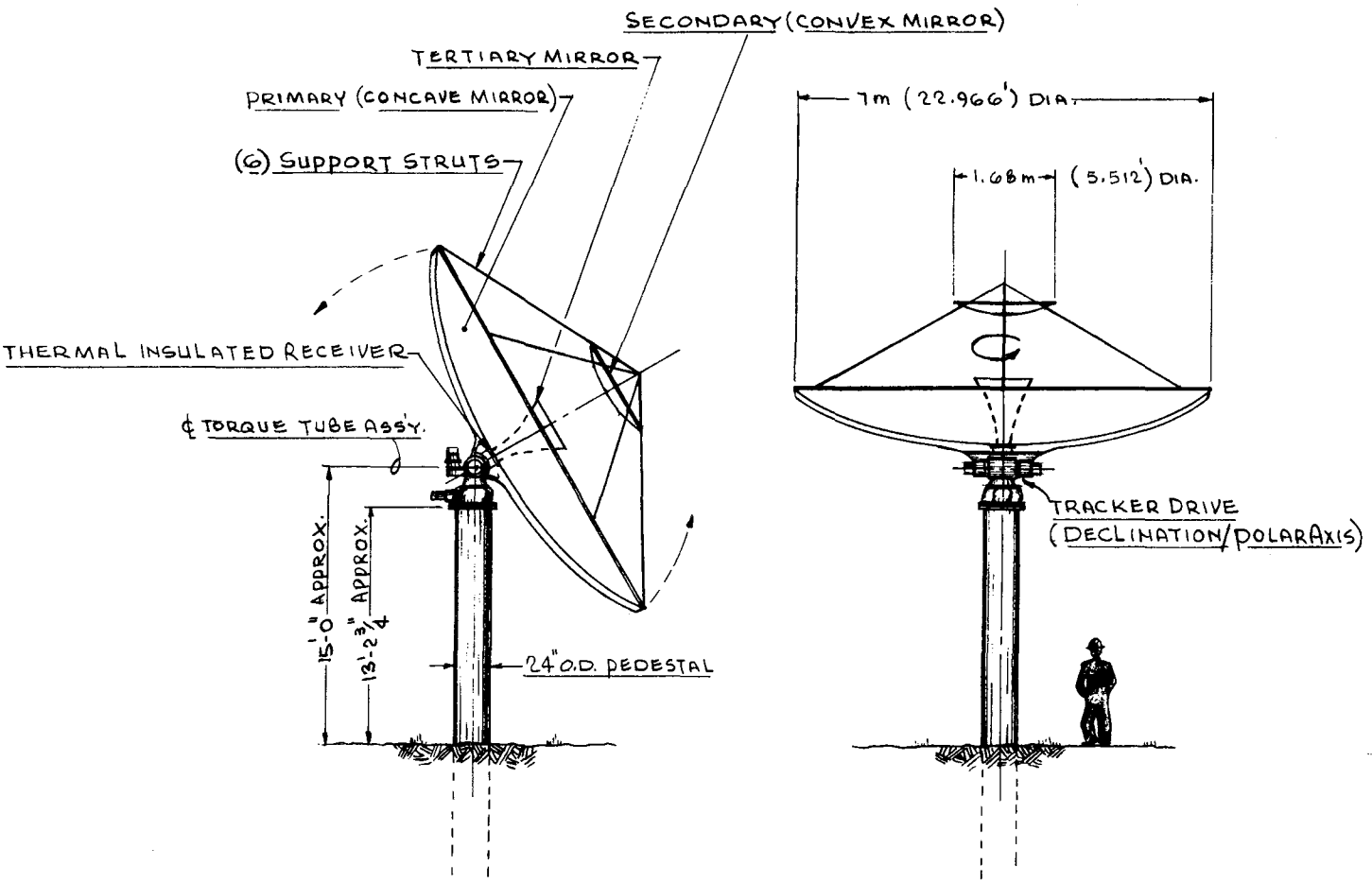

• 7 METER DIA. COLLECTOR •
(CASSEGRAINIAN CONFIGURATION)

Figure V-7. Pylon Support Concept

from the Northrup Heliostat study (reference 40). This single pylon concept minimizes material and labor for installation of the primary support. Based on data in reference 40, this support costs $1260 for a driven steel pipe pile.

Another support and tracker concept, shown in figure V-8, was used with the Shenandoah collector. In this concept, the major structural members attached to the primary mirror would fit between and be attached to the mounting points on the Shenandoah frame. A calorimeter or receiver can be attached to the primary at the system focal point for testing.

The receiver could be bolted to the base and structural members and to the primary mirror structure. If replacement is necessary, it could be unbolted and slid out between the structural members using a crane.

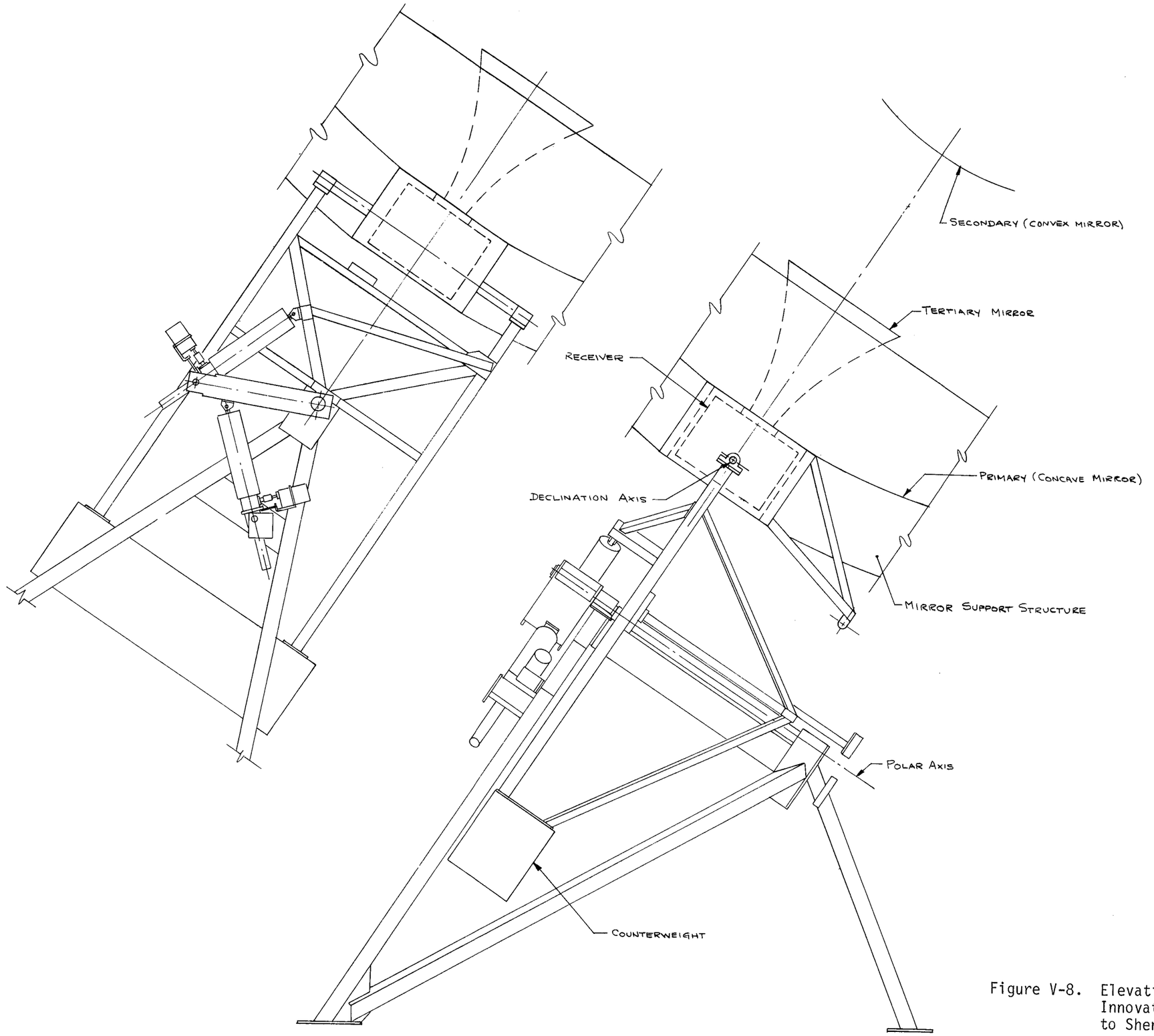

Figure V-8. Elevation Mounting Detail - Innovative Solar Thermal Receiver to Shenandoah Support

CHAPTER VI
SUMMARY AND RECOMMENDATIONS

A. SUMMARY

A Cassegrainian point focus solar concentrator system has been analyzed and a conceptual design developed. A Cassegrainian system with the receiver located at the vertex of the primary eliminates the limitations of receiver size and weight associated with a standard parabolic dish collector which has the receiver located at the focal point of the primary. However, the Cassegrainian system also has disadvantages such as increased reflection loss at the secondary mirror, and increased beam spreading associated with the longer focal length.

We have found that a non-imaging, trumpet shaped tertiary reflector located at the receiver aperture increases the system efficiency by 15 to 20 percent. The temperature of the secondary mirror may reach 110° C which eliminates consideration of reflective film as a mirror surface. We have recommended the use of thin (0.777mm thick) polished stainless steel, stamped into shape, as the mirror substrate, and vacuum deposited silver as the reflecting surface. A transparent coating will be required to protect the silver from the environment.

Both the secondary and the primary require radial supports on the back surface to minimize deflection under wind loading. The primary structure consists of eighteen 22-gage low carbon steel petals each stamped into the shape of a paraboloid. A reflective film, 3-m's ECP-300x, is recommended for the reflective surface.

A cost/performance analysis was performed for the Cassegrainian, standard parabolic dish collector, and a linear parabolic trough. A summary of the results is shown in table VI-1. At this point the cost of assembly of the supporting structure to the secondary mirror and primary mirror petals is not included in the costs. Also it is assumed that the cost of the primary mirror will be the same for the Cassegrainian and the standard dish collector.

TABLE VI-1. COST AND PERFORMANCE COMPARISON SUMMARY

Cost Item	Cassegrainian	PDC	LPT
Primary Mirror	2847.00	2847.00	
Secondary Mirror	362.60		
Secondary Support	11.00		
Testiary Mirror	217.50		
Receiver Support (126kg)		17.34	
Piping and Insulation		1794.00	
Total Cost per m^2 of Aperture	$89.33	$121.00	$110.80

STEADY STATE PERFORMANCE AND COST

		Cassegrainian		PDC		LPT	
RECEIVER TEMP ^oC	RECEIVER Dia.(m)	PERFORMANCE (kW/m^2)	COST ($/kW)	PERFORMANCE (kW/m^2)	COST ($/kW)	PERFORMANCE (kW/m^2)	COST ($/kW)
370	0.609	0.815	109.60	0.867	139.60		
370	1.22	0.811	110.15	0.833	145.25		
815	0.609	0.813	109.90	0.832	145.40		
815	1.22	0.809	110.40	0.791	153.00		
350	0.0318					0.63	$175.90

As seen in table VI-1, the efficiency of the Cassegrainian system is greater than that of the standard dish only at high operation temperatures and for large receivers. However, the cost per kilowatt into the receiver aperture is less for the Cassegrainian. This is primarily due to the high cost of piping and insulation running to the receiver of the standard disk. The cost of piping and insulation shown in table VI-1 includes material only, if labor were to be included, the cost of a standard dish would be even greater.

B. RECOMMENDATIONS

Based on this preliminary analysis of a Cassegrainian collector and the comparison with a standard parabolic dish, it appears that additional analysis and design of the Cassegrainian concept is warranted. There are four areas of additional effort which could lead toward improved performance and/or lower cost. These areas are:

(1) Receiver design
(2) Materials and manufacturing investigation and analysis
(3) Detailed structural analysis and design
(4) Optical design

1. Receiver Design

Because the Cassegrainian concentrator receiver faces upward, its thermal loss mechanisms may be significantly different than those encountered by a more conventional parabolic dish receiver. In particular, the convection losses may require more extensive reduction, and innovative techniques may be required to accomplish this reduction. Such techniques may include the use of a quartz window or an air curtain across the aperture.

The use of a window or air curtain may depend on the system application. For example, an air curtain could not be used in a large cavity, high pressure chemical reaction chamber. The application will also drive the requirements of the internal design. For example, internal reflective surfaces, or selective surfaces may be used to minimize radiative and convective losses.

The receiver should also be integrated with the tertiary reflector. Since the tertiary narrows the field of view for radiation losses, the receiver may be designed to use this factor to advantage. Also, since the receiver is deep within the tertiary, convection losses due to wind would be reduced.

Receiver design can be optimized through an engineering analysis and design effort. This work must be performed to continue the development of the Cassegrainian concept.

2. Materials and Fabrication

The secondary mirror is subject to higher fluxes than can be tolerated by conventional reflective films. Therefore, other materials and techniques must be used for the secondary. Several methods were discussed in chapter IV; however, testing of these methods is required to define optical performance and weatherability. A more detailed investigation of materials and cooling techniques for the tertiary reflector is also required. A materials program is required with Sandia performing the detailed optical and environmental tests. A scaled down prototype mirror system should be fabricated and tested on a two-axis tracker for performance and weatherability.

In addition to a materials study, fabrication techniques to minimize cost and surface errors need to be identified. We have suggested stamping for the primary and secondary, spinning for the tertiary, and radial supports applied to the back surface of the primary and secondary mirror with structural acrylic adhesive. This, and other concepts need to be investigated in more detail for cost, structural integrity, and attainable tolerances in order to continue the development of the Cassegrainian concept.

3. Structural Analysis and Design

A detailed structural analysis and design is required to define the minimum cost system and the minimum number of supports required. This would be coupled to the manufacturing analysis task to determine the lowest cost structure which meets the defined operational requirements. In addition, a detailed design of the interface between the mirror,

receiver, and tracking system would lead to the next step of prototype fabrication and test.

4. Optical Analysis

A second order Ritchey-Chretien Cassegrainian has been studied in this program, and no improvement in performance was noted. It is possible to generate higher order reflective surfaces, and thus reduce optical aberrations to a greater extent than was possible with the second order Ritchey-Chretien. A high order Ritchey Chretien could be designed using an optical design code such as ORS's CODE V. An optimized Ritchey-Chretien could be constructed with no more difficulty than a standard Cassegrainian, and could result in a higher concentration ratio for a given intercept factor, or it could reduce the size of the tertiary, slightly reducing the cost of the system. However, slope errors on the primary would still affect the peformance of the Cassegrainian, and will limit the gains possible by an improved optical design. An improved optical design is not critical to the deployment of a Cassegrainian concentrator.

REFERENCES

1. Novikov, V. V., Baranov, et al, "Cassegrain System Modified for Solar Concentrators," Geliotekhnika, Vol. 2, No. 5, pg 15-18, 1966.

2. Buzin, E. I., "Conical Concentrator with Point Focusing Secondary Reflector," Geliotekhnika, Vol. 4, No. 2, pg 25-31, 1968.

3. Umarov, G. Ya, et al, "Determining the Geometric Parameters of a Solar-Power Element Consisting of a Hyperboloid and Paraboloid of Revolution," Geliotekhnika, Vol. 9, No. 4, pg 39-43, 1973.

4. Kirgizbuev, D. A., et al, "Energy Distribution in the Concentration Field of a Solar Installation with a Hyperboloidal Counter-Reflector," Geliotekhnika, Vol. 10, No. 4, pg 13-19, 1974.

5. Zakhidov, R. A., et al, "Paraboloid-Hyperboloid Concentrating Systems and Their Accuracy," Geliotekhnika, Vol. 13, No. 1, pg 42-49, 1977.

6. Zakhidov, R. A., "General Principles of Multielement Concentrating System Design," Geliotekhnika, Vol. 14, No. 1, pg 22-29, 1978.

7. Zakhidov, R. A., et al, "Integrated Precision Parameter for a Cassegrain System," Geliotekhnika, Vol. 11, Nos. 3/4, pg 133-134, 1975.

8. Umarov, G. Ya, et al, "A Cassegrain System for Solar Radiation," Geliotekhnika, Vol. 12, No. 2, pg 68-69, 1976.

9. Alimov, A. K., et al, "Two-Mirror Unit with Plane and Hyperboloidal Counter-Reflectors," Geliotekhnika, Vol. 15, No. 3, pg 44-46, 1979.

10. Umarov, G. Ya, et al, "Investigation of Two-Mirror Systems Consisting of a Paraboloidal Mirror and an Inflated Film Reflector," Geliotekhnika, Vol. 4, No. 3, pg 62-66, 1968.

11. Cobble, M. H., et al, "Analysis of a Cassegrain Solar Furnace," SPIE Vol. 161, Optics Applied to Solar Energy IV, 1978.

12. Cobble, M. H., et al, "Concentration of Solar Energy Using a Cassegrain Type Solar Furnace," NMSU.

13. Mank, C. E., et al, "Optical and Thermal Analysis of a Cassegrainian Solar Concentrator," Solar Energy, Vol. 23, pg 157-167, 1979.

14. Bass, A. H., Schrenk, G. L., Poon, P.T.Y., Higgins, S. N., "Optical Analysis of Cassegrainian Concentrator Systems," ISES Proceedings, 1979 ISES/ASES Conference, pg 1261-1265.

15. McDanal, A. J., "Optical Analysis of Paraboloidal Concentrators with Secondary Reflectors," ISES Proceedings, 1979 ISES/ASES Conference, pg 1256-1260.

16. Vittitoe, C. N., "Users Guide to HELIOS-Computer Program for Modelling the Optical Behavior of Reflecting Solar Concentrators," SAND81-1180 and SAND81-1562.

17. Personal Communication, Optical Research Associates, Pasadena, CA.

18. Schrenk, G. L., "Analysis of Solar Reflectors-Mathematical Theory and Methodology for Simulation of Real Reflectors," Final Report, Contract AF04(695)-335, Allison Div., GMC, EDR 3693, 1963.

19. Personal Communication, Jim Monroe, LANL, 1983.

20. "Survey-Mirrors and Lenses and Their Required Surface Accuracy," Honeywell, Inc., DOE/CS/35348-T1.

21. Jones, R. T., "Coma of Modified Gregorian and Cassegrainian Mirror Systems," J. Opt. Soc. Am. Vol. 44, No. 8, 1954.

22. Wetherell, W. B., and Rimmer, M. P., "General Analysis of Aplanatic Cassegrain, Gregorian, and Schwarzschild Telescopes," Applied Optics, Vol. 11, No. 12, 1972, Erratum: Applied Optics, Vol. 13, No. 2, 1974.

23. Winston, R. and Welford, W. T., "Geometrical Vector Flux and Some New Non-Imaging Concentrators," J. Opt. Soc. Am. Vol. 69, No. 4, 1979.

24. O'Gallagher, J. and Winston, R., "Test of a 'Trumpet' Secondary Concentrator with a Paraboloidal Dish Primary," Enrico Fermi Institute, EFI Preprint #83-58, 1983.

25. Winston, R., and O'Gallagher, J. "Non-Imaging Secondary Concentrators," Fourth Parabolic Dish Solar Thermal Power Program Review, DOE/JPL-1060-58, 1982.

26. Atkinson, J. and Hobgood, J., "Advanced Solar Power System, Fifth JPL Parabolic Dish Solar Thermal Power Program Review, December 6-8, 1983, Indian Wells, California.

27. Dudley, V. E., Workhoven, R. M., "Performance Testing of the Solar Kinetics T-700A Solar Collector," SAND81-0984, 1982.

28. "Solar Total Energy Large Scale Experiment at Shenandoah, Georgia. Phase III Preliminary Design," Space Division, General Electric Company, ALO-3985-1, September 1978.

29. Kinoshita, G. S., "Development and Testing of the Shenandoah Collector," Parabolic Dish Solar Thermal Power Annual Review, Pasadena, California, January 1981, DOE/JPL 1060-46, May 1981.

30. Zimmerman, D. K., "A Conceptual Design Study of Point Focusing Thin Film Concentrators," The Boeing Co., Solar Systems Group, Boeing Engineering and Construction, Seattle, Washington, JPL Contract 955804, November 1981.

31. Roark, R. R., and Young, W. C., Formulas for Stress and Strain, 5th Edition, McGraw-Hill, N.Y., 1975.

32. Ostwald, Phillip B., The American Machinist Manufacturing Cost Estimating Guide (1983 edition) McGraw Hill, New York.

33. Fawcett, W. M. and York, L. J., Manhour Estimating Relationships for Fabrication of Aircraft Parts, ERR-FW-1604, General Dynamics Corporation, Fort Worth Division, December 1974.

34. Pettit, R. B. and Roth, E. P., "Solar Mirror Materials: Their Properties and Uses in Solar Concentrating Collectors," SAND79-2190, Sandia National Laboratories, Albuquerque, NM, June 1980.

35. Gordon, S., "Acrylic Structural Adhesives Cut Bonding Costs," Mechnical Engineering, Vol 105, No. 9, pp 60-65, September, 1983.

36. Hughson Lord Chemicals, Versilok 201 Data Sheet DS10-3102A, Erie, Pa.

37. American National Standards Institute," American National Standard Building Code Requirements for Minimum Design Loads in Buildings and other Structures", ANSI A58.1-1982.

38. -----, "Wind Forces on Structures, Final Report," ASCE Transactions, Vol. 126, part ii, 1961, paper 3269, pp. 1124-1198.

39. Timoshenko, S. P. and J. M. Gere, Theory of Elastic Stability, 2nd Edition, McGraw-Hill, N.Y.

40. Northrup, Inc., "Second Generation Heliostat Development for Solar Central Receiver Systems, Detailed Design Report," Volumes 1 and 2, Sandia Contract No. 83-2729E, May 1980.

APPENDIX A

The following plots are the results of the parametric study of the Standard Cassegrainian, and the Ritchey-Chretien configurations. For each rim angle and set of slope errors there are four plots. They are as follows:

(1) Integrated power into the receiver versus receiver radius,

(2) Intensity of solar radiation at the receiver versus receiver radius,

(3) Optical efficiency versus Z/F_p

(4) Intercept factor (IF_R) versus concentration ratio

Unless otherwise noted, each line plotted corresponds in position to the legend, i.e. in figure 1, the line that is highest from 0 to 4 cm corresponds to a Z/F_p value of 0.55. When it is not clear which line belongs to the parameters in the legend, explanatory lines are drawn to identify the curves.

Figures 1 through 44 show the results for the standard Cassegrainian, and figures 45 through 64 show the results for the Ritchey-Chretien (R-C) configuration.

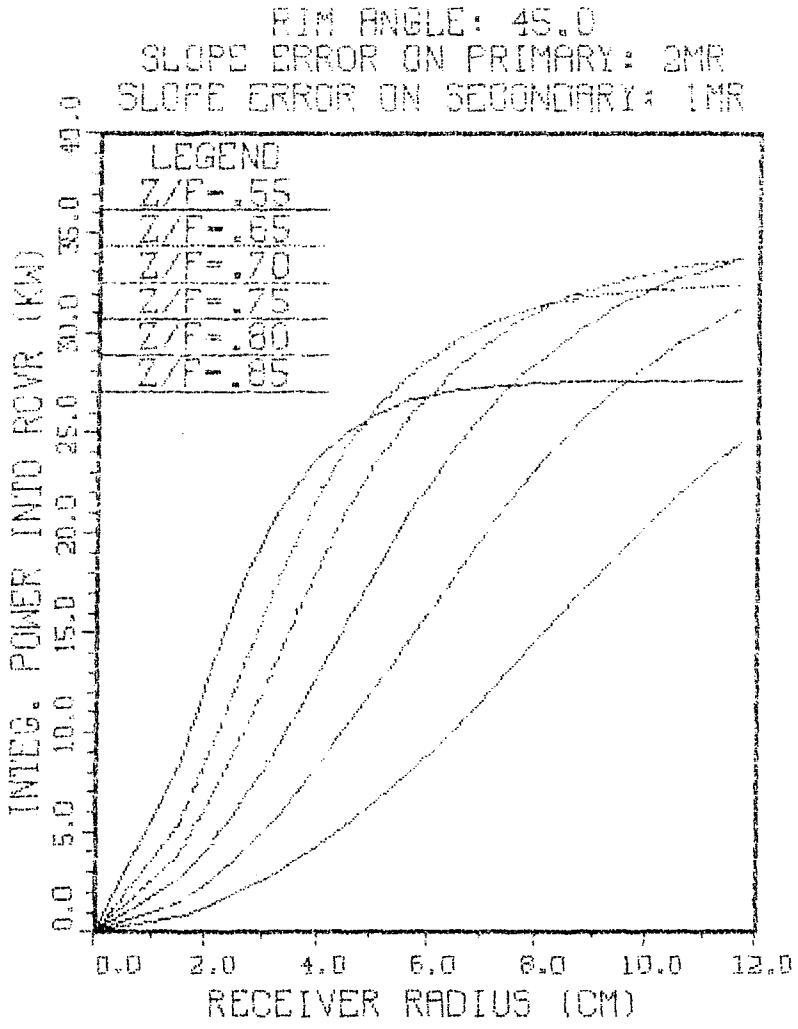
RIM ANGLE: 45.0
SLOPE ERROR ON PRIMARY: 2MR
SLOPE ERROR ON SECONDARY: 1MR
LEGEND
Z/F=.55
Z/F=.65
Z/F=.70
Z/F=.75
Z/F=.80
Z/F=.85
INTEG. POWER INTO RCVR (KW)
0.0
5.0
10.0
15.0
20.0
25.0
30.0
35.0
40.0
0.0
2.0
4.0
6.0
8.0
10.0
12.0
RECEIVER RADIUS (CM)

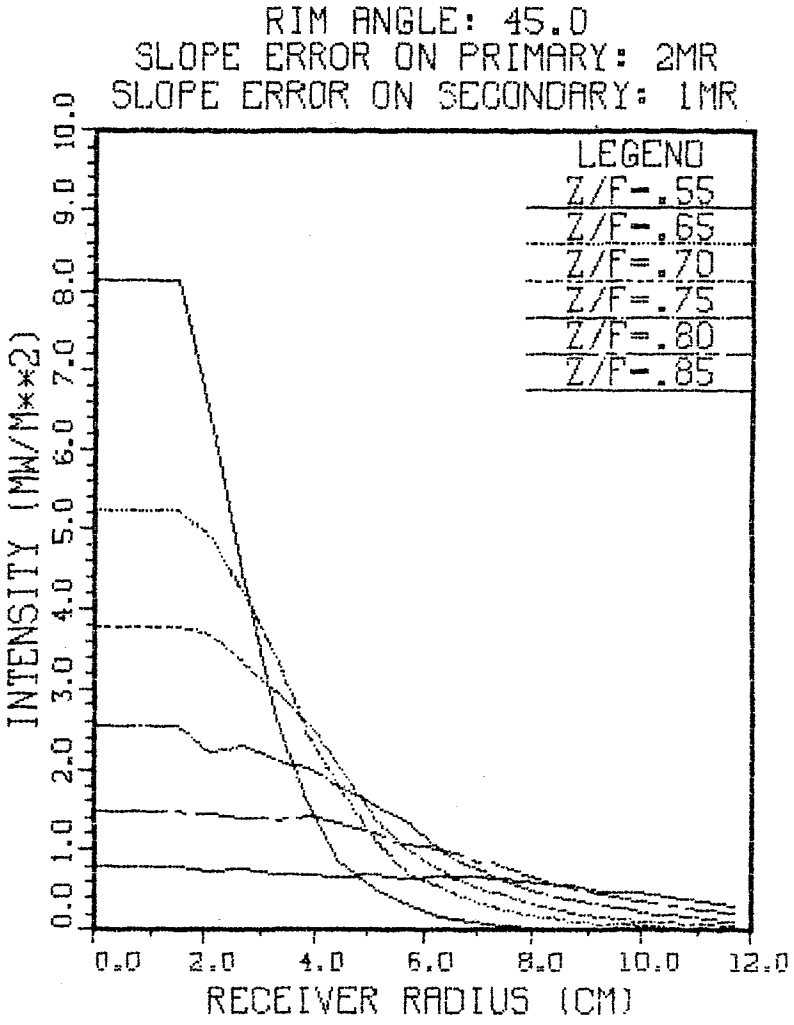
RIM ANGLE: 45.0
SLOPE ERROR ON PRIMARY: 2MR
SLOPE ERROR ON SECONDARY: 1MR
LEGEND
Z/F=.55
Z/F=.65
Z/F=.70
Z/F=.75
Z/F=.80
Z/F=.85
INTENSITY (MW/M**2)
0.0 1.0 2.0 3.0 4.0 5.0 6.0 7.0 8.0 9.0 10.0
0.0 2.0 4.0 6.0 8.0 10.0 12.0
RECEIVER RADIUS (CM)

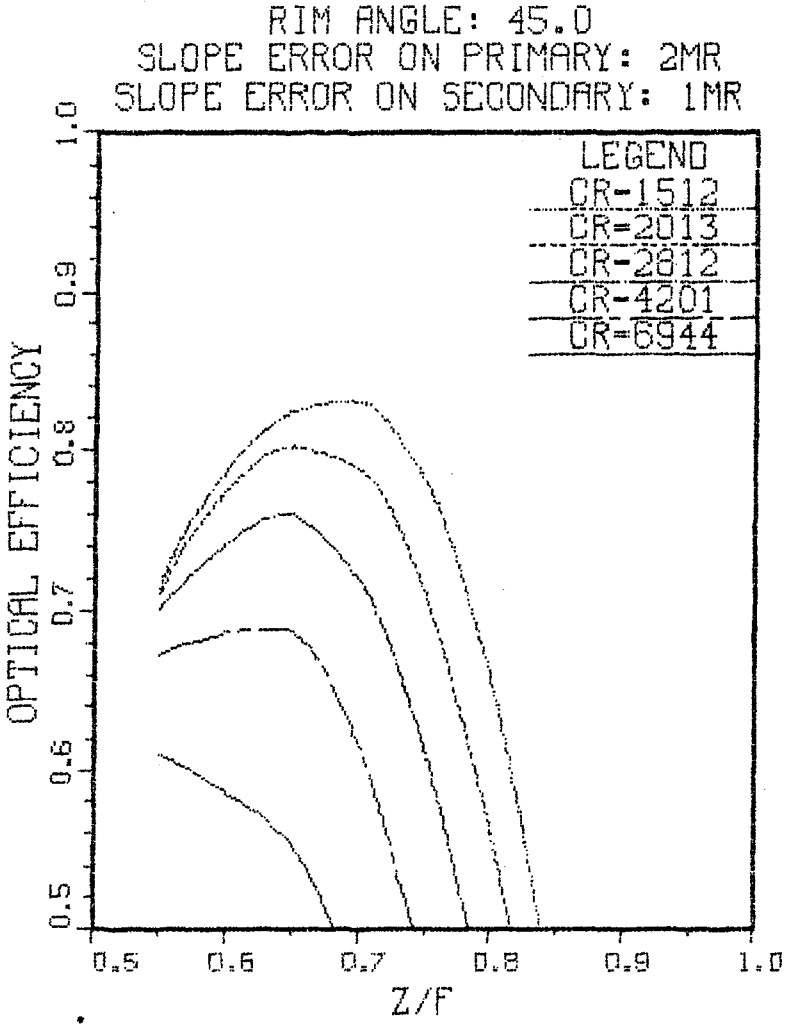
RIM ANGLE: 45.0
SLOPE ERROR ON PRIMARY: 2MR
SLOPE ERROR ON SECONDARY: 1MR
LEGEND
CR-1512
CR=2013
CR-2812
CR-4201
CR=6944
OPTICAL EFFICIENCY
1.0
0.9
0.8
0.7
0.6
0.5
0.5
0.6
0.7
0.8
0.9
1.0
Z/F

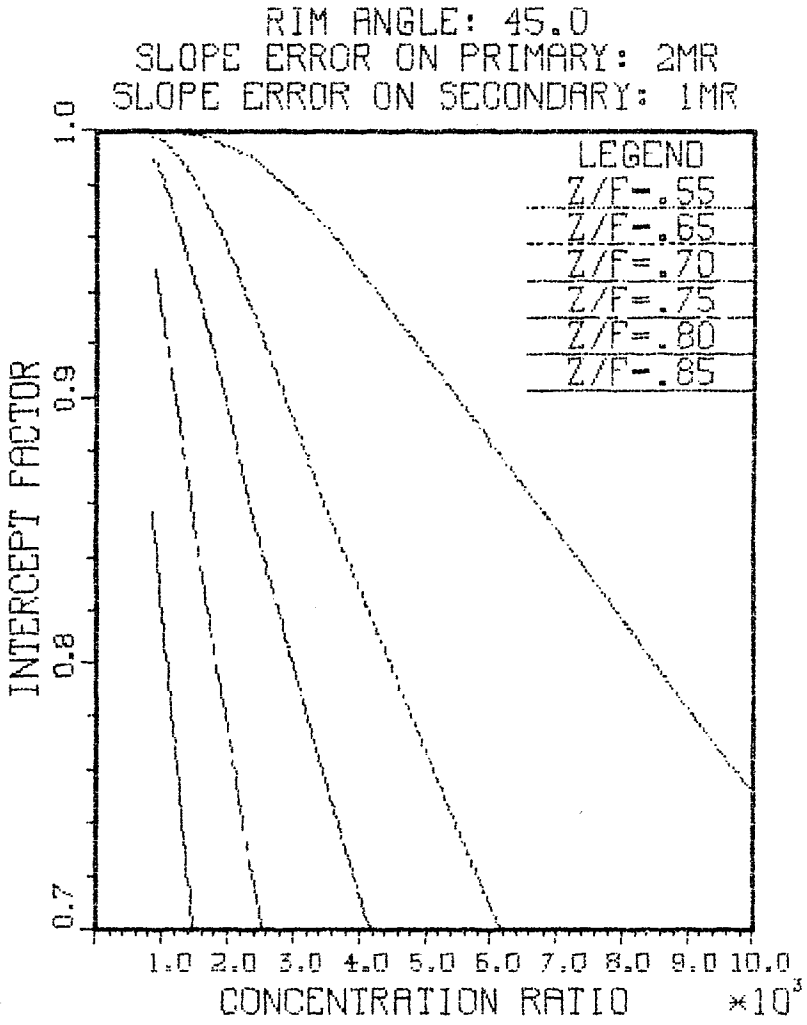
RIM ANGLE: 45.0
SLOPE ERROR ON PRIMARY: 2MR
SLOPE ERROR ON SECONDARY: 1MR
LEGEND
Z/F=.55
Z/F=.65
Z/F=.70
Z/F=.75
Z/F=.80
Z/F=.85
INTERCEPT FACTOR
1.0
0.9
0.8
0.7
1.0 2.0 3.0 4.0 5.0 6.0 7.0 8.0 9.0 10.0
CONCENTRATION RATIO
×10³

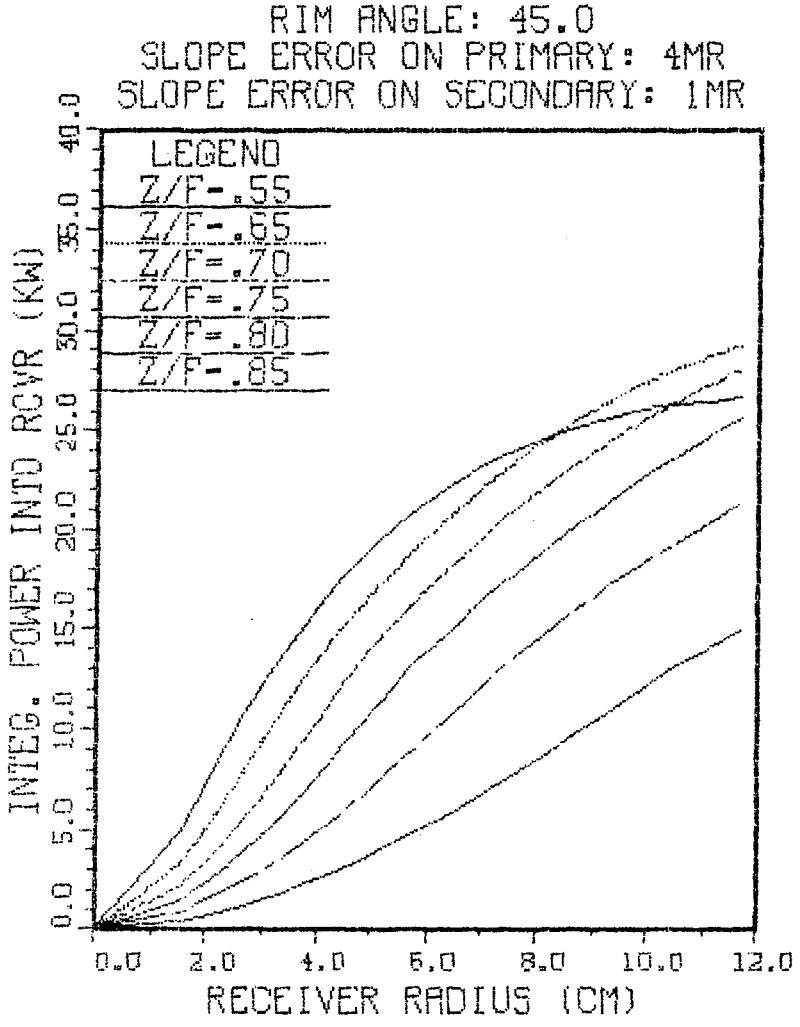
RIM ANGLE: 45.0
SLOPE ERROR ON PRIMARY: 4MR
SLOPE ERROR ON SECONDARY: 1MR
LEGEND
Z/F=.55
Z/F=.65
Z/F=.70
Z/F=.75
Z/F=.80
Z/F=.85
INTEG. POWER INTO RCVR (KW)
0.0
5.0
10.0
15.0
20.0
25.0
30.0
35.0
40.0
0.0
2.0
4.0
6.0
8.0
10.0
12.0
RECEIVER RADIUS (CM)

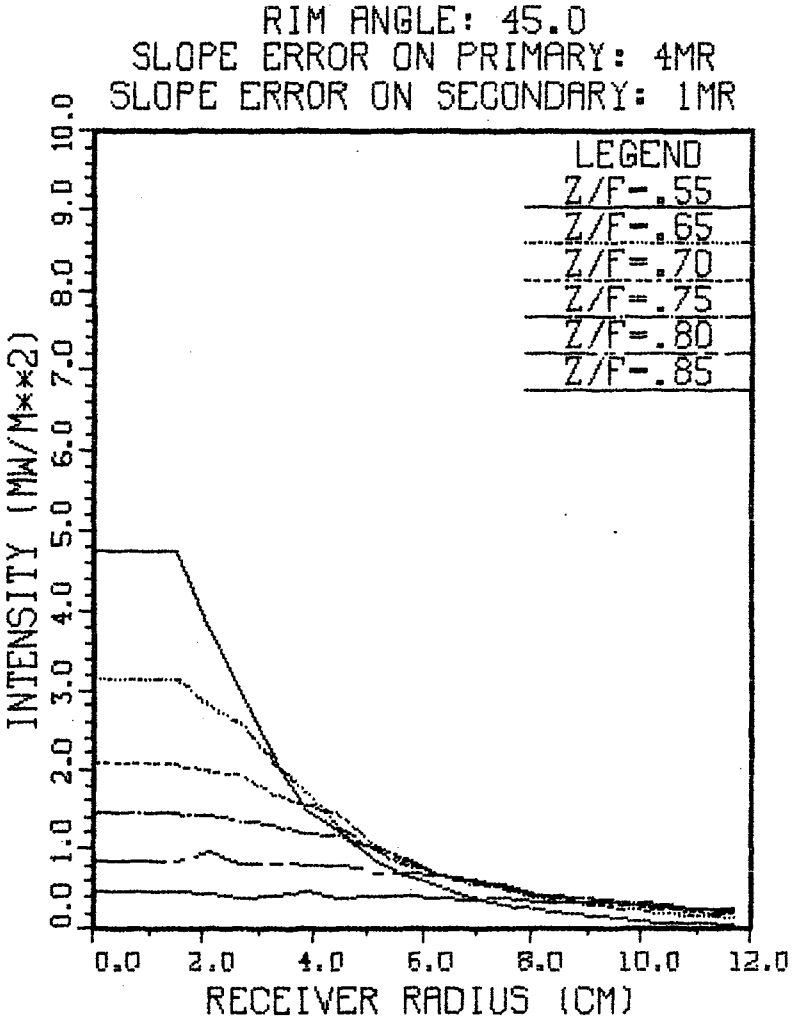
RIM ANGLE: 45.0
SLOPE ERROR ON PRIMARY: 4MR
SLOPE ERROR ON SECONDARY: 1MR
LEGEND
Z/F=.55
Z/F=.65
Z/F=.70
Z/F=.75
Z/F=.80
Z/F=.85
INTENSITY (MW/M**2)
0.0 1.0 2.0 3.0 4.0 5.0 6.0 7.0 8.0 9.0 10.0
0.0 2.0 4.0 6.0 8.0 10.0 12.0
RECEIVER RADIUS (CM)

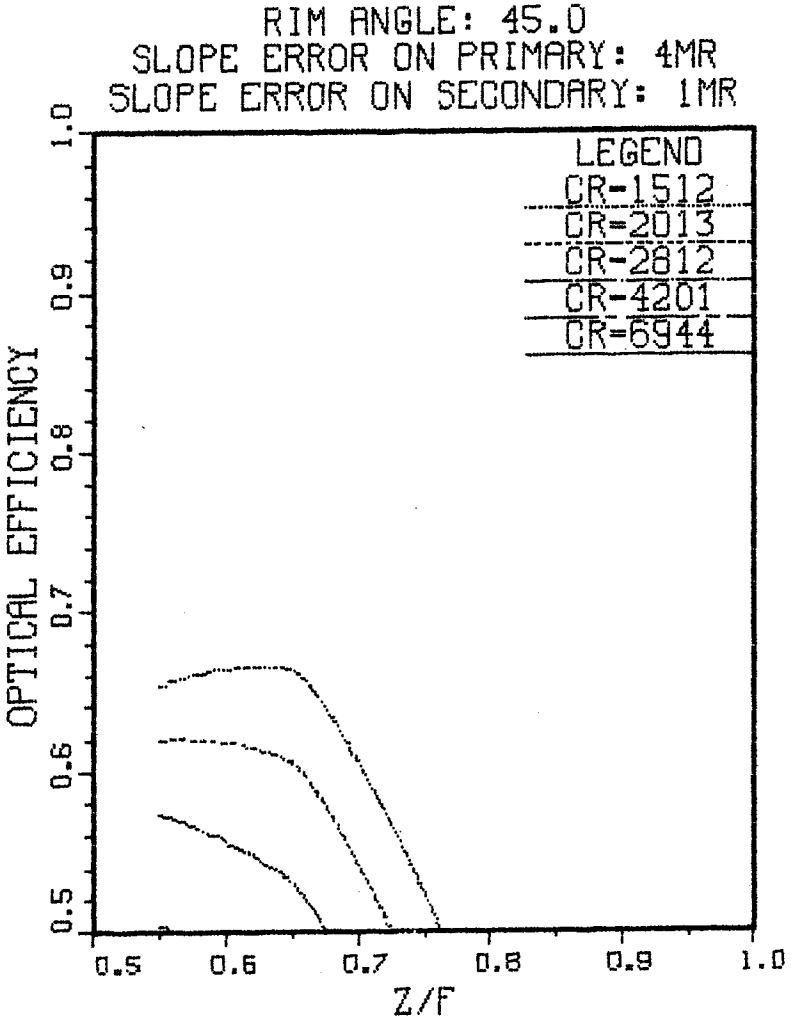
RIM ANGLE: 45.0
SLOPE ERROR ON PRIMARY: 4MR
SLOPE ERROR ON SECONDARY: 1MR
LEGEND
CR-1512
CR=2013
CR-2812
CR-4201
CR=6944
OPTICAL EFFICIENCY
0.5
0.6
0.7
0.8
0.9
1.0
Z/F

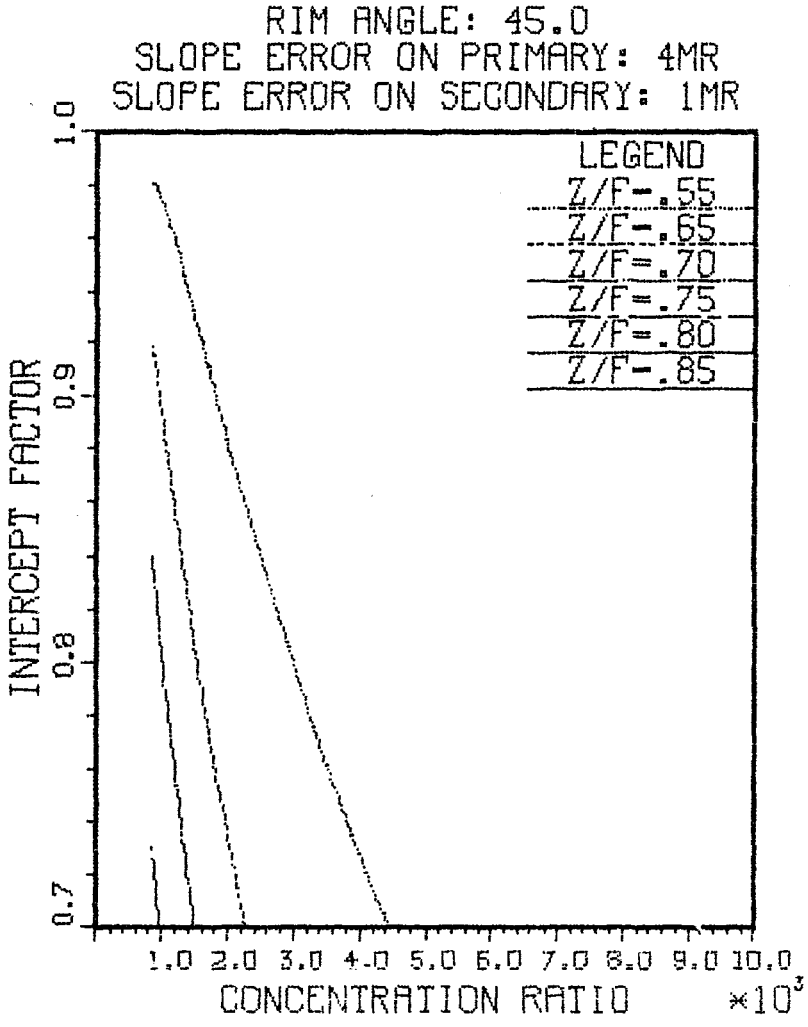
RIM ANGLE: 45.0
SLOPE ERROR ON PRIMARY: 4MR
SLOPE ERROR ON SECONDARY: 1MR
LEGEND
Z/F=.55
Z/F=.65
Z/F=.70
Z/F=.75
Z/F=.80
Z/F=.85
INTERCEPT FACTOR
1.0
0.9
0.8
0.7
1.0 2.0 3.0 4.0 5.0 6.0 7.0 8.0 9.0 10.0
CONCENTRATION RATIO
*10³

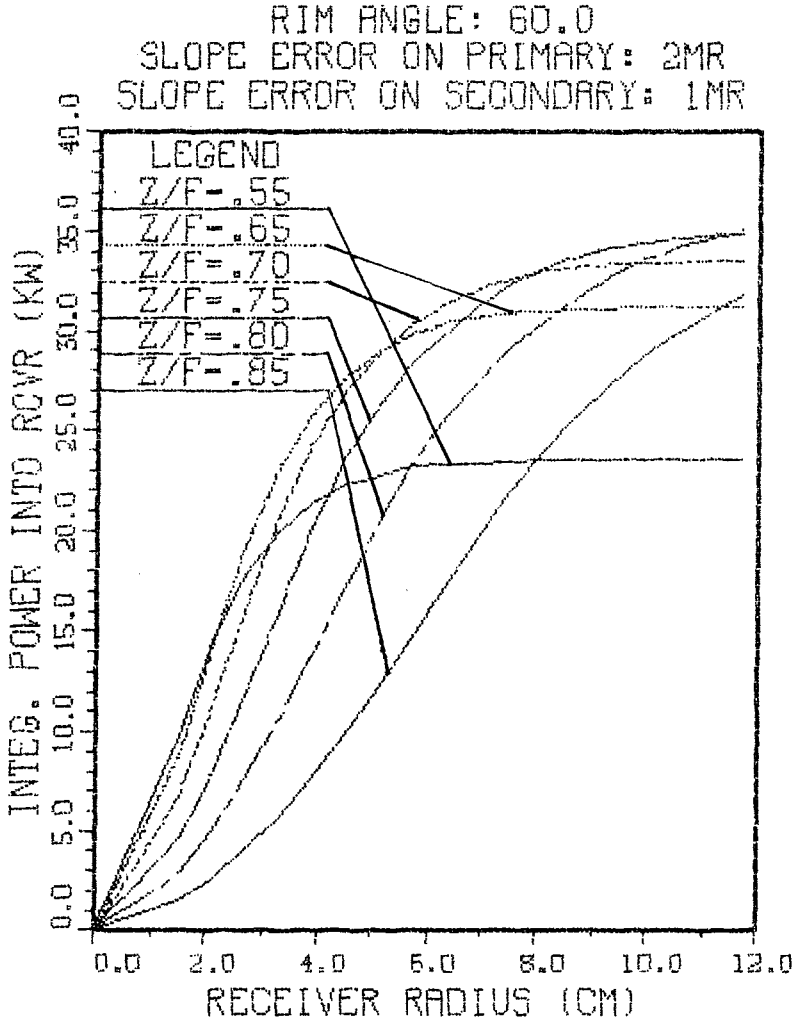
RIM ANGLE: 60.0
SLOPE ERROR ON PRIMARY: 2MR
SLOPE ERROR ON SECONDARY: 1MR
LEGEND
Z/F=.55
Z/F=.65
Z/F=.70
Z/F=.75
Z/F=.80
Z/F=.85
INTEG. POWER INTO RCVR (KW)
0.0
5.0
10.0
15.0
20.0
25.0
30.0
35.0
40.0
0.0
2.0
4.0
6.0
8.0
10.0
12.0
RECEIVER RADIUS (CM)

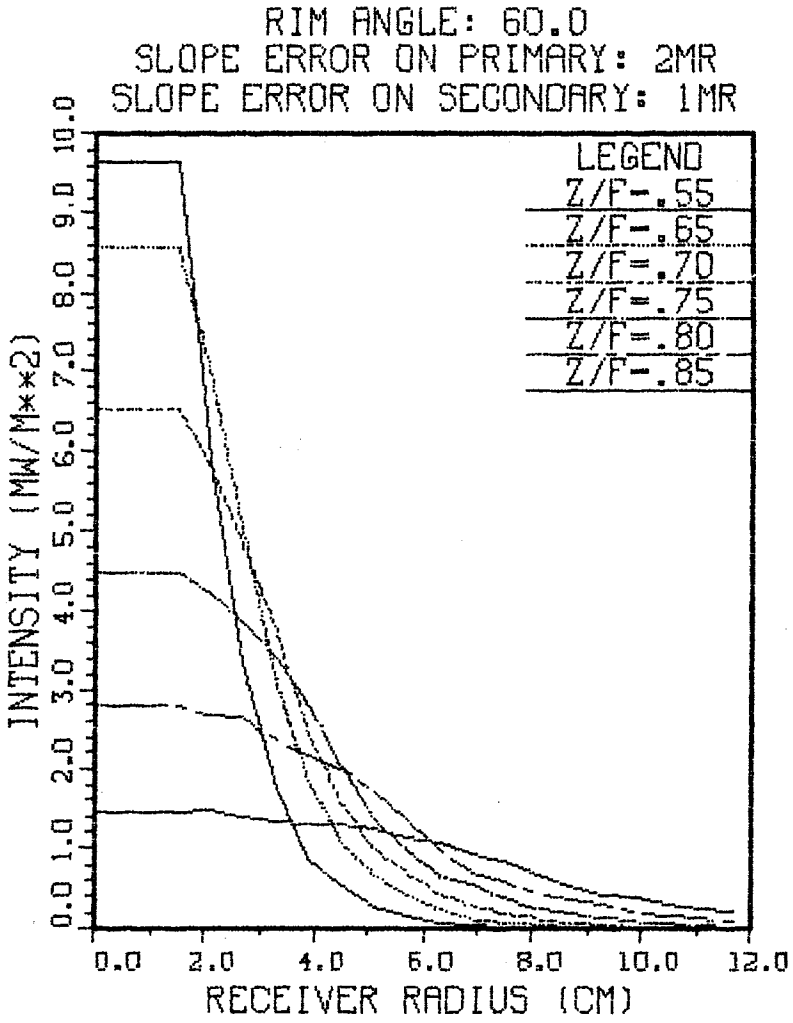
RIM ANGLE: 60.0
SLOPE ERROR ON PRIMARY: 2MR
SLOPE ERROR ON SECONDARY: 1MR
LEGEND
Z/F=.55
Z/F=.65
Z/F=.70
Z/F=.75
Z/F=.80
Z/F=.85
INTENSITY (MW/M**2)
0.0 1.0 2.0 3.0 4.0 5.0 6.0 7.0 8.0 9.0 10.0
0.0 2.0 4.0 6.0 8.0 10.0 12.0
RECEIVER RADIUS (CM)

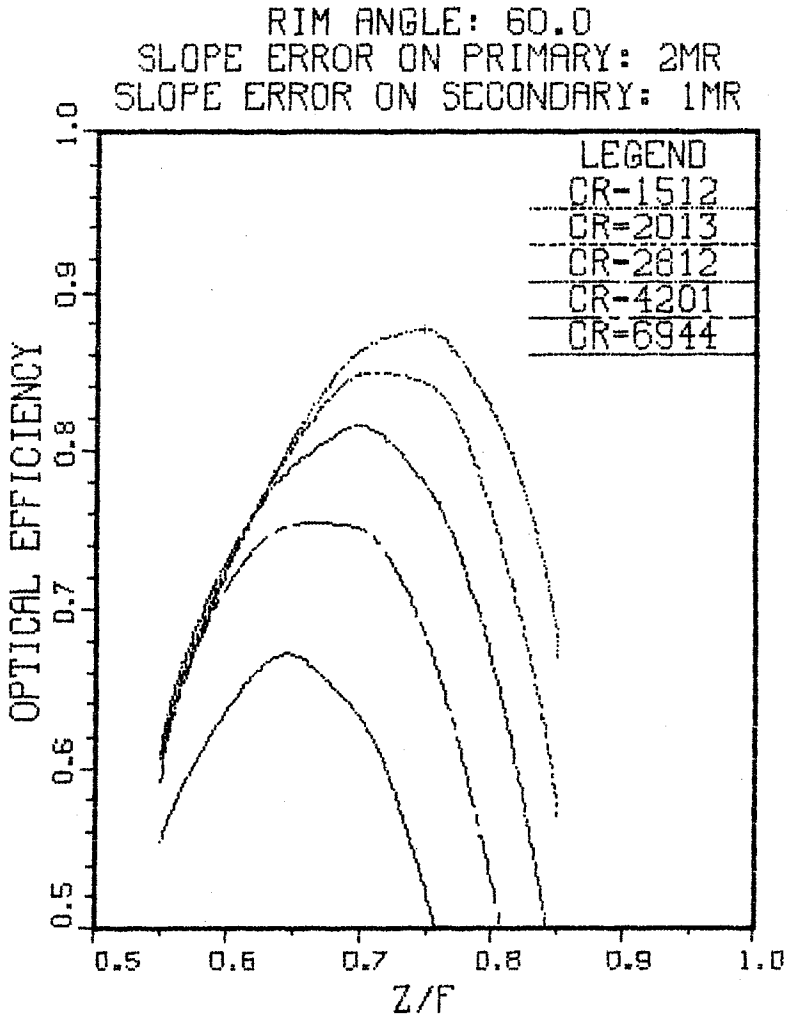
RIM ANGLE: 60.0
SLOPE ERROR ON PRIMARY: 2MR
SLOPE ERROR ON SECONDARY: 1MR
LEGEND
CR-1512
CR=2013
CR-2812
CR-4201
CR=6944
OPTICAL EFFICIENCY
1.0
0.9
0.8
0.7
0.6
0.5
0.5
0.6
0.7
0.8
0.9
1.0
Z/F

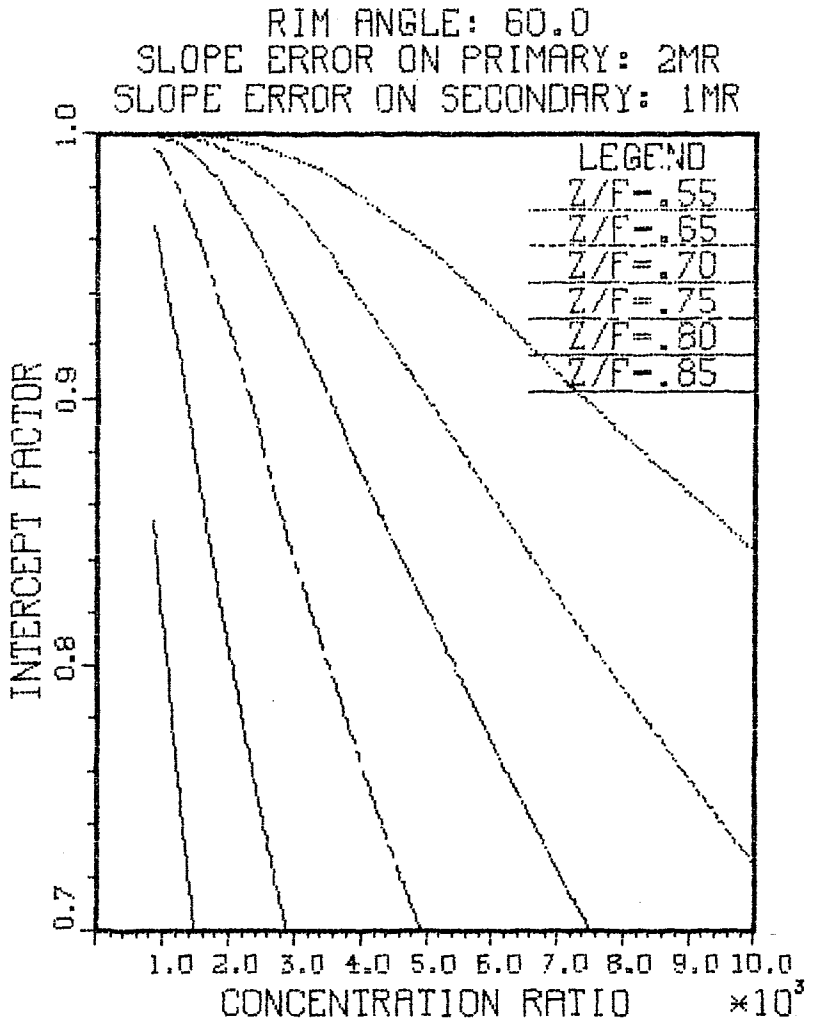
RIM ANGLE: 60.0
SLOPE ERROR ON PRIMARY: 2MR
SLOPE ERROR ON SECONDARY: 1MR
LEGEND
Z/F=.55
Z/F=.65
Z/F=.70
Z/F=.75
Z/F=.80
Z/F=.85
INTERCEPT FACTOR
1.0
0.9
0.8
0.7
1.0 2.0 3.0 4.0 5.0 6.0 7.0 8.0 9.0 10.0
CONCENTRATION RATIO
×10³

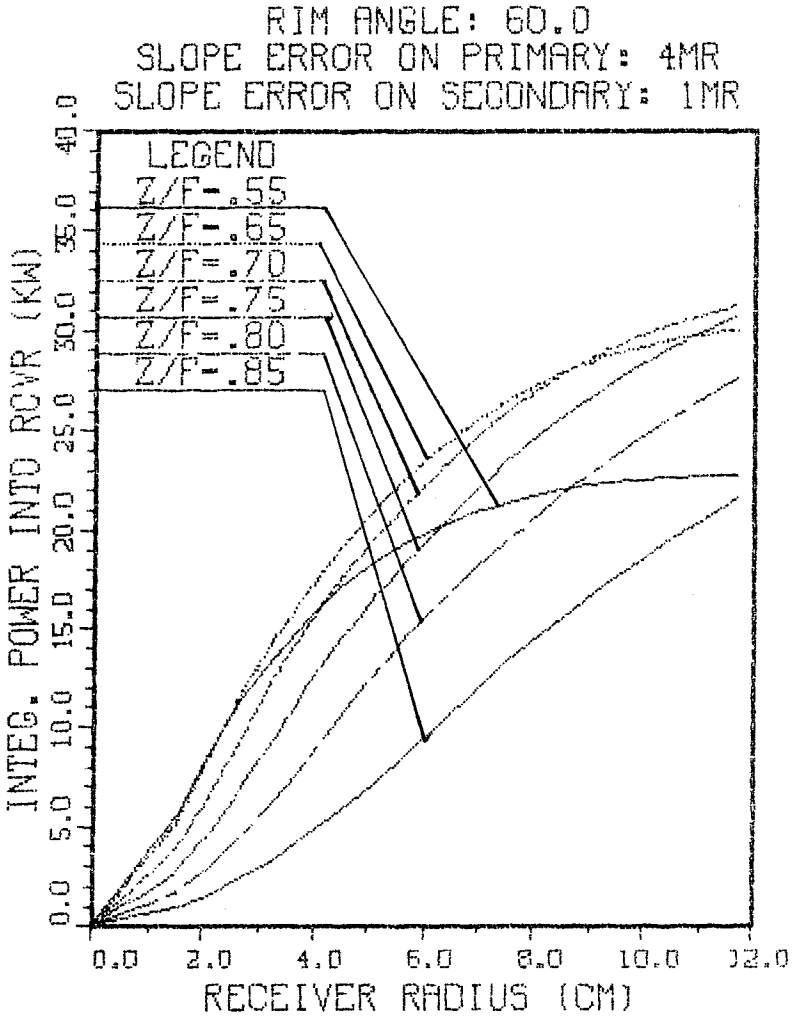
RIM ANGLE: 60.0
SLOPE ERROR ON PRIMARY: 4MR
SLOPE ERROR ON SECONDARY: 1MR
LEGEND
Z/F=.55
Z/F=.65
Z/F=.70
Z/F=.75
Z/F=.80
Z/F=.85
INTEG. POWER INTO RCVR (KW)
0.0
5.0
10.0
15.0
20.0
25.0
30.0
35.0
40.0
0.0
2.0
4.0
6.0
8.0
10.0
12.0
RECEIVER RADIUS (CM)

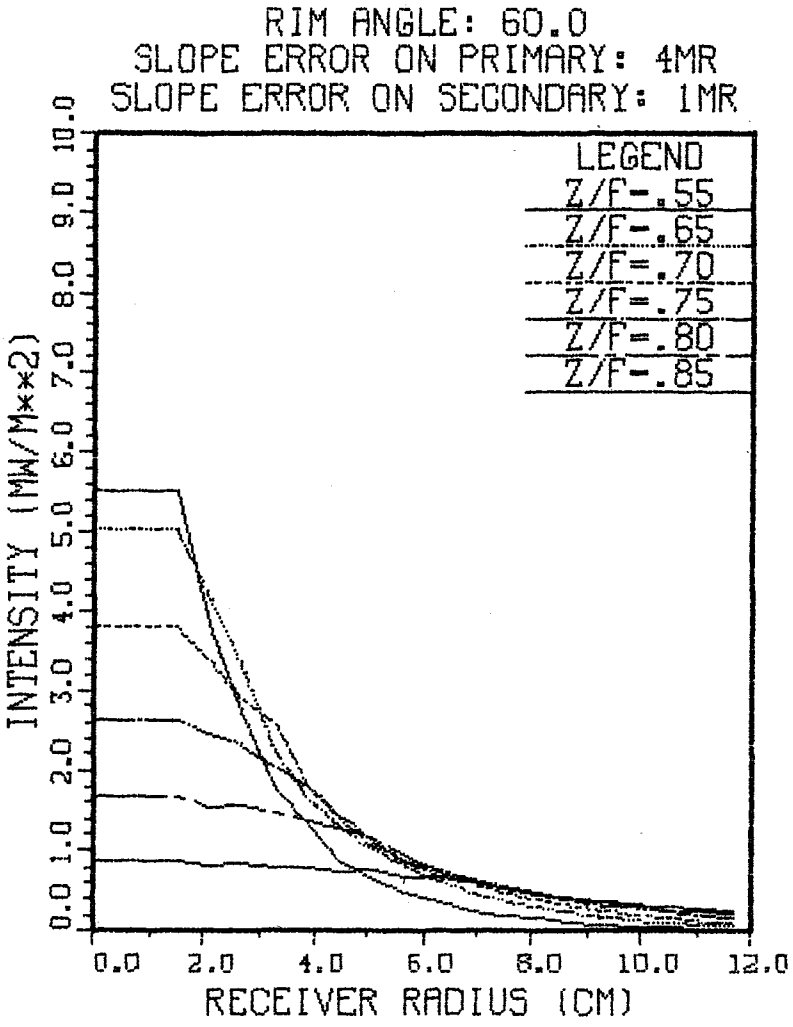
RIM ANGLE: 60.0
SLOPE ERROR ON PRIMARY: 4MR
SLOPE ERROR ON SECONDARY: 1MR
LEGEND
Z/F=.55
Z/F=.65
Z/F=.70
Z/F=.75
Z/F=.80
Z/F=.85
INTENSITY (MW/M**2)
0.0 1.0 2.0 3.0 4.0 5.0 6.0 7.0 8.0 9.0 10.0
0.0 2.0 4.0 6.0 8.0 10.0 12.0
RECEIVER RADIUS (CM)

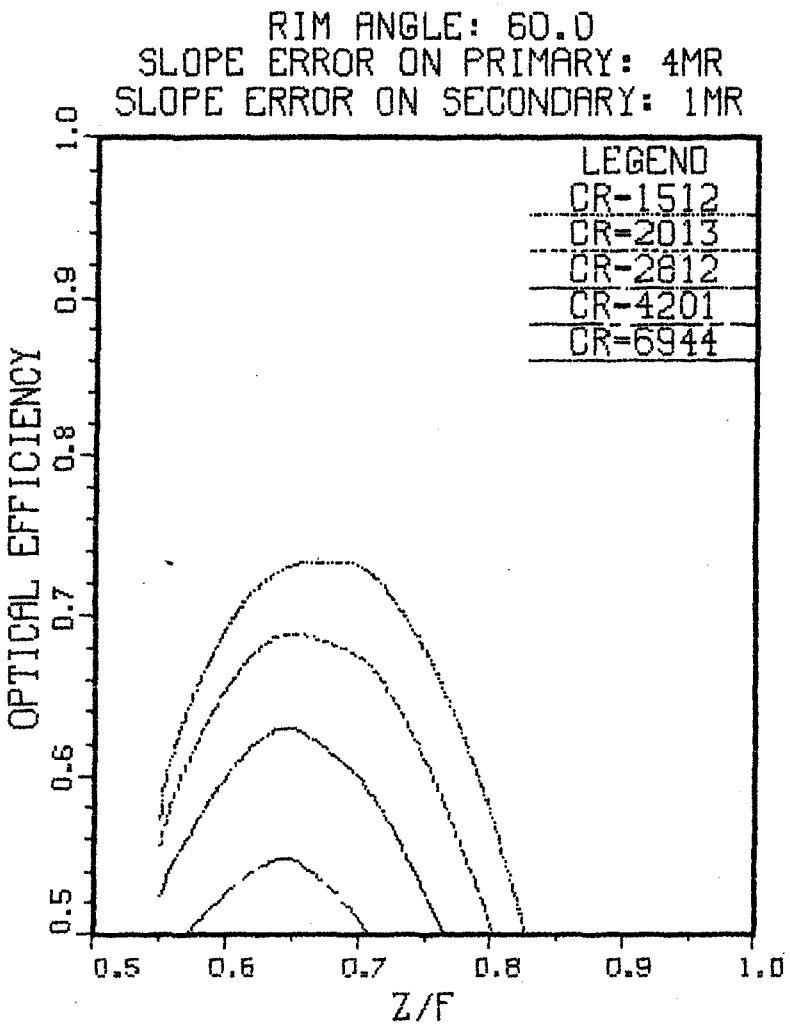
RIM ANGLE: 60.0
SLOPE ERROR ON PRIMARY: 4MR
SLOPE ERROR ON SECONDARY: 1MR
LEGEND
CR-1512
CR=2013
CR-2812
CR-4201
CR=6944
OPTICAL EFFICIENCY
1.0
0.9
0.8
0.7
0.6
0.5
0.5
0.6
0.7
0.8
0.9
1.0
Z/F

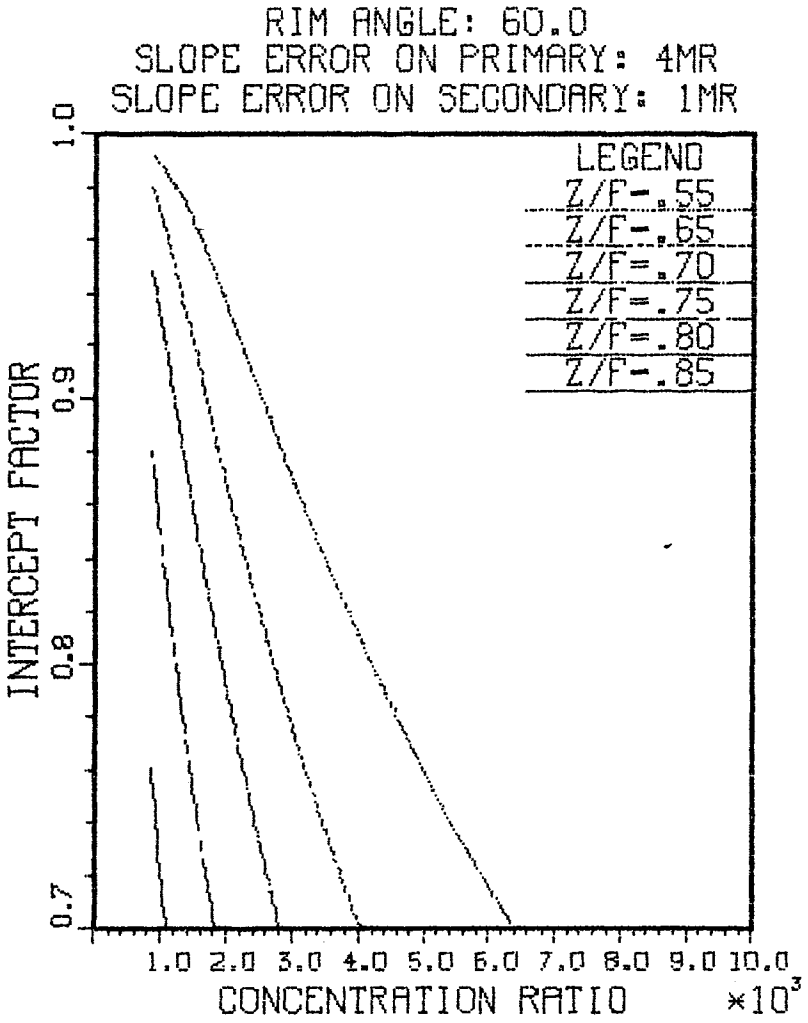
RIM ANGLE: 60.0
SLOPE ERROR ON PRIMARY: 4MR
SLOPE ERROR ON SECONDARY: 1MR
LEGEND
Z/F=.55
Z/F=.65
Z/F=.70
Z/F=.75
Z/F=.80
Z/F=.85
INTERCEPT FACTOR
1.0
0.9
0.8
0.7
1.0 2.0 3.0 4.0 5.0 6.0 7.0 8.0 9.0 10.0
CONCENTRATION RATIO
*10^3

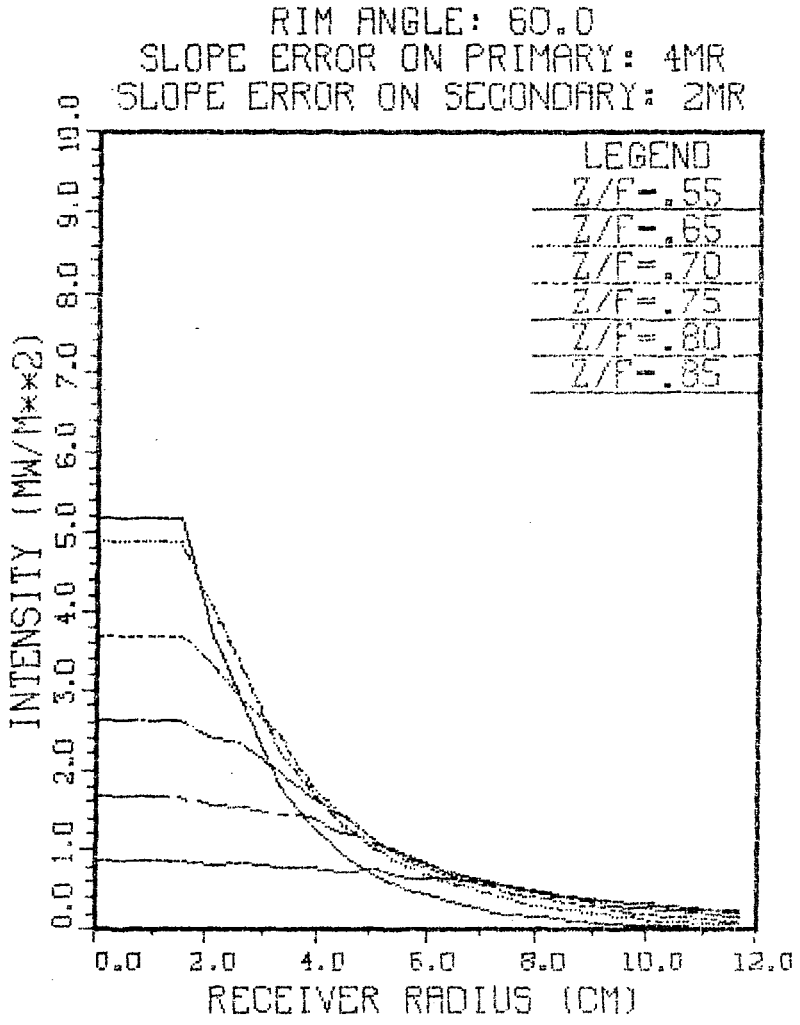
RIM ANGLE: 60.0
SLOPE ERROR ON PRIMARY: 4MR
SLOPE ERROR ON SECONDARY: 2MR
LEGEND
Z/F=.55
Z/F=.65
Z/F=.70
Z/F=.75
Z/F=.80
Z/F=.85
INTENSITY (MW/M**2)
0.0 1.0 2.0 3.0 4.0 5.0 6.0 7.0 8.0 9.0 10.0
0.0 2.0 4.0 6.0 8.0 10.0 12.0
RECEIVER RADIUS (CM)

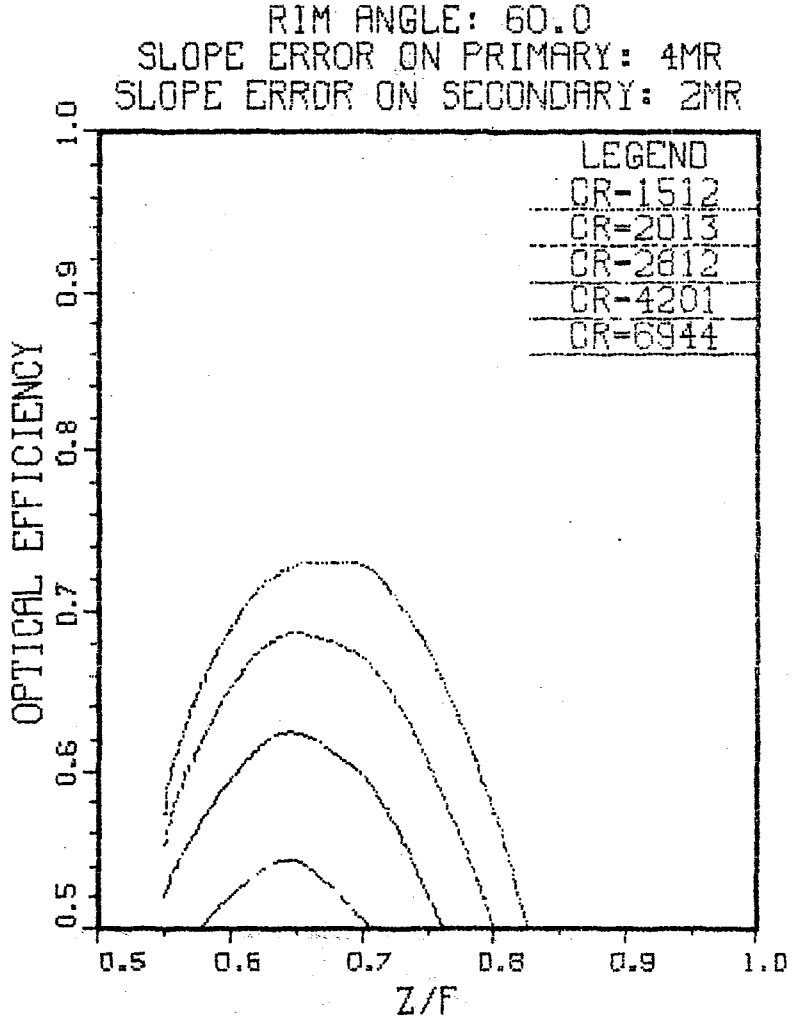
RIM ANGLE: 60.0
SLOPE ERROR ON PRIMARY: 4MR
SLOPE ERROR ON SECONDARY: 2MR
LEGEND
CR-1512
CR=2013
CR-2812
CR-4201
CR=6944
OPTICAL EFFICIENCY
0.5
0.6
0.7
0.8
0.9
1.0
Z/F

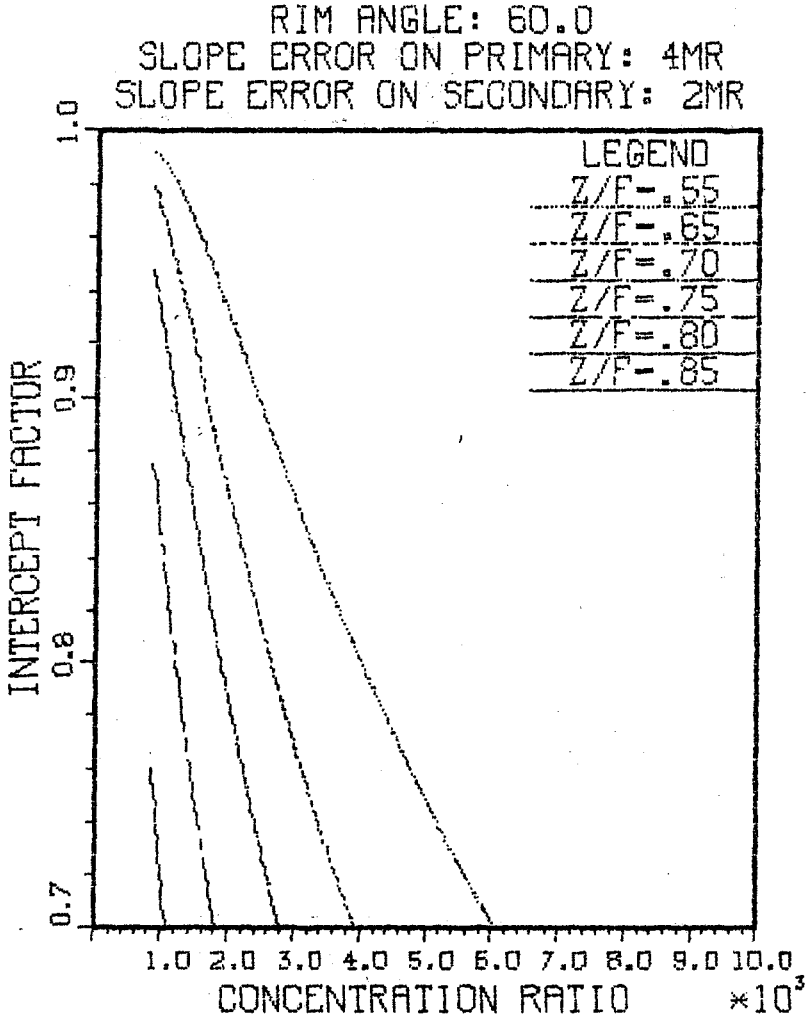
RIM ANGLE: 60.0
SLOPE ERROR ON PRIMARY: 4MR
SLOPE ERROR ON SECONDARY: 2MR
LEGEND
Z/F=.55
Z/F=.65
Z/F=.70
Z/F=.75
Z/F=.80
Z/F=.85
INTERCEPT FACTOR
1.0
0.9
0.8
0.7
1.0 2.0 3.0 4.0 5.0 6.0 7.0 8.0 9.0 10.0
CONCENTRATION RATIO
×10³

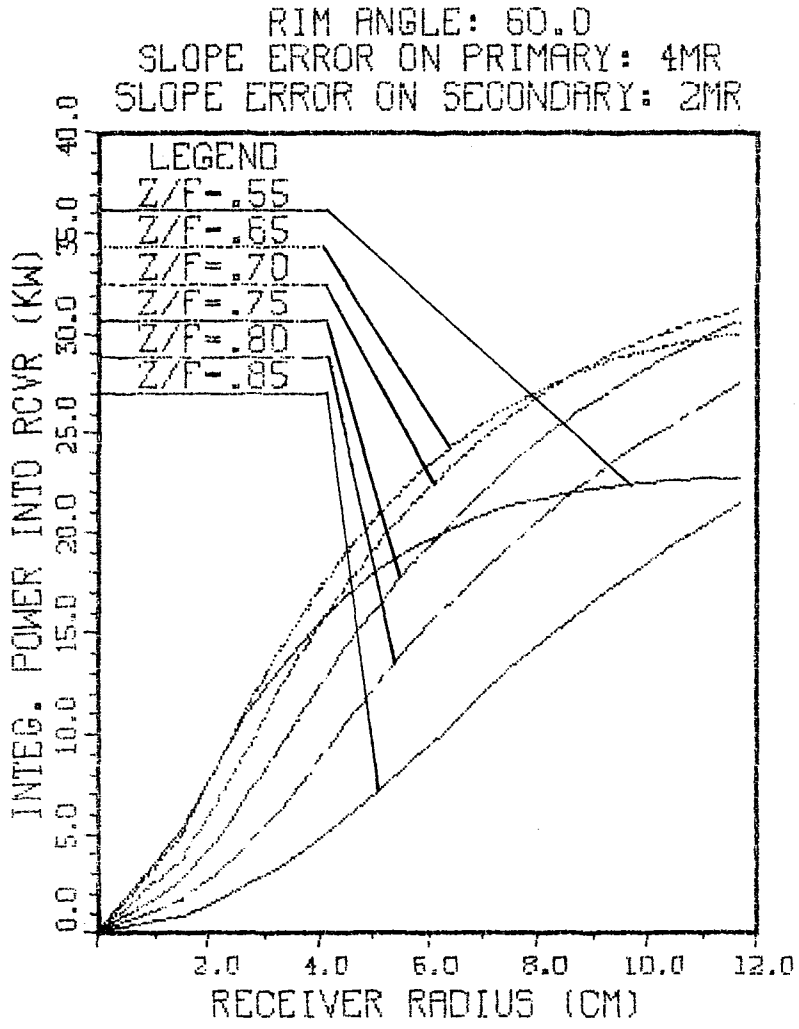
RIM ANGLE: 60.0
SLOPE ERROR ON PRIMARY: 4MR
SLOPE ERROR ON SECONDARY: 2MR
LEGEND
Z/F=.55
Z/F=.65
Z/F=.70
Z/F=.75
Z/F=.80
Z/F=.85
INTEG. POWER INTO RCVR (KW)
0.0
5.0
10.0
15.0
20.0
25.0
30.0
35.0
40.0
2.0
4.0
6.0
8.0
10.0
12.0
RECEIVER RADIUS (CM)

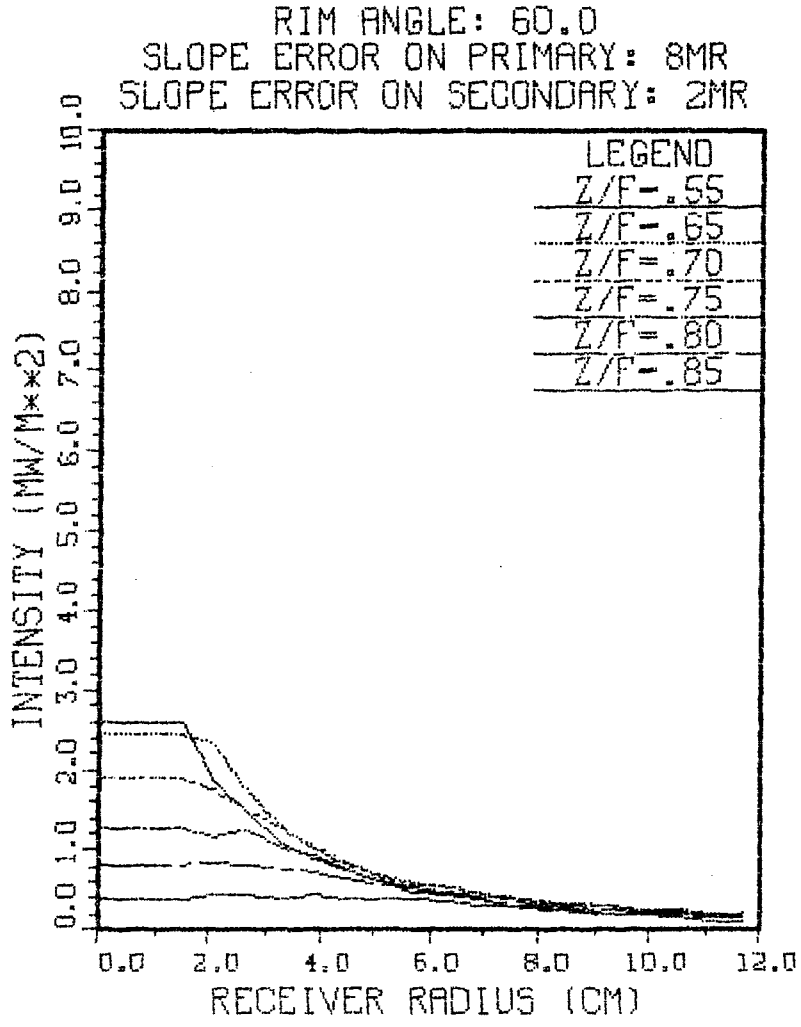
RIM ANGLE: 60.0
SLOPE ERROR ON PRIMARY: 8MR
SLOPE ERROR ON SECONDARY: 2MR
LEGEND
Z/F=.55
Z/F=.65
Z/F=.70
Z/F=.75
Z/F=.80
Z/F=.85
INTENSITY (MW/M**2)
0.0 1.0 2.0 3.0 4.0 5.0 6.0 7.0 8.0 9.0 10.0
0.0 2.0 4.0 6.0 8.0 10.0 12.0
RECEIVER RADIUS (CM)

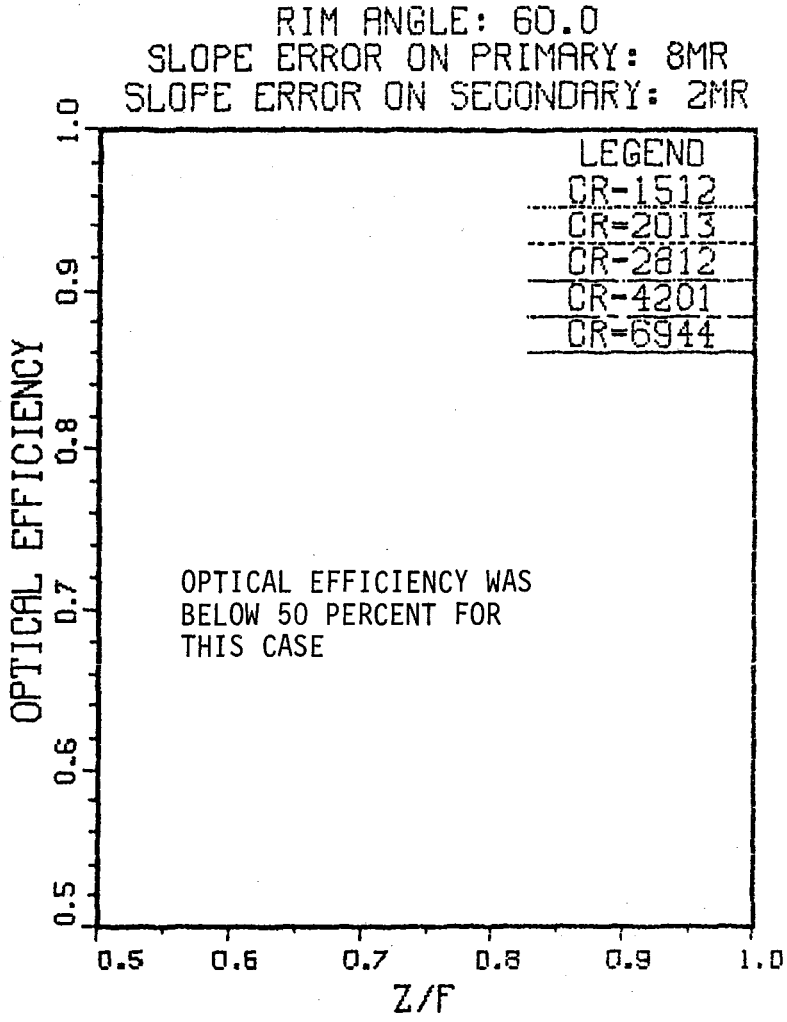
RIM ANGLE: 60.0
SLOPE ERROR ON PRIMARY: 8MR
SLOPE ERROR ON SECONDARY: 2MR
LEGEND
CR-1512
CR=2013
CR-2812
CR-4201
CR=6944
OPTICAL EFFICIENCY WAS
BELOW 50 PERCENT FOR
THIS CASE
OPTICAL EFFICIENCY
1.0
0.9
0.8
0.7
0.6
0.5
0.5
0.6
0.7
0.8
0.9
1.0
Z/F

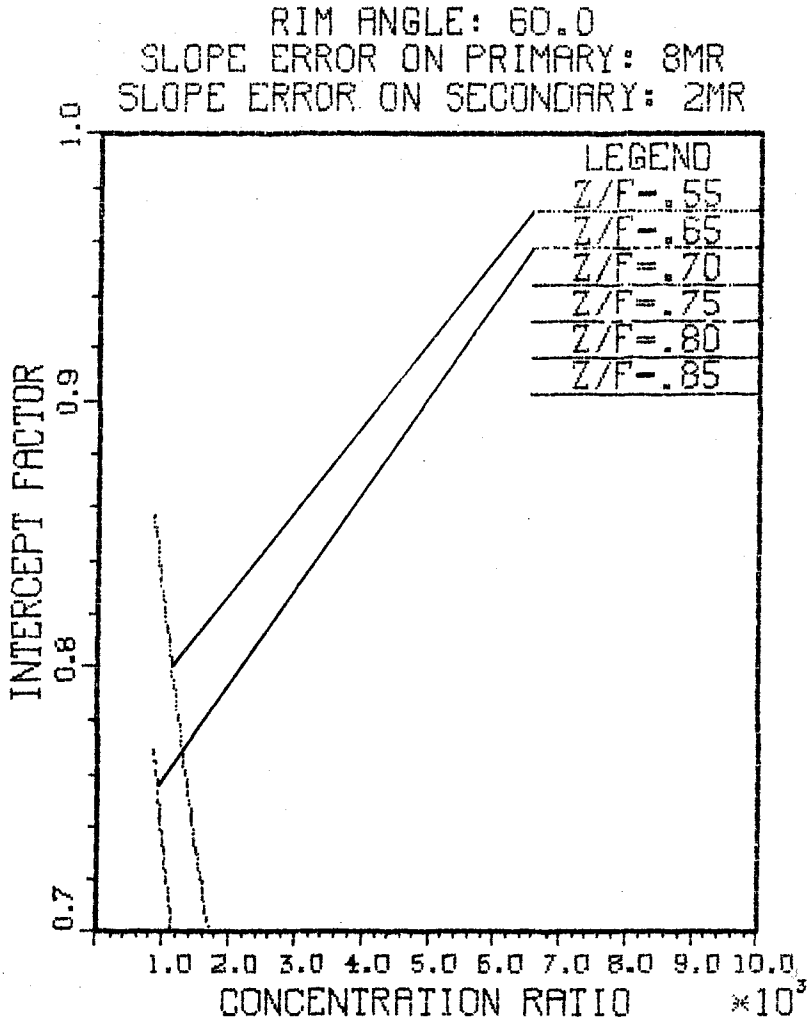
RIM ANGLE: 60.0
SLOPE ERROR ON PRIMARY: 8MR
SLOPE ERROR ON SECONDARY: 2MR
LEGEND
Z/F=.55
Z/F=.65
Z/F=.70
Z/F=.75
Z/F=.80
Z/F=.85
INTERCEPT FACTOR
1.0
0.9
0.8
0.7
1.0 2.0 3.0 4.0 5.0 6.0 7.0 8.0 9.0 10.0
CONCENTRATION RATIO
*10^3

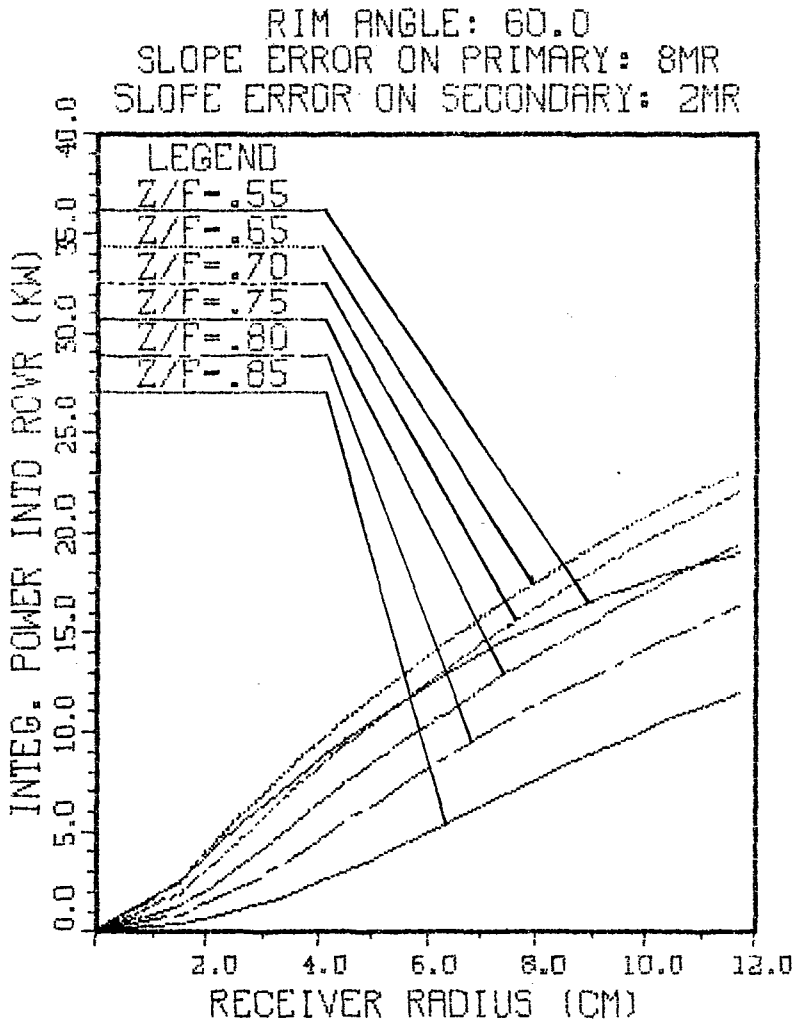
RIM ANGLE: 60.0
SLOPE ERROR ON PRIMARY: 8MR
SLOPE ERROR ON SECONDARY: 2MR
LEGEND
Z/F=.55
Z/F=.65
Z/F=.70
Z/F=.75
Z/F=.80
Z/F=.85
INTEG. POWER INTO RCVR (KW)
0.0
5.0
10.0
15.0
20.0
25.0
30.0
35.0
40.0
2.0
4.0
6.0
8.0
10.0
12.0
RECEIVER RADIUS (CM)

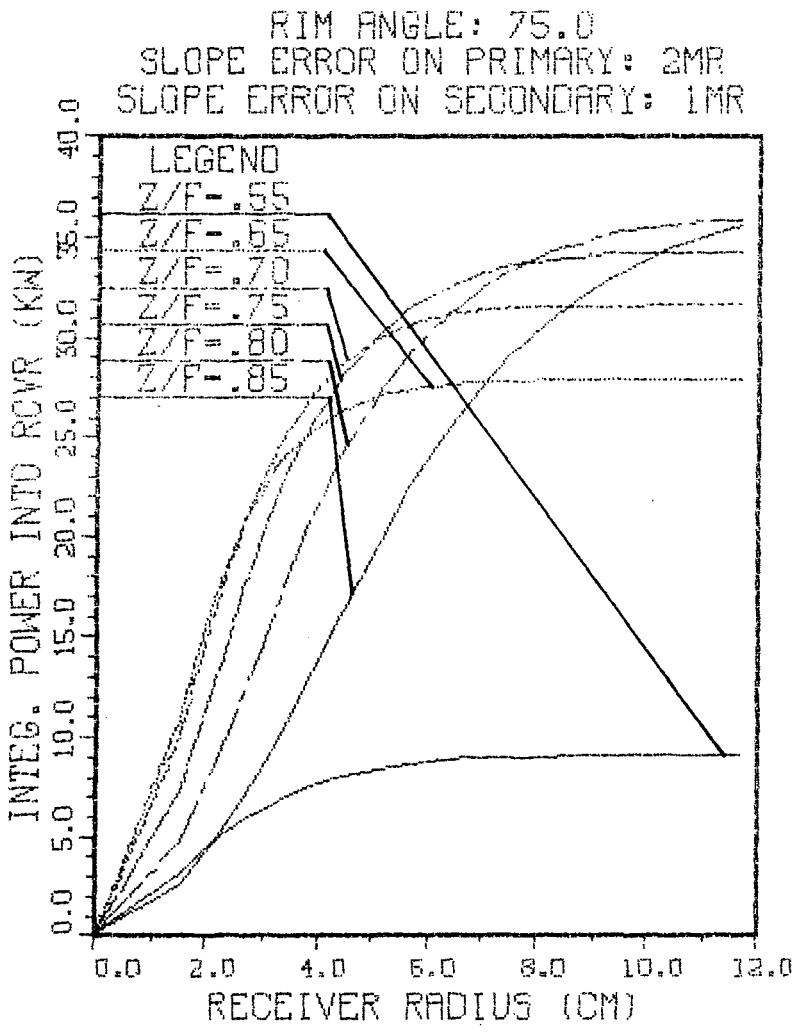
RIM ANGLE: 75.0
SLOPE ERROR ON PRIMARY: 2MR
SLOPE ERROR ON SECONDARY: 1MR
LEGEND
Z/F=.55
Z/F=.65
Z/F=.70
Z/F=.75
Z/F=.80
Z/F=.85
INTEG. POWER INTO RCVR (KW)
0.0
5.0
10.0
15.0
20.0
25.0
30.0
35.0
40.0
0.0
2.0
4.0
6.0
8.0
10.0
12.0
RECEIVER RADIUS (CM)

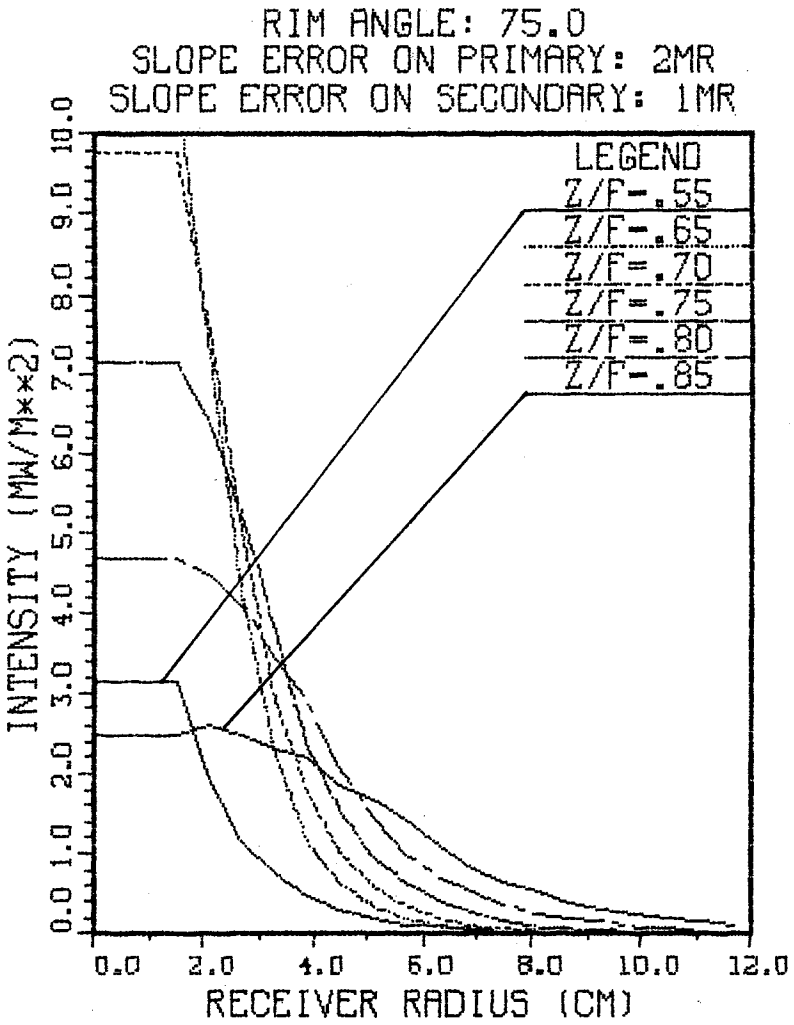
RIM ANGLE: 75.0
SLOPE ERROR ON PRIMARY: 2MR
SLOPE ERROR ON SECONDARY: 1MR
LEGEND
Z/F=.55
Z/F=.65
Z/F=.70
Z/F=.75
Z/F=.80
Z/F=.85
INTENSITY (MW/M**2)
0.0 1.0 2.0 3.0 4.0 5.0 6.0 7.0 8.0 9.0 10.0
0.0 2.0 4.0 6.0 8.0 10.0 12.0
RECEIVER RADIUS (CM)

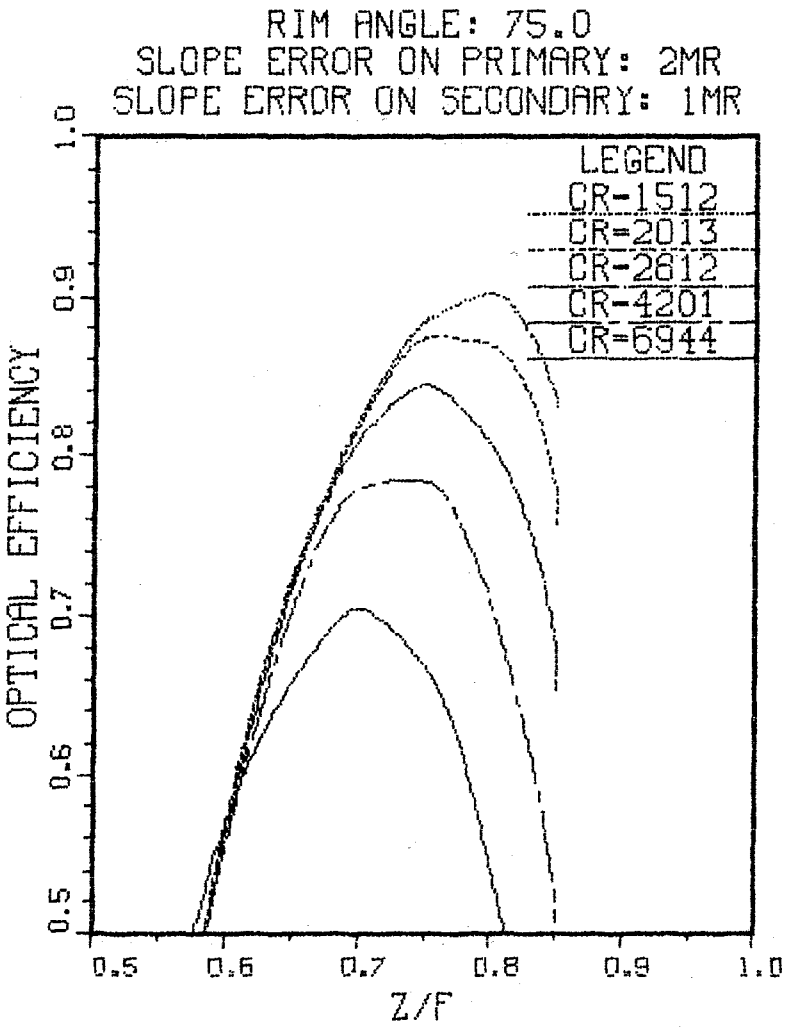
RIM ANGLE: 75.0
SLOPE ERROR ON PRIMARY: 2MR
SLOPE ERROR ON SECONDARY: 1MR
LEGEND
CR-1512
CR=2013
CR-2812
CR-4201
CR=6944
OPTICAL EFFICIENCY
1.0
0.9
0.8
0.7
0.6
0.5
0.5
0.6
0.7
0.8
0.9
1.0
Z/F

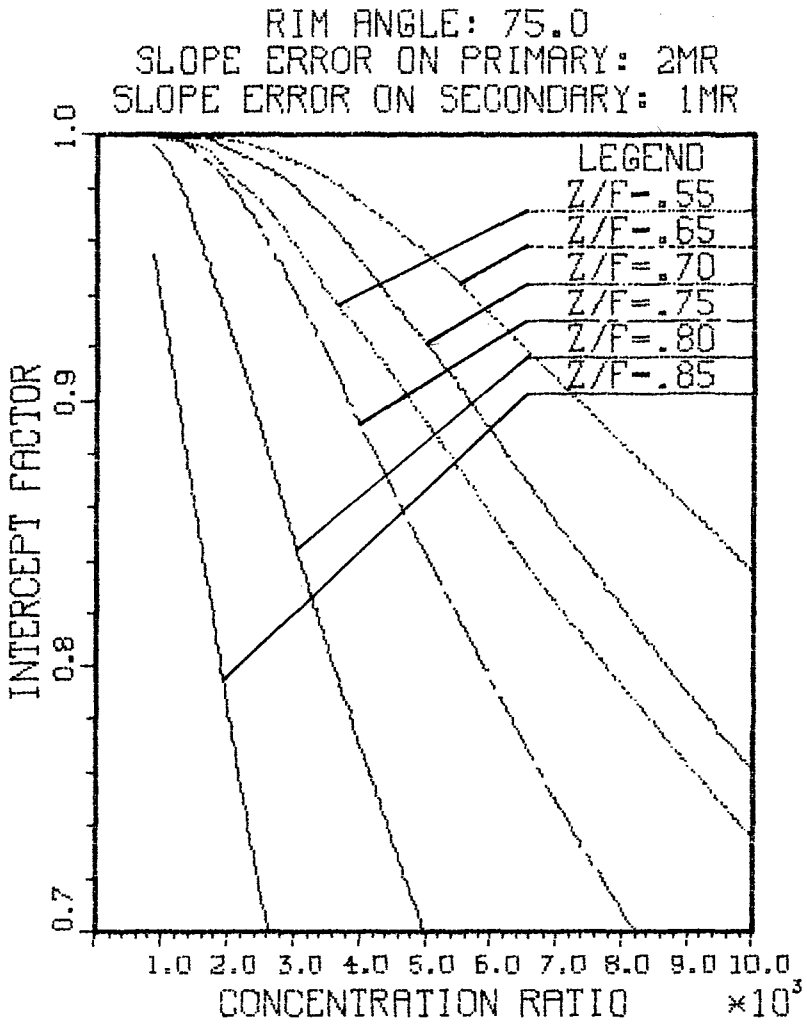
RIM ANGLE: 75.0
SLOPE ERROR ON PRIMARY: 2MR
SLOPE ERROR ON SECONDARY: 1MR
LEGEND
Z/F=.55
Z/F=.65
Z/F=.70
Z/F=.75
Z/F=.80
Z/F=.85
INTERCEPT FACTOR
1.0
0.9
0.8
0.7
1.0 2.0 3.0 4.0 5.0 6.0 7.0 8.0 9.0 10.0
CONCENTRATION RATIO
*10^3

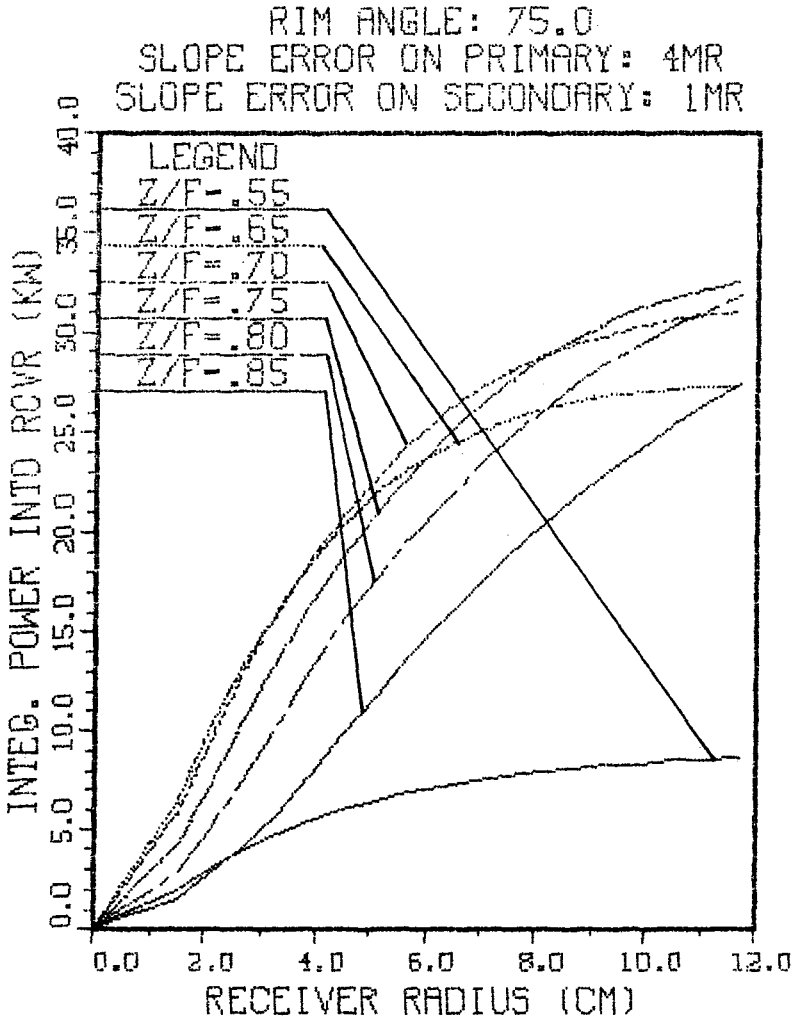
RIM ANGLE: 75.0
SLOPE ERROR ON PRIMARY: 4MR
SLOPE ERROR ON SECONDARY: 1MR
LEGEND
Z/F=.55
Z/F=.65
Z/F=.70
Z/F=.75
Z/F=.80
Z/F=.85
INTEG. POWER INTO RCVR (KW)
0.0
5.0
10.0
15.0
20.0
25.0
30.0
35.0
40.0
0.0
2.0
4.0
6.0
8.0
10.0
12.0
RECEIVER RADIUS (CM)

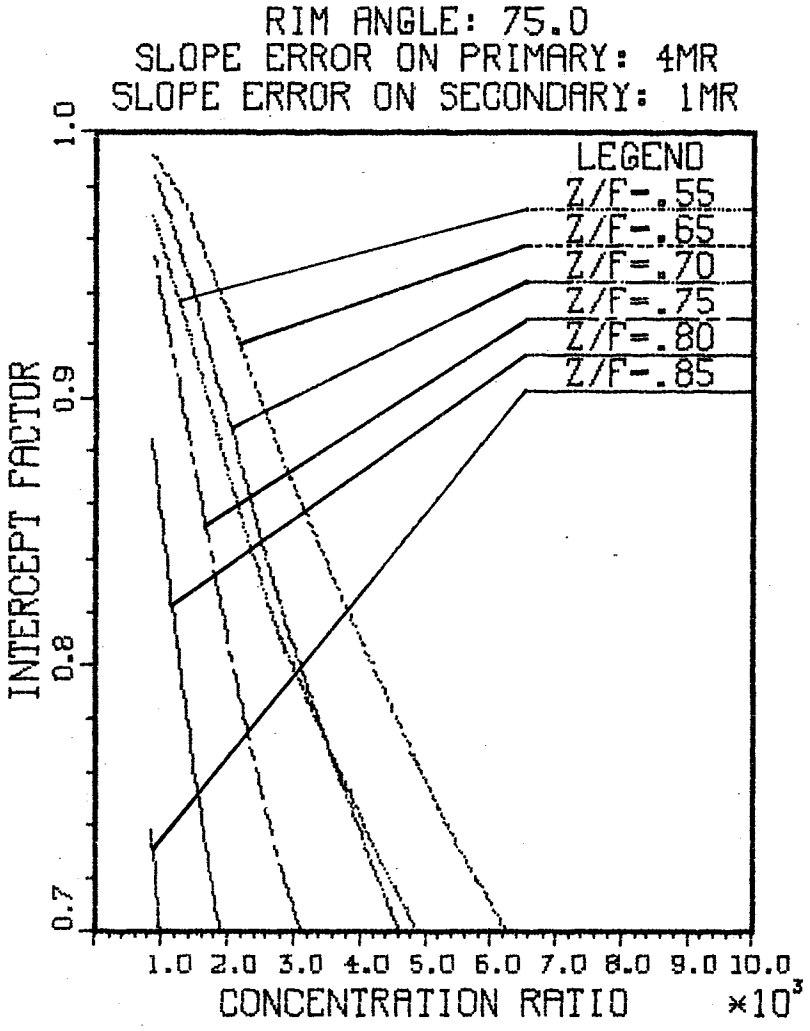
RIM ANGLE: 75.0
SLOPE ERROR ON PRIMARY: 4MR
SLOPE ERROR ON SECONDARY: 1MR
LEGEND
Z/F=.55
Z/F=.65
Z/F=.70
Z/F=.75
Z/F=.80
Z/F=.85
INTERCEPT FACTOR
1.0
0.9
0.8
0.7
1.0 2.0 3.0 4.0 5.0 6.0 7.0 8.0 9.0 10.0
CONCENTRATION RATIO
×10³

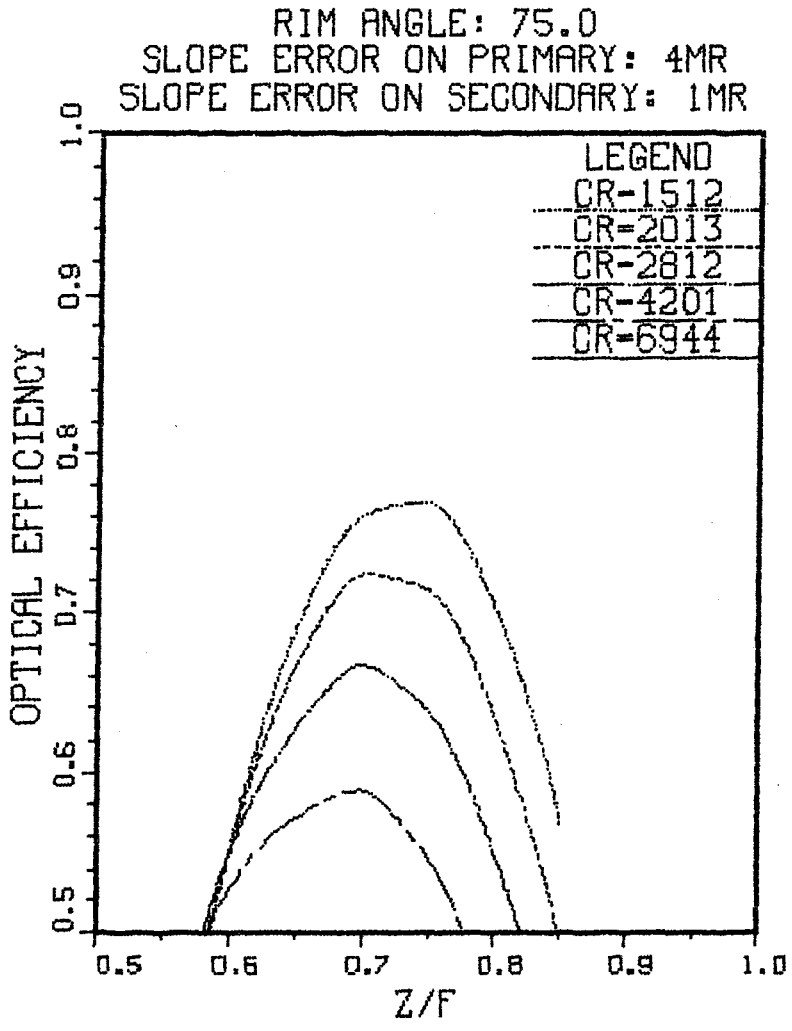
RIM ANGLE: 75.0
SLOPE ERROR ON PRIMARY: 4MR
SLOPE ERROR ON SECONDARY: 1MR
LEGEND
CR-1512
CR=2013
CR-2812
CR-4201
CR=6944
OPTICAL EFFICIENCY
1.0
0.9
0.8
0.7
0.6
0.5
0.5
0.6
0.7
0.8
0.9
1.0
Z/F

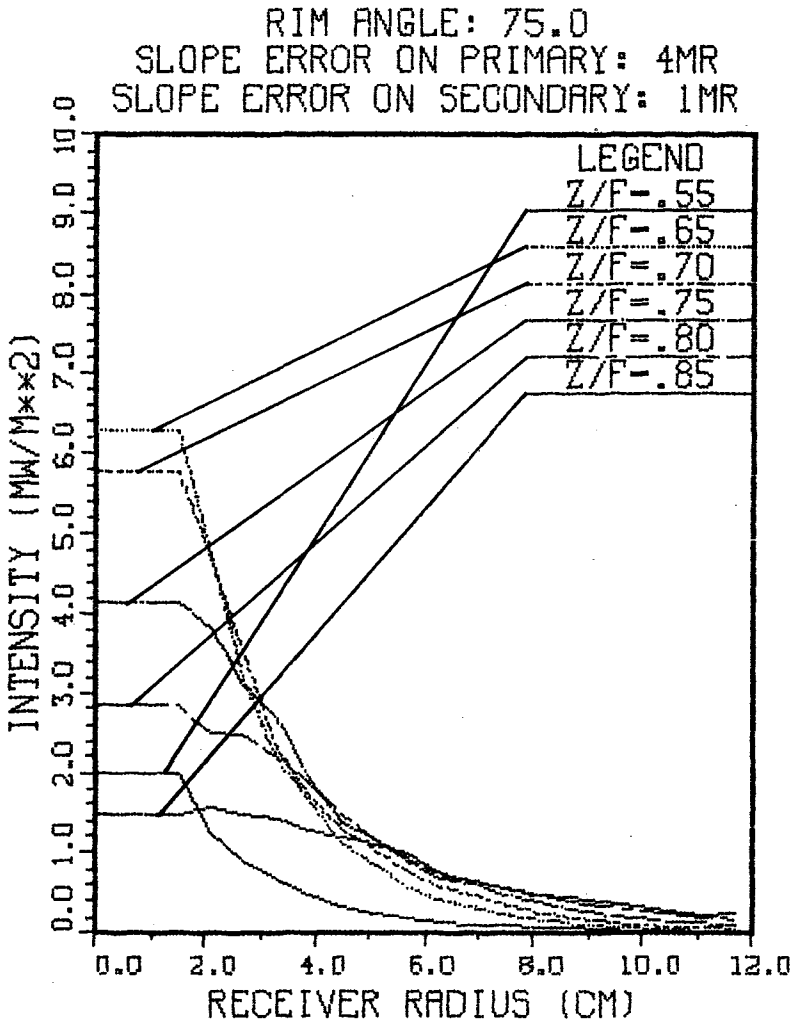
RIM ANGLE: 75.0
SLOPE ERROR ON PRIMARY: 4MR
SLOPE ERROR ON SECONDARY: 1MR
LEGEND
Z/F=.55
Z/F=.65
Z/F=.70
Z/F=.75
Z/F=.80
Z/F=.85
INTENSITY (MW/M**2)
0.0 1.0 2.0 3.0 4.0 5.0 6.0 7.0 8.0 9.0 10.0
0.0 2.0 4.0 6.0 8.0 10.0 12.0
RECEIVER RADIUS (CM)

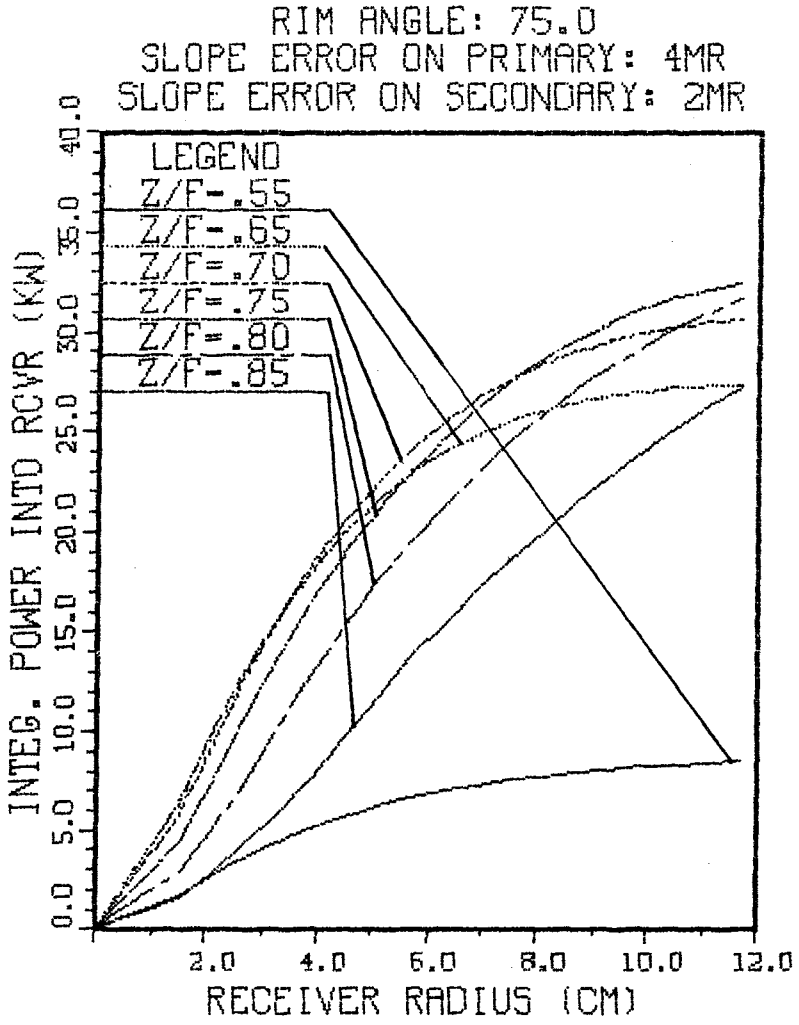
RIM ANGLE: 75.0
SLOPE ERROR ON PRIMARY: 4MR
SLOPE ERROR ON SECONDARY: 2MR
LEGEND
Z/F=.55
Z/F=.65
Z/F=.70
Z/F=.75
Z/F=.80
Z/F=.85
INTEG. POWER INTO RCVR (KW)
0.0
5.0
10.0
15.0
20.0
25.0
30.0
35.0
40.0
2.0
4.0
6.0
8.0
10.0
12.0
RECEIVER RADIUS (CM)

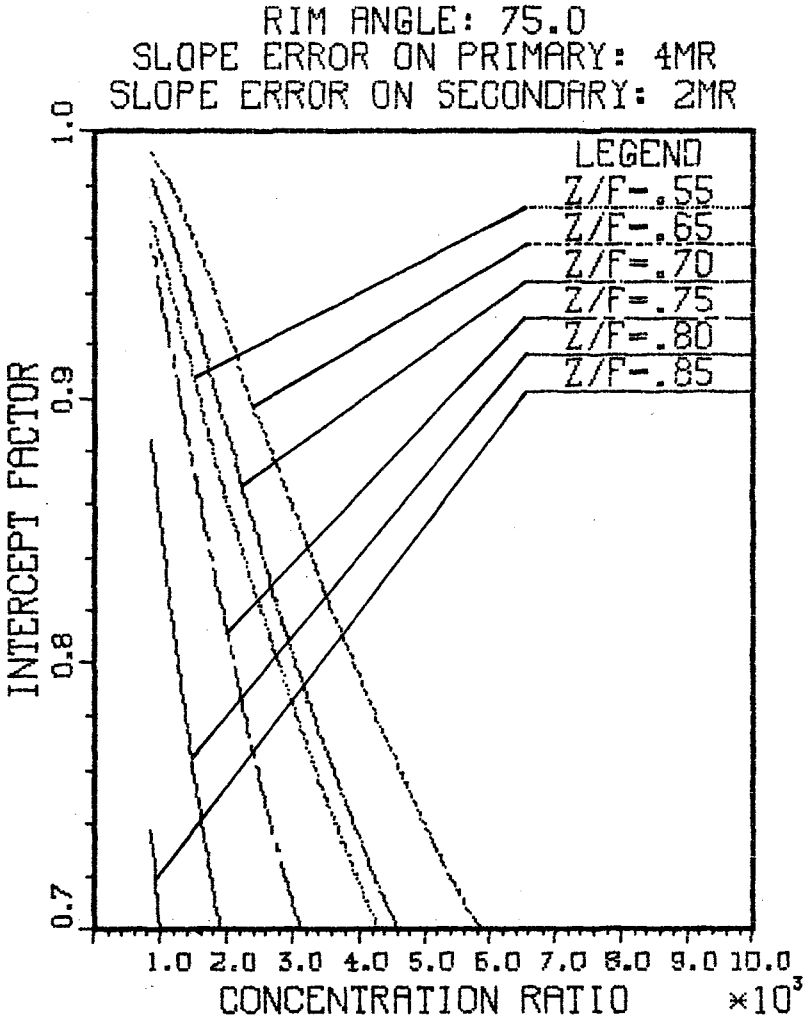
RIM ANGLE: 75.0
SLOPE ERROR ON PRIMARY: 4MR
SLOPE ERROR ON SECONDARY: 2MR
LEGEND
Z/F=.55
Z/F=.65
Z/F=.70
Z/F=.75
Z/F=.80
Z/F=.85
INTERCEPT FACTOR
1.0
0.9
0.8
0.7
1.0 2.0 3.0 4.0 5.0 6.0 7.0 8.0 9.0 10.0
CONCENTRATION RATIO ×10³

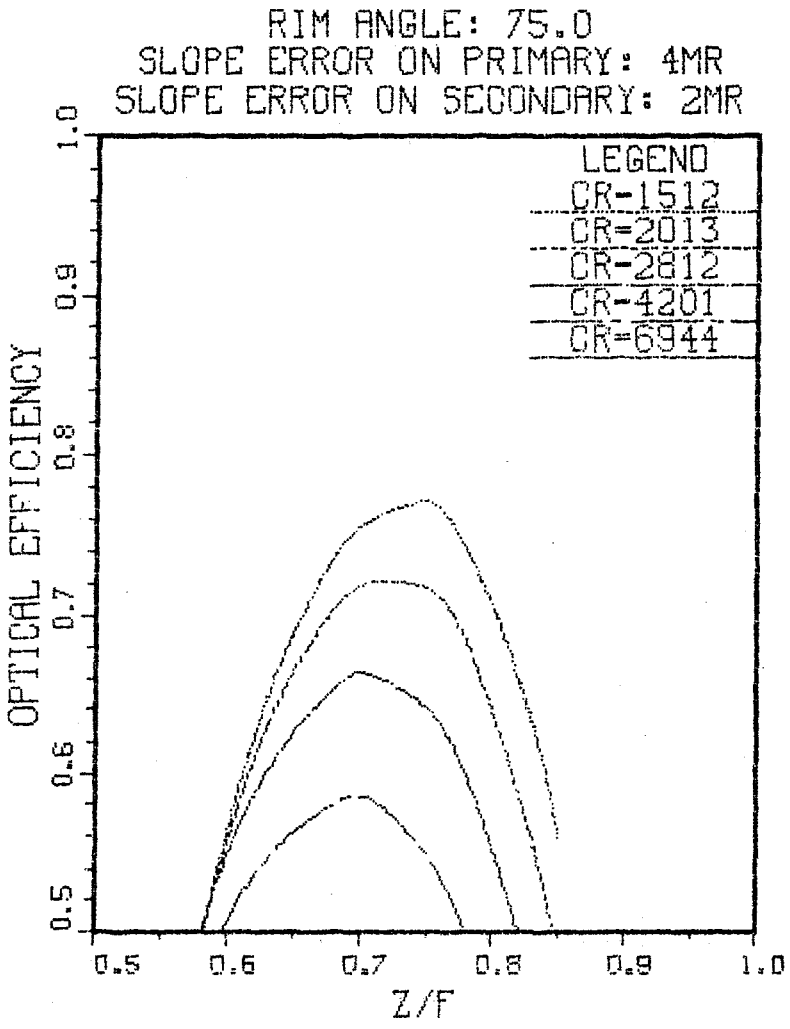
RIM ANGLE: 75.0
SLOPE ERROR ON PRIMARY: 4MR
SLOPE ERROR ON SECONDARY: 2MR
LEGEND
CR-1512
CR=2013
CR-2812
CR-4201
CR=6944
OPTICAL EFFICIENCY
0.5
0.6
0.7
0.8
0.9
1.0
Z/F

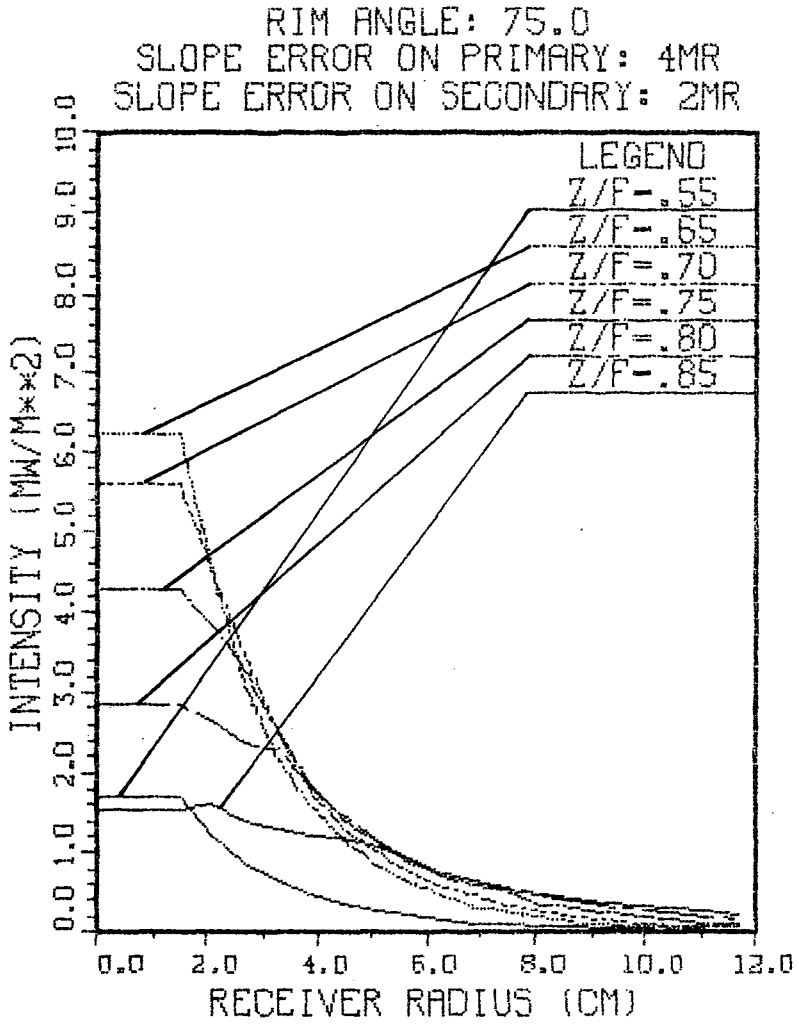
RIM ANGLE: 75.0
SLOPE ERROR ON PRIMARY: 4MR
SLOPE ERROR ON SECONDARY: 2MR
LEGEND
Z/F=.55
Z/F=.65
Z/F=.70
Z/F=.75
Z/F=.80
Z/F=.85
INTENSITY (MW/M**2)
0.0 1.0 2.0 3.0 4.0 5.0 6.0 7.0 8.0 9.0 10.0
0.0 2.0 4.0 6.0 8.0 10.0 12.0
RECEIVER RADIUS (CM)

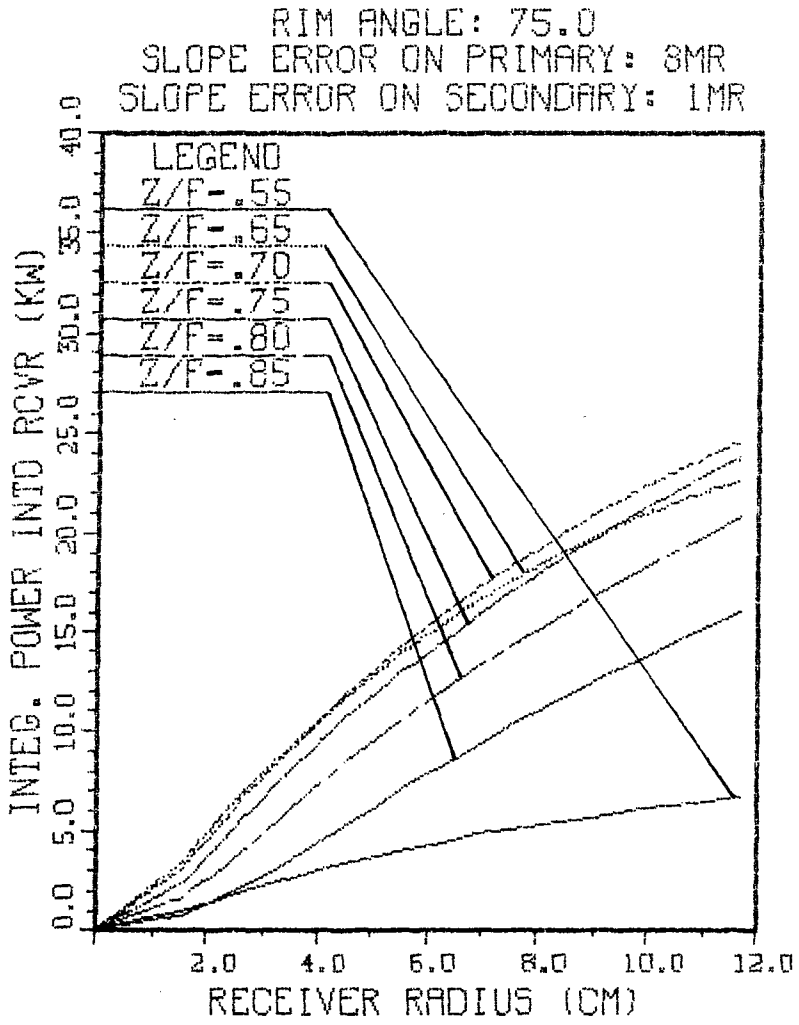
RIM ANGLE: 75.0
SLOPE ERROR ON PRIMARY: 8MR
SLOPE ERROR ON SECONDARY: 1MR
LEGEND
Z/F=.55
Z/F=.65
Z/F=.70
Z/F=.75
Z/F=.80
Z/F=.85
INTEG. POWER INTO RCVR (KW)
0.0
5.0
10.0
15.0
20.0
25.0
30.0
35.0
40.0
2.0
4.0
6.0
8.0
10.0
12.0
RECEIVER RADIUS (CM)

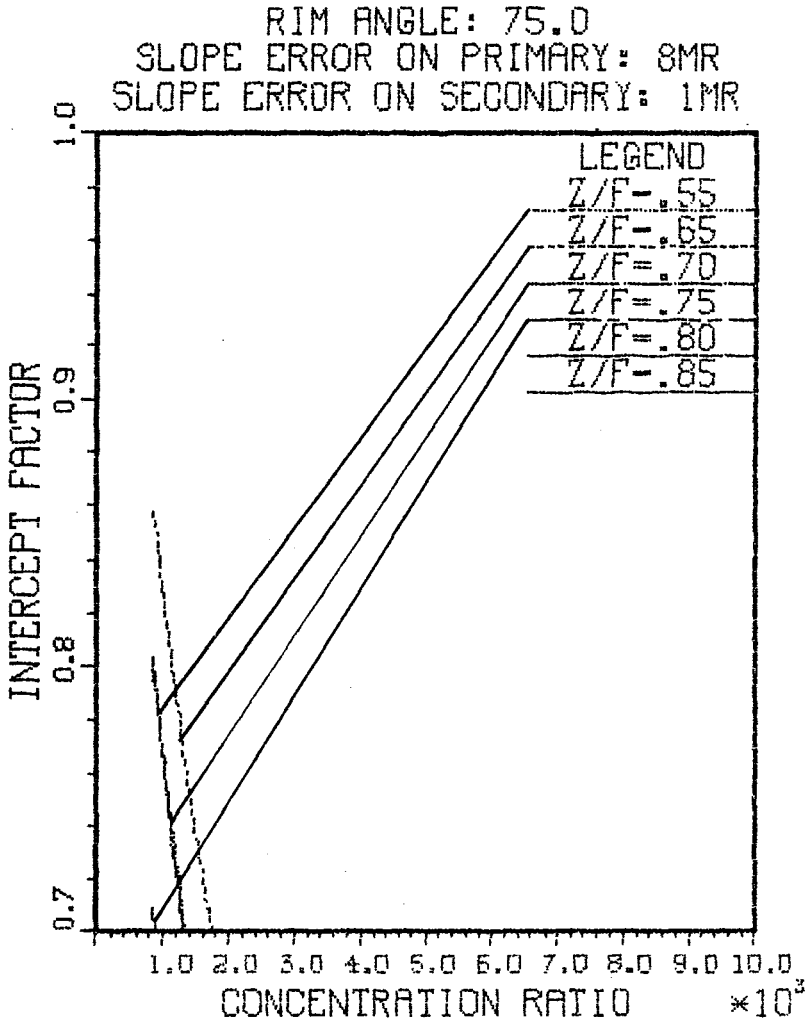
RIM ANGLE: 75.0
SLOPE ERROR ON PRIMARY: 8MR
SLOPE ERROR ON SECONDARY: 1MR
LEGEND
Z/F=.55
Z/F=.65
Z/F=.70
Z/F=.75
Z/F=.80
Z/F=.85
INTERCEPT FACTOR
1.0
0.9
0.8
0.7
1.0 2.0 3.0 4.0 5.0 6.0 7.0 8.0 9.0 10.0
CONCENTRATION RATIO
×10³

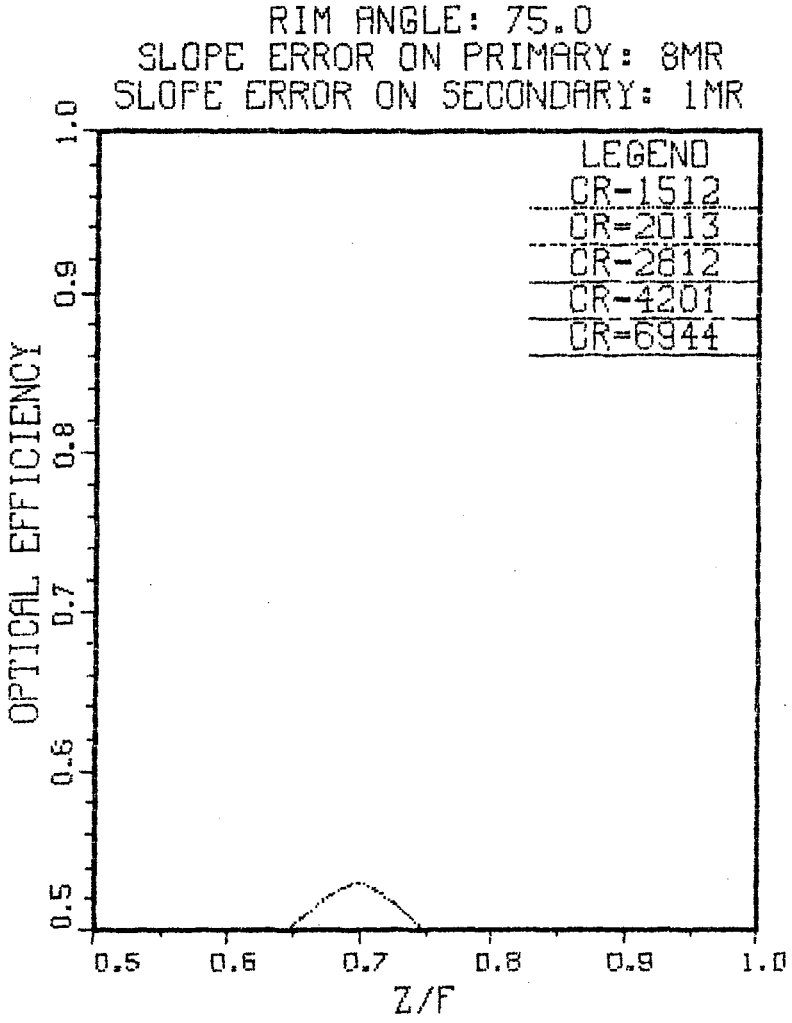
RIM ANGLE: 75.0
SLOPE ERROR ON PRIMARY: 8MR
SLOPE ERROR ON SECONDARY: 1MR
LEGEND
CR-1512
CR=2013
CR-2812
CR-4201
CR=6944
OPTICAL EFFICIENCY
0.5
0.6
0.7
0.8
0.9
1.0
Z/F

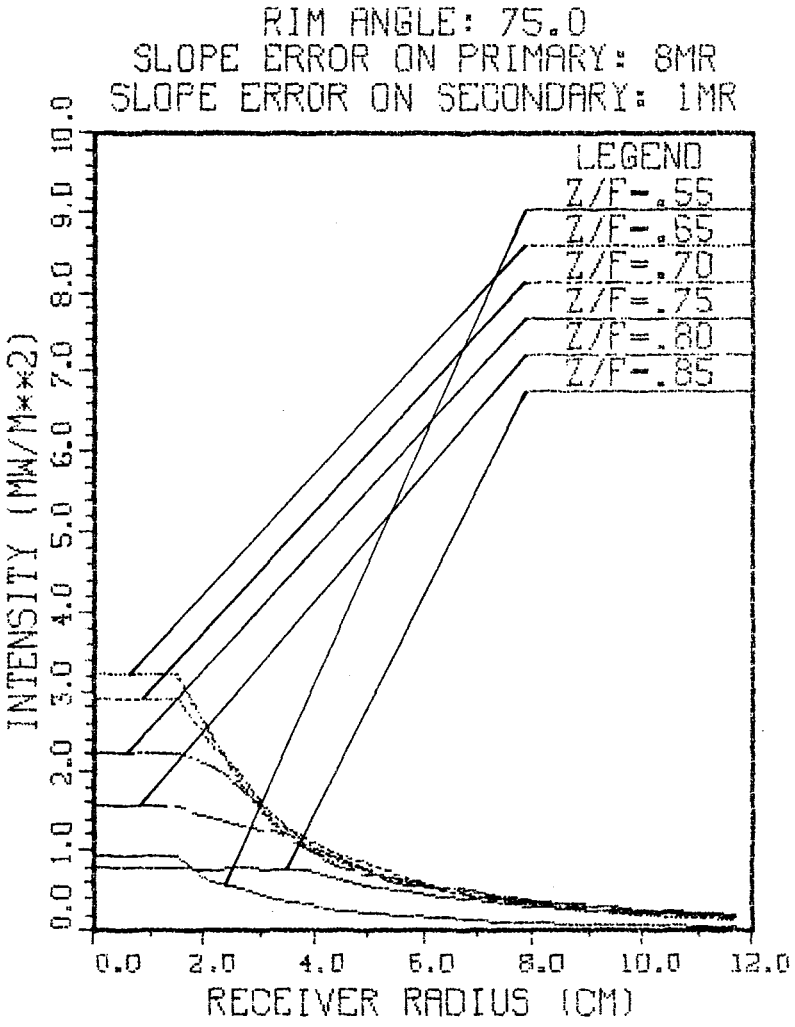
RIM ANGLE: 75.0
SLOPE ERROR ON PRIMARY: 8MR
SLOPE ERROR ON SECONDARY: 1MR
LEGEND
Z/F=.55
Z/F=.65
Z/F=.70
Z/F=.75
Z/F=.80
Z/F=.85
INTENSITY (MW/M**2)
0.0 1.0 2.0 3.0 4.0 5.0 6.0 7.0 8.0 9.0 10.0
0.0 2.0 4.0 6.0 8.0 10.0 12.0
RECEIVER RADIUS (CM)

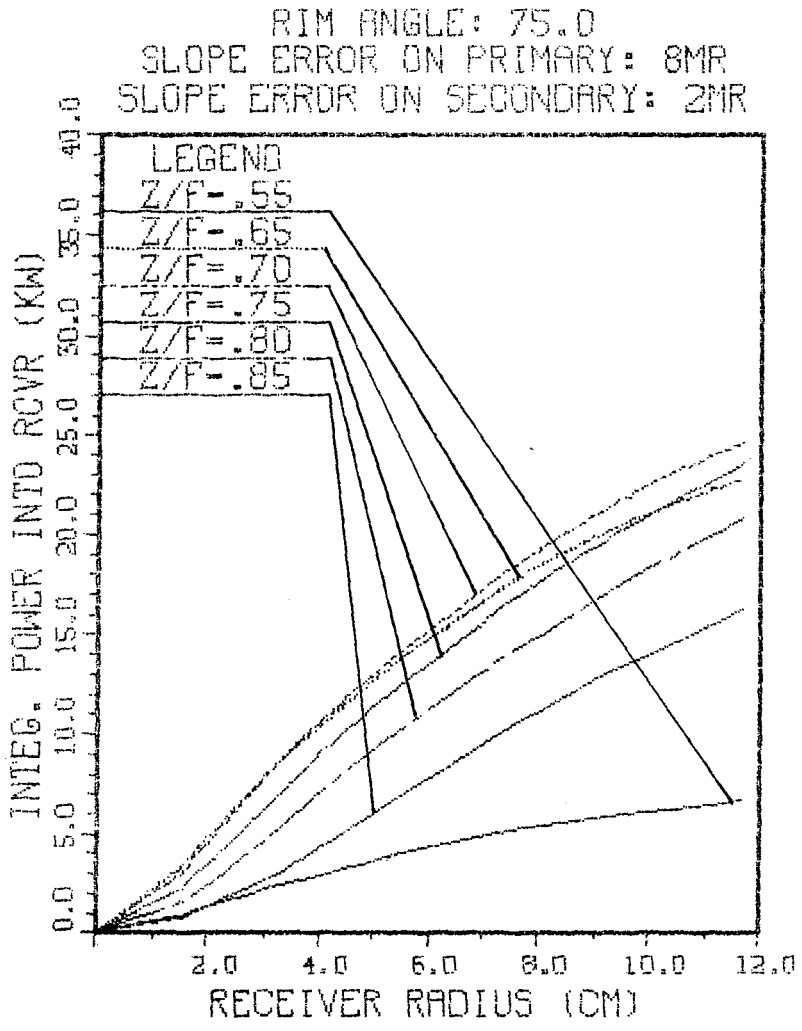
RIM ANGLE: 75.0
SLOPE ERROR ON PRIMARY: 8MR
SLOPE ERROR ON SECONDARY: 2MR
LEGEND
Z/F=.55
Z/F=.65
Z/F=.70
Z/F=.75
Z/F=.80
Z/F=.85
INTEG. POWER INTO RCVR (KW)
0.0
5.0
10.0
15.0
20.0
25.0
30.0
35.0
40.0
2.0
4.0
6.0
8.0
10.0
12.0
RECEIVER RADIUS (CM)

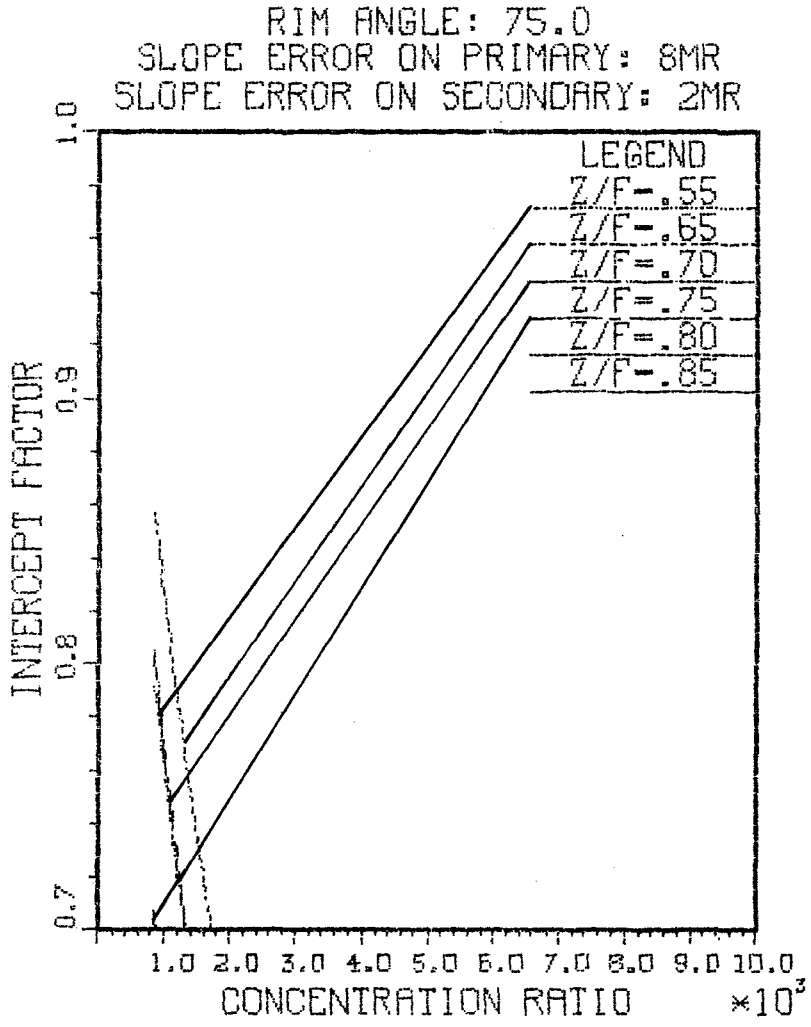
RIM ANGLE: 75.0
SLOPE ERROR ON PRIMARY: 8MR
SLOPE ERROR ON SECONDARY: 2MR
LEGEND
Z/F=.55
Z/F=.65
Z/F=.70
Z/F=.75
Z/F=.80
Z/F=.85
INTERCEPT FACTOR
1.0
0.9
0.8
0.7
1.0 2.0 3.0 4.0 5.0 6.0 7.0 8.0 9.0 10.0
CONCENTRATION RATIO
×10³

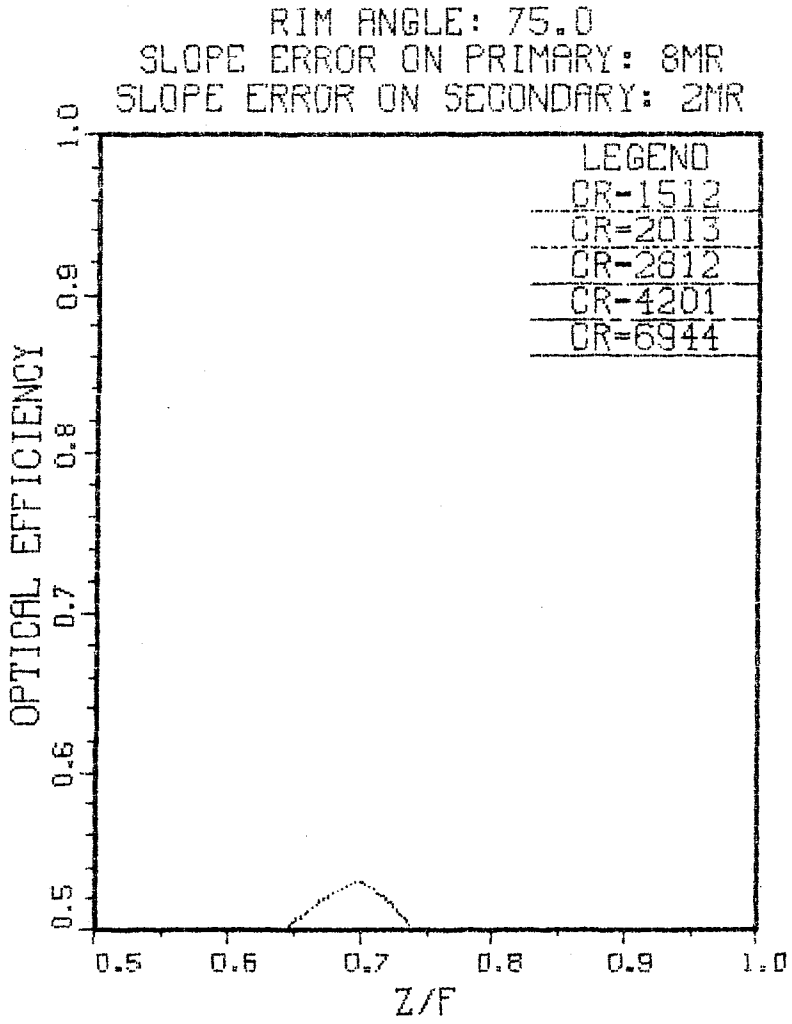
RIM ANGLE: 75.0
SLOPE ERROR ON PRIMARY: 8MR
SLOPE ERROR ON SECONDARY: 2MR
LEGEND
CR-1512
CR=2013
CR-2812
CR-4201
CR=6944
OPTICAL EFFICIENCY
0.5
0.6
0.7
0.8
0.9
1.0
Z/F

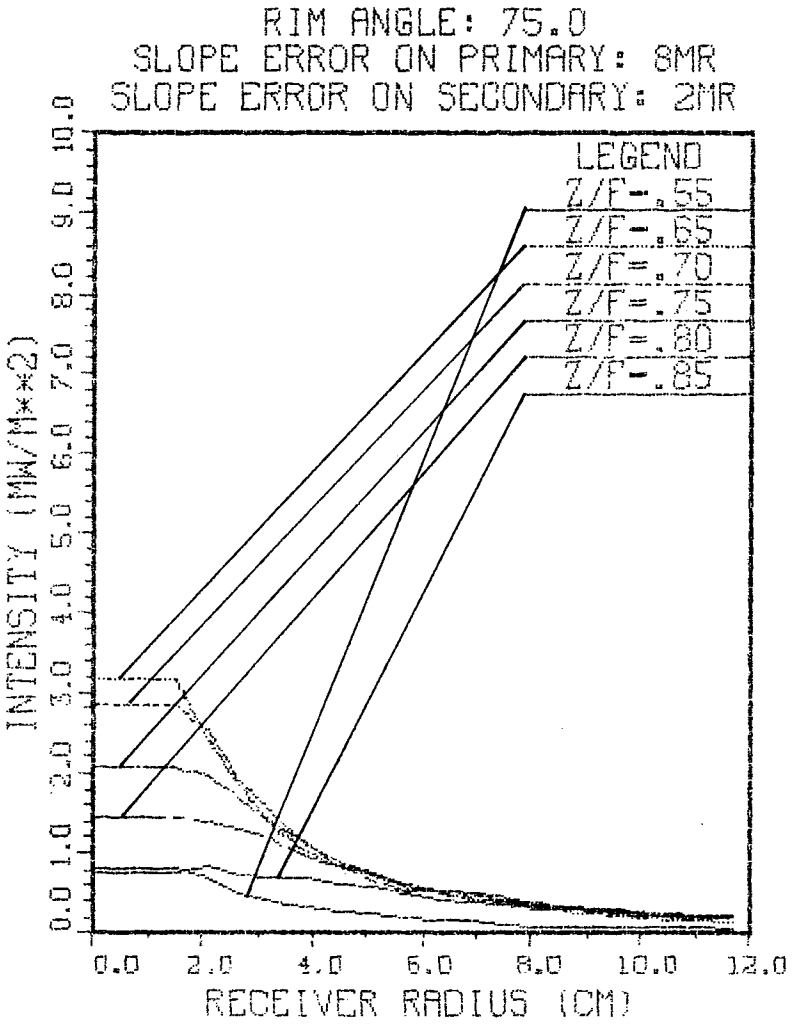
RIM ANGLE: 75.0
SLOPE ERROR ON PRIMARY: 8MR
SLOPE ERROR ON SECONDARY: 2MR
LEGEND
Z/F=.55
Z/F=.65
Z/F=.70
Z/F=.75
Z/F=.80
Z/F=.85
INTENSITY (MW/M**2)
0.0 1.0 2.0 3.0 4.0 5.0 6.0 7.0 8.0 9.0 10.0
0.0 2.0 4.0 6.0 8.0 10.0 12.0
RECEIVER RADIUS (CM)

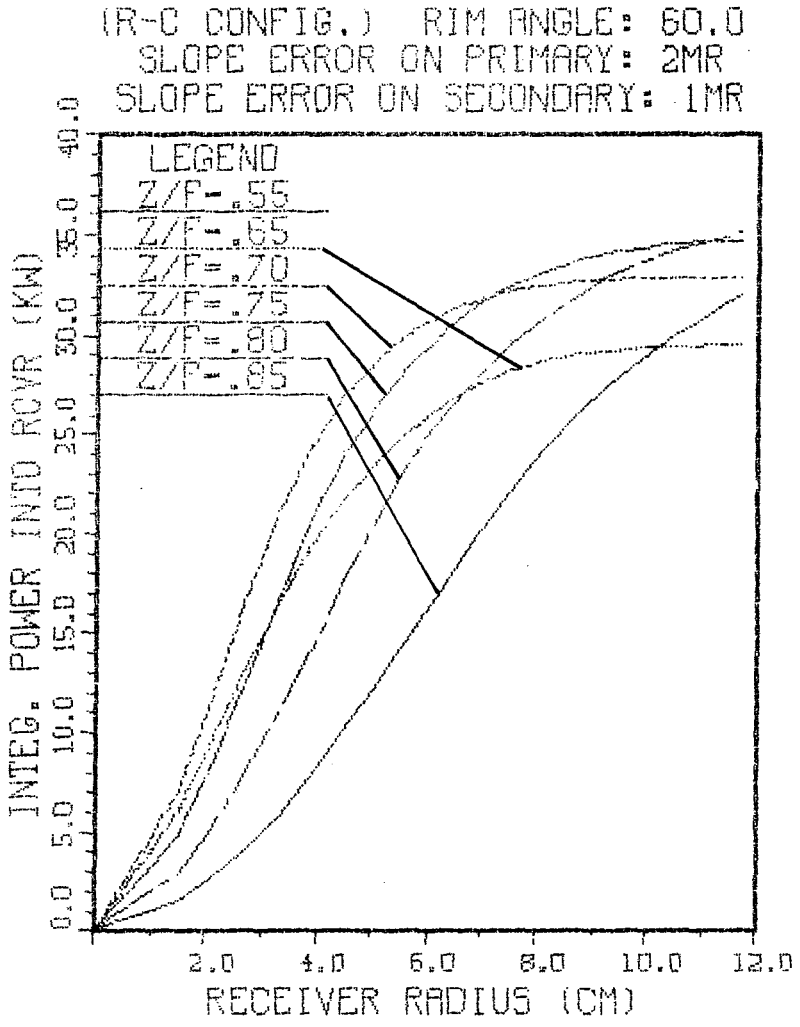
(R-C CONFIG.) RIM ANGLE: 60.0
SLOPE ERROR ON PRIMARY: 2MR
SLOPE ERROR ON SECONDARY: 1MR
LEGEND
Z/F=.55
Z/F=.65
Z/F=.70
Z/F=.75
Z/F=.80
Z/F=.85
INTEG. POWER INTO RCVR (KW)
0.0
5.0
10.0
15.0
20.0
25.0
30.0
35.0
40.0
2.0
4.0
6.0
8.0
10.0
12.0
RECEIVER RADIUS (CM)

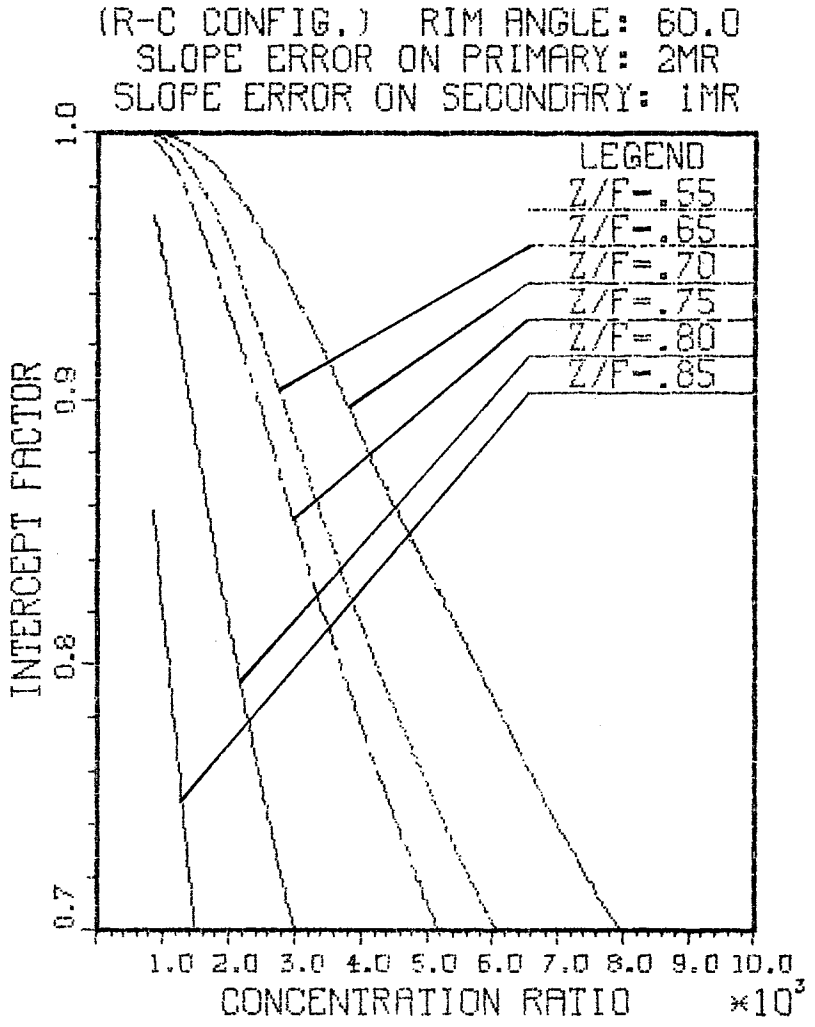
(R-C CONFIG.) RIM ANGLE: 60.0
SLOPE ERROR ON PRIMARY: 2MR
SLOPE ERROR ON SECONDARY: 1MR
LEGEND
Z/F=.55
Z/F=.65
Z/F=.70
Z/F=.75
Z/F=.80
Z/F=.85
INTERCEPT FACTOR
1.0
0.9
0.8
0.7
1.0 2.0 3.0 4.0 5.0 6.0 7.0 8.0 9.0 10.0
CONCENTRATION RATIO
*10^3

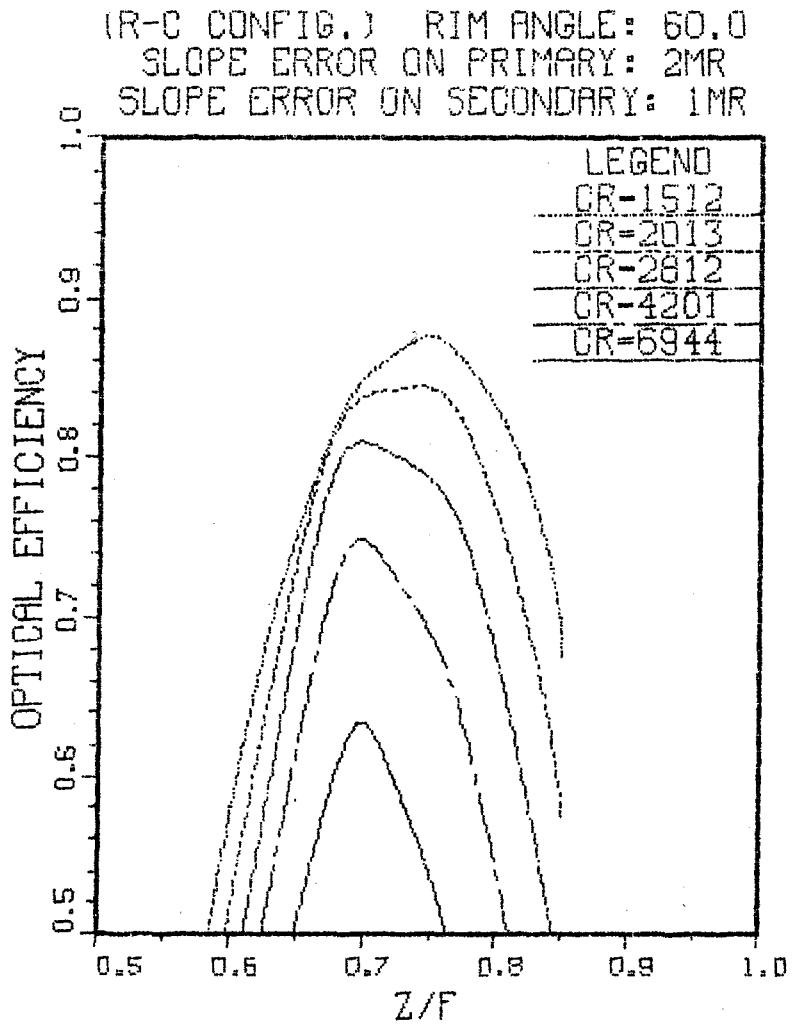
(R-C CONFIG.) RIM ANGLE: 60.0
SLOPE ERROR ON PRIMARY: 2MR
SLOPE ERROR ON SECONDARY: 1MR
LEGEND
CR-1512
CR=2013
CR-2812
CR-4201
CR=6944
OPTICAL EFFICIENCY
0.5
0.6
0.7
0.8
0.9
1.0
Z/F

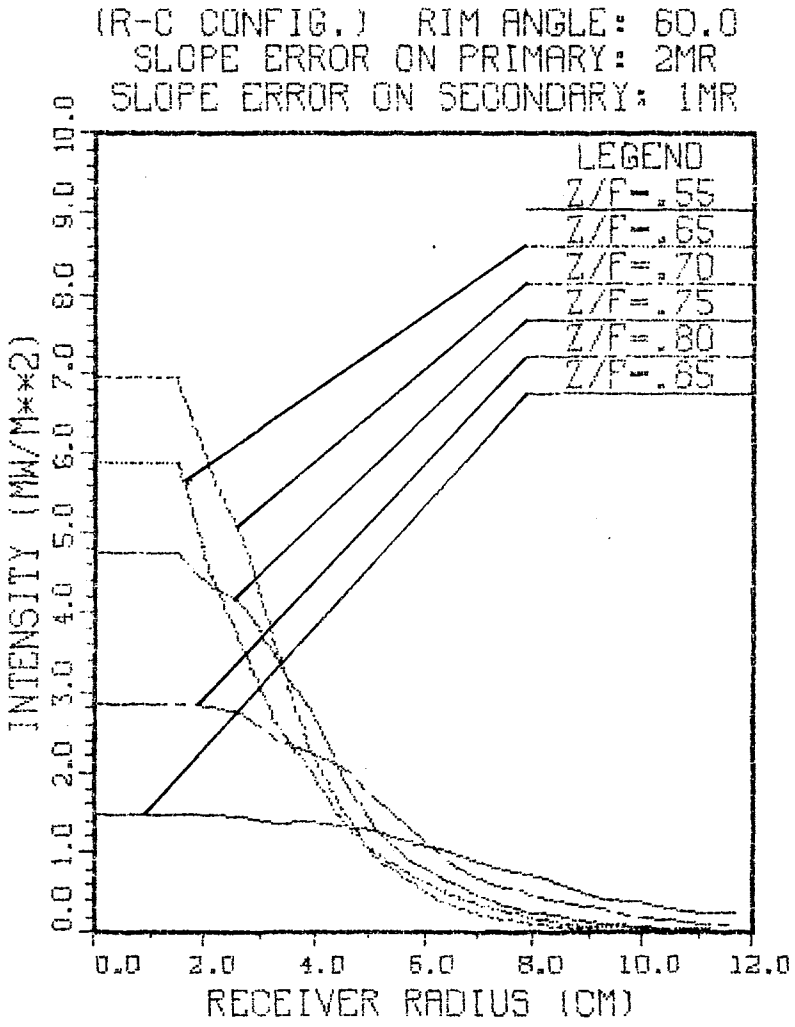
(R-C CONFIG.) RIM ANGLE: 60.0
SLOPE ERROR ON PRIMARY: 2MR
SLOPE ERROR ON SECONDARY: 1MR
LEGEND
Z/F=.55
Z/F=.65
Z/F=.70
Z/F=.75
Z/F=.80
Z/F=.85
INTENSITY (MW/M**2)
0.0 1.0 2.0 3.0 4.0 5.0 6.0 7.0 8.0 9.0 10.0
0.0 2.0 4.0 6.0 8.0 10.0 12.0
RECEIVER RADIUS (CM)

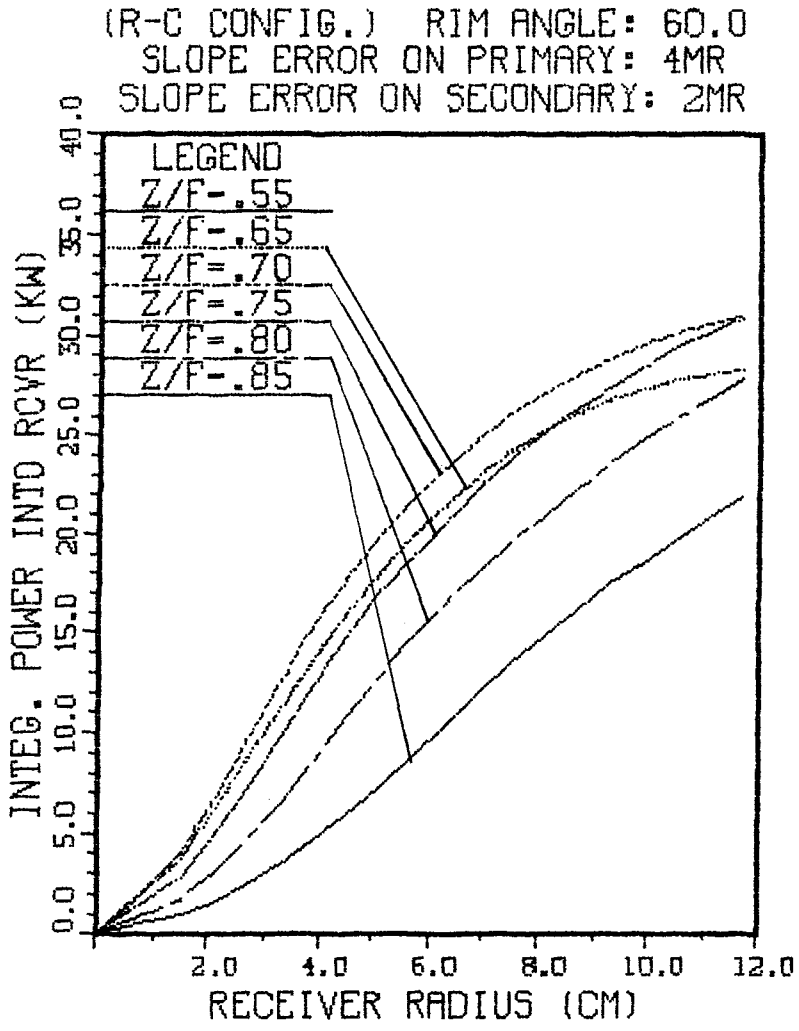
(R-C CONFIG.) RIM ANGLE: 60.0
SLOPE ERROR ON PRIMARY: 4MR
SLOPE ERROR ON SECONDARY: 2MR
LEGEND
Z/F=.55
Z/F=.65
Z/F=.70
Z/F=.75
Z/F=.80
Z/F=.85
INTEG. POWER INTO RCVR (KW)
0.0
5.0
10.0
15.0
20.0
25.0
30.0
35.0
40.0
2.0
4.0
6.0
8.0
10.0
12.0
RECEIVER RADIUS (CM)

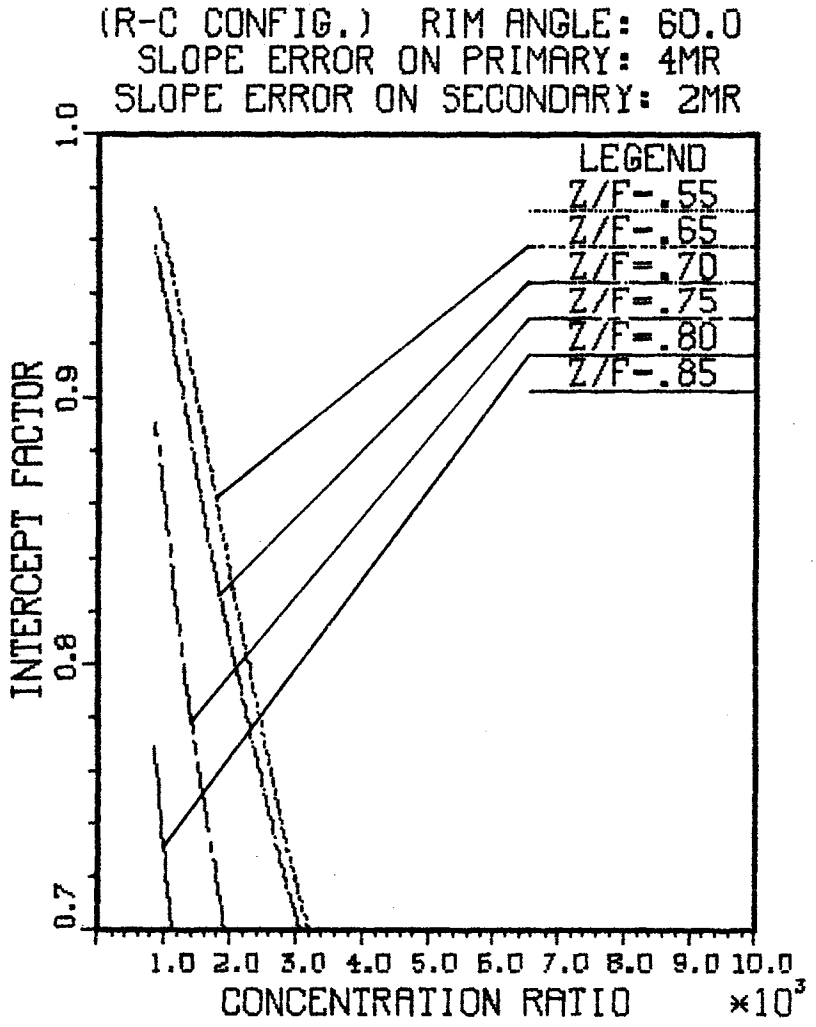
(R-C CONFIG.) RIM ANGLE: 60.0
SLOPE ERROR ON PRIMARY: 4MR
SLOPE ERROR ON SECONDARY: 2MR
LEGEND
Z/F=.55
Z/F=.65
Z/F=.70
Z/F=.75
Z/F=.80
Z/F=.85
INTERCEPT FACTOR
1.0
0.9
0.8
0.7
1.0 2.0 3.0 4.0 5.0 6.0 7.0 8.0 9.0 10.0
CONCENTRATION RATIO
×10³

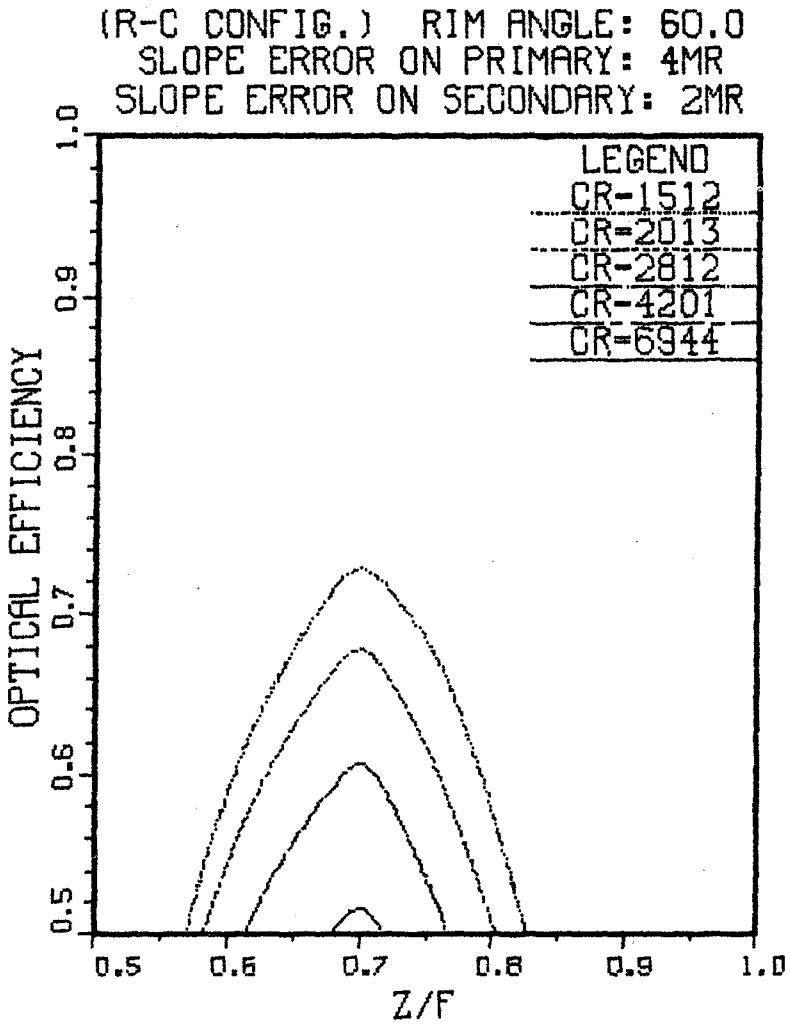
(R-C CONFIG.) RIM ANGLE: 60.0
SLOPE ERROR ON PRIMARY: 4MR
SLOPE ERROR ON SECONDARY: 2MR
LEGEND
CR-1512
CR=2013
CR-2812
CR-4201
CR-6944
OPTICAL EFFICIENCY
0.5
0.6
0.7
0.8
0.9
1.0
Z/F

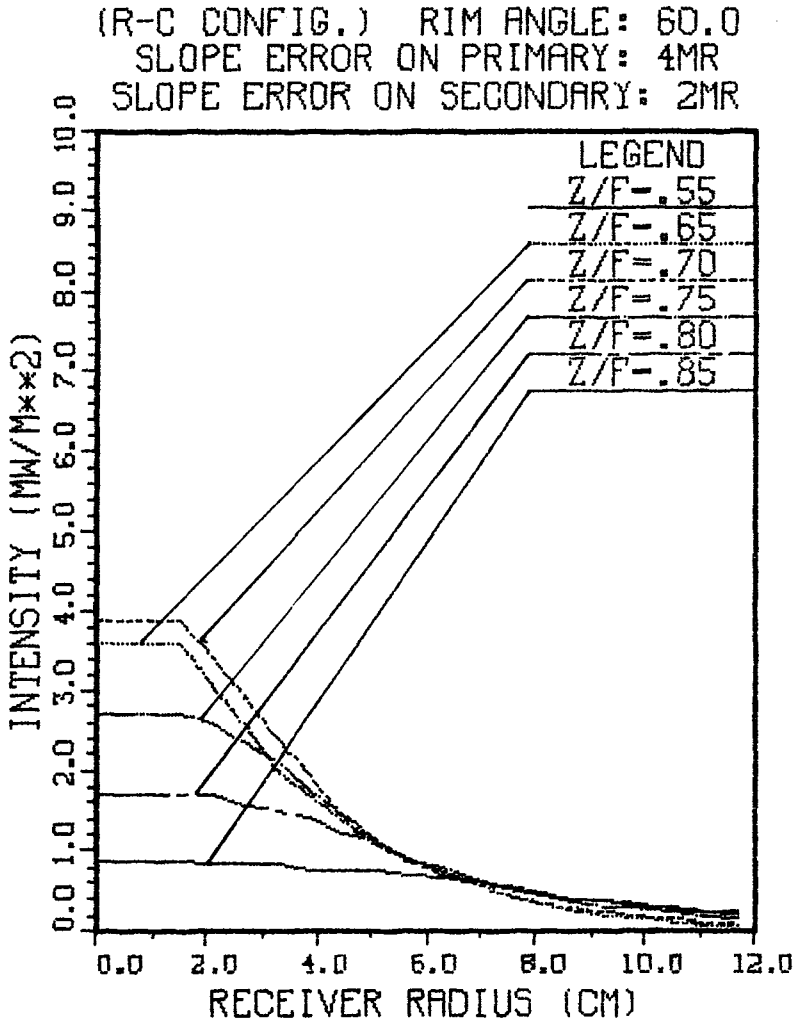
(R-C CONFIG.) RIM ANGLE: 60.0
SLOPE ERROR ON PRIMARY: 4MR
SLOPE ERROR ON SECONDARY: 2MR
LEGEND
Z/F=.55
Z/F=.65
Z/F=.70
Z/F=.75
Z/F=.80
Z/F=.85
INTENSITY (MW/M**2)
0.0 1.0 2.0 3.0 4.0 5.0 6.0 7.0 8.0 9.0 10.0
0.0 2.0 4.0 6.0 8.0 10.0 12.0
RECEIVER RADIUS (CM)

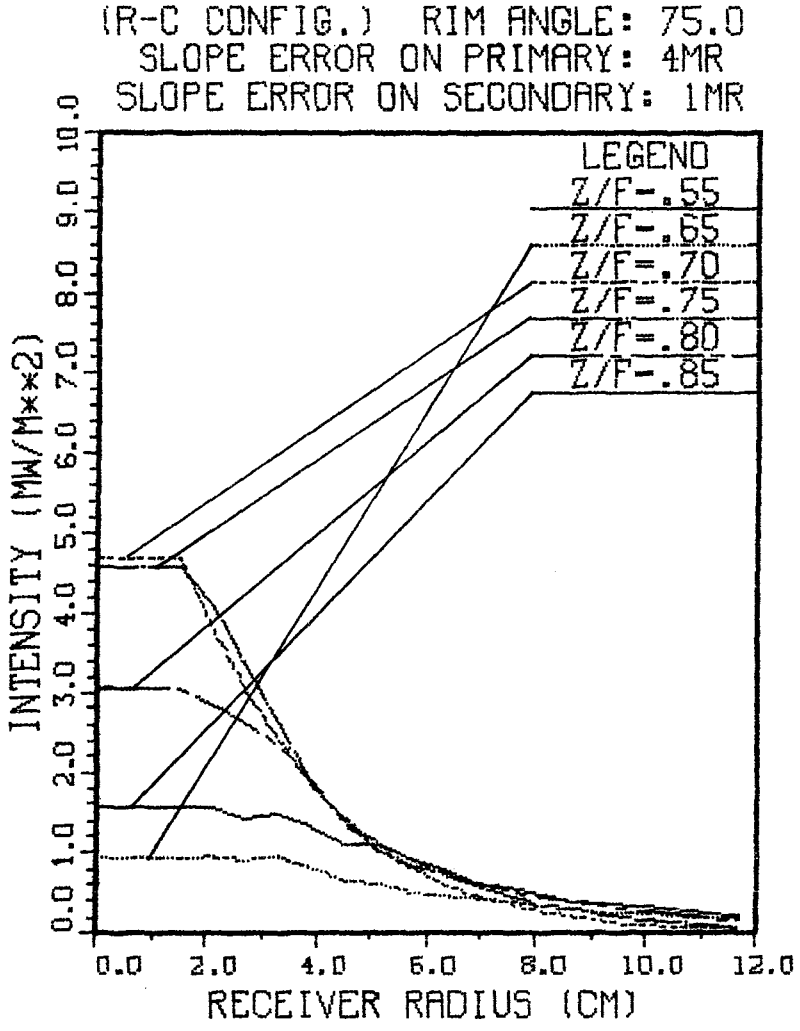
(R-C CONFIG.) RIM ANGLE: 75.0
SLOPE ERROR ON PRIMARY: 4MR
SLOPE ERROR ON SECONDARY: 1MR
LEGEND
Z/F=.55
Z/F=.65
Z/F=.70
Z/F=.75
Z/F=.80
Z/F=.85
INTENSITY (MW/M**2)
0.0
1.0
2.0
3.0
4.0
5.0
6.0
7.0
8.0
9.0
10.0
0.0
2.0
4.0
6.0
8.0
10.0
12.0
RECEIVER RADIUS (CM)

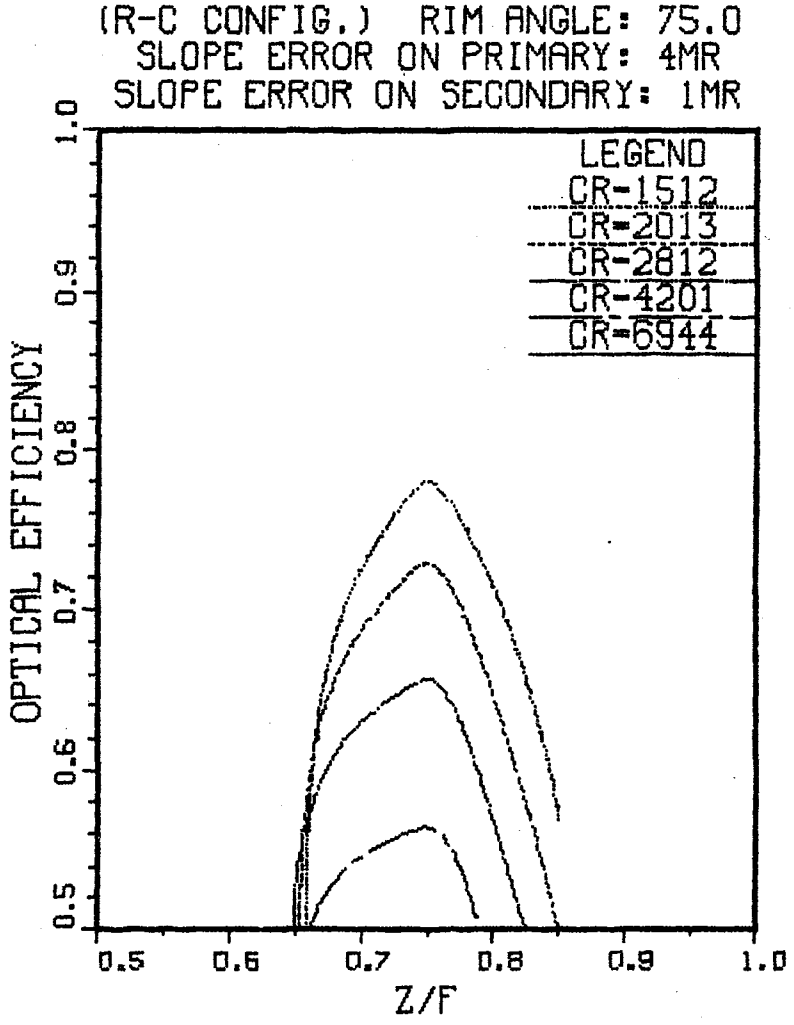
(R-C CONFIG.) RIM ANGLE: 75.0
SLOPE ERROR ON PRIMARY: 4MR
SLOPE ERROR ON SECONDARY: 1MR
LEGEND
CR-1512
CR-2013
CR-2812
CR-4201
CR-6944
OPTICAL EFFICIENCY
1.0
0.9
0.8
0.7
0.6
0.5
0.5
0.6
0.7
0.8
0.9
1.0
Z/F

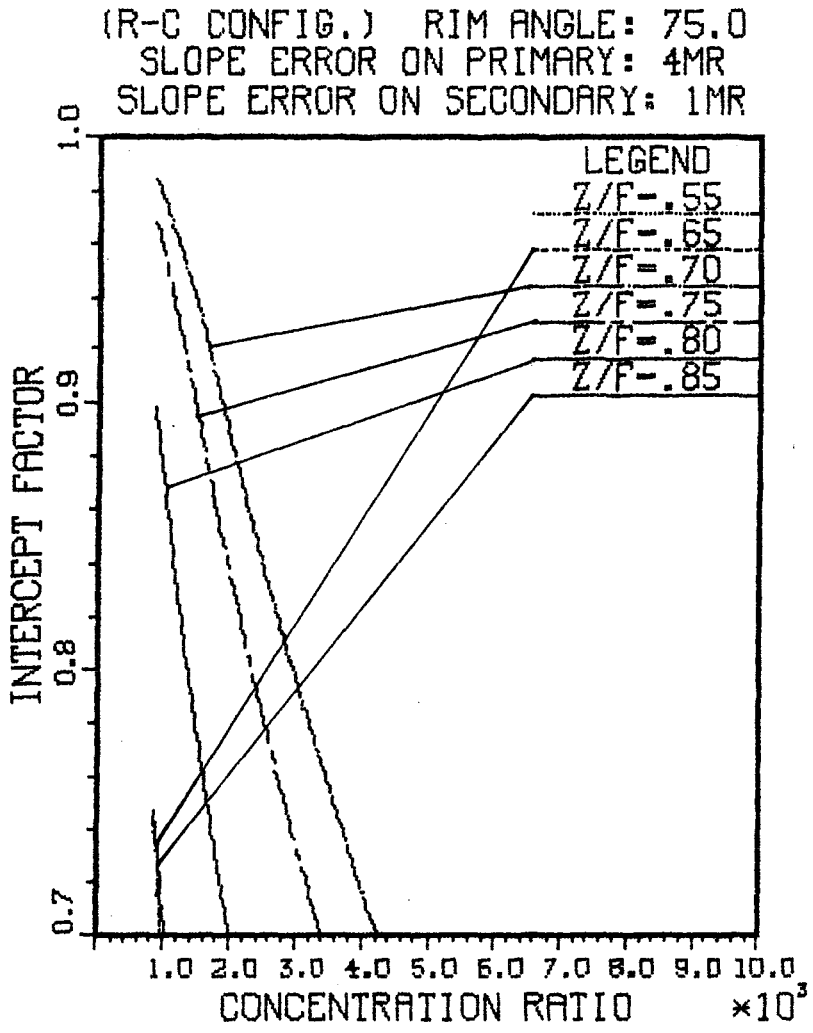
(R-C CONFIG.) RIM ANGLE: 75.0
SLOPE ERROR ON PRIMARY: 4MR
SLOPE ERROR ON SECONDARY: 1MR
LEGEND
Z/F=.55
Z/F=.65
Z/F=.70
Z/F=.75
Z/F=.80
Z/F=.85
INTERCEPT FACTOR
1.0
0.9
0.8
0.7
1.0 2.0 3.0 4.0 5.0 6.0 7.0 8.0 9.0 10.0
CONCENTRATION RATIO
×10³

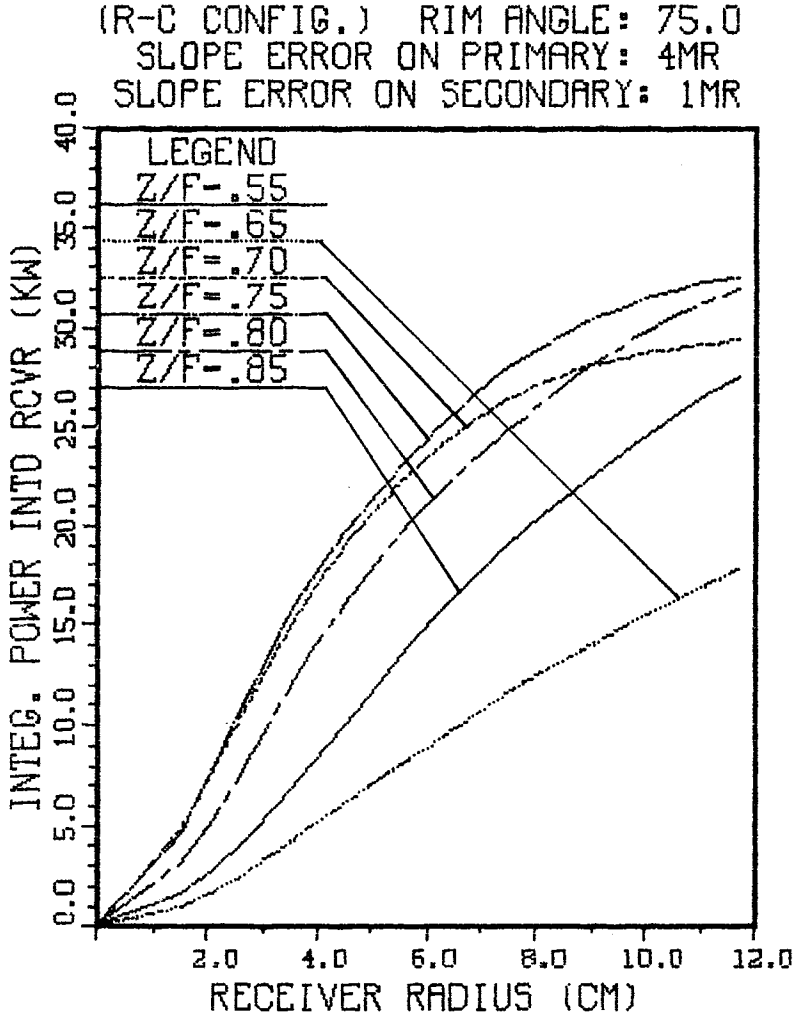
(R-C CONFIG.) RIM ANGLE: 75.0
SLOPE ERROR ON PRIMARY: 4MR
SLOPE ERROR ON SECONDARY: 1MR
LEGEND
Z/F=.55
Z/F=.65
Z/F=.70
Z/F=.75
Z/F=.80
Z/F=.85
INTEG. POWER INTO RCVR (KW)
0.0
5.0
10.0
15.0
20.0
25.0
30.0
35.0
40.0
2.0
4.0
6.0
8.0
10.0
12.0
RECEIVER RADIUS (CM)

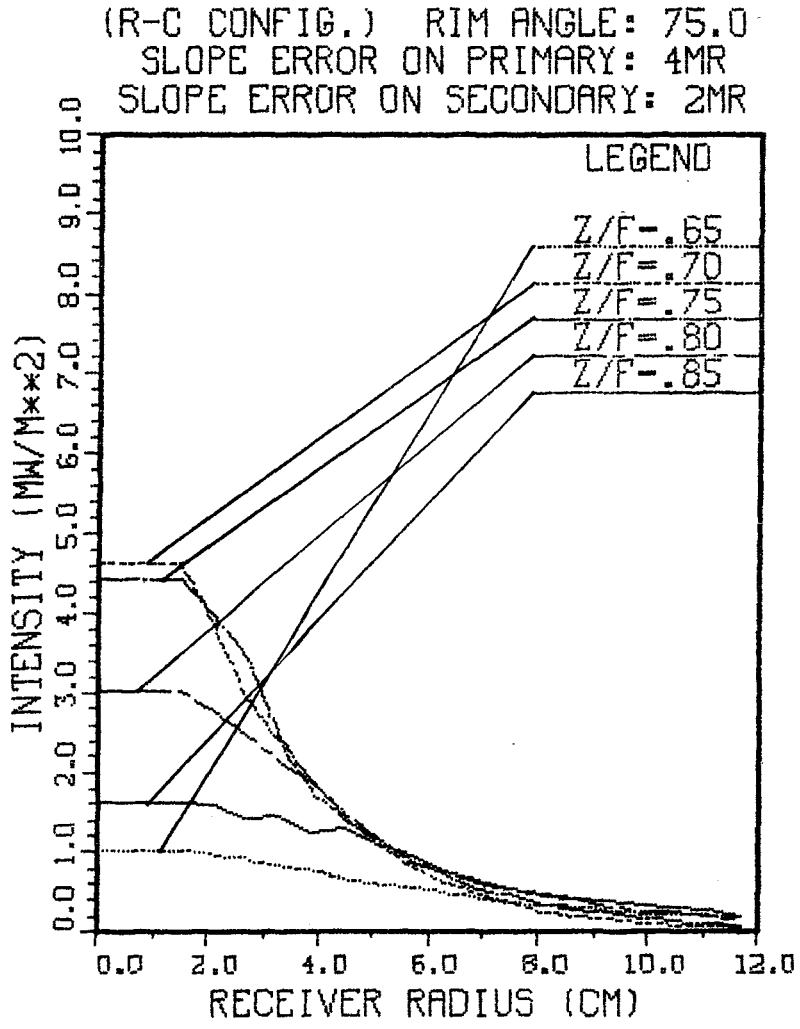
(R-C CONFIG.) RIM ANGLE: 75.0
SLOPE ERROR ON PRIMARY: 4MR
SLOPE ERROR ON SECONDARY: 2MR
LEGEND
Z/F=.65
Z/F=.70
Z/F=.75
Z/F=.80
Z/F=.85
INTENSITY (MW/M**2)
0.0 1.0 2.0 3.0 4.0 5.0 6.0 7.0 8.0 9.0 10.0
0.0 2.0 4.0 6.0 8.0 10.0 12.0
RECEIVER RADIUS (CM)

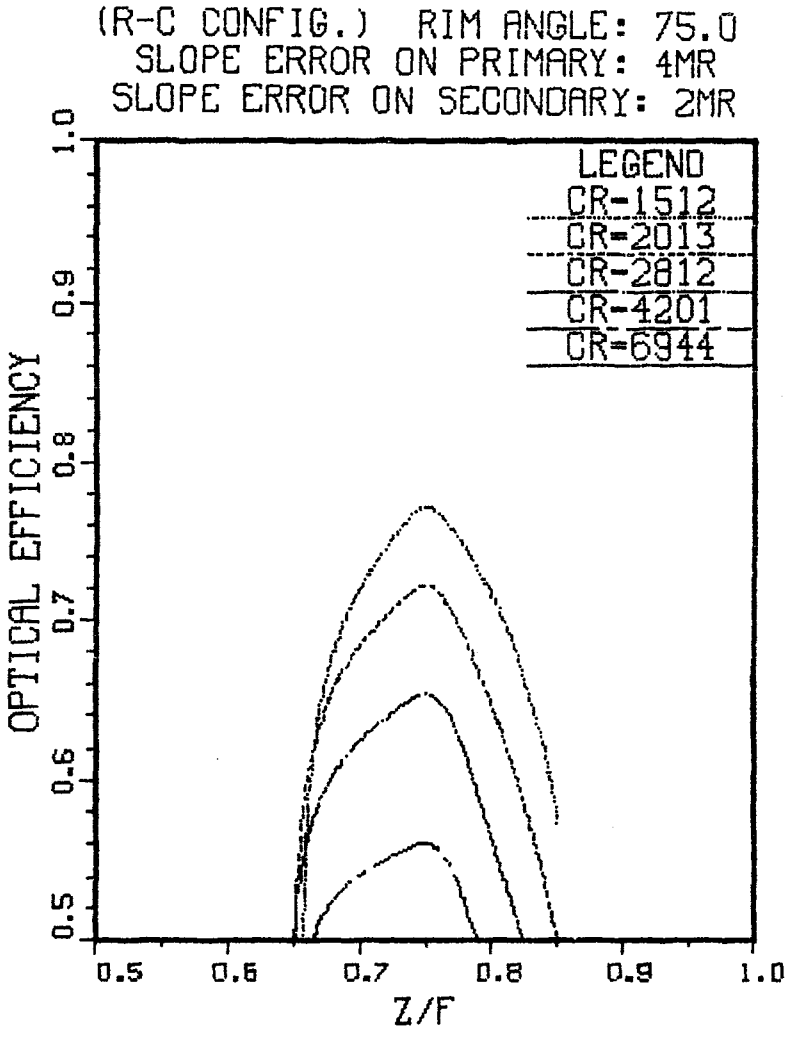
(R-C CONFIG.) RIM ANGLE: 75.0
SLOPE ERROR ON PRIMARY: 4MR
SLOPE ERROR ON SECONDARY: 2MR
LEGEND
CR-1512
CR-2013
CR-2812
CR-4201
CR-6944
OPTICAL EFFICIENCY
0.5
0.6
0.7
0.8
0.9
1.0
Z/F

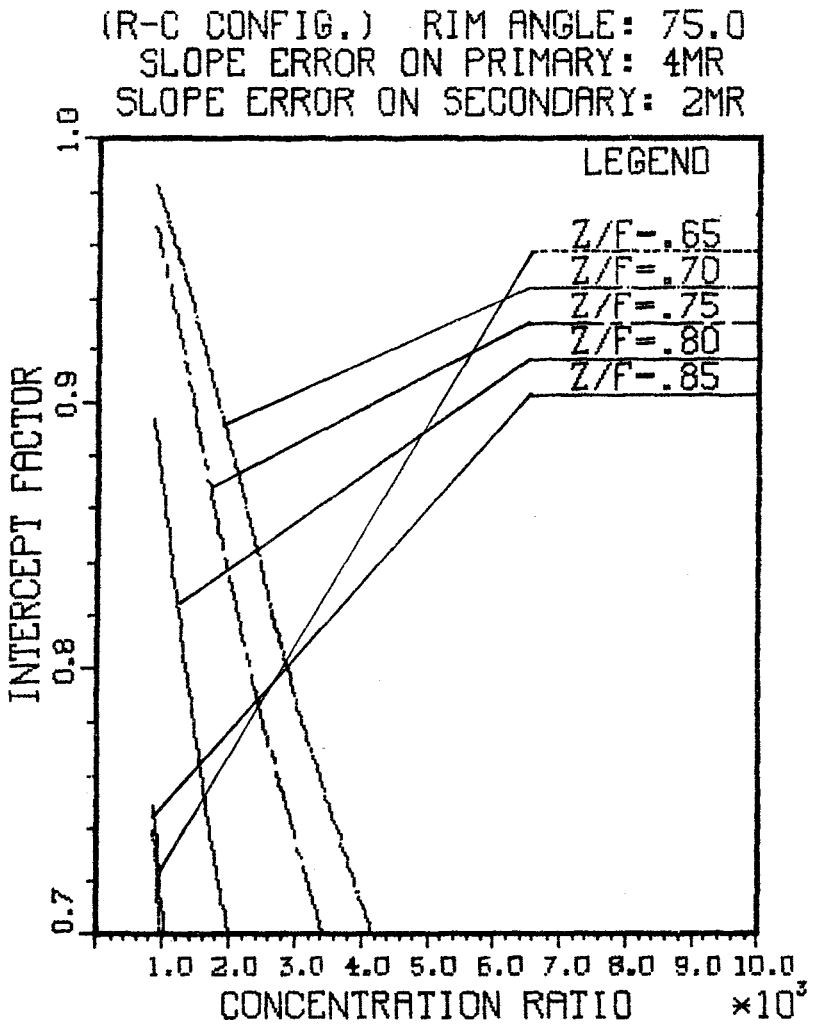
(R-C CONFIG.) RIM ANGLE: 75.0
SLOPE ERROR ON PRIMARY: 4MR
SLOPE ERROR ON SECONDARY: 2MR
LEGEND
Z/F=.65
Z/F=.70
Z/F=.75
Z/F=.80
Z/F=.85
INTERCEPT FACTOR
1.0
0.9
0.8
0.7
1.0 2.0 3.0 4.0 5.0 6.0 7.0 8.0 9.0 10.0
CONCENTRATION RATIO ×10³

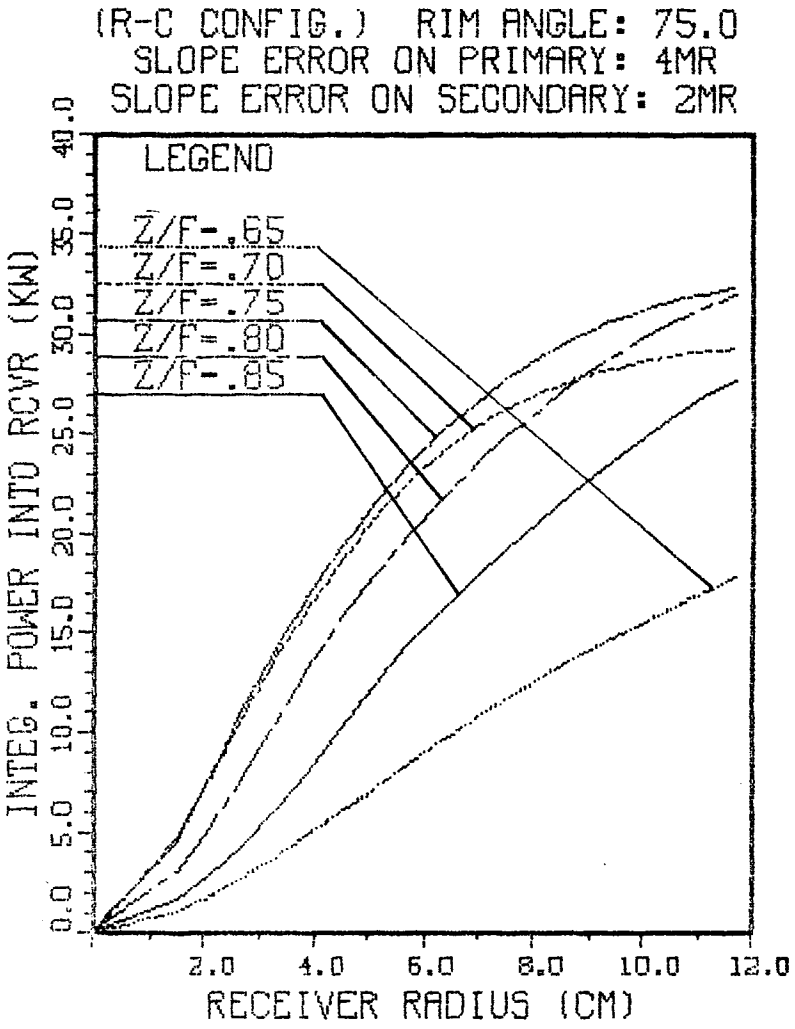
(R-C CONFIG.) RIM ANGLE: 75.0
SLOPE ERROR ON PRIMARY: 4MR
SLOPE ERROR ON SECONDARY: 2MR
LEGEND
Z/F=.65
Z/F=.70
Z/F=.75
Z/F=.80
Z/F=.85
INTEG. POWER INTO RCVR (KW)
0.0
5.0
10.0
15.0
20.0
25.0
30.0
35.0
40.0
2.0
4.0
6.0
8.0
10.0
12.0
RECEIVER RADIUS (CM)

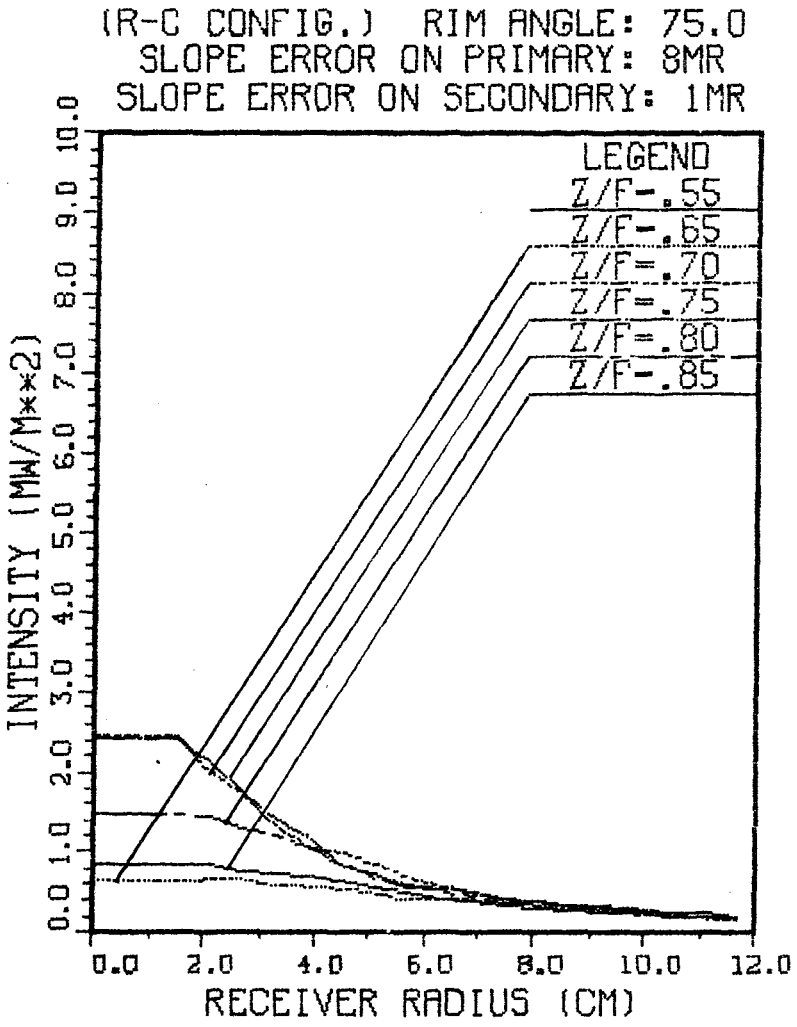
(R-C CONFIG.) RIM ANGLE: 75.0
SLOPE ERROR ON PRIMARY: 8MR
SLOPE ERROR ON SECONDARY: 1MR
LEGEND
Z/F=.55
Z/F=.65
Z/F=.70
Z/F=.75
Z/F=.80
Z/F=.85
INTENSITY (MW/M**2)
0.0 1.0 2.0 3.0 4.0 5.0 6.0 7.0 8.0 9.0 10.0
0.0 2.0 4.0 6.0 8.0 10.0 12.0
RECEIVER RADIUS (CM)

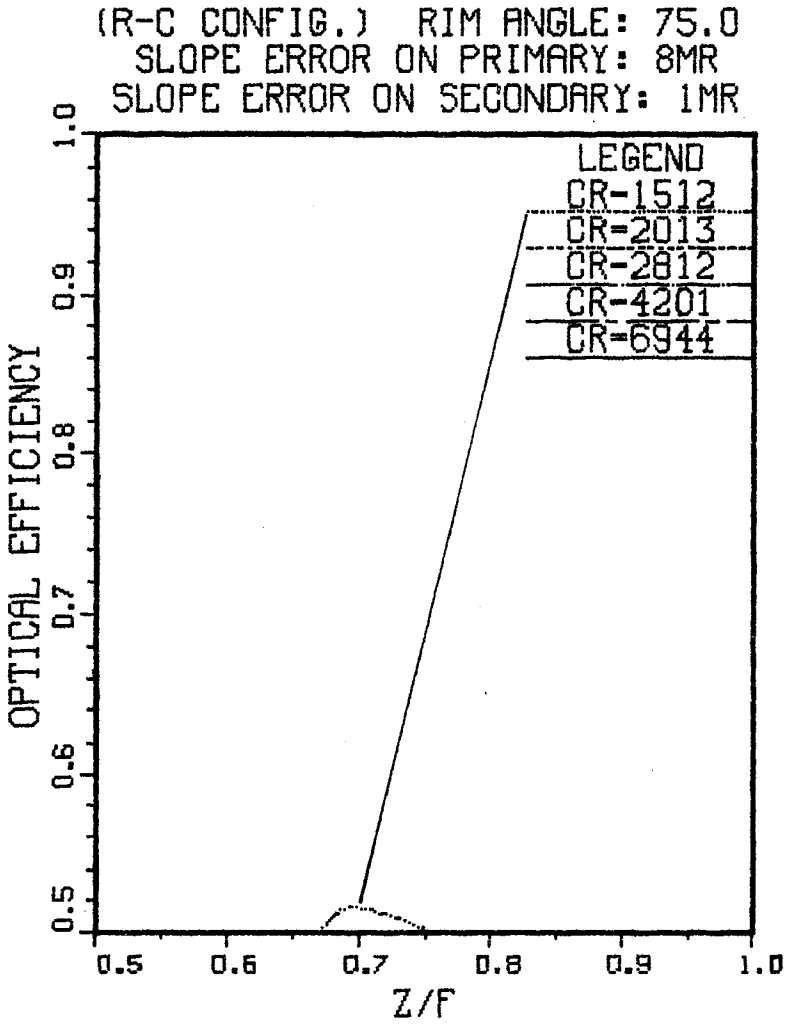
(R-C CONFIG.) RIM ANGLE: 75.0
SLOPE ERROR ON PRIMARY: 8MR
SLOPE ERROR ON SECONDARY: 1MR
LEGEND
CR-1512
CR=2013
CR-2812
CR-4201
CR=6944
OPTICAL EFFICIENCY
0.5
0.6
0.7
0.8
0.9
1.0
Z/F

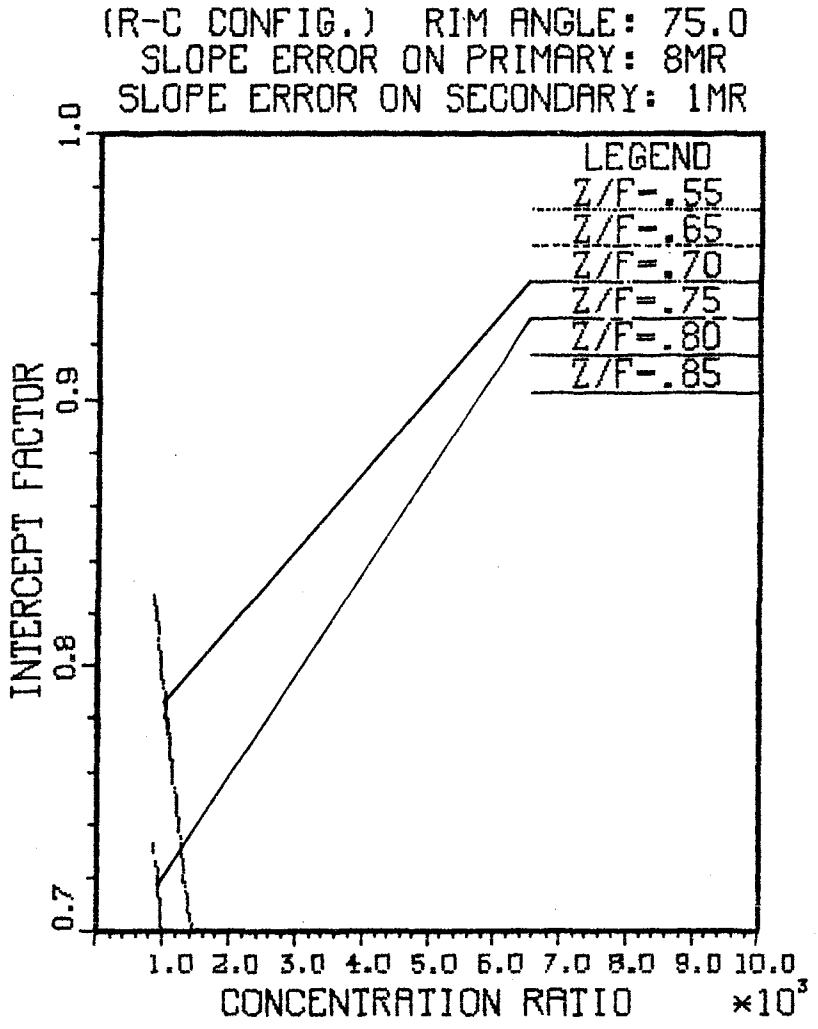
(R-C CONFIG.) RIM ANGLE: 75.0
SLOPE ERROR ON PRIMARY: 8MR
SLOPE ERROR ON SECONDARY: 1MR
LEGEND
Z/F=.55
Z/F=.65
Z/F=.70
Z/F=.75
Z/F=.80
Z/F=.85
INTERCEPT FACTOR
1.0
0.9
0.8
0.7
1.0 2.0 3.0 4.0 5.0 6.0 7.0 8.0 9.0 10.0
CONCENTRATION RATIO
*10^3

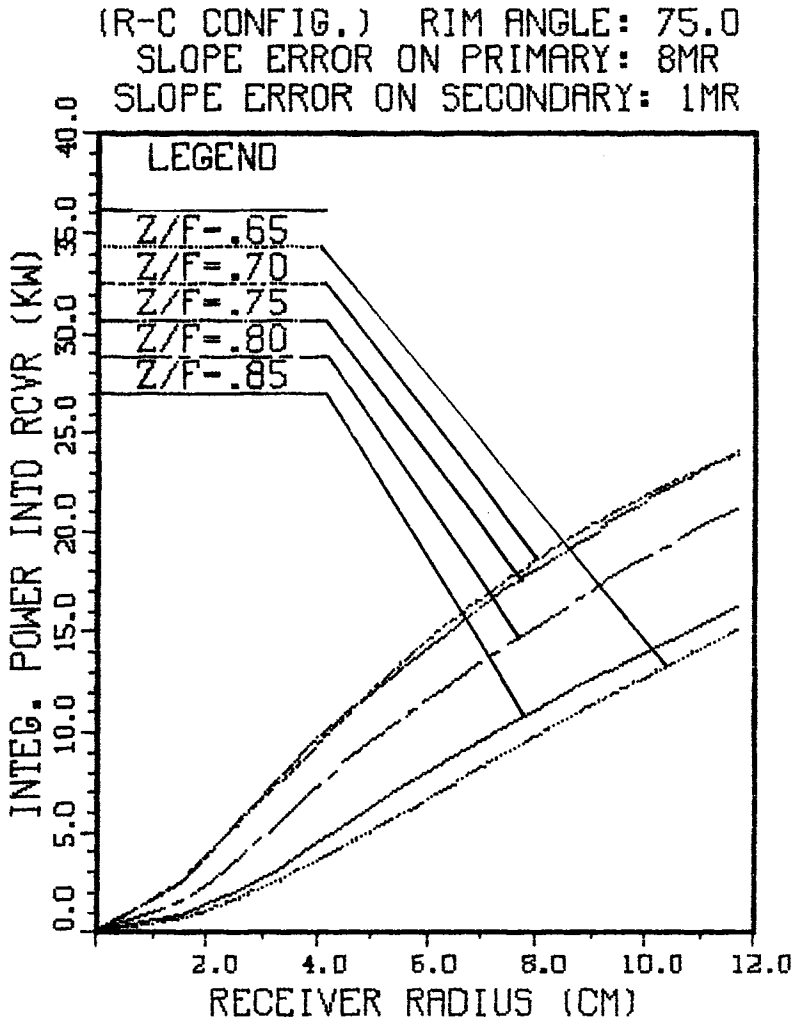
(R-C CONFIG.) RIM ANGLE: 75.0
SLOPE ERROR ON PRIMARY: 8MR
SLOPE ERROR ON SECONDARY: 1MR
LEGEND
Z/F=.65
Z/F=.70
Z/F=.75
Z/F=.80
Z/F=.85
INTEG. POWER INTO RCVR (KW)
0.0
5.0
10.0
15.0
20.0
25.0
30.0
35.0
40.0
2.0
4.0
6.0
8.0
10.0
12.0
RECEIVER RADIUS (CM)

APPENDIX B
LISTING OF CONCENTRATOR OPTICAL PERFORMANCE SIMULATION (COPS) COMPUTER CODE

COPS.FOR;1 26-JAN-1984 15:32 Page 1

```
      PROGRAM COPS
C     DEVELOPED BY HONEYWELL.
C     THIS PROGRAM HAS BEEN MODIFIED BY STUART WATERBURY OF BDM TO PERFORM
C     ANALYSES ON:
C       1.   CASSEGRAINIAN SOLAR CONCENTRATORS
C       2.   RITCHEY CHRETIEN MODIFIED CASSEGRAINIAN CONCENTRATORS
C       3.   TRUMPET TYPE NON-IMAGING CONCENTRATORS
C
      LOGICAL*1 FNOUT(11)
      COMMON/RUNC/ NDRAW,TAZ,TEL,TIME,XLAT,XLONG,TZONE,IDAY,ICONC,ISTOP,
     + NMAT,MAPS,NMATL
      COMMON/VECTOR/ ULE(3),ULV(3),ULS(3),UCN(3),UCA(3),UCP(3),US(3)
      DRAD=0.0174532925
C   SET LOCAL DIRECTION VECTORS
      DO 3 I =1,3
      ULE(I)=0.0
      ULS(I)=0.0
    3 ULV(I)=0.0
      ULS(1)=1.0
      ULE(2)=1.0
      ULV(3)=1.0
C  SET DEFAULT AZIMUTH AND ELEVATION
      TAZ=0.0
      TEL=1.57079633
      TIME=12.
C   LAT AND LONG IN DEGREES
      XLAT=33.
      XLONG=90.
      TZONE=6.
      IDAY=0
C
C  OPEN INPUT DATA FILE
      OPEN(UNIT=7,FILE='CASSPAR.DAT',STATUS='OLD')
C    READ INPUT DATA
    5 READ(7,10) (FNOUT(I),I=1,11),NDRAW,ICONC,ISTOP
   10 FORMAT(1X,11A1,3I10)
      OPEN(UNIT=8,FILE=FNOUT,STATUS='NEW',RECL=9999)
      IF(ICONC.EQ.1)CALL UNMODC
      IF(ICONC.EQ.2) CALL RCCASS
      IF (ICONC.EQ.3) CALL PDISH2
      ENDFILE 8
      CLOSE(UNIT=8,STATUS='SAVE')
      IF(ISTOP.NE.1) GO TO 5
      STOP
      END
      SUBROUTINE UNMODC
C
C   THIS SUBROUTINE MODELS AN UNMODIFIED CASSEGRAINIAN SOLAR
C   CONCENTRATOR, WITH A PARABOLOIDAL PRIMARY REFLECTOR AND A
C   HYPERBOLOIDAL SECONDARY REFLECTOR.  THE COMMON FOCAL POINT FOR THE
C   TWO REFLECTORS IS AT THE PRIMARY SURFACE FOCAL POINT.  THE
C   SYSTEM FOCUS IS AT THE VERTEX OF THE PRIMARY REFLECTOR.
C
      DIMENSION D(3),UT(3),UN(3),UNP(3),UR(3),USP(3),RHIT(3),UDUM(3),
     + UNH(3),UDUMH(3),UTH(3),UTH2(3),UNPH(3),URH(3),XIF(20),RINT(20),
     + ARPI(20),RR(20),CR(20),EOPTI(20),UT2(3),HARPI(20),RRH(20)
     + ,XINT(20),X2INT(20),IFIRST(16)
      INTEGER*4 ISEED
      COMMON/RUNC/ NDRAW,TAZ,TEL,TIME,XLAT,XLONG,TZONE,IDAY,ICONC,ISTOP,
```

```
     + NMAT,MAPS,NMATL
      COMMON/VECTOR/ ULE(3),ULV(3),ULS(3),UCN(3),UCA(3),UCP(3),US(3)
      COMMON/CASSEG/ RMANGL,F,R2,Z,SD1,SD2,NRZR,NRZ2,RMAX,REFL1,REFL2,
     + PSM1,PSM2,R1
      COMMON/TPAR/TRANGL(16),EXAPR(16),ZTRUN(16),ZPOS(16)
     + ,PWRTER(20,16),ZTER(20,16),MIST(16),
     + XLOST(16),NLOST(16),NABS(16),PRCVR(20,16),
     + RRCVR(20,16),TREFL(16),SDT(16),ANGR(14),ANGPWR(14,16)
      DATA ACC/0.0/,DRAD/0.0174532925/,ISEED/8473957/,ICONC/1/
CC    READ CONCENTRATOR PARAMETERS
      READ(7,9000) RMANGL,F,R2,Z,SD1,SD2,ITYPE,NCR
 9000 FORMAT(1X,6F10.5,2I5)
      READ(7,9005)NRZR,NRZ2,RMAX,REFL1,REFL2,PSM1,PSM2,R1
      READ(7,9007)DXS,DYS,DZS,THTAS,DXT,DYT,DZT,THTAT
 9007 FORMAT(1X,8F9.5)
 9005 FORMAT(1X,2I5,6F10.5)
      IF(ITYPE.EQ.0)GO TO 4
      NCR=0
 8000 NCR=NCR+1
      IFIRST(NCR)=1
      READ(7,9010)TRANGL(NCR),EXAPR(NCR),ZTRUN(NCR)
     + ,ZPOS(NCR),TREFL(NCR),SDT(NCR)
      IF(TRANGL(NCR).GT.0.) GO TO 8000
      NCR=NCR-1
 9010 FORMAT(1X,6F10.5)
    4 RMANGL=RMANGL*DRAD
      AHYP=Z-F/2
      BHYP=SQRT(F*F/4-AHYP*AHYP)
      ASBS=SQRT(AHYP*AHYP+BHYP*BHYP)
      AMIR=3.141592654*(R1*R1)
      DO 5I=1,NRZR
      EOPTZ(I)=0.
      ARPI(I)=0.
      RR(I)=(I+2)*RMAX/(NRZR+2)
    5 CR(I)=AMIR/(3.141592654*RR(I)*RR(I))
      DO 6 I=1,NRZ2
      HARPI(I)=0.
    6 RRH(I)=I*R2/NRZ2
      MISR=0
      RPWR=0.
      MIS2=0
      HPWR=0.
      ISHAD=0
C
C   SET SUN VECTORS
      CALL SUN1(TAZ,TEL)
      CALL TRACK(TAZ,TEL)
      REFLT=REFL1*REFL2
      ECCEN=SQRT(AHYP*AHYP+BHYP*BHYP)/AHYP
      NLOOP=0
C   DRAW RAYS OVER SURFACE
      DO 300 NLOOP=1,NDRAW
      RANF=RAN(ISEED)
      RTH=6.2831853*RANF
      RANF=RAN(ISEED)
      RD=SQRT(R1*R1*RANF)
C   CHECK FOR SHADOWING
      ROFFAX=SQRT((R2*COS(RTH)+DXS)**2+(R2*SIN(RTH)+DYS)**2)
```

```
      ISHAD=ISHAD+1
      GO TO 300
C    CONVERT TO SURFACE POINTS
   15 X0=RD*COS(RTH)
      Y0=SIN(RTH)*RD
      Z0=(X0*X0+Y0*Y0)*.25/F
C    FIND THE UNPERTURBED SURFACE NORMAL UN
      PHI=ATAN(RD/(2.*F))
      CPHI=COS(PHI)
      SPHI=SIN(PHI)
      DO 30 J=1,3
      UDUM(J)=(X0*UCA(J)+Y0*UCP(J))/RD
      UN(J)=-SPHI*UDUM(J)+CPHI*UCN(J)
   30 UT(J)=CPHI*UDUM(J)+SPHI*UCN(J)
C   FIND THE PERTURBED NORMAL USING SD1
      CALL CROSS(UN,UT,UT2)
      CALL ERNORM (SD1,0.,UN,UT,UT2,UNP,PSM1,ISEED)
C   PERTURB SUN RAY FOR FINITE SUN SIZE
C   AND VARIATION IN SUN INTENSITYU
      CALL SUN2(ACC,USP,DRAD,ISEED)
C    CALCULATE REFLECTED RAY USING SNELL
      CALL SNELL(UR,UNP,USP)
C    HERE ARE THE MODS FOR THE SECONDARY REFLECTOR.
C
C    CALL TRANS FOR MISALIGNED SECONDARY
      ZTRAN=F/2+AHYP
      IDIR=1
      CALL TRANS(X0,Y0,Z0,UR,DXS,DYS,DZS,ZTRAN,THTAS,IDIR)
C    SOLVE FOR INTERSECTION OF RAY ON HYPERBOLOID.
      A=UR(3)*UR(3)/(AHYP*AHYP)-(UR(1)*UR(1)+UR(2)*UR(2))/(BHYP*BHYP)
      B= 2.*UR(3)*(Z0-ASBS)/(AHYP*AHYP)-2.*(Y0*UR(2)+X0*UR(1))/(BHYP*
     +BHYP)
      C=(Z0-ASBS)*(Z0-ASBS)/(AHYP*AHYP)-(X0*X0+Y0*Y0)/(BHYP*BHYP)-1.
      XL=(-B-SQRT(B*B-4*A*C))/(2.*A)
      Z1=Z0+XL*UR(3)
      AMAXLN=SQRT(X0*X0+Y0*Y0+(F-Z0)*(F-Z0))
      IF((XL.LT.AMAXLN) .AND.( XL .GT. 0.0).AND.(Z1.GT. F/2.))GO TO 50
      XL=(-B+SQRT(B*B-4.*A*C))/(2.*A)
   50 X1=X0+XL*UR(1)
      Y1=Y0+XL*UR(2)
      Z1=Z0+XL*UR(3)
C    FIND RADIUS OF HIT POINT OF HYPERBOLOID
      RHYP=SQRT(X1*X1+Y1*Y1)
      IF(RHYP.LE.R2) GO TO 35
C     WRITE(9,51)X0,Y0,Z0,UR(1),UR(2),UR(3),XL,X1,Y1,Z1
C   51 FORMAT(1X,'X0Y0Z0',2X,3F8.4,5X,'UR123',2X,3F9.6,5XX'XL',1X,F9.5,
C     + 5X,'X1Y1Z1',2X,3F8.4)
       MIS2= MIS2+1
      GO TO 300
C
C    FILL POWER RINGS ON HYPERBOLOID
   35 J=0
   36 J=J+1
      IF(RHYP.GT.RRH(J)) GO TO 36
      HARPI(J)=HARPI(J)+REFL1
      HPWR=HPWR+REFL1

C
```

```
      DZDRRH=AHYP*AHYP*RHYP/(BHYP*BHYP*SQRT(AHYP*AHYP*(1+(RHYP*RHYP)
     + /(BHYP*BHYP))))
      PHIH=ATAN(DZDRRH)
 7025 CPHIH=COS(PHIH)
      SPHIH=SIN(PHIH)
      DO 38J=1,3
      UDUMH(J)=(X1*UCA(J)+Y1*UCP(J))/RHYP
      UNH(J)=SPHIH*UDUMH(J)-CPHIH*UCN(J)
   38 UTH(J)=CPHIH*UDUMH(J)+SPHIH*UCN(J)
C
C    PERTURB UNH TO GET UNHP
      CALL CROSS(UNH,UTH,UTH2)
      CALL  ERNORM(SD2,0.,UNH,UTH,UTH2,UNPH,0.,ISEED)
C    FOR SNELL SETUP
      DO 40 J = 1,3
   40 UR(J)=-UR(J)
C
C    FIND REFLECTED RAY
      CALL SNELL(URH,UNPH,UR)
C
C    RETURN VECTOR TO MAIN COORDINATE SYSTEM
      IDIR=-1
      CALL TRANS(X1,Y1,Z1,URH,DXS,DYS,DZS,ZTRAN,THTAS,IDIR)
C
C    FIND INTERSECTION OF RAY AT Z=0 (RECEIVER AT PARABOLOID VERTEX)
      Z2=0
      XL=-Z1/URH(3)
      X2=X1+XL*URH(1)
      Y2=Y1+XL*URH(2)
      RMAG=SQRT(X2*X2+Y2*Y2)
C    FILL POWER RINGS AT RECEIVER
      IF(RMAG.LE.RMAX) GO TO 41
      MISR=MISR+1
      GO TO 290
   41 J=0
   44 J=J+1
      IF(RMAG.GT.RR(J)) GO TO 44
      ARPI(J)=ARPI(J)+REFLT
      RPWR=RPWR+REFLT
  290 IF(ITYPE.EQ.0)GO TO 300
C     WRITE(9,1000)NLOOP,X1,Y1,Z1,(URH(I),I=1,3),A,B,C
C1000 FORMAT(1X,'NRAY,X1Y1Z1',I5,3F8.4,1X,'URH1,2,3',3F7.4,1X,
C    + 'ABC',3F10.5)
C
C    CALL TRANS FOR MISALIGNED TERTIARY
      ZTRAN=0.
      IDIR=1
      POS=0.
      CALL TRANS(X1,Y1,Z1,URH,DXT,DYT,DZT,ZTRAN,THTAT,IDIR)
      DO 295 ICR=1,NCR
  295 CALL NOIMUJ(URH,X1,Y1,Z1,ITYPE,IFIRST(ICR),ISEED,ICR,ICONC,POS)
  300 CONTINUE
C    DO CALCULATIONS AND WRITE RESULTS TO FILE
      SUM=0.
      SUMIF=0.
      DO 500I=1,NRZR
      SUMIF=SUMIF+ARPI(I)
      XIF(I)=SUMIF/(NDRAW-ISHAD-MIS2)
```

```
      SUM=SUM+ARPI(I)
      RINT(I) =SUM/(RR(I)*RR(I)*3.141592654)
      EOPTZ(I)=SUM/AMIR
      IF(I.GT.1) GO TO 650
      AREA=RR(I)*RR(I)*3.14159
      GO TO 651
  650 AREA=(RR(I)*RR(I)-RR(I-1)*RR(I-1))*3.14159
  651 XINT(I)=ARPI(I)/AREA
  500 CONTINUE
      DO 501 I=1,NRZ2
      IF(I.GT.1) GO TO 660
      AREA=RRH(I)*RRH(I)*3.14159
      GO TO 661
  660 AREA=(RRH(I)*RRH(I)-RRH(I-1)*RRH(I-1))*3.14159
  661 HARPI(I)=HARPI(I)*AMIR/NDRAW
  501 X2INT(I)=HARPI(I)/AREA
      RM=RMANGL/DRAD
      ZFRAC=Z/F
      WRITE(8,604) F,RM,ZFRAC,Z,R1,R2,ECCEN,SD1,SD2,DXS,DYS,DZS,
     + THTAS,DXT,DYT,DZT,THTAT
  604 FORMAT(5X,'CONCENTRATOR PARAMETERS:  FPRIM:'F7.4,3X,
     + 'RIM ANGLE:',F5.1,3X,'ZFRAC:',
     + F7.4,2X,'Z:',F7.4,2X,'R1:',F7.4,2X,'R2:',F7.4,/,5X
     + ,'ECCENTRICITY:'
     +,F7.4,5X,'SLOPE ERROR 1:',F4.1,2X,'SLOPE ERROR 2:',F4.1,
     + /,5X,'DXS,DYS,DZS,THTAS',4F8.4,2X,'DXT,DYT,DZT,THTAT',
     + 4F8.4,/)
      WRITE(8,599)
  599 FORMAT(20X,'CONCENTRATOR PERFORMANCE RESULTS',/,10X,'RADIUS',
     + 4X,'GEOMETRIC',4X,'POWER',5X,'OVERALL',4X,'INTERCEPT',
     + 4X,'INTEGRATED',7X,'RADIAL'
     + /,20X,'CONC RATIO',12X,'EFFICIENCY',3X,'FACTOR',
     + 7X,'INTENSITY',5X,'INTENSITY',/)
      WRITE(8,600)(RR(I),CR(I),ARPI(I),EOPTZ(I),XIF(I),RINT(I),XINT(I)
     + ,I=1,NRZR)
  600 FORMAT(10X,F6.3,3X,F11.1,3X,F7.2,4X,F6.4,6X,F5.3,5X,F11.1,2X,
     + F11.1)
      WRITE(8,601)
  601 FORMAT(///,14X,'FLUX MAP ON SECONDARY',/,10X,'RADIUS',3X,'POWER'
     +,10X,'RADIAL INTENSITY',/)
      WRITE(8,602)(RRH(I),HARPI(I),X2INT(I),I=1,NRZ2)
  602 FORMAT(10X,F5.3,3X,F8.2,10X,F11.1)
      WRITE(8,603) NDRAW,MIS2,MISR,ISHAD
  603 FORMAT(//,5X,I6,' RAYS DRAWN',5X,I6,' RAYS MISSED SECONDARY',
     +5X, I6,' RAYS MISSED THE RECEIVER',5X,I6,' RAYS WERE SHADOWED',/)
      IF(ITYPE .EQ.0)RETURN
      DO 700 ICR=1,NCR
  700 CALL TRTOUT(ITYPE,NDRAW,ISHAD,MIS2,ICR,R1)
      RETURN
      END
      SUBROUTINE RCCASS
C
C   THIS SUBROUTINE MODELS AN APLANATIC CASSEGRAINIAN SOLAR
C   CONCENTRATOR USING THE RITCHEY-CHRETIAN CONFIGURATION.  THE
C   SYSTEM FOCUS IS AT THE VERTEX OF THE PRIMARY REFLECTOR.
C
C   THE REFERENCE FOR THIS CONFIGURATION AS USED IN THIS CODE IS:
C     "GENERAL ANALYSIS OF APLANATIC CASSEGRAINIAN, GREGORIAN,
```

```
C       BY W. B. WETHERELL AND M. P. RIMMER
C       PUBLISHED IN " APPLIED OPTICS" DEC 72  VOL 11,NO.12 PG2817-2832.
C
      DIMENSION D(3),UT(3),UN(3),UNP(3),UR(3),USP(3),RHIT(3),UDUM(3),
     + UNH(3),UDUMH(3),UTH(3),UTH2(3),UNPH(3),URH(3),XIF(20),RINT(20),
     + ARPI(20),RR(20),CR(20),EOPTZ(20),UT2(3),HARPI(20),RRH(20)
     + ,XINT(20),X2INT(20),IFIRST(16)
      INTEGER*4 ISEED
      COMMON/RUNC/ NDRAW,TAZ,TEL,TIME,XLAT,XLONG,TZONE,IDAY,ICONC,ISTOP,
     + NMAT,MAPS,NMATL
      COMMON/VECTOR/ ULE(3),ULV(3),ULS(3),UCN(3),UCA(3),UCP(3),US(3)
      COMMON/CASSEG/ RMANGL,F,R2,Z,SD1,SD2,NRZR,NRZ2,RMAX,REFL1,REFL2,
     + PSM1,PSM2,R1
      COMMON/TPAR/TRANGL(16),EXAPR(16),ZTRUN(16),ZPOS(16)
     + ,PWRTER(20,16),ZTER(20,16),MIST(16),
     + XLOST(16),NLOST(16),NABS(16),PRCVR(20,16),
     + RRCVR(20,16),TREFL(16),SDT(16),ANGR(14),ANGPWR(14,16)
      DATA ACC/0.0/,DRAD/0.0174532925/,ISEED/8473957/,ICONC/2/
C   READ CONCENTRATOR PARAMETERS
      READ(7,9000) RMANGL,F,R2,Z,SD1,SD2,ITYPE,NCR
 9000 FORMAT(1X,6F10.5,2I5)
      READ(7,9005)NRZR,NRZ2,RMAX,REFL1,REFL2,PSM1,PSM2,R1
      IF(ITYPE.EQ.0)GO TO 4
      NCR=0
 8000 NCR=NCR+1
      IFIRST(NCR)=1
      READ(7,9010)TRANGL(NCR),EXAPR(NCR),ZTRUN(NCR)
     + ,ZPOS(NCR),TREFL(NCR),SDT(NCR)
      IF(TRANGL(NCR).GT.0.) GO TO 8000
      NCR=NCR-1
 9010 FORMAT(1X,6F10.5)
 9005 FORMAT(1X,2I5,6F10.5)
C   SET PARAMETERS FOR R - C CONFIGURATION
    4 RMANGL=RMANGL*DRAD
      XMAG=1/(F/Z-1.)
      XMAG2=XMAG*XMAG
      FTOTL=XMAG*F
      XKAPP=-2*F/(FTOTL*XMAG2)
      XKAPS=-2*((XMAG+1)/(XMAG-1)**3+2*XMAG/(XMAG-1)**2)
      CURVP=-1/(2*F)
      CURVS=(1-XMAG2)/(2*XMAG*F)
      CPKP=XKAPP*CURVP**2
      CSKS=XKAPS*CURVS**2
      AMIR=3.141592654*(R1*R1)
      DO 5I=1,NRZR
      EOPTZ(I)=0.
      ARPI(I)=0.
      RR(I)=(I+2)*RMAX/(NRZR+2)
    5 CR(I)=AMIR/(3.141592654*RR(I)*RR(I))
      DO 6 I=1,NRZ2
      HARPI(I)=0.
    6 RRH(I)=I*R2/NRZ2
      MISR=0
      RPWR=0.
      MIS2=0
      HPWR=0.
      ISHAD=0
C
```

```
      CALL SUN1(TAZ,TEL)
      CALL TRACK(TAZ,TEL)
      REFLT=REFL1*REFL2
      NLOOP=0
C   DRAW RAYS OVER SURFACE
      DO 300 NLOOP=1,NDRAW
      RANF=RAN(ISEED)
      RTH=6.2831853*RANF
      RANF=RAN(ISEED)
      RD=SQRT(R1*R1*RANF)
C   CHECK FOR SHADOWING
      IF(RD.GT. R2) GO TO 15
      ISHAD=ISHAD+1
      GO TO 300
C   CONVERT TO SURFACE POINTS
   15 X0=RD*COS(RTH)
      Y0=SIN(RTH)*RD
      R1SQ=RD*RD
      R1SQK=SQRT(1-R1SQ*CPKP)
      Z0=-CURVP*R1SQ/(1+R1SQK)
C   FIND THE UNPERTURBED SURFACE NORMAL UN
      ANG=-CURVP*RD*(2/(1+R1SQK)+(R1SQ*CPKP)/((1+R1SQK)**2*R1SQK))
      PHI=ATAN(ANG)
      CPHI=COS(PHI)
      SPHI=SIN(PHI)
      DO 30 J=1,3
      UDUM(J)=(X0*UCA(J)+Y0*UCP(J))/RD
      UN(J)=-SPHI*UDUM(J)+CPHI*UCN(J)
   30 UT(J)=CPHI*UDUM(J)+SPHI*UCN(J)
C  FIND THE PERTURBED NORMAL USING SD1
      CALL CROSS(UN,UT,UT2)
      CALL ERNORM (SD1,0.,UN,UT,UT2,UNP,PSM1,ISEED)
C  PERTURB SUN RAY FOR FINITE SUN SIZE
C  AND VARIATION IN SUN INTENSITY
      CALL SUN2(ACC,USP,DRAD,ISEED)
C   CALCULATE REFLECTED RAY USING SNELL
      CALL SNELL(UR,UNP,USP)
C   HERE ARE THE MODS FOR THE SECONDARY REFLECTOR.
C
C   SOLVE FOR INTERSECTION OF RAY ON SECONDARY.
      MAXCNT=10
      XLNU=(F-Z0)
      NCNT=0
  800 NCNT=NCNT+1
      XL=XLNU
      IF(NCNT.GT.MAXCNT) STOP
      RS2=(X0+UR(1)*XL)*(X0+UR(1)*XL)+(Y0+UR(2)*XL)*(Y0+UR(2)*XL)
      DRS2=2*((X0+UR(1)*XL)*UR(1)+(Y0+UR(2)*XL)*UR(2))
      ARC=SQRT(1-CSKS*RS2)
      DARC=-CSKS*DRS2/(2*ARC)
      FOFL=Z-CURVS*RS2/(1+ARC)-Z0-UR(3)*XL
      FPRIM=-(CURVS*(DRS2/(1+ARC)-RS2*DARC/(
     + (1.+ARC)*(1.+ARC))))-UR(3)
      XLNU=XL-FOFL/FPRIM
      IF(ABS(XLNU-XL).GT.0.000001) GO TO 800
      XL=XLNU
      X1=X0+XL*UR(1)
      Y1=Y0+XL*UR(2)
```

```
   50 CONTINUE
C    FIND RADIUS OF HIT POINT ON SECONDARY
       RHYP=SQRT(X1*X1+Y1*Y1)
       IF(RHYP.LE.R2) GO TO 35
        MIS2= MIS2+1
       GO TO 300
C
C    FILL POWER RINGS ON SECONDARY
   35 J=0
   36 J=J+1
       IF(RHYP.GT.RRH(J)) GO TO 36
       HARPI(J)=HARPI(J)+REFL1
       HPWR=HPWR+REFL1
C
C    FIND NORMAL UHN ON SECONDARY
       R2SQ=RHYP*RHYP
       RSQK=SQRT(1-R2SQ*CSKS)
       AG=-CURVS*RHYP*(2/(1+RSQK)+(R2SQ*CSKS)/((1+RSQK)**2*RSQK))
       PHIH=ATAN(AG)
       CPHIH=COS(PHIH)
       SPHIH=SIN(PHIH)
       DO 38J=1,3
       UDUMH(J)=(X1*UCA(J)+Y1*UCP(J))/RHYP
       UNH(J)=SPHIH*UDUMH(J)-CPHIH*UCN(J)
   38 UTH(J)=CPHIH*UDUMH(J)+SPHIH*UCN(J)
C
C    PERTURB UNH TO GET UNHP
       CALL CROSS(UNH,UTH,UTH2)
       CALL  ERNORM(SD2,0.,UNH,UTH,UTH2,UNPH,0.,ISEED)
C    FOR SNELL SETUP
       DO 40 J = 1,3
   40 UR(J)=-UR(J)
C
C    FIND REFLECTED RAY
       CALL SNELL(URH,UNPH,UR)
C
C    FIND INTERSECTION OF RAY AT Z=0 (RECEIVER AT PRIMARY VERTEX)
       Z2=0
       XL=-Z1/URH(3)
       X2=X1+XL*URH(1)
       Y2=Y1+XL*URH(2)
       RMAG=SQRT(X2*X2+Y2*Y2)
C    FILL POWER RINGS AT RECEIVER
       IF(RMAG.LE.RMAX) GO TO 41
       MISR=MISR+1
       GO TO 290
   41 J=0
   44 J=J+1
       IF(RMAG.GT.RR(J)) GO TO 44
       ARPI(J)=ARPI(J)+REFLT
       RPWR=RPWR+REFLT
  290 IF(ITYPE.EQ.0)GO TO 300
       POS=0
       DO 295 ICR=1,NCR
  295 CALL NOIMUJ(URH,X1,Y1,Z1,ITYPE,IFIRST(ICR),ISEED,ICR,ICONC,POS)
  300 CONTINUE
C    DO CALCULATIONS AND WRITE RESULTS TO FILE
       SUM=0.
```

```
      DO 500I=1,NRZR
      SUMIF=SUMIF+ARPI(I)
      XIF(I)=SUMIF/(NDRAW-ISHAD-MIS2)
      ARPI(I)=ARPI(I)*AMIR/NDRAW
      SUM=SUM+ARPI(I)
      RINT(I) =SUM/(RR(I)*RR(I)*3.141592654)
      EOPTI(I)=SUM/AMIR
      IF(I.GT.1) GO TO 650
      AREA=RR(I)*RR(I)*3.14159
      GO TO 651
  650 AREA=(RR(I)*RR(I)-RR(I-1)*RR(I-1))*3.14159
  651 XINT(I)=ARPI(I)/AREA
  500 CONTINUE
      DO 501 I=1,NRZ2
      IF(I.GT.1) GO TO 660
      AREA=RRH(I)*RRH(I)*3.14159
      GO TO 661
  660 AREA=(RRH(I)*RRH(I)-RRH(I-1)*RRH(I-1))*3.14159
  661 HARPI(I)=HARPI(I)*AMIR/NDRAW
  501 X2INT(I)=HARPI(I)/AREA
      RM=RMANGL/DRAD
      ZFRAC=Z/F
      WRITE(8,604) F,RM,ZFRAC,Z,R1,R2,SD1,SD2
  604 FORMAT(5X,'CONCENTRATOR PARAMETERS:  FPRIM:'F7.4,3X,
     + 'RIM ANGLE:',F5.1,3X,'ZFRAC:',
     + F7.4,2X,'Z:',F7.4,2X,'R1:',F7.4,2X,'R2:',F7.4,/,30X,
     + 'SLOPE ERROR 1:',F4.1,2X,'SLOPE ERROR 2:',F4.1,//)
      WRITE(8,599)
  599 FORMAT(20X,'CONCENTRATOR PERFORMANCE RESULTS (R-C CONFIGURATION)',
     + /,10X,'RADIUS',
     + 4X,'GEOMETRIC',4X,'POWER',5X,'OVERALL',4X,'INTERCEPT',
     + 4X,'INTEGRATED',7X,'RADIAL'
     + /,20X,'CONC RATIO',12X,'EFFICIENCY',3X,'FACTOR',
     + 7X,'INTENSITY',5X,'INTENSITY',/)
      WRITE(8,600)(RR(I),CR(I),ARPI(I),EOPTI(I),XIF(I),RINT(I),XINT(I)
     + ,I=1,NRZR)
  600 FORMAT(10X,F6.3,3X,F11.1,3X,F7.2,4X,F6.4,6X,F5.3,5X,F11.1,2X,
     + F11.1)
      WRITE(8,601)
  601 FORMAT(///,14X,'FLUX MAP ON SECONDARY',/,10X,'RADIUS',3X,'POWER'
     +,10X,'RADIAL INTENSITY',/)
      WRITE(8,602)(RRH(I),HARPI(I),X2INT(I),I=1,NRZ2)
  602 FORMAT(10X,F5.3,3X,F8.2,10X,F11.1)
      WRITE(8,603) NDRAW,MIS2,MISR,ISHAD
  603 FORMAT(//,5X,I6,' RAYS DRAWN',5X,I6,' RAYS MISSED SECONDARY',
     +5X, I6,' RAYS MISSED THE RECEIVER',5X,I6,' RAYS WERE SHADOWED',/)
      IF(ITYPE .EQ.0)RETURN
      DO 700 ICR=1,NCR
  700 CALL TRTOUT(ITYPE,NDRAW,ISHAD,MIS2,ICR,R1)
C
C
C
      RETURN
      END
      SUBROUTINE PDISH2
C
C   THIS SUBROUTINE MODELS AN PARABOLOIDAL SOLAR
C   CONCENTRATOR, WITH A PARABOLOIDAL PRIMARY REFLECTOR .
```

```
      DIMENSION D(3),UT(3),UN(3),UNP(3),UR(3),USP(3),RHIT(3),UDUM(3),
     + XIF(20),RINT(20),
     + ARPI(20),RR(20),CR(20),EOPTZ(20),UT2(3)
     + ,XINT(20),X2INT(20),IFIRST(16)
      INTEGER*4 ISEED
      COMMON/RUNC/ NDRAW,TAZ,TEL,TIME,XLAT,XLONG,TZONE,IDAY,ICONC,ISTOP,
     + NMAT,MAPS,NMATL
      COMMON/VECTOR/ ULE(3),ULV(3),ULS(3),UCN(3),UCA(3),UCP(3),US(3)
      COMMON/PDISH/ RMANGL,F,R2,SD1,NRZR,RMAX,REFL1,
     + PSM1,R1
      COMMON/TPAR/TRANGL(16),EXAPR(16),ZTRUN(16),ZPOS(16)
     + ,PWRTER(20,16),ZTER(20,16),MIST(16),
     + XLOST(16),NLOST(16),NABS(16),PRCVR(20,16),
     + RRCVR(20,16),TREFL(16),SDT(16),ANGR(14),ANGPWR(14,16)
      DATA ACC/0.0/,DRAD/0.0174532925/,ISEED/8473957/,ICONC/3/
CC    READ CONCENTRATOR PARAMETERS
      READ(7,9000) RMANGL,F,R2,SD1,ITYPE,NCR
 9000 FORMAT(1X,4F10.5,2I5)
      READ(7,9005)NRZR,RMAX,REFL1,PSM1,R1
 9005 FORMAT(1X,1I5,4F10.5)
      IF(ITYPE.EQ.0)GO TO 4
      NCR=0
 8000 NCR=NCR+1
      IFIRST(NCR)=1
      READ(7,9010)TRANGL(NCR),EXAPR(NCR),ZTRUN(NCR)
     + ,ZPOS(NCR),TREFL(NCR),SDT(NCR)
      IF(TRANGL(NCR).GT.0.) GO TO 8000
      NCR=NCR-1
 9010 FORMAT(1X,6F10.5)
    4 RMANGL=RMANGL*DRAD
      AMIR=3.141592654*(R1*R1)
      DO 5I=1,NRZR
      EOPTZ(I)=0.
      ARPI(I)=0.
      RR(I)=(I+2)*RMAX/(NRZR+2)
    5 CR(I)=AMIR/(3.141592654*RR(I)*RR(I))
      MISR=0
      RPWR=0.
      ISHAD=0
C
C     SET SUN VECTORS
      CALL SUN1(TAZ,TEL)
      CALL TRACK(TAZ,TEL)
      REFLT=REFL1
      NLOOP=0
C     DRAW RAYS OVER SURFACE
      DO 300 NLOOP=1,NDRAW
      RANF=RAN(ISEED)
      RTH=6.2831853*RANF
      RANF=RAN(ISEED)
      RD=SQRT(R1*R1*RANF)
C     CHECK FOR SHADOWING
      IF(RD.GT. R2) GO TO 15
      ISHAD=ISHAD+1
      GO TO 300
C     CONVERT TO SURFACE POINTS
   15 X0=RD*COS(RTH)
      Y0=SIN(RTH)*RD
```

```
C    FIND THE UNPERTURBED SURFACE NORMAL UN
       PHI=ATAN(RD/(2.*F))
       CPHI=COS(PHI)
       SPHI=SIN(PHI)
       DO 30 J=1,3
       UDUM(J)=(X0*UCA(J)+Y0*UCP(J))/RD
       UN(J)=-SPHI*UDUM(J)+CPHI*UCN(J)
    30 UT(J)=CPHI*UDUM(J)+SPHI*UCN(J)
C   FIND THE PERTURBED NORMAL USING SD1
       CALL CROSS(UN,UT,UT2)
       CALL ERNORM (SD1,0.,UN,UT,UT2,UNP,PSM1,ISEED)
C   PERTURB SUN RAY FOR FINITE SUN SIZE
C   AND VARIATION IN SUN INTENSITYU
       CALL SUN2(ACC,USP,DRAD,ISEED)
C    CALCULATE REFLECTED RAY USING SNELL
       CALL SNELL(UR,UNP,USP)

C
C    FIND INTERSECTION OF RAY AT Z=F (RECEIVER AT PARABOLOID FOCUS)
       Z2=F
       XL=(Z2-Z0)/UR(3)
       X2=X0+XL*UR(1)
       Y2=Y0+XL*UR(2)
       RMAG=SQRT(X2*X2+Y2*Y2)
C    FILL POWER RINGS AT RECEIVER
       IF(RMAG.LE.RMAX) GO TO 41
       MISR=MISR+1
       GO TO 290
    41 J=0
    44 J=J+1
       IF(RMAG.GT.RR(J)) GO TO 44
       ARPI(J)=ARPI(J)+REFLT
       RPWR=RPWR+REFLT
   290 CONTINUE
C      WRITE(9,1000)NLOOP,X0,Y0,Z0,(UR(I),I=1,3)
C1000 FORMAT(1X,'NRAY,X0Y0Z0',I5,3F8.4,1X,'UR1,2,3',3F7.4)
       IF(ITYPE.EQ.0)GO TO 300
       DO 295 ICR=1,NCR
   295 CALL NOIMUJ(UR,X0,Y0,Z0,ITYPE,IFIRST(ICR),ISEED,ICR,ICONC,F)
   300 CONTINUE
C    DO CALCULATIONS AND WRITE RESULTS TO FILE
       SUM=0.
       SUMIF=0.
       DO 500I=1,NRZR
       SUMIF=SUMIF+ARPI(I)
       XIF(I)=SUMIF/(NDRAW-ISHAD-MIS2)
       ARPI(I)=ARPI(I)*AMIR/NDRAW
       SUM=SUM+ARPI(I)
       RINT(I) =SUM/(RR(I)*RR(I)*3.141592654)
       EOPTZ(I)=SUM/AMIR
       IF(I.GT.1) GO TO 650
       AREA=RR(I)*RR(I)*3.14159
       GO TO 651
   650 AREA=(RR(I)*RR(I)-RR(I-1)*RR(I-1))*3.14159
   651 XINT(I)=ARPI(I)/AREA
   500 CONTINUE
       RM=RMANGL/DRAD
       WRITE(8,604) F,RM,R1,R2,SD1
```

```
     + 'RIM ANGLE:',F5.1,3X,
     + 'R1:',F7.4,2X,'BLOCKING RADIUS:',F7.4,/,5X
     + ,'SLOPE ERROR 1:',F4.1,//)
      WRITE(8,599)
  599 FORMAT(20X,'CONCENTRATOR PERFORMANCE RESULTS',/,10X,'RADIUS',
     + 4X,'GEOMETRIC',4X,'POWER',5X,'OVERALL',4X,'INTERCEPT',
     + 4X,'INTEGRATED',7X,'RADIAL'
     + /,20X,'CONC RATIO',12X,'EFFICIENCY',3X,'FACTOR',
     + 7X,'INTENSITY',5X,'INTENSITY',/)
      WRITE(8,600)(RR(I),CR(I),ARPI(I),EOPTZ(I),XIF(I),RINT(I),XINT(I)
     + ,I=1,NRZR)
  600 FORMAT(10X,F6.3,3X,F11.1,3X,F7.2,4X,F6.4,6X,F5.3,5X,F11.1,2X,
     + F11.1)
      WRITE(8,603) NDRAW,MIS2,MISR,ISHAD
  603 FORMAT(//,5X,I6,' RAYS DRAWN',5X,I6,' RAYS MISSED SECONDARY',
     +5X, I6,' RAYS MISSED THE RECEIVER',5X,I6,' RAYS WERE SHADOWED',/)
      IF(ITYPE .EQ.0)RETURN
      DO 700 ICR=1,NCR
  700 CALL TRTOUT(ITYPE,NDRAW,ISHAD,MIS2,ICR,R1)
      RETURN
      END
      SUBROUTINE NOIMUJ(UDIN,XIN,YIN,ZIN,ITYPE,IFIRST,ISEED,ICR,ICONC,
     + FPOS)
      COMMON/TPAR/TRANGL(16),EXAPR(16),ZTRUN(16),ZPOS(16)
     + ,PWRTER(20,16),ZTER(20,16),MIST(16),
     + XLOST(16),NLOST(16),NABS(16),PRCVR(20,16),
     + RRCVR(20,16),TREFL(16),SDT(16),ANGR(14),ANGPWR(14,16)
      COMMON/VECTOR/ULE(3),ULV(3),ULS(3),UCN(3),UCA(3),UCP(3),US(3)
      DIMENSION TNANGL(16),RTRUN(16),AHYP(16),BHYP(16),NCALL(16)
      DIMENSION UD(3),UDIN(3),UN(3),UNP(3),UDUM(3),UT(3),UT2(3),UR(3)
      INTEGER*4 ISEED
      DATA ANGR/10.,20.,30.,40.,45.,50.,55.,60.,65.,70.,75.,80.,85.,90./
      IF(IFIRST.EQ.0) GO TO 20
C     IDIAG=0
      NCALL(ICR)=0
      MIST(ICR)=0
      NLOST(ICR)=0
      XLOST(ICR)=0.
      NABS(ICR)=0
      IFIRST=0
C  CALCULATE GEOMETRIC CONSTANTS
      TNANGL(ICR)=TAND(TRANGL(ICR))
      IF(ITYPE.EQ.2) GO TO 10
C  CONE TYPE NON-IMAGING CONCENTRATOR
      RTRUN(ICR)=ZTRUN(ICR)*TNANGL(ICR)+EXAPR(ICR)
      GOTO 15
C  TRUMPET TYPE NON-IMAGING CONCENTRATOR
   10 AHYP(ICR)=EXAPR(ICR)
      BHYP(ICR)=AHYP(ICR)/TNANGL(ICR)
      RTRUN(ICR)=AHYP(ICR)*SQRT(ZTRUN(ICR)*ZTRUN(ICR)
     + /(BHYP(ICR)*BHYP(ICR))+1)
   15 DO 16 I=1,20
      RRCVR(I,ICR)=(I+2)*EXAPR(ICR)/22.
      ZTER(I,ICR)=I*ZTRUN(ICR)/20.
      PRCVR(I,ICR)=0.
   16 PWRTER(I,ICR)=0.
      DO 17 I=1,14
   17 ANGPWR(I,ICR)=0.
```

```
      DO 21 I=1,3
   21 UD(I)=UDIN(I)
      X=XIN
      Y=YIN
      Z=ZIN
      IF (ICONC.NE.3) GO TO 22
C  TRANSLATE UNIT VECTOR AND VECTOR ORIGINATION POINT TO KEEP
C  COORDINATE SYSTEM CONSISTENT
      XL=(FPOS-Z)/UD(3)
      XTR=X+XL*UD(1)
      YTR=-(Y+XL*UD(2))
      ZTR=0.
      UD(2)=-UD(2)
      UD(3)=-UD(3)
      X=XTR-XL*UD(1)
      Y=YTR-XL*UD(2)
      Z=ZTR-XL*UD(3)
   22 CONTINUE
C     WRITE(9,105)ICR,NCALL(ICR),X,Y,Z,UD(1),UD(2),UD(3)
C 105 FORMAT(1X,'ICR,NCALL',2I5,2X,'X,Y,Z,UD1,2,3',6F10.5,/)
      NCALL(ICR)=NCALL(ICR)+1
      NREFL=0
C    IS RAY WITHIN THE ENTRANCE APERTURE?
      XL=(ZTRUN(ICR)-Z)/UD(3)
      XI=X+XL*UD(1)
      YI=Y+XL*UD(2)
      RI=SQRT(XI*XI+YI*YI)
      IF(RI.LE.RTRUN(ICR)) GO TO 30
C    RAY MISSED THE APERTURE
      MIST(ICR)=MIST(ICR)+1
C     WRITE(6,104)RI
C  104 FORMAT(' MISSED THE TERTIARY.  RI=',F10.5)
      RETURN
C    IS RAY INCIDENT ON RECEIVER?
   30 XL=-Z/UD(3)
      XR=X+XL*UD(1)
      YR=Y+XL*UD(2)
      RR=SQRT(XR*XR+YR*YR)
      IF(RR.GT.EXAPR(ICR)) GO TO 40
C    RAY IS ON THE RECEIVER.  SUM INTO REGISTERS.
   35 J=0
   36 J=J+1
      IF(J.LE.20) GO TO 37
      J=J-1
      GO TO 38
   37 IF(RR.GT.RRCVR(J,ICR)) GO TO 36
   38 PRCVR(J,ICR)=PRCVR(J,ICR)+RAYVAL
C    SUM INTO ANGLE OF INCIDENCE REGISTERS
      ANGINC=ACOSD(-UD(3))
  335 J=0
  336 J=J+1
      IF(J.LE.14) GO TO 337
      J=J-1
      GO TO 338
  337 IF(ANGINC.GT.ANGR(J)) GO TO 336
  338 ANGPWR(J,ICR)=ANGPWR(J,ICR)+RAYVAL
C
C    DIAGNOSTICS
```

```
C 100 FORMAT(10X,'NREFL,RAYVAL,XR,YR',5X,I5,3F10.6,/)
      RETURN
C   FIND INTERSECTION OF RAY ON TERTIARY
   40 IF(ITYPE.EQ.2) GO TO 50
C   CONE CONCENTRATOR
      A=UD(1)*UD(1)+UD(2)*UD(2)-UD(3)*UD(3)*TNANGL(ICR)*TNANGL(ICR)
      B=2.*(UD(1)*X+UD(2)*Y-UD(3)*(Z*TNANGL(ICR)*TNANGL(ICR)
     + +TNANGL(ICR)*EXAPR(ICR)))
      C=X*X+Y*Y-Z*Z*TNANGL(ICR)*TNANGL(ICR)
     + -2.*TNANGL(ICR)*Z*EXAPR(ICR)-EXAPR(ICR)*EXAPR(ICR)
      GO TO 55
C   TRUMPET CONCENTRATOR
   50 A=(UD(1)*UD(1)+UD(2)*UD(2))/(AHYP(ICR)*AHYP(ICR))-(UD(3)*UD(3))
     + /(BHYP(ICR)*BHYP(ICR))
      B=2.*((X*UD(1)+Y*UD(2))/(AHYP(ICR)*AHYP(ICR))
     + -(Z-ZPOS(ICR))*UD(3)/(BHYP(ICR)*BHYP(ICR)))
      C=(X*X+Y*Y)/(AHYP(ICR)*AHYP(ICR))
     + -(Z-ZPOS(ICR))*(Z-ZPOS(ICR))/(BHYP(ICR)*BHYP(ICR))-1.
   55 XL=(-B+SQRT(B*B-4.*A*C))/(2.*A)
C   CHECK ROOT
      Z2=Z+UD(3)*XL
      IF(Z2.LT.0..OR.XL.LE.0.000001)XL=(-B-SQRT(B*B-4.*A*C))/(2*A)
      X=X+XL*UD(1)
      Y=Y+XL*UD(2)
      Z=Z+XL*UD(3)
      R2=SQRT(X*X+Y*Y)
C     WRITE(8,101)X,Y,Z,R2,UD(1),UD(2),UD(3)
C 101 FORMAT(1X,' X,Y,Z,R2',5X,4F10.5,10X,'UD1,2,3 ',5X,3F10.7)
C   SUM ABSORPTION INTO REFLECTOR SURFACE
      ABSORB=(1.-TREFL(ICR))*RAYVAL
      J=0
   56 J=J+1
      IF(J.LE.20) GO TO 57
      J=J-1
      WRITE(8,110)ICR,NCALL(ICR),NREFL,X,Y,Z,XL,(UD(I),I=1,3),A,B,C
  110 FORMAT(1X,3I5,1X,'X,Y,Z',3F8.3,2X,'XL',F10.5,2X,'UD123',
     +3F7.4,2X,'ABC',3F10.4)
      GO TO 58
   57 IF(Z.GT.ZTER(J,ICR)) GO TO 56
   58 PWRTER(J,ICR)=PWRTER(J,ICR)+ABSORB
C   DECREASE RAYVAL BY AMOUNT ABSORBED
      RAYVAL=RAYVAL-ABSORB
      IF(NREFL.LT.40) GO TO 59
      PWRTER(J,ICR)=PWRTER(J,ICR)+RAYVAL
      NABS(ICR)=NABS(ICR)+1
      RETURN
   59 NREFL=NREFL+1
C   FIND NORMAL ON SURFACE
      DZDR=1/TNANGL(ICR)
      ZP=Z
      IF(ITYPE.EQ.2)DZDR=BHYP(ICR)*BHYP(ICR)
     + *SQRT(ZP*ZP/(BHYP(ICR)*BHYP(ICR))+1.)/(AHYP(ICR)*ZP)
      PHI=ATAN(DZDR)
      CPHI=COS(PHI)
      SPHI=SIN(PHI)
      DO 60 I=1,3
      UDUM(I)=(X*UCA(I)+Y*UCP(I))/R2
      UN(I)=-SPHI*UDUM(I)+CPHI*UCN(I)
```

```
C    PERTURN UN USING SDT
       CALL CROSS(UN,UT,UT2)
       CALL ERNORM(SDT(ICR),DUMY,UN,UT,UT2,UNP,DUMY,ISEED)
C    FIND REFLECTED RAY
       DO 61 I=1,3
    61 UD(I)=-UD(I)
       CALL SNELL(UR,UNP,UD)
       DO 65 I=1,3
    65 UD(I)=UR(I)
C      WRITE(6,102) X,Y,Z,UD(1),UD(2),UD(3)
C 102 FORMAT(10X,'X,Y,Z',5X,3F10.5,5X,'UD1,2,3',5X,3F10.5,/)
C    CHECK DIRECTION OF RAY
       IF(UD(3).LT.0.) GO TO 30
       IF(UD(3).EQ.0.) GO TO 40
C    DID RAY LEAVE APERTURE?
       XL=(ZTRUN(ICR)-Z)/UD(3)
       XI=X+XL*UD(1)
       YI=Y+XL*UD(2)
       RI=SQRT(XI*XI+YI*YI)
       IF(RI.GT.RTRUN(ICR)) GO TO 40
C    RAY HAS LEFT APERTURE
    75 XLOST(ICR)=XLOST(ICR)+RAYVAL
       NLOST(ICR)=NLOST(ICR)+1
       RETURN
       END
       SUBROUTINE TRTOUT(ITYPE,NDRAW,ISHAD,MIS2,ICR,R1)
       COMMON/TPAR/TRANGL(16),EXAPR(16),ZTRUN(16),ZPOS(16)
      + ,PWRTER(20,16),ZTER(20,16),MIST(16),
      + XLOST(16),NLOST(16),NABS(16),PRCVR(20,16),
      + RRCVR(20,16),TREFL(16),SDT(16),ANGR(14),ANGPWR(14,16)
C
C    THIS SUBROUTINE FORMATS THE OUTPUT GENERATED BY NOIMUJ
C
       SUMT=0.
       SUMR=0
       AMIR=R1*R1*3.1415926
       DO 10 I=1,20
       PWRTER(I,ICR)=PWRTER(I,ICR)*AMIR/NDRAW
       PRCVR(I,ICR)=PRCVR(I,ICR)*AMIR/NDRAW
       SUMT=SUMT+PWRTER(I,ICR)
    10 SUMR=SUMR+PRCVR(I,ICR)
       DO 11 I=1,14
    11 ANGPWR(I,ICR)=ANGPWR(I,ICR)*AMIR/NDRAW
       PLOST=XLOST(ICR)*AMIR/NDRAW
       PMIST=MIST(ICR)*AMIR/NDRAW
       TOTLP=SUMT+SUMR+PLOST+PMIST
       XIF=0.
       IF(TOTLP.GT.0.)XIF=SUMR/TOTLP
       SHADOW=ISHAD
       BF=1.-SHADOW/NDRAW
       CR=R1*R1/(EXAPR(ICR)*EXAPR(ICR))
       VSPOT=SQRT(EXAPR(ICR)**2*(1+1/(TAND(TRANGL(ICR))**2)))
       EFFOPT=BF*XIF*(1-FLOAT(MIS2)/(FLOAT(NDRAW)-FLOAT(ISHAD)))
C
C    WRITE RESULTS
       WRITE(8,20)
       WRITE(8,30) ITYPE,SUMT,ZPOS(ICR),SUMR,ZTRUN(ICR)
      + ,PLOST,EXAPR(ICR),PMIST,
```

```
      WRITE(8,40)(ZTER(I,ICR),PWRTER(I,ICR),
     + RRCVR(I,ICR),PRCVR(I,ICR),ANGR(I),ANGPWR(I,ICR),I=1,14)
      WRITE(8,41)(ZTER(I,ICR),PWRTER(I,ICR),
     + RRCVR(I,ICR),PRCVR(I,ICR),I=15,20)
   20 FORMAT('1',43X,'NONIMAGING CONCENTRATOR PERFORMANCE RESULTS',
     + //,24X,'PARAMETERS',55X,'SUMMARY',//)
   30 FORMAT(20X,'TYPE:  ',I1,'  (1-CONIC, 2-HYPERBOLIC)',T68,7X,
     + 'POWER ABSORBED BY CONCENTRATOR:  ',F7.4,1X,'KW',/,
     + 10X,'POSITION OF HYPERBOLIC WAIST: ',F7.4,1X,'M',
     + T68,11X,'POWER INCIDENT ON RECEIVER:  ',F7.4,1X,'KW',/,
     + 16X,'HEIGHT OF CONCENTRATOR: ',F7.4,1X,'M',
     + T68,7X,'POWER REJECTED BY CONCENTRATOR:  ',F7.4,1X,'KW',/,
     + 20X,'RADIUS OF RECEIVER: ',F7.4,1X,'M',
     + T68,'POWER NOT INTERCEPTED BY CONCENTRATOR:  ',F7.4,1X,'KW',/,
     + 16X,'CONIC-ASYMPTOTIC ANGLE: ',F7.4,1X,'DEG',
     + T68,8X,'GEOMETRIC CONCENTRATION RATIO:  ',F7.2,/,
     + 26X,'REFLECTIVITY: ',F7.4,
     + T68,21X,'INTERCEPT FACTOR:  ',F7.4,/,
     + 25X,'SURFACE ERROR: ',F7.4,1X,'MR',
     + T68,22X,'BLOCKING FACTOR:  ',F7.4,/,
     + 19X,'VIRTUAL SPOT RADIUS: ',F7.4,1X,'M',
     + T68,19X,'OPTICAL EFFICIENCY:  ',F7.4,//)
   40 FORMAT(5X,'DISTRIBUTION OF POWER ABSORBED BY TERTIARY',
     + 5X,'DISTRIBUTION OF POWER INCIDENT ON RECEIVER',
     + 5X,'ANGULAR DISTRIBUTION OF POWER',//,
     + 15X,'HEIGHT(M)',4X,'POWER(KW)',25X,'RADIUS(M)',4X,
     + 'POWER(KW)',15X,'ANGLE(DEG)',5X,'POWER(KW)',
     + //,14(15X,F8.4,5X,F8.4,26X,F8.4,5X,F8.4,18X,F5.0,9X,F8.4,/))
   41 FORMAT(6(15X,F8.4,5X,F8.4,26X,F8.4,5X,F8.4,/))
      RETURN
      END

      SUBROUTINE CROSS(A,B,C)
      DIMENSION A(3),B(3),C(3)
      C(1)=A(2)*B(3)-A(3)*B(2)
       C(2)=-A(1)*B(3)+A(3)*B(1)
      C(3)=A(1)*B(2)-A(2)*B(1)
      RETURN
      END
      SUBROUTINE LIMDR(YRN,LIMC,ROERN)
C    THIS SUBR. GENERATES THE INTENSITY DISTRIBUTION OF ENERGY
C    CROSS THE SURFACE OF THE SUN.  IT HS 2 DIFERENT SUN MODES.
C    LIMC=1    FLAT SUN
C    LIMC=3    SUN WITH LIMB DRKENING

      IF (LIMC.EQ.3) GO TO 23
C
C    FLAT SUN
C      WRITE(3,9000) YRN
C9000 FORMAT(2X,'IN LIMDR.  YRN=',F10.6)
      ROERN=.2665*SQRT(YRN)
      RETURN
C    NON-UNIFORM SUN
   23 Y=YRN*15.94
      IF(Y.GT.7.) GO TO 41
      ROERN=.06408*(Y**.4878)
      RETURN
   41 ROERN=.010956*Y+.092413
```

```
      END
C
      SUBROUTINE SUN2(AC,USP,DRAD,ISEED)
C    THIS ROUTINE PERTURBS THE SUN VECTOR FOR A FINITE SUN
      INTEGER*4 ISEED
      DIMENSION USP(3)
      COMMON/VECTOR/ULE(3),ULV(3),ULS(3),UCN(3),UCA(3),UCP(3),US(3)
      COMMON/SUNC/UST1(3),UST2(3)
      R1=RAN(ISEED)
      R2=RAN(ISEED)
      CRN=COS(6.2831853*R1)
      SRN=SIN(6.2831853*R1)
      CALL LIMDR(R2,3,ROE)
      CP=COS(ROE*DRAD)
      SP=SIN(ROE*DRAD)
      DO30I=1,3
   30 USP(I)=CP*US(I)+SP*CRN*UST1(I)+SP*SRN*UST2(I)
      RETURN
      END
C
      SUBROUTINE SNELL(UREFL,UNORM,USOL)
      DIMENSION UREFL(3),UNORM(3),USOL(3)
C
C    THIS ROUTINE SOLVES FOR A REFLECTED RAY USING SNELLS LAW
      FCTRUN=2*DOTER(UNORM,USOL)
      DO 20I=1,3
   20 UREFL(I)=FCTRUN*UNORM(I)-USOL(I)
      RETURN
      END
C
      SUBROUTINE ERNORM(SDS,DUM,UN,UT,UCA,UNP,PSM,ISEED)
      INTEGER*4 ISEED
      DIMENSION UN(3),UT(3),UCA(3),UNP(3)

      DATA NORCT/0/
      CALL RNORM(R1,NORCT,ISEED)
      NORCT=NORCT+1
      IF (NORCT.EQ.2) NORCT=0
      PHI=SDS*R1*.001+PSM
      RN=RAN(ISEED)
      PH2=RN*6.2831853
      C1=COS(PHI)
      C2=COS(PH2)
      S1=SIN(PHI)
      S2=SIN(PH2)
      DO 90 I=1,3
   90 UNP(I)=C1*UN(I)+S1*(C2*UT(I)+S2*UCA(I))
      RETURN
      END
C
      SUBROUTINE RNORM(D1,ICOUNT,ISEED)
      INTEGER*4 ISEED
C    THIS SUBR GENERATES PAIRS OF INDEPENDENT NORMAL RANDOM DEVIATES.
      IF(ICOUNT.GT.0) GO TO 30
   10 X=RAN(ISEED)
      RN=RAN(ISEED)
      Y=2.*RN-1.0
      XX=X*X
```

```
      S=XX+YY
      IF(S-1.) 20,20,10
   20 RN=RAN(ISEED)
      IF(RN.LT.0.0000001)RN=.000001
      ARGU=-2.*ALOG(RN)
      XL=SQRT(ARGU)/S
      D1=(XX-YY)*XL
      D2=2*X*Y*XL
      RETURN
   30 D1=D2
      RETURN
      END
C
      SUBROUTINE SUN1(TAZ,TEL)
C    SET SUN CENTER TO VECTOR US
      COMMON /VECTOR/ULE(3),ULV(3),ULS(3),UCN(3),UCA(3),UCP(3),US(3)
      COMMON/SUNC/ UST1(3),UST2(3)
      CA=COS(TAZ)
      SA=SIN(TAZ)
      CE=COS(TEL)
      SE=SIN(TEL)
      DO 10 I=1,3
   10 US(I)=CA*CE*ULS(I)+SA*CE*ULE(I)+SE*ULV(I)
      COFF=DOTER(ULV,US)
      SOFF=SQRT(1-COFF*COFF)
      IF(SOFF.NE.0.) GO TO 20
C    SUN IS OVERHEAD
      DO 12 I=1,3
      UST1(I)=0.
   12 UST2(I)=0.
      UST1(1)=1.
      UST2(2)=1.
      RETURN
   20 DO11I=1,3
   11 UST1(I)=(ULV(I)-COFF*US(I))/SOFF
      CALL CROSS(UST1,US,UST2)
C    UST1,UST2, AND US ARE TRIAD ON SUN FACE
C    CHECK FOR ARTHOGANALITY
      DUM=DOTER(UST1,US)
      IF(DUM.GT.0.00001) WRITE(8,60) DUM
   60 FORMAT(' ERROR IN SUN TANGENT',10X,F10.7)
      RETURN
      END
C
      SUBROUTINE TRACK(TAZ,TEL)
C    THIS ROUTINE SETS THE COLLECTOR POSITION VECTOR
C    TRIAD FOR ALL CONCENTRATORS AND CALCULATES THE OFF AXIS
C    SUN ANGLE BASED UPON THE PERFECT SUN VECTOR.
C      NEEDED VARIABLES INCLUDE:
C       NAXIS - 2 FOR 2AXIS TRACKING
C       TAZ,TEL
      DIMENSION DUM(3)
C
      COMMON/TRAC/NAXIS,TLTANG,OFFSUN,THTAAX,DTRCRL,DTRCAZ,IRPI
      COMMON/VECTOR/ULE(3),ULV(3),ULS(3),UCN(3),UCA(3),UCP(3),US(3)
      DATA NAXIS,TLTANG,IRPI/2,0.,0/
      IF (IRPI.EQ.1) GO TO 200
      IF(ABS(COS(TEL)).GT.0.001) GO TO 30
```

```
      DO 15 I=1,3
      UCN(I)=0.
      UCA(I)=0.
   15 UCP(I)=0.
      UCN(3)=1.
      UCA(1)=1.
      UCP(2)=1.
      OFFSUN=0.0
      RETURN
   30 IF(NAXIS.EQ.2) THTAAX=-TAZ+DTRCAZ
      TANEL=SIN(TEL)/COS(TEL)
      THTARL=ATAN2(COS(THTAAZ+TAZ),TANEL)+DTRCRL
      IF (NAXIS.EQ.0) THTARL=TLTANG
      SAX=SIN(THTAAX)
      CAX=COS(THTAAX)
      SRL=SIN(THTARL)
      CRL=COS(THTARL)
      DO 40 I=1,3
      UCA(I)=CAX*ULE(I)+SAX*ULS(I)
      UCP(I)=-SAX*CRL*ULE(I)+CAX*CRL*ULS(I)-SRL*ULV(I)
   40 UCN(I)=-SRL*SAX*ULE(I)+SRL*CAX*ULS(I)+CRL*ULV(I)
C    ACOS(X)=ATAN(SQRT(1-X*X)/X)
      X=DOTER(UCN,US)
      OFFSUN=ATAN(SQRT(1-X*X)/X)
      OFFSUN=OFFSUN*SIGN(1.,THTAAX+TAZ)
      RETURN
  200 SA=SIN(TAZ)
      CA=COS(TAZ)
      ST=SIN(TILT)
      CT=COS(TILT)
      DO 10 I=1,3
   10 DUM(I)=CA*ULS(I)+SA*ULE(I)
      DO 20 I=1,3
      UCN(I)=CT*ULV(I)+ST*DUM(I)
      UCP(I)=CT*DUM(I)-ST*ULV(I)
   20 UCA(I)=CA*ULE(I)-SA*ULS(I)
C    ACOS(X)=ATAN(SQRT(1-X*X)/X)
      X=DOTER(UCN,US)
      OFFSUN=ATAN(SQRT(1-X*X)/X)
      OFFSUN=OFFSUN*SIGN(1.,THTAAX+TAZ)
      RETURN
      END
C
      SUBROUTINE TRANS(X,Y,Z,U,DX,DY,DZ,ZTRAN,THETA,IDIR)
      DIMENSION U(3)
C
C    IDIR=1, TRANSFORMING VECTOR TO MISALIGNED HYPERBOLOID
C    IDIR=-1,TRANSFORMING VECTOR TO MAIN COORDINATE SYSTEM.
      IF(IDIR.LT.0) GO TO 10
C   TRANSLATE XYZ
      X=X-DX
      Y=Y-DY
      Z=Z-(DZ+ZTRAN)
C    ROTATE SYSTEM
      XROT=X*COSD(THETA)-Z*SIND(THETA)
      ZROT=X*SIND(THETA)+Z*COSD(THETA)+ZTRAN
      X=XROT
      Z=ZROT
```

```
      UZROT=U(1)*SIND(THETA)+U(3)*COSD(THETA)
      U(1)=UXROT
      U(3)=UZROT
      RETURN
   10 Z=Z-ZTRAN
C    DEROTATE SYSTEM
      XROT=X*COSD(-THETA)-Z*SIND(-THETA)
      ZROT=X*SIND(-THETA)+Z*COSD(-THETA)
      X=XROT
      Z=ZROT
      UXROT=U(1)*COSD(-THETA)-U(3)*SIND(-THETA)
      UZROT=U(1)*SIND(-THETA)+U(3)*COSD(-THETA)
      U(1)=UXROT
      U(3)=UZROT
      X=X+DX
      Y=Y+DY
      Z=Z+DZ+ZTRAN
      RETURN
      END
C
C
      FUNCTION DOTER(V1,V2)
      DIMENSION V1(3),V2(3)
C     THIS FUNCTION FINDS THE MAGNITUDE OF A DOT PRODUCT
      DOTER = 0.
      DO 10 I=1,3
   10 DOTER=DOTER+V1(I)*V2(I)
      RETURN
      END
```

TIC-4500-R70-UC-62 (170)

AAl Corporation
P.O. Box 6787
Baltimore, MD 21204

Acurex Aerotherm(2)
485 Clyde Avenue
Mountain View, CA 94042
Attn: J. Vindum
H. Morse

Advanco Corporation
2250 E. Imperial Hwy.
Suite 252
El Segundo, CA 90245

Alpha Solarco
1014 Vine Street
Suite 2230
Cincinatti, OH 45202

Anaconda Metal Hose Co.
698 South Main Street
Waterbury, CT 06720
Attn: W. Genshino

Applied Concepts Corp.
2501 S. Larimer County Rd. 21
Berthoud, CO 80513
Attn: Stan Pond

BDM Corporation
1801 Randolph Street
Albuquerque, NM 87106
Attn: W. E. Schwinkendorf

Battelle Memorial Institute
Pacific Northwest Laboratory
San Francisco, CA 94119
ATtn: E. Y. Lam

Bechtel National, Inc.
P.O. Box 3965
50 Beale Street
San Francisco, CA 94119
Attn: E. Y. Lam

Black & Veatch
P.O. Box 8405
Kansas City, MO 64114
Attn: J. C. Grosskreutz

Boeing
Engineering & Construction
P.O. Box 3707
Seattle, WA 98124
Attn: J. R. Gintz

Budd Company (The)
Fort Washington, PA 19034
Attn: W. W. Dickhart

Budd Company (The)
Plastic R&D Center
356 Executive Drive
Troy, MI 48084
Attn: J. N. Epel

Burns & Roe
800 Kinderkamack Road
Oradell, NJ 07649
Attn: G. Fontana

Burns & Roe, Inc.
185 Crossways Park Drive
Wooodbury, NY 11797
Attn: R. J. Vondrasket
J. Wysocki

Carrier Corporation
Energy System Division
Summit Landing
P.O. Box 4895
Syracuse, NY 13221
Attn: R. A. English

Chicago Bridge and Iron
800 Jorie Blvd.
Oak Brook, IL
Attn: J. M. Shah

Colorado State University
Ft. Collins, CO 80521
Attn: T. G. Lene

Columbia Gas System Service Corp.
1600 Dublin Road
Columbus, OH 43215
Attn: J. Philip Dechow

Corning Glass Company
Corning, NY 14830
Attn: A. F. Shoemaker
W. Baldwin

Custom Engineering, Inc.
2805 South Tejon Street
Englewood, CO 80110
Attn: C. Demoraes

Datron Systems, Inc.
20700 Plummer Street
Chatsworth, CA 91311

DFVLR
Apto. 649
Almeria, SPAIN
Attn: C. Selvage

DSET
Black Canyon Stage
P.O. Box 185
Phoenix, AZ 85029
Attn: G. A. Zerlaut

Donnelly Mirrors, Inc.
49 West Third Street
Holland, MI 49423
Attn: J. A. Knister

Dow Corning Corporation
Midland, MI 48640
Attn: R. S. Woodward
G. A. Lane

Electric Power Research
Institute
3412 Hillview Avenue
Palo Alto, CA 94303
Attn: E. A. Demaeo

Energetics Corporation
1201 Richardson Drive
Suite 216
Richardson, TX 75080
Attn: Lee Wilson

Energy Technology Engr. Ctr.
P.O. Box 1449
Canoga Park, CA 91304
Attn: W. Bigelow

ENTECH, Inc.
P.O. Box 612246
DFW Airport, TX 75261
Attn: R. R. Walters

Eurodrive, Inc.
2001 W. Main Street
Troy, OH 45373

Florida Solar Energy Center
300 State Road, Suite 401
Cape Canaveral, FL 32920
Attn: Library

Ford Aerospace
Ford Road
Newport Beach, CA 92663
Attn: Al Gates

Ford Motor Company
Glass Div., Technical Center
25500 West Outer Drive
Lincoln Park, MI 48246
Attn: V. L. Lindberg

Foster Wheeler Solar Dev. Corp.
12 Peach Tree Hill Road
Livingston, NJ 07039
Attn: M. D. Garber

General Atomic
P.O. Box 81608
San Diego, CA 92138
Attn: D. Williamson

General Motors
Harrison Radiator Division
Lockport, NY 14094
Attn: L. Brock

Georgia Institute of Technology
Atlanta, GA
Attn: T. Stelson

Georgia Power Co. (3)
270 Peachtree Street
PO. Box 4545
Atlanta, GA 309302
Attn: J. Roberts
W. Davis
E. Ney

Haveg Industries, Inc.
1287 E. Imperial Highway
Santa Fe Springs, CA 90670
Attn: J. Flynt

Highland Plating
10001 N. Orange Drive
Los Angeles, CA 90038
Attn: D. May

Honeywell, Inc.
Energy Resources Center
2600 Ridgeway Parkway
Minneapolis, MN 55413

Insights West
14022 Condessa Drive
Del Mar, CA 92014
Attn: David W. Kearney

Institute of Gas Technology
34245 State Street
Chicago, IL 60616

Jacobs Engineering Co.
251 South Lake Avenue
Pasadena, CA 91101
Attn: Meyer Schwartz

Jet Propulsion Laboratory (3)
4800 Oak Grove Drive
MS 502-419
Pasadena, CA 91103
Attn: J. Lucas
Dr. Paul M. McElroy

LaJet Energy Co.
3130 Antilley Road
Abilene, TX 79606
Attn: Monte McGlaun

Lawrence Livermore Laboratory
University of California
P.O. Box 808
Livermore, CA 94500
Attn: W. C. Dickinson

L'Garde, Inc.
1555 Placentia Avenue
Newport Beach, CA 92663
Attn: Dr. Mitchell Thomas

Los Alamos National Laboratory (2)
Los Alamos, NM 87545
Attn: J. D. Balcomb

Martin Marietta Corp. (2)
P.O. Box 179
MS S8120
Denver, CO 80201
Attn: P. Brown
T. Tracy

McDonnell-Douglas Astronautics
Company (3)
5301 Bolsa Avenue
Huntington Beach, CA 92647
Attn: J. B. Blackmon
J. Rogan
D. Steinmeyer

Mechanical Technology, Inc. (2)
968 Albany Shaker Road
Latham, NY 12110
Attn: H. M. Leibowitz
G. R. Dochat

Midwest Research Institute (2)
425 Volker Blvd.
Kansas City, MO 64110
Attn: R. L. Martin
J. Williamson

NASA Lewis Research Center (2)
21000 Brook Park Road
Cleveland, OH 44135
Attn: R. Bermand 500-202
W. Goette

Naval Civil Engr. Laboratory
Port Hueneme Naval Station
Port Hueneme, CA 93043
Attn: Lewis Huang

New Mexico Solar University
Solar Energy Department
Box 3SOL
Las Cruces, NM 88003

Owens-Illinois
1020 N. Westwood
Toledo, OH 43614
Attn: Y. K. Pei

PPG Industries
One Gateway Center
Pittsburgh, PA 15222
Attn: C. R. Frownfelter

Parsons of California
3437 S. Airport Way
Stockton, CA 95206
Attn: D. R. Biddle

Power Kinetics, Inc.
1223 Peoples Avenue
Troy, NY 12180
Attn: Mark Rice

Research Systems, Inc.
Suburban Trust Bldg.,
Suite 203
5410 Indian Head Hwy.
Oxon Hill, MD 20745
Attn: Dr. T. A. Chubb

Rocket Research Company
11441 Willows Rd. NE
Redmond, WA 98052
Attn: E. W. Schmidt

Rockwell International
Energy Systems Group
8900 De Soto Avenue
Canoga Park, Ca 91304
Attn: T. Springer

Rockwell International
Space Transportation &
Systems Group
12214 Lakeweek Blvd.
Downey, CA 90241
Attn: I. M. Chen

Sanders Associates
C.S. 2035
Nashua, NH 03061-2035
Attn: B. Davis

Solar Energy Information Center
1536 Cole Blvd.
Golden, CO 80401
Attn: R. Ortiz

Solar Energy Research Inst. (3)
1617 Cole Blvd.
Golden, CO. 80401
Attn: G. Gross
B. P. Gupta
J. Thornton

Shelltech Associates
809 Tolman Drive
Stanford, CA 94305
Attn: C. R. Steele

Solar Kinetics, Inc.
P.O. Box 47045
Dallas, TX 75247
Attn: J. A. Hutchison

Solar Steam
Suite 400
Old City Hall
625 Commerce Street
Tacoma, WA 98402
Attn: D. E. Wood

Southwest Research Institute
P.O. Box 28510
San Antonio, TX 78284
Attn: D. M. Deffenbaugh

Stanford Research Institute
Menlo Park, CA 94025
Attn: A. J. Slemmons

Stearns-Roger
4500 Cherry Creek
Denver, CO 80217
Attn: W. R. Lang

W. B. Stine
1230 Grace Drive
Pasadena, CA 91105

Sun Gas Company
Suite 930
3 N Park E
Dallas, TX 75221
Attn: R. I. Benner

Sundstrand Electric Power
4747 Harrison Avenue
Rockford, IL 61101
Attn: A. W. Adam
B. G. Johnson

Sunpower Systems
510 S 52 Street
Tempe, AZ 85281
Attn: W. Matlock

Suntec Systems, Inc.
2101 Wooddale Drive
St. Paul, MN 55110
Attn: Harrison Randolph

Swedlow, Inc. (2)
12122 Western Avenue
Garden Grove, CA 92645
Attn: E. Nixon
M. M. Friefeld

3M-Decorative Products Div.
209-2N 3M Center
St. Paul, MN 55144
Attn: B. Benson

3M-Product Development
Energy Control Products
207-1W 3M Center
St. Paul, MN 55144
Attn: J. B. Roche

Texas Tech University
Dept. of Electrical Engineering
P.O. Box 4709
Lubbock, TX 79409
Attn: E. A. O'Hair

Toltec Industries, Inc.
40th and East Main
Clear Lake, IA 50428
Attn: D. Chenault

TRW
Space & Technology Group
One Space Park
Redondo Beach, CA 90278
Attn: G. M. Reppucci
A. D. Schoenfeld
J. S. Archer

US Department of Energy (3)
Albuquerque Operations Office
P.O. Box 5400
Albuquerque, NM 87185
Attn: D. Graves
D. L. Krenz
J. Weisiger

US Department of Energy
Division of Energy Storage Sys.
Washington, DC 20585
Attn: J. Gahimer

US Department of Energy (6)
Division of Solar Thermal Tech.
Washington, DC 20585
Attn: H. S. Coleman
C. Carwile
J. E. Greyerbiehl
C. Mangold
M. R. Scheve
F. Wilkins

US Department of Energy (2)
San Francisco Operations Ofc.
1333 Broadway
Wells Fargo Building
Oakland, CA 94612
Attn: R. W. Hughey
W. L. Lambert

University of Houston
Houston, TX 77004
Attn: Lorin Vant-Hull

University of New Mexico (2)
Department of Mechanical Engr.
Albuquerque, NM 87113
Attn: M. W. Wilden
W. A. Gross

0400 R. P. Stromberg
1510 J. W. Nunziato
1513 D. W. Larson
1520 D. McCloskey
1810 R. G. Kepler
1820 R. E. Whan
1830 M. J. Davis
1840 R. J. Eagan
2540 G. N. Beeler
2541 J. P Abbin
3141 C. M. Ostrander (5)
3151 W. L. Garner (3)
3160 J. E. Mitchell
6200 V. L. Dugan
6220 D. G. Schueler
6221 E. L. Burgess
6222 J. V. Otts
6223 G. J. Jones
6224 D. E. Arvizu
6225 R. H. Braasch
6226 E. C. Boes
6227 J. A. Leonard (50)
6228 J. F. Banas
8424 M. A. Pound
8450 J. B. Wright
8452 A. C. Skinrood
8453 J. C. Swearengen
8454 J. B. Woodard

☆U.S. GOVERNMENT PRINTING OFFICE:1984—776-027/4379